Reverse electron transfer in the ischemic myocardium: role of succinate as a biomarker and modulation by internal and external factors

Marta Consegal Pérez

UAB
Universitat Autònoma de Barcelona

DOCTORAL THESIS

Reverse electron transfer in the ischemic myocardium: role of succinate as a biomarker and modulation by internal and external factors.

Doctoral thesis presented by **Marta Consegal Pérez** to obtain the degree of Doctor from the Universitat Autònoma de Barcelona.

Directors	Antonio Rodríguez Sinovas
	David García Dorado † (2019)
Tutors	Ignacio Ferreira González
	David García Dorado † (2019)

Doctorate in Medicine Program
Department of Medicine

Barcelona, 2023

Sé prou que la claror
germina dins la fosca.

Joan Vinyoli

AKNOWLEDGEMENTS

Sembla mentida que estigui aquí escrivint aquestes línies, després d'un dels anys més llargs de la meva vida però que tanca els cinc anys d'una etapa meravellosa. Qui ho hauria dit, la primera vegada que vaig trepitjar el laboratori de Malalties Cardiovasculars, que arribaríem fins aquí. Aquesta tesi doctoral ha sigut un gran repte però sobretot un gran aprenentatge, tant a nivell científic com personal, i no hauria sigut possible sense moltíssimes persones que, d'una manera o altra, hi han format part.

En primer lugar, si a alguien he de agradecerle este trabajo es al Dr. Antonio Rodríguez Sinovas, director de esta tesis. Gracias por apostar por mí, por haberme enseñado tanto y por guiarme con mucha paciencia hasta la pequeña científica que soy ahora. Por suerte no le diste demasiada importancia a mi cara de susto en mi primera cirugía de cerdo, que desapareció muy rápido, y aquí estamos. Gracias, Antonio, por responder a cada pregunta y duda y ser tan cercano.

Mi agradecimiento también para el Dr. David García Dorado, director del Laboratorio de Enfermedades Cardiovasculares, por haberme dado la oportunidad de incorporarme a su laboratorio para realizar este doctorado, aunque desafortunadamente sólo pudo ser codirector y tutor de esta tesis durante unos meses. También me gustaría agradecer al Dr. Ignacio Ferreira por aceptar amablemente coger el relevo y ser el tutor de esta tesis.

És necessari anomenar a l'Ignasi Barba, la persona que va fer possible tots els experiments amb la ressonància magnètica nuclear. Gracies per confiar en mi i deixar la reso al meu càrrec, per les extenses explicacions sobre camps magnètics i spins, que he intentat transmetre a les següents generacions, i pels consells sobre la ciència i la vida mentre es feia el manteniment de l'heli.

També cal una menció especial per l'Elisabet Miró. Eli, t'estic molt agraïda per haver-me introduït en el món de les mitocòndries, per haver-me ajudat a cultivar el criteri científic i per la paciència en classes magistrals sobre la cadena de transport d'electrons. No puc pensar en el CoQ sense recordar-me de tu. I al final, tot i els entrebancs, vam guanyar la batalla contra la HPLC!

A tots els meus companys de laboratori, començant pels que van marxar aviat o van estar només uns mesos, passant pels que han estat des del principi i acabant pels que acaben d'arribar. Entre tots heu creat un entorn fantàstic i ha sigut una sort poder treballar al vostre costat. A la Laura Valls, la meva pre-predoc, que em vas introduir al laboratori i em vas ensenyar tantes coses en tant poc temps. Al David Aluja, la Diana Bou-Teen, la Laia Yáñez i la Sara Delgado, el meus companys de despatx i de batalla que us heu convertit en la meva segona família, i als que sense dubte he vist durant aquest temps bastant més que a la meva família. Fer aquest camí al vostre costat ha estat un plaer, m'heu ajudat a fer els dies difícils menys difícils i el vostre suport ha sigut inestimable. SarA, dit amb la meva millor "a" de Barcelona, ara comences la marató d'escriure la tesi, però si jo he pogut, sé que tu ho bordaràs. A el team Antonio: Freddy, you have probably already realized that the moment is here and you are the new "Marta" now, which only means you are older and more experienced. I'm sure you will do great, and I hope you enjoy it as much as I did. Y Laura, ahora que empiezas aprende todo lo que puedas y, sobre todo, ¡disfruta del camino! A més, a tots els estudiants de pràctiques que han passat pel lab, Enric, Carmen, Andrés, Berta, i altres que segur em deixo, gràcies per haver-me ensenyat a ensenyar. And Maria, it was a pleasure to spend with you a strange but fantastic month, I am sure we will meet again, of course, in the next congress. A tota la resta de membres del laboratori, Ángeles, Begoña, Javier, Marisol i Tere, i als que hi han passat sense quedar-se, Andrea, Kelly i Ricardo, gràcies per aportar cadascú el seu granet de sorra a aquesta tesi.

No puc oblidar-me de la gent de la UAT que sempre ha estat disposada a ajudar, en especial al Norberto, que ha sigut indispensable pels experiments amb la HPLC i ens ha ajudat a navegar entre tots els problemes que han sorgit. I per suposat, un agraïment especial també als tots els membres dels dos estabularis, sobretot a l'Àngel, l'Albert i la Marielle i la Raquel.

Fora del laboratori, vull agrair a totes les persones que han patit les conseqüències d'aquesta tesi i que han estat sempre allà per ajudar-me a afrontar-les.

Al "Patatal", Aixa, Blanca, Lourdes i Lucía, no us podeu imaginar com d'importants heu estat. Gràcies per els berenars i els sopars, per ajudar-me a desconnectar i per passar per alt tots els meus "ho sento noies, arribo tard que

vinc del lab", tot i no acabar de saber mai què he estat fent exactament. Lourdes, les converses fins les tantes han sigut molt necessàries. I ara que saps el que és... estàs segura que t'hi vols ficar? Al grup de sempre, prometo venir a la pròxima, del que sigui. Als "enciams" amb qui, compartint anècdotes bioquímiques, hem tingut vides científiques paral·leles des de la distància. A la Laura, la teva forma de veure la vida sempre em dona perspectiva, gràcies per la paciència i perquè sé que, passi el que passi, sempre estaràs quan et necessito.

Qui m'ha donat suport des del principi ha sigut la meva família, els que estan i els que malauradament ja no, moltes gràcies a tots. Avis, Mila, finalmente he acabado y podréis ver en papel qué es eso a lo que le he estado dedicando tanto tiempo estos últimos años, gracias por vuestro apoyo siempre.

Definitivament aquesta tesi no hauria estat possible sense els meus pares i el meu germà, us estimo molt. Jordi, t'admiro moltíssim i ets per mi un exemple de com fer les coses bé, gràcies per estar sempre allà i et desitjo el millor en la teva tesi, que pel que sembla és contagiós. Papa, des del principi has cregut en mi i m'has donat suport incondicional, gràcies per seguir pensant que el que he fet és extraordinari, ets el meu referent del que significa treballar dur. Mama, gràcies per escoltar hores i hores d'explicacions de ciència i fer l'esforç de entendre-la, fins i tot a partir de les 10 de la nit. Sempre has confiat en mi i has estat darrere meu donant-me forces tot i les dificultats, has sigut imprescindible per mantenir-me sencera i la millor mare que hauria pogut desitjar. Les teves abraçades i els teus consells m'han fet arribar fins aquí.

Finalment, vull dedicar l'últim paràgraf a qui sempre ha estat agafant-me la mà. Alex, em costa posar en paraules com d'important ha sigut el teu suport constant. Moltes gràcies per esperar-me, sempre, sota la pluja o sota el sol, i per escoltar-me, sempre, i entendre'm. Has estat el meu pilar i la boia a la que m'he agafat per mantenir-me a la superfície. T'estimo.

ABREVIATIONS

^{1}H-NMR	nuclear magnetic resonance
4OHT	4-hydroxytamoxifen
ADP	adenosine 5'-diphosphate
AEMPS	Agencia española de medicamentos y productos sanitarios
AMP	adenosine 5'-monophosphate
ANOVA	analysis of variance
ANT	adenine nucleotide translocase
AP	aortic pressure
APAF-1	apoptotic protease activating factor 1
ATP	adenosine 5'-triphosphate
BA/BB	benzyl alcohol/benzyl benzoate
BCAA	branched-chain amino acid
BCKA	branched-chain keto acid
BCL-2	B-cell lymphoma-2
BH_4	tetrahydrobiopterin
BSA	bovine serum albumin
CD36	fatty acid translocase
CMR	cardiac magnetic resonance
CO_2	carbon dioxide
CoA	coenzyme A
CoQ	coenzyme Q
CPT	carnitine palmitoyl transferase I
CS	citrate synthase
CsA	cyclosporin A
Cx43	connexin 43
Cx43^{Crefl}+4OHT	connexin 43-deficient animals
Cx43^{flfl}+4OHT	control animals
CypD	cyclophilin D
Cyt C	cytochrome C
DEP	diesel exhaust particles
DHE	dihydroethidium
DNA	deoxyribonucleic acid
dP/dt	left ventricular pressure derivate divided by time
DTNB	dithiobis-(2-nitrobenzoic) acid

ECG	electrocardiogram
EDL	end diastolic length
eNOS	endothelial nitric oxide synthase
ESI	electrospray
ESL	end systolic length
ETC	electron transport chain
$FABP_{(pm)}$	fatty acid binding protein (plasma membrane)
FACS	fatty acyl-CoA synthetase
$FADH_2$	reduced flavin adenine dinucleotide
Fe-S	iron-sulfur cluster
FFA	free fatty acid
FMN	flavin mononucleotide
GLUTs	glucose transporters
GPx	glutathione peroxidase
GRP75	glucose-regulated protein 75
GSH	glutathione
GSSG	glutathione disulfide
GTP	guanosine 5-triphosphate
H_2O	water
H_2O_2	oxygen peroxide
HKII	hexokinase II
HRP	horseradish peroxidase
IFM	interfibrillar mitochondria
IMM	inner mitochondrial membrane
iNOS	inducible nitric oxide synthase
IP	intraperitoneal
IV	intravenous
LAD	left anterior descending
LC-MS/MS	liquid chromatography tandem mass spectrometry
LDH	lactate dehydrogenase
LDL	low density lipoproteins
LGE	late gadolinium enhancement
LV	left ventricular
LVdevP	left ventricular developed pressure
LVEDP	left ventricular end-diastolic pressure
LVEDV	left ventricular end-diastolic volume

LVEF	left ventricular ejection fraction
LVESV	left ventricular end-systolic volume
MAM	mitochondrial associated sarcoplasmic reticulum membranes
mCK	mitochondrial creatine kinase
MCU	mitochondrial calcium uniporter
MPC	mitochondrial pyruvate carrier
mPTP	mitochondrial permeability transition pore
MRM	multiple reaction monitoring
NAD^+	oxidized nicotinamide adenine dinucleotide
NADH	reduced nicotinamide adenine dinucleotide
NCX	Na^+/Ca^{2+} exchanger
NHE	Na^+/H^+ exchanger
nNOS	neuronal nitric oxide synthase
NO	nitric oxide
NOS	nitric oxide synthase
NOX	NADPH oxidases
O_2	molecular oxygen
$O_2^{-\cdot}$	superoxide anion
OAA	oxalacetate
OH^-	hydroxyl radical
OMM	outer mitochondrial membrane
$ONOO^-$	peroxynitrite anion
OXPHOS	oxidative phosphorilation
PCR	polimerase-chain reaction
PDH	pyruvate dehydrogenase
PiC	inorganic phosphate carrier
PKA	protein kinase A
PKC	protein kinase C
PNC	purine nucleotide cycle
pPCI	percutaneous coronary intervention
Prx	peroxiredoxin
RCR	respiratory control ratio
RET	reverse electron transfer
RIC	remote ischemic conditioning
ROS	reactive oxygen species
RyR2	ryanodine receptor 2

S2	state 2
S3	state 3
SDH	succinate dehydrogenase
SDS-PAGE	sodium dodecylsulphate-poliacrylamide gel electrophoresis
SEM	standard error of the mean
SERCA	sarcoendoplasmic reticulum calcium ATPase
SLC16A1	monocarboxylate transporter
SOD	superoxide dismutase
SR	sarcoplasmic reticulum
SS	systolic segment shortening ratio
SSM	subsarcolemmal mitochondria
STEMI	ST-elevated myocardial infarction
TAE	tris-acetate-EDTA
TBS-T	tris buffered saline-Tween
TEMED	tetramethyl ethylene diamide
TMRE	tetramethyl rhodamine ethyl ester perchlorate
TNB	2-nitro-5-thiobenzoate
TNF	tumor necrosis factor
Trx	thioredoxin
TrxR	thioredoxin reductase
TSP	3-(trimethylsilyl)propionic-2,2,3,3-d4 acid sodium salt
TSPO	translocator protein
TTC	2,3,5-triphenyltetrazolium chloride
UPLC-MS/MS	ultra-performance liquid chromatography coupled with mass spectrometry
VDAC	voltage dependent anion channel
VF	ventricular fibrillation
VT	ventricular tachycardia
XDH	xanthine dehydrogenase
XO	xanthine oxidases
XOR	xanthine oxidoreductases
β-HO-B	β-hydroxybutyrate
Δp	protonmotive force
ΔΨ	mitochondrial membrane potential

TABLE OF CONTENTS

ABSTRACT

Reperfusion injury triggered by blood flow restoration following an ischemic event account for an important part of cellular injury occurring during myocardial infarction. Although the mechanisms of reperfusion injury are complex, opening of the mitochondrial permeability transition pore, induced by a burst of reactive oxygen species (ROS) production at the onset of reperfusion, has a prominent role in this process. The main source of ROS during reperfusion is the mitochondria, mainly by a mechanism known as reverse electron transfer (RET). During ischemia succinate, the endogenous substrate of the citric acid cycle enzyme succinate dehydrogenase (SDH) (or mitochondrial complex II), accumulates in the myocardium. At the onset of reperfusion, this accumulated succinate is rapidly oxidized by SDH, a process coupled with transfer of electrons from complex II to complex I, where ROS are generated. Despite the extensive research done in this subject, many questions remain to be answered.

RET inhibition during reperfusion by the SDH reversible inhibitor malonate has been proved to protect against ischemia-reperfusion injury. Since evidence suggests that multitarget approaches may be beneficial to reduce infarct size in the clinical setting, here we assessed, in an *in vivo* porcine model of transient coronary occlusion, whether malonate, intracoronary administered into the area at risk at the onset of reperfusion, had additive effects against infarction with remote ischemic conditioning (RIC), applied to a femoral artery during ischemia. Our results confirm previous findings on the strong protective actions of both malonate and RIC and demonstrate that their combination does not result in additive effects.

Part of the succinate that accumulates in the myocardium is released into the circulation upon reperfusion. Accordingly, we also aimed to evaluate the potential for succinate and other citric acid cycle metabolites to become biomarkers of myocardial injury. In our porcine model, plasma levels of these metabolites were determined by UPLC-MS/MS, in blood samples obtained from both a peripheral vein and from the great cardiac vein. Plasma succinate levels were markedly increased during reperfusion in samples obtained from the great cardiac vein, but not from peripheral blood. Remarkably, succinate concentrations at the great cardiac vein correlated with infarct size, as assessed by TTC staining. Afterwards, we moved to the clinical scenario, where only

peripheral blood is easily available. In contrast to our findings in pigs, we were not able to detect any correlation between plasma levels of succinate or other metabolites, as assessed by ^{1}H-NMR, and cardiac magnetic resonance variables, including infarct size and area at risk, in patients with ST-segment elevation myocardial infarction submitted to primary percutaneous coronary intervention. These data indicate that the use of succinate as a biomarker would be restricted to blood obtained from the coronary sinus. In addition, our data suggest that succinate concentrations in peripheral plasma may increase over time, and that longer periods after reperfusion may be needed for its analysis.

ROS production by RET is modulated by the mitochondrial membrane potential, the coenzyme Q (CoQ) pool and its redox state, and succinate concentrations. However, no data are available on endogenous RET modulators. The gap junction protein connexin 43 (Cx43) is a good candidate for it, since it is found at the inner mitochondrial membrane of subsarcolemmal mitochondria where it modulates ROS production under specific circumstances. Therefore, we assessed the effects of Cx43 deficiency on ROS production by RET in isolated mitochondria from $Cx43^{Cre(ER)T/fl}$ mice treated with 4-hydroxytamoxifen (4OHT), which develop a global deletion of the protein. Cx43 deficiency decreased ROS production by RET in isolated subsarcolemmal mitochondria, as compared with control animals ($Cx43^{fl/fl}$+4OHT), but not in interfibrillar mitochondria. This effect was associated with a reduction in the amount of CoQ and in its reduced state, but not with changes in mitochondrial membrane potential or succinate accumulation at the end of ischemia. This fact may explain, at least in part, the marked protection these Cx43-deficient animals have against myocardial ischemia-reperfusion injury, as assessed in isolated hearts submitted to global ischemia-reperfusion, and that transient, reversible inhibition of SDH with malonate does not exert additional protection.

ROS production has been reported to be a key player in the deleterious cardiovascular effects of air pollution exposure. Thus, we assessed whether air pollution influences RET, using mitochondria isolated from rats intratracheally instilled with saline containing or not diesel exhaust particles. Our data demonstrate that particulate matter exposure reduces the number of viable mitochondria and enhances mitochondrial ROS production when using substrates feeding complex I, both in subsarcolemmal and interfibrillar mitochondria. However, these effects are independent of RET. In addition, diesel

exhaust particle exposure did not modify infarct size in isolated rat hearts submitted to global ischemia-reperfusion.

In conclusion, despite combination of SDH inhibition and RIC do not show additive effects against infarct size, concentrations of succinate, the endogenous substrate of the enzyme, correlate with infarct size in blood from the great cardiac vein, but not in peripheral blood. In addition, RET is modulated by Cx43 in a CoQ-dependent manner, but it is not altered by diesel exhaust particle exposure.

RESUMEN

El daño por reperfusión producido tras la restauración del flujo sanguíneo posterior a un evento isquémico es responsable de una parte muy relevante del daño celular que ocurre durante un infarto de miocardio. Aunque los mecanismos causantes del daño por reperfusión son complejos, la apertura del poro de transición mitocondrial, inducida por un rápido aumento en la producción de especies reactivas del oxígeno (ROS) al inicio de la restauración del flujo, desempeña un papel destacado en este proceso. La principal fuente de ROS durante la reperfusión son las mitocondrias, principalmente por un mecanismo conocido como transferencia reversa de electrones (RET). El succinato, que es el substrato endógeno de la succinato deshidrogenasa (SDH) (o complejo II), una enzima del ciclo de Krebs, se acumula en el miocardio durante la isquemia. Al inicio de la reperfusión, el succinato acumulado es rápidamente oxidado por esta enzima, en un proceso acoplado con la transferencia de electrones desde el complejo II al complejo I, donde se generan las ROS. A pesar de todos los estudios realizados, aún quedan muchas preguntas por responder al respecto.

Se ha demostrado que la inhibición de la transferencia reversa de electrones durante la reperfusión mediante malonato, un inhibidor reversible de la SDH, es protectora contra el daño por isquemia-reperfusión. Puesto que existen evidencias que sugieren que terapias combinadas podrían ser beneficiosas para reducir el tamaño del infarto, en esta tesis hemos evaluado, en un modelo porcino de oclusión coronaria transitoria *in vivo*, si el malonato, administrado de forma intracoronaria en el área en riesgo al inicio de la reperfusión, podría tener efectos aditivos con el condicionamiento isquémico remoto (RIC), aplicado en una arteria femoral durante la isquemia. Nuestros resultados confirman los importantes efectos protectores tanto del malonato como del RIC observados en estudios anteriores, y demuestran que su combinación no resulta en efectos aditivos.

Parte del succinato que se acumula en el miocardio durante la isquemia es liberado al torrente sanguíneo al inicio de la reperfusión. Por ello, nos propusimos evaluar el potencial del succinato y otros metabolitos del ciclo de Krebs como biomarcadores de daño miocárdico. En nuestro modelo porcino, determinamos los niveles de estos metabolitos por UPLC-MS/MS en muestras de

plasma obtenidas tanto de una vena periférica cómo de la gran vena cardíaca. La concentración de succinato en plasma aumentó, durante la reperfusión, en las muestras obtenidas de la gran vena cardíaca, pero no en las provenientes de sangre periférica. De forma importante, las concentraciones de succinato en la gran vena cardíaca correlacionaron con el tamaño del infarto evaluado mediante tinción de TTC. Seguidamente, pasamos al ámbito clínico, dónde sólo la sangre periférica es de fácil acceso. En oposición a nuestros hallazgos en los cerdos, no pudimos detectar ninguna correlación entre los niveles plasmáticos de succinato u otros metabolitos, analizados por ^{1}H-NMR, y las variables de resonancia magnética cardíaca, que incluyeron el tamaño del infarto y el área en riesgo, en pacientes con infarto de miocardio con elevación del segmento ST sometidos a angioplastia primaria. Estos resultados indican que el uso del succinato como biomarcador quedaría restringido a sangre obtenida del seno coronario. Además, nuestros datos sugieren que las concentraciones plasmáticas de succinato en sangre periférica podrían aumentar con el tiempo, y que para su análisis serían necesarios periodos más prolongados después de la reperfusión.

La producción de ROS por RET está modulada por el potencial de membrana mitocondrial, los niveles y estado de oxidación de la coenzima Q (CoQ), y las concentraciones de succinato al final de la isquemia. Sin embargo, no se conoce la existencia de moduladores endógenos de la RET. Un buen candidato para serlo es la proteína conexina 43 (Cx43), que forma parte de las uniones gap. Esta proteína se encuentra en la membrana mitocondrial interna de las mitocondrias subsarcolemales, dónde modula la producción de ROS en condiciones concretas. Por lo tanto, evaluamos los efectos de la deficiencia de Cx43 en la producción de ROS por RET en mitocondrias aisladas de animales Cx43$^{Cre(ER)T/fl}$ tratados con 4-hidroxitamoxifeno (4OHT), que desarrollan una deleción global de esta proteína. Comparando con animales control (Cx43$^{fl/fl}$+4OHT), la deficiencia de Cx43 disminuyó la producción de ROS por RET en las mitocondrias subsarcolemales pero no en las interfibrilares. Este efecto se asoció con una reducción en la cantidad de coenzima Q y de su estado reducido, pero no con cambios en el potencial de membrana mitocondrial o en la acumulación de succinato al final de la isquemia. Este hecho podría explicar, al menos en parte, la protección tan importante que presentan los animales deficientes de Cx43 frente al daño por reperfusión, evaluada en corazones aislados sometidos a isquemia global seguida de reperfusión, y el hecho de que la inhibición transitoria y reversible de la SDH con malonato no ejerza ninguna protección adicional.

Se ha demostrado que la producción de ROS es un factor clave en los efectos cardiovasculares perjudiciales de la exposición a contaminación ambiental. Por esta razón, evaluamos si la contaminación ambiental puede modular la RET utilizando mitocondrias aisladas de ratas sometidas a instilación intratraqueal de suero fisiológico conteniendo o no partículas diésel. Nuestros resultados demuestran que la exposición a materia particulada reduce el número de mitocondrias viables y aumenta la producción de ROS al utilizar substratos del complejo I, tanto en mitocondrias subsarcolemales como interfibrilares, aunque estos efectos son independientes de la RET. Además, la exposición a partículas diésel no modificó el tamaño del infarto en corazones aislados de rata sometidos a isquemia-reperfusión global.

En conclusión, aunque la combinación de la inhibición de la SDH y el RIC no muestran efectos aditivos contra el tamaño del infarto, las concentraciones de succinato, el substrato endógeno de esta enzima, correlacionan con el tamaño del infarto en sangre de la gran vena cardíaca, pero no en sangre periférica. Además, la RET está modulada por la Cx43 de forma dependiente de la CoQ, pero no se ve alterada por la exposición a partículas diésel.

1. INTRODUCTION

Cardiovascular diseases are the leading cause of global mortality, accounting for 19 million deaths in 2020 and representing about 32% of all deaths worldwide [1,2]. They are also a major contributor to disability, and its prevalence is increasing steadily, as a result of population growth and aging [3]. Specifically, in Spain, cardiovascular diseases account for 1 out of 3 deaths in women and 1 out of 4 deaths in men [4].

Ischemic heart disease is the most prevalent cause of cardiovascular death. It is usually due to occlusion of a coronary artery by an atherosclerotic plaque, leading to reduced blood flow in distal vessels, and to subsequent depletion in oxygen supply to the myocardial tissue. Atherosclerosis is a chronic inflammatory process which starts with a complex interaction of risk factors such as dyslipidemia and hypertension that disrupts the endothelium. Circulating low-density lipoproteins (LDL) have the ability to permeate the disrupted endothelium and undergo oxidation. Modified LDL, then, attract leukocytes into the intima of the coronary vessels, and are scavenged by macrophages, leading to formation of foamy cells. The replication of these cells induces the formation of lesions which are the earliest visualized sign of atherosclerosis. Consequently, smooth muscle cells start proliferating and producing extracellular matrix, the accumulation of which leads to progression of the atherosclerotic lesion to a fibrous plaque. The coronary lumen is then invaded, reducing blood flow. Fibrous plaques have an increased susceptibility to glycation and oxidative modification and give rise to an enhanced inflammatory response. As the lesion progresses, calcification, new vessel formation and cell death in the core of the atherosclerotic plaque may occur [5].

Even a 50% reduction in coronary artery diameter would not lead to symptoms at rest, despite a decrease in distal coronary perfusion pressure. However, with an increase in oxygen demand, for example during physical exercise, blood flow would become insufficient, giving rise to the appearance of symptoms, including angina [6].

Large plaques may occlude completely the vessel, leading to the appearance of myocardial ischemia. In addition, physical disruption of vulnerable atherosclerotic plaques would result in exposure of the necrotic core to the blood stream. Since the necrotic core is highly thrombogenic, it triggers the

initiation of the coagulation cascade and induces thrombus formation, which may also occlude the vessel in an already narrowed artery lumen.

An acute coronary syndrome comprises the events that follow a sudden coronary artery occlusion and the subsequent myocardial ischemia. When the ischemia lasts long enough it leads to the appearance of cardiomyocyte cell death and therefore to myocardial infarction. The ST-segment elevation myocardial infarction (STEMI) is the most serious presentation of acute coronary syndrome and is characterized by persistent ST segment elevation in the electrocardiogram (ECG) [7].

The extent of cell death during myocardial infarction is proportional to the duration of the ischemic insult. Thus, a prolonged ischemic period will lead to a large myocardial necrotic or infarcted area [8]. Infarct size is also influenced by the location of the obstructive plaque and the size of the myocardial territory distal to the occlusion and therefore affected by the ischemia, the so-called area at risk. The presence of residual blood flow at the obstruction site and the amount of coronary collateral circulation to the ischemic tissue also contribute to the final infarct size [9,10].

In accordance with the direct relation between the duration of the ischemic insult and infarct size, the current treatment of choice for a patient presenting with an acute coronary syndrome is the immediate application of reperfusion therapies, including primary percutaneous coronary intervention (pPCI) or administration of thrombolytics, aimed to restore coronary blood flow as quick as possible [11]. In fact, the area of myocardium salvaged by reperfusion decreases with any delay in its application, and after 3 hours of ischemia, the benefits of reperfusion on infarct size are questionable [10]. Thus, there is a window of opportunity in which reperfusion can rescue a significant part of the affected myocardium, thus reducing cell death, limiting infarct size and increasing survival until hospital discharge, but also improving long-term morbidity, life expectancy and quality of life.

However, the process of myocardial reperfusion itself can induce further cell death, additional to the damage caused by ischemia, in the form of necrosis occurring during the first minutes of flow restoration. This phenomenon has been called reperfusion injury and there is still no effective therapeutic

intervention to limit its deleterious effects in the myocardium. Therefore, reperfusion injury is being extensively studied with the objective of understanding the underlying molecular mechanisms, and it has been proposed that it may become an important therapeutic target aimed to reduce infarct size and the impact myocardial infarction has in the society [12,13].

1.1 CELLULAR AND MOLECULAR MECHANISMS OF MYOCARDIAL ISCHEMIA-REPERFUSION INJURY

Myocardial reperfusion injury is defined as the damage caused by restoration of blood flow and oxygen re-supply in cells that were only reversibly injured by the preceding ischemic insult. Therefore, ischemia-reperfusion injury could theoretically be prevented by a timely and effective intervention given at the onset of blood flow restoration *(Figure 1)* [14]. The most relevant consequence of reperfusion injury is the death of cardiomyocytes, the contractile units of the heart, subsequently producing a detrimental effect on myocardial functional capacity.

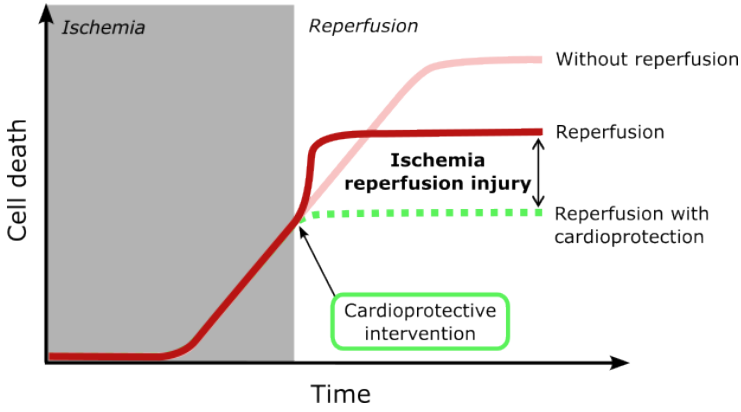

Figure 1: Representative illustration of the ischemia-reperfusion injury concept. During ischemia, cell death increases in proportion to insult duration. Reperfusion limits this process but at the same time induces additional cell death on the first minutes of flow restoration, which could be prevented by appropriate cardioprotective treatments administered at the onset of reperfusion. Modified from [12].

Multiple studies over the last decades have identified some critical and complex physiopathological changes that trigger necrotic cell death after ischemia-reperfusion injury, being deeply interconnected, but still not completely understood. Nevertheless, ischemia has been described to induce energy deprivation, changes in intracellular pH, and loss of ionic homeostasis which continue after reperfusion and lead to the development of hypercontracture and mitochondrial permeability transition pore (mPTP) opening.

1.1.1 ISCHEMIA

Coronary occlusion during myocardial ischemia causes cessation of blood flow to the myocardium, preventing delivery of oxygen and nutrients. Therefore, oxygen available to cardiomyocytes is quickly exhausted and adenosine 5'-triphosphate (ATP) synthesis is halted due to cessation of electron flow through the mitochondrial electron transport chain (ETC). In order to overcome ATP shortage, the anaerobic metabolism is enhanced, and the glycolytic pathway is activated. However, the detrimental consequences of this metabolic switch are the intracellular accumulation of lactic acid which, together with the impossibility to eliminate carbon dioxide (CO_2), causes tissue acidosis [12,15]. As a consequence of these events, the contractile activity of the heart is stopped, and when ATP concentration is reduced beyond a critical threshold, ischemic rigor contracture develops [16]. In addition, in order to maintain the mitochondrial membrane potential, the activity of the mitochondrial ATP synthase is reversed, further reducing ATP concentrations [17].

Simultaneously, activity of the Na^+/H^+ exchanger (NHE) and the Na^+/HCO_3^- cotransporter tries to correct intracellular acidosis, even though it induces a significant increase in cytosolic Na^+. Such excess of Na^+ cannot be pumped out of the cell, as exhaustion of ATP inhibits the sarcolemmal Na^+/K^+ ATPase pump, thus resulting in a progressive and significant Na^+ overload [18]. Consequently, the reverse mode of the Na^+/Ca^{2+} exchanger (NCX) is activated, introducing Ca^{2+} into the cytosol and producing a Ca^{2+} overload. This situation is worsened by the fact that the sarcoendoplasmic reticulum Ca^{2+} ATPase (SERCA), also dependent on ATP, is unable to store this Ca^{2+} into the sarcoplasmic reticulum (SR) [12,18,19]. Therefore, ischemia leads to dysregulation of ionic homeostasis that include enhanced intracellular Ca^{2+} and Na^+ concentrations in a low pH environment.

1.1.2 REPERFUSION

In a situation in which the period of ischemia and energy depletion is not excessively prolonged, blood flow restoration would repolarize cardiomyocyte mitochondria, reactivating ATP synthesis. Furthermore, re-flow of blood into the area at risk would allow the washout of the extracellular space, removing lactate and other metabolites accumulated during ischemia, and returning pH to its physiological values. Despite the positive implications of reperfusion, this same

condition, together with the alterations already produced during ischemia, can be the starting point for posterior cell death caused by reperfusion itself. The two main mechanisms that lead to cardiomyocyte death during ischemia-reperfusion injury are the development of hypercontracture and the opening of the mPTP (*Figure 2*).

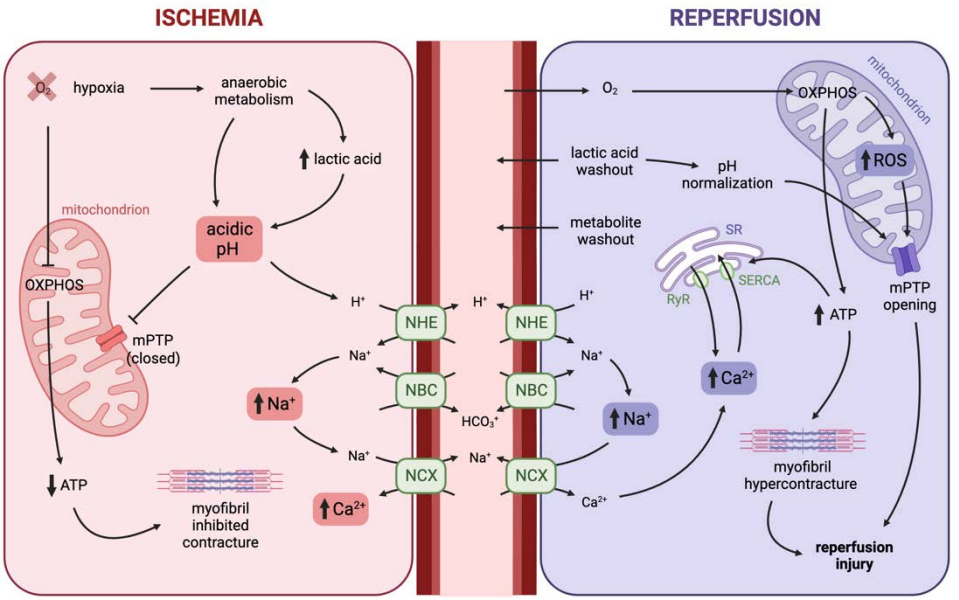

Figure 2: Schematic representation of the different intracellular mechanisms modified by ischemia-reperfusion. Complete explanation in main text. mPTP: mitochondrial permeability transition pore; NBC: Na^+/HCO_3^- cotransporter; NCX: Na^+/Ca^{2+} exchanger: NHE: Na^+/H^+ exchanger; OHPHOS: oxidative phosphorylation; ROS: reactive oxygen species; RyR: ryanodine receptor; SERCA: sarcoendoplasmic reticulum Ca^{2+} ATPase; SR: sarcoplasmic reticulum. Based on [13,435].

1.1.2.1 Hypercontracture

The phenomenon of hypercontracture refers to an excessive activation of cardiomyocyte contractile machinery causing an abrupt shortening of cell length. As cardiomyocytes are well connected with neighboring cells, the resulting mechanical forces would induce cardiomyocyte cell membrane (sarcolemmal) rupture and consequently cell death, which later spreads through the affected myocardial tissue. From a histological point of view, myocardial infarcts are

characterized by the presence of a typical pattern of connected hypercontracted dead cardiomyocytes, known as contraction band necrosis [19–22].

The mechanisms responsible for sarcolemmal rupture due to hypercontracture are complex and not completely elucidated, but the four main factors that contribute to final infarct size are changes in ionic homeostasis, osmolarity and oedema, cell fragility due to calpain activation and, finally, propagation of cell death through gap junctions.

1.1.2.1.1 Ionic homeostasis and pH alterations

Following restoration of oxygen supply during reperfusion, mitochondria of surviving cardiomyocytes recover the ability to synthesize ATP. Simultaneously, blood flow restoration allows for a rapid washout of accumulated catabolites that built up during ischemia at the interstitial space, including lactate and H^+. The quick reduction in extracellular proton concentrations induces a pH gradient between the intra and the extracellular spaces, stimulating the cardiomyocyte to rapidly restore the cytosolic pH through the activation of the NHE exchanger and the Na^+/HCO_3- cotransporter.

However, the activity of both transporters further increases the cytosolic Na^+ concentration, already enhanced during the preceding ischemia. Although excess Na^+ should be pumped out of the cell by the sarcolemmal Na^+/K^+ ATPase, it became structurally and functionally damaged by calpain activation occurring at the start of reperfusion [23]. As a consequence, Na^+ overload is increased during initial reperfusion. In order to reduce the Na^+ concentration, the NCX exchanger is then activated in its reverse mode but this, in turn, worsens the Ca^{2+} overload already started during ischemia [24].

In addition to these events, restoration of ATP synthesis at the onset of reperfusion leads to reactivation of SERCA, which would cause sequestration of Ca^{2+} into the SR. As a result, the SR storage capacity for this ion is rapidly saturated, surpassing the necessary threshold for opening of the ryanodine receptor Ca^{2+} channel (RyR), which would release Ca^{2+} again into the cytosol. Cyclic repetitions of this process of Ca^{2+} uptake and release by the SR results in marked cytosolic Ca^{2+} oscillations [25]. This situation is worsened by the key role of

mitochondria in Ca^{2+} homeostasis and the close interconnection of mitochondria and the SR through RyR [26].

Intracellular pH normalization has an additional important consequence. During ischemia, acidosis presents a protective role, as it inhibits the myofibrillar contractile machinery by modifying myofilament sensibility to Ca^{2+} [27]. However, the rapid recovery of cytosolic pH at the beginning of reperfusion removes this beneficial factor. Therefore, cytosolic Ca^{2+} cyclic oscillations, in the presence of ATP, and after normalization of intracellular pH during the initial moments of reperfusion triggers an excessive contractile activation of cardiomyocyte myofibrils leading to a disproportionate cardiomyocyte shortening termed hypercontracture [13].

Importantly, Ca^{2+} oscillations also affect membrane potential and generate concomitant transmembrane potential oscillations, which could originate early afterdepolarizations and induce the genesis of ventricular arrhythmias at the start of reperfusion [28].

1.1.2.1.2 Osmolarity and oedema

The rapid wash-out of the end-products of anaerobic metabolism that were accumulated in the extracellular space during ischemia, generates a transarcolemmal osmotic gradient between the intra and extracellular compartments. This, together with the increased cytosolic Na^{+} concentration present at the beginning of reperfusion, induces water uptake into the cytoplasm leading to intracellular oedema and enlargement of cell volume [14,22,29]. The consequent mechanical stress caused by cell swelling, will join with that caused by hypercontracture, leading to sarcolemmal rupture and cell death.

1.1.2.1.3 Cellular fragility and calpains

Calpains are a non-lysosomal family of cysteine proteases directly activated by Ca^{2+} that are fundamental in the generation of sarcolemmal fragility upon reoxygenation. Whereas calpain activity is inhibited by acidosis during ischemia, pH normalization and changes in intracellular Ca^{2+} homeostasis occurring in the early stages of reperfusion induce an excessive and dysregulated activation of this family of proteases [30]. Calpain substrates include an extensive list of proteins, many of which are components of the cytoskeleton and contractile cell

machinery. Its proteolysis at reperfusion plays a critical role in the induction of sarcolemmal and cytoskeleton fragility, contractile dysfunction and, consequently, cardiomyocyte death [31,32].

One of the most relevant calpain substrates is α-fodrin, a key component of the cytoskeleton that forms a complex with ankyrin. The α-fodrin-ankyrin complex interacts with several receptors and channels including the Na^+/K^+ ATPase, determining its correct function and position in the sarcolemma. Therefore, its degradation at the onset of reperfusion prevents a fast recovery of Na^+ concentrations, thus contributing to the loss of ionic homeostasis occurring at reperfusion [30,33]. Furthermore, several cytoskeletal-associated proteins are also cleaved by calpains, such as dystrophin, paxillin, tallin and vinculin, disrupting membrane-cytoskeleton connection and increasing cell permeability [31]. Cardiac troponin I and T, important components of the actin-tropomyosin complex, are also proteolyzed by calpains, leading to an impairment in the contractile apparatus during reperfusion [34,35].

1.1.2.1.4 Cell death propagation through gap junctions

The last factor in this scenario is propagation of hypercontracture and cell death through gap junctions. Gap junctions are aggregates of intercellular channels located in specialized areas of the cell membrane allowing electrical and chemical communication between adjacent cells [36]. These channels are formed by connexins, a family of transmembrane proteins, with connexin 43 (Cx43) being the predominant isoform in atrial and ventricular myocardium. The oligomerization of six connexin monomers around a central pore forms an hemichannel, that docks with another hemichannel in the cell membrane of an adjacent cell to create an intercellular channel connecting both cytoplasms [37].

In cardiomyocytes, gap junctions contain thousands of hemichannels clustered in plaques that are usually found within the intercalated disks, at cardiomyocyte poles. The main function of these channels in the myocardium is the correct propagation of electrical current across the heart allowing the existence of a coordinated cardiac contraction [38]. The importance of their role in electrical conduction is supported by the observation of an increased incidence of ventricular arrhythmias after ischemia-reperfusion in transgenic mice models of reduced Cx43 expression [39].

Besides from electrical coupling, gap junctions are also key players in chemical coupling. These intercellular channels are permeable to a diverse variety of ions and second messengers with molecular weights below 1500 Da, allowing propagation of reperfusion injury between connected cells. It is important to note that conditions present in ischemia such as acidosis, reduced ATP levels and increased Ca^{2+} concentrations induce gap junction closure [40], hence the quick recovery of energy levels and normal pH associated with reperfusion allows reopening of the channels [37,41]. For this reason, even if propagation of ionic changes can happen during the first minutes of ischemia [42], the main contribution of gap junctions to ischemia-reperfusion injury occurs at the onset of reperfusion. In fact, Na^{+} overload occurring early during reperfusion has been demonstrated to propagate to adjacent cells through opened gap junctional channels, with subsequent exchange by Ca^{2+} through the reverse activation of the NCX, thus spreading hypercontracture and cell death [43,44].

Classical studies in histological preparations proved that some kind of interaction between neighboring cells was needed in order to develop the pattern of connected hypercontracted cardiomyocytes that form contraction band necrosis [45]. This interaction was later demonstrated to be dependent on connexin-formed channels, as gap junction uncouplers administered at the onset of reperfusion reduced contraction band necrosis, prevented cell death progression, and reduced infarct size in several animal models [41,46]. Furthermore, deletion or substitution of Cx43 in transgenic mice was also associated with a marked reduction in infarct size [39,47,48].

1.1.2.2 Regulation of mitochondrial permeability transition pore opening

Several factors occurring at the onset of reperfusion, as pH normalization, together with Ca^{2+} overload and ROS production, favor the opening of the mPTP, a marked and non-selective increase in mitochondrial membrane permeability that compromises the homeostasis of the organelle. This phenomenon leads to the release of mitochondrial components into the cytosol, eliciting a cascade of events which lead to cardiomyocyte death. A complete explanation of the role of the mPTP in cardiomyocyte death will be exposed in subsequent sections.

1.2 ROLE OF MITOCHONDRIA IN MYOCARDIAL ISCHEMIA-REPERFUSION INJURY

Mitochondria are intracellular organelles essential for normal cellular function in eukaryote organisms. It is widely accepted that they have a bacterial evolutionary origin, through the incorporation of an α-proteobacterium into an ancestor of the modern eukaryotic cell [49]. While most of the mitochondrial proteins come from nuclear genes, some of them remain encoded by the circular mitochondrial genome [50].

Mitochondria are comprised of two physically and functionally separate compartments, the matrix and the intermembrane space. They are divided by the inner mitochondrial membrane (IMM), which presents an abundance of key proteins for mitochondrial function and a unique lipid composition, and separated from the cytosol by the highly permeable outer mitochondrial membrane (OMM). Numerous IMM invaginations that penetrate the matrix constitute the cristae, which greatly increase the area of the IMM and consequently contribute to enhance ATP production [51,52].

The cell type with the highest mitochondrial content are cardiomyocytes, where mitochondria represent more than 30% of total cell volume [53]. Depending on its location, mitochondria in adult cardiomyocytes are classified in three subpopulations. Interfibrillar (IF) mitochondria are tightly and longitudinally aligned with the most energy consuming sites, the myofibrilles, and also located in close proximity to t-tubules and SR, where Ca^{2+} release occurs. Its main function is to provide ATP for contractile function. On the other hand, subsarcolemmal (SSM) mitochondria are arranged in clusters just beneath the sarcolemma and could be involved in ion channel functions or signaling pathways, whereas perinuclear mitochondria, located around the nucleus, are probably involved in nuclear transcription [54,55].

1.2.1 MAIN FUNCTIONS OF MITOCHONDRIA

Usually known as the “powerhouse” of the cell, the central task of mitochondria is the production of most of the ATP required to perform the numerous cellular

physiological processes. Besides energy supply, however, mitochondria also constitute an important player in cellular Ca^{2+} storage, regulation of cellular metabolism, control of many intracellular signaling pathways and regulation of cell death. Therefore, mitochondrial function greatly impacts cell fate, and consequently, various pathological conditions such as cancer, neurodegenerative conditions, and cardiovascular diseases [56].

1.2.1.1 ATP production

The continuous cardiac pumping activity needed to provide a sustained nutrient supply to all body systems and tissues is maintained by an incessant and significant energy consumption. Thus, to maintain proper functioning, cardiomyocytes consume a lot of energy and strongly depend on the formation of ATP, 95% of which is provided by mitochondria as a result of oxidative phosphorylation (OXPHOS). The remaining 5% comes mostly from glycolysis and to a lesser extent from the Krebs cycle in the form of guanidine triphosphate (GTP). Consequently, it is not surprising that an impairment in energy production can easily lead to cardiac contractile dysfunction [57].

Mitochondria, as the main ATP source of the cell, host the final common catabolic pathways for oxidative metabolism, as it contains all the necessary enzymatic machinery to complete the oxidation of carbohydrates, free fatty acids (FFA) and proteins originated throughout the cell. In cardiomyocytes of a normal adult human heart, FFA β-oxidation is the predominant origin for mitochondrial ATP, representing from 70 to 90% of the total amount consumed. The remaining 10 to 30% is produced mainly by glycolysis and oxidation of lactate, as well as ketone bodies and amino acids [57,58] (*Figure 3*).

Myocardial FFA uptake into the cytoplasm is facilitated by transport proteins including fatty acid translocase (CD36) and plasma membrane fatty acid binding protein ($FABP_{pm}$). Once inside the cell, FFA can be stored as triglycerides, but most of them are esterified to fatty acyl-coenzyme A (CoA) by the fatty acyl-CoA synthetase (FACS) and converted to long chain acylcarnitine by the carnitine palmitoyl transferase (CPT) I located in the outer mitochondrial membrane. Long chain acylcarnitine are then transported inside the mitochondrial matrix and converted back to acyl-CoA by CPT II, where it undergoes β-oxidation generating acetyl-CoA and the reducing equivalents NADH (reduced nicotinamide adenine dinucleotide) and $FADH_2$ (reduced flavin adenine dinucleotide)[57,59,60] (*Figure 3*).

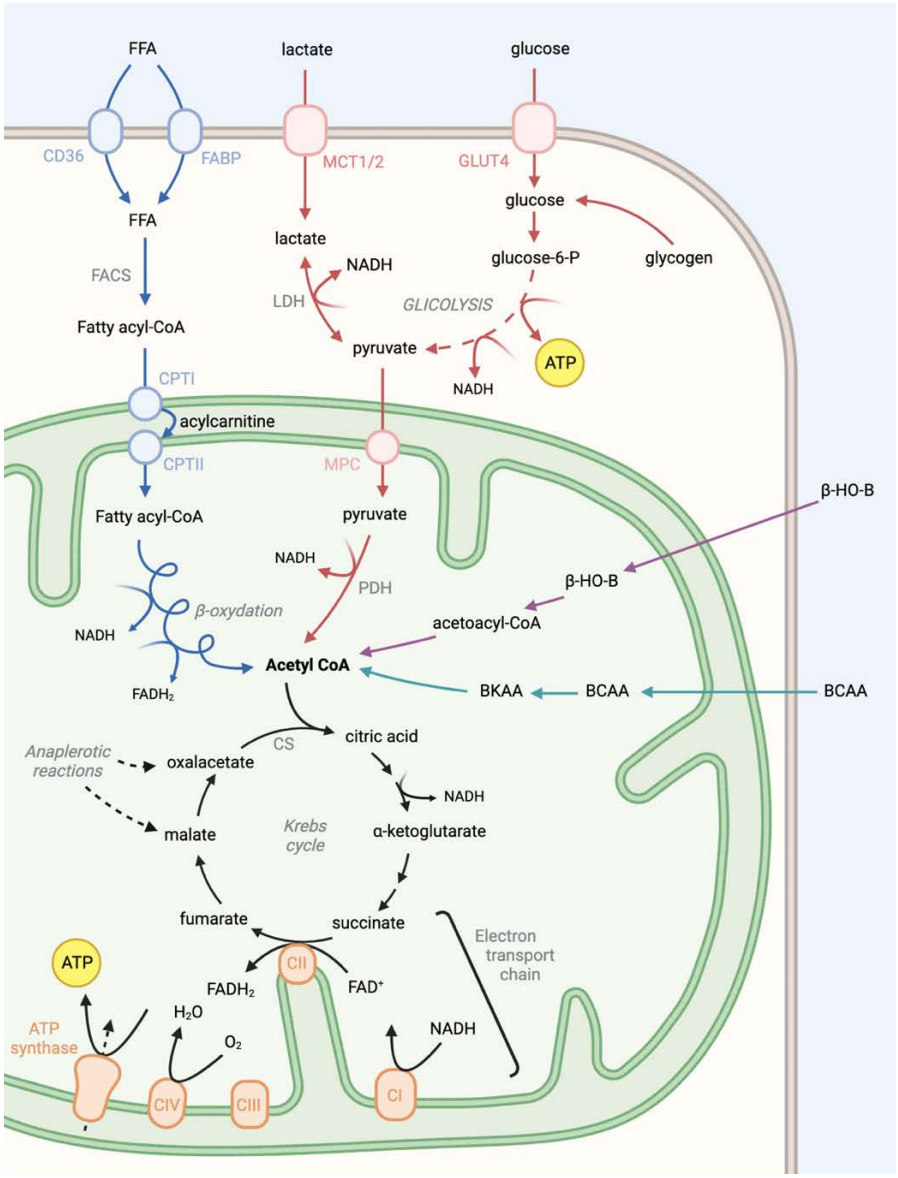

Figure 3: Schematic representation of classic catabolic pathways of cardiac metabolism. Substrates are transported into the cell and metabolized into intermediates. Metabolic intermediates are transported across the inner mitochondrial membrane by specific mechanisms, and once in the mitochondria, are oxidized to feed the Krebs cycle. There, reducing equivalents are generated and used to feed the ETC and synthetize ATP. BCAA: Branched-chain amino acids, BCKA: branched-chain keto acids, CD36: Fatty-acid translocase, CPT: carnitine palmitoyl transferase, CS: citrate synthase, FABP: Fatty acid binding protein, FACS: Faty acyl-CoA synthetase, GLUT4: Glucose transporter 4, LDH: Lactate dehydrogenase, MCT1: monocarboxylate transporter 1, MPC: mitochondrial pyruvate carrier, PDH: pyruvate dehydrogenase, β-HO-B: β-hydroxybutyrate. Based on [57,60,436]. Created with Biorender.

Glucose in cardiomyocytes is either derived from internal glycogen stores, which are moderately small but with a high turnover rate or comes directly from the blood. Glucose uptake is driven by the glucose gradient across the cardiomyocyte plasma membrane, and it is transported into the cytosol by glucose transporters (GLUTs) [61]. In adult healthy myocardium, the most predominant isoform is GLUT4 [62,63]. Free glucose inside cardiomyocytes is rapidly phosphorylated into glucose-6-phosphate to start glycolysis, leading to the production of 2 pyruvate, 2 ATP and 2 NADH molecules. In conditions of limited oxygen availability, such as ischemia or severe exercise, pyruvate can be converted to lactate by lactate dehydrogenase (LDH) in the anaerobic catabolism, where NAD^+ is regenerated from NADH to be reused again in glycolysis. Pyruvate can also undergo oxidation to acetyl-CoA to enter the mitochondria. Oxidation of pyruvate is catalyzed by pyruvate dehydrogenase (PDH), the activity of which is strongly regulated by its products acetyl-CoA and NADH [57] (*Figure 3*).

Ketone bodies gain importance as an energetic substrate in situations such as starvation. Ketone bodies enter the cell via monocarboxylate transporter I (SLC16A1) and migrate inside the mitochondria, where β-hydroxybutyrate, the major ketone body in the heart, is oxidized to acetoacetate. Ketone bodies oxidation ultimately ends with the synthesis of 2 molecules of acetyl-CoA [64]. Branched-chain amino acids (BCAA) are converted to the corresponded branched-chain ketoacids (BCKA) and eventually oxidized into acetyl-CoA [65] (*Figure 3*).

The common end-product into which the different catabolic pathways previously mentioned converge is acetyl-CoA which, inside the mitochondria, is incorporated into the citric acid cycle, also known as Krebs cycle or tricarboxylic-acid cycle. Citric acid cycle is a metabolic hub consisting of an eight reactions cycle that occurs in the mitochondrial matrix. It begins with the condensation of the two-carbon acetyl group of acetyl-CoA into the four-carbon molecule oxalacetate to generate citric acid, reaction synthetized by the enzyme citrate synthase (CS). Throughout the cycle, citric acid is progressively oxidized, and the energy released by this process is transferred into the reducing equivalents NADH and $FADH_2$, while the excess of carbon is carried away by the release of CO_2. The last reaction regenerates oxalacetate as the starting point for another round of the cycle. In particular, one molecule of acetyl-CoA incorporated into the cycle produces three NADH, one $FADH_2$, one guanidine triphosphate (GTP)

and two molecules of CO_2 [66] (*Figure 3*). On the other hand, citric acid cycle also provides precursors to different biosynthetic pathways. Its intermediates are removed from the cycle to fuel anabolic reactions, becoming the building blocks for macromolecule synthesis such as carbohydrates, lipids, proteins, and nucleotides. To maintain the citric acid cycle running, anaplerotic reactions replenish the intermediates lost in other reactions [67].

The energy released by the citric acid cycle, as well as by the different catabolic reactions described above, is carried by the reducing equivalents NADH and $FADH_2$ into the electron transport chain (ETC), a crucial and final step in the transformation of catabolic substrates into usable energy. The ETC consists of four intermembrane proteins located in the IMM where the electrons stored into NADH and $FADH_2$ are used to power the pumping of protons (at complexes I, III and IV) from the matrix to the intermembrane space generating a potential difference across the IMM. The energy generated by this gradient is then used by the ATP synthase to produce ATP, in a process coupled with proton re-introduction into the matrix. This process in which the energy stored in NADH and $FADH_2$ is used, in multiple steps, to synthetize ATP is known as oxidative phosphorylation (OXPHOS) [51,68]. The final electron acceptor is molecular oxygen (O_2), which is converted in complex IV into H_2O.

1.2.1.2 Ca^{2+} homeostasis

Intracellular Ca^{2+} mediates most of the rapid events that lead to changes in cellular function, energy metabolism and cell death, regulating excitation-contraction coupling, ion channel and transporter activity, gene transcription and signaling cascades. For this reason, Ca^{2+} homeostasis is strictly regulated, and mitochondria plays a crucial role in this process [51].

To be incorporated into the mitochondria, Ca^{2+} must cross both mitochondrial membranes. The OMM is permeable to all energy production related metabolites, including Ca^{2+}, due to the presence of the voltage dependent anion channel (VDAC) 1. However, IMM crossing constitute the limiting step to Ca^{2+} uptake and occurs via the mitochondria calcium uniporter (MCU), a Ca^{2+} selective channel that requires the electrochemical gradient generated by the ETC to facilitate Ca^{2+} accumulation into the mitochondrial matrix [69,70]. For this reason, Ca^{2+} entry into the mitochondria is driven by mitochondrial membrane potential and competes with proton import and ATP synthesis. This process is highly

regulated and is counterbalanced by the extrusion of this cation in exchange of Na^+ through the mitochondrial sodium-calcium exchanger (NCLX) [70–73].

Changes in cardiomyocyte cytosolic Ca^{2+} concentration are fundamental for myocardial excitation-contraction coupling. When action potential reaches the cardiomyocyte, cell membrane is depolarized facilitating a moderate Ca^{2+} influx from the extracellular space into the cytoplasm via the voltage gated L-type calcium channels. The increased Ca^{2+} intracellular concentration triggers the opening of the ryanodine receptor 2 (RyR2) located in the SR, the main reservoir of Ca^{2+} within the cell and a key player in Ca^{2+} homeostasis. The transient rise in cytosolic Ca^{2+} resulting from its release through the RyR2 is known as calcium-induced calcium-release [74]. Cytosolic Ca^{2+} binds to troponin C and, jointly with the interaction of myosin with ADP and inorganic phosphate produced by ATP hydrolysis, induces actin and myosin crossbridge formation and the start of cardiac contraction. Subsequently the elevated Ca^{2+} is mainly taken back into the SR by the SERCA pump, but also extruded from the cytoplasm to the extracellular space through the NCX. This process induces the start of the diastolic phase, in which ATP is consumed. The diastolic phase lasts until the next transient rise of Ca^{2+}, as myofibril contraction is only possible as long as Ca^{2+} is attached to troponin C [75,76].

The cytosolic Ca^{2+} oscillations occurring during contraction are transmitted into the mitochondria. Thus, the close communication between both organelles coordinates the balance between the changing energy demands of the cardiomyocyte and ATP production by OXPHOS. When physiological myocardial workload is increased, the amplitude and frequency of cytosolic Ca^{2+} transient rises, leading to more ATP consumption by the accelerated myofibrillar contraction-relaxation process. Cytosolic Ca^{2+} oscillations are transferred to mitochondria and proportionally enhance ATP production to allow metabolic adaptation to the additional energy requirements [74,77,78]. For instance, a moderate increase in mitochondrial Ca^{2+} directly activates several key rate-limiting enzymes of the citric acid cycle that include α-ketoglutarate and isocitrate dehydrogenases, leading to an increased conversion rate of NAD^+ to NADH, fueling the respiratory chain. Mitochondrial Ca^{2+} also directly regulates PDH activation via posttranslational mechanisms, playing a central role in coupling glycolysis with citric acid cycle activity. Furthermore, ATP synthase is also upregulated by mitochondrial Ca^{2+}. All these mechanisms highlight the

importance of mitochondrial Ca^{2+} homeostasis in matching energy supply and demands [78].

The rapid and efficient transduction of cytosolic Ca^{2+} signals into the mitochondrial matrix is attributable to the close location of mitochondria and Ca^{2+} releasing sites from the intracellular stores. Specific microdomains of high Ca^{2+} transfer are created in the contact locations between mitochondria and SR and are termed mitochondria-associated sarcoplasmic reticulum membranes (MAM) [79,80]. In cardiomyocytes, MAMs are enriched with RyR2, required for Ca^{2+} outflow from the SR, and VDAC and MCU, which take up Ca^{2+} into the mitochondria. This multiprotein complex is also formed by other units, as the glucose regulated protein 75 (GRP75), acting as a connector between RyR2 and VDAC [80].

1.2.2 MITOCHONDRIAL DYNAMICS

Mitochondria are highly dynamic organelles and its changes in morphology are determined by two strictly regulated and opposing processes, fusion and fission. Mitochondrial dynamics play a role in apoptosis, mitophagy and a variety of stress responses [80].

The molecular machinery that mediates mitochondrial fusion includes three GTPases of the dynamin family that work in concert to fuse, in a coordinated manner, the mitochondrial membranes of two neighboring mitochondria. Mitofusins (Mfn) 1 and 2 are required for OMM fusion, while forming oligomeric complexes [81], and Optic Atrophy 1 (Opa1) activity mediates fusion of the IMM. Opa1 also plays a role in the maintenance of the cristae structure [82].

Mitochondrial fission is mediated by the GTPase dynamin related protein 1 (Drp1) which, upon activation, assembles in multimeric helical structures that wrap around the OMM to facilitate the constriction of the mitochondria and eventually its scission [83]. Drp1 is strictly regulated by other GTPases and by posttranslational modifications, and the sites of Drp1 assembly to start mitochondrial fission colocalize with the contact points between SR and mitochondria [84].

Cells with dysfunctional mitochondria have developed a quality control mechanism, mediated by the fission machinery, which leads to degradation of aberrant mitochondria before further damage can occur. This process is termed mitophagy and consists in the selective scission of the damaged portion of the mitochondrion, which is then targeted to be recognized by autophagic machinery, leading to lysosomal degradation [85,86]. Consequently, an alteration in mitophagy is linked to an impaired stress response and ultimately to cell death.

Mitochondrial fusion, fission and mitophagy work together to maintain mitochondrial homeostasis, structure and distribution throughout the cell in response to cellular needs. Thus, maintaining a proper equilibrium in mitochondrial morphology is essential for an accurate regulation of metabolic function and ATP production. It also plays an important role homogenizing the mitochondrial population, as these processes allow content exchange, reduce the probability of mutational defects by protecting the integrity of the mitochondrial deoxyribonucleic acid (DNA), and ensures an equitable distribution of the mitochondria population among daughter cells [83,87].

1.2.3 INVOLVEMENT OF MITOCHONDRIA IN CELL DEATH

Apoptosis and necrosis, the two main forms of cell death, are highly regulated processes with complex mechanisms that have, in both cases, mitochondria as a central player [88].

Apoptosis, often referred as programmed cell death, results in a controlled death of the cell, where plasma membrane integrity is maintained until the apoptotic cell is phagocytized by macrophages. The start of apoptosis is dependent on the activation of caspases, a family of cysteine-aspartate proteases that proteolyze multiple cellular substrates and initiate a cascade of events that lead to DNA fragmentation, crosslinking and degradation of proteins, destruction of the cytoskeleton, formation of apoptotic bodies and, ultimately, cell death [89]. The apoptotic signal can be originated outside the cell and be detected through death receptors located at the plasma membrane, including the tumor necrosis factor (TNF) receptor superfamily, initiating what is known as the extrinsic pathway of apoptosis. On the other hand, when internal damage occurs, a variety of stimuli

activates intracellular sensors that induces the release of apoptotic factors from the mitochondria, which start the intrinsic pathway of apoptosis [88,89].

The intrinsic pathway of apoptosis is triggered either by negative signals such as the absence of cytokines or growth factors in the cellular environment, leading to the activation of pro-apoptotic molecules otherwise inhibited, or by positive stress factors including toxins, reactive oxygen species, viruses and DNA damage, directly activating the mediators of apoptosis [90]. In any case, the intrinsic apoptotic events are orchestrated by the B-cell lymphoma 2 (BCL-2) family of proteins, which can have pro-apoptotic effects, such as BAX, BAK, BID, PUMA, NOXA and BAD, or anti-apoptotic, like BCL-2 and its homologous. Activated BAX and BAK form homodimers and then oligomers that target mitochondria and lead to OMM permeabilization [91,92]. This is a critical point in the apoptotic pathway since it leads to irreversible damage in mitochondrial function and ATP production and causes the release of mitochondrial components into the cytosol. The released proteins, which in normal conditions perform their expected functions in the mitochondria, become toxic in the cytoplasmic environment, playing a pro-apoptotic role and triggering the end-stage apoptotic events. Cytochrome C is one of the released mitochondrial components that, once in the cytosol, binds to apoptosis protease activating factor 1 (APAF1) allowing a conformational change and subsequent oligomerization into the apoptosome [93,94]. Procaspase 9 is then recruited by the apoptosome and activated into caspase 9, which in turn activates the executioner caspases 3 and 7 inducing the final cascade of proteolysis that completes apoptosis [89,95]. Other pro-apoptotic factors released by mitochondria are high-temperature requirement protein A2 (HTRA2)/OMI [96] and second mitochondria-derived activator of caspase/direct inhibitor of apoptotic protein-binding protein with low pI (SMAC/DIABLO) [97,98], that contribute to the initiation of apoptosis by competing with the inhibitors of caspase 9 and allowing its activation. In this context, however, it is important to notice that experimental data indicate that the caspase-dependent signaling is repressed in adult cardiomyocytes [99] and does not play a significant role in cell death, at least during myocardial infarction [100].

Necrosis is usually the result of a metabolic cellular failure and is characterized by plasma membrane breakdown and cytoplasmatic content leakage that, unlike apoptosis, leads to the release of inflammatory mediators causing additional loss of homeostasis, breakdown of ion gradients, cell swelling, and structural

disorganization. It is usually caused by an external injury or sudden shock such as hypoxia, chemicals, or inflammation [88]. In mitochondrial-mediated necrosis, the triggering event is the opening of the mPTP in the IMM, resulting in the immediate collapse of mitochondrial membrane potential and the abrupt cessation of ATP production, since proton gradient is needed for ATP synthesis. Mitochondrial matrix swelling is another consequence of mPTP opening due to water import into the organelle in response to the osmotic gradient. Mitochondrial damage elicits the rest of the necrotic consequences and ultimately cell death [101]. Albeit the molecular identity of the mPTP is still unresolved, necrotic cell death mediated by mPTP opening has been demonstrated to be one of the main causes of cell death after myocardial ischemia-reperfusion [102], together with hypercontracture [103].

1.2.4 NORMAL FUNCTION OF THE MITOCHONDRIAL ELECTRON TRANSPORT CHAIN

The ETC, also known as the mitochondrial respiratory chain, is a crucial event in cell metabolism where chemical energy originated throughout a plethora of catabolic reactions is transformed into electrical power which fuels the synthesis of usable energy in the form of ATP. The underlying principle of this process is the chemiosmotic theory, first described by the British biochemist Peter Mitchell in 1961 [104]. Even if controversial initially, it was later confirmed, and he was awarded with the Novel Prize in 1978 for his innovative and transcendental discoveries.

As previously mentioned, the respiratory machinery comprises four multiprotein complexes embedded in the IMM which enable proton translocation from the matrix to the mitochondrial intermembrane space using the energy stored in the reducing equivalents NADH and $FADH_2$. The maintenance of the resulting electrochemical gradient or protonmotive force (Δp) (and its thermodynamically equivalent membrane potential ($\Delta\psi$) is supported by the proton impermeability of the IMM. Ultimately this gradient drives the return of hydrogen ions through the ATP synthase, which is coupled with the synthesis of ATP, the universal source of energy within the cells [105].

The components of the ETC are complex macromolecular structures formed by several subunits encoded both by the mitochondrial and the nuclear DNA. To function properly, they also need to be associated with different cofactors such as iron clusters and haem groups. The proton-pumping activity is only presented by three of the complexes and by three different mechanisms [105].

Complex I or NADH-ubiquinone oxidoreductase is the largest component of the ETC and the first entry point for electrons in the respiratory chain. It couples the oxidation of NADH to NAD^+ with the reduction of ubiquinone while pumping four protons across the IMM to the intermembrane space [106]. NADH oxidation occurs in the hydrophilic arm of the complex which protrudes into the matrix. The primary electron acceptor from NADH is the cofactor flavin mononucleotide (FMN), from which two electrons move along a pathway formed by iron-sulphur clusters (Fe-S clusters) of increasing redox potential. Electrons are then transferred from the last cluster, N2, to ubiquinone at the interface of the hydrophilic arm with the membrane domain. Ubiquinone reduction initiates a cascade of conformational changes that results in the transport of four protons from the matrix to the intermembrane space [107,108] (*Figure 4*).

Respiratory complex II, also known as succinate dehydrogenase (SDH), is a crucial player in cellular metabolism, given its position as a direct component of both the citric acid cycle and the ETC. It is the only complex of the chain whose activity does not result in proton pumping across the IMM. Complex II couples the oxidation of succinate to fumarate in the citric acid cycle with the reduction of ubiquinone to ubiquinol [109]. Succinate is oxidized by the covalently bound FAD^+ cofactor in the hydrophilic domain of the complex and the electrons are passed down, similarly to complex I, through a series of three Fe-S clusters responsible of electron transfer to ubiquinone [106,110] (*Figure 4*).

Both complex I and complex II donate electrons and reduce ubiquinone, a lipid soluble redox carrier which transfer the electrons to complex III. Also known as Coenzyme Q (CoQ), it can exist in three different redox states: fully oxidized (ubiquinone or CoQ), partially reduced (semiubiquinone or $CoQ^{\cdot-}$) and fully reduced (ubiquinol or $CoQH_2$). The reversible redox cycling capacity of CoQ between these three states is the basis of its function as an electron carrier. Its lipophilic structure is also important, as it allows its free movements throughout the IMM, from complex I and II to complex III [111,112] (*Figure 4*).

Complex III, or CoQ-cytochrome C reductase, couples the oxidation of $CoQH_2$ with the reduction of cytochrome C, together with the release of protons to the intermembrane space [113,114]. However, the mechanisms involved in complex III function are much more complicated than the overall reaction might imply, which helps to increase the efficiency of energy transfer from electron transport to proton translocation. This complex has a homodimeric structure, with three catalytic subunits per monomer: cytochrome b, which harbors two distinct quinone-binding haem groups b_L and b_H, cytochrome c_1, and the Rieske Fe-S protein. $CoQH_2$ oxidation occurs in the b_L quinone binding site, where the first electron follows a high potential pathway running through the Fe-S cluster in the Rieske center to cytochrome c_1, which subsequently transfers the electron to the soluble carrier cytochrome C to leave complex III. The resulting highly reactive semiubiquinone radical is then fully oxidized and its remaining electron is accepted by the low potential heme b_H, located in the opposite side of the complex. From there, this second electron is passed down to an oxidized ubiquinone to generate $CoQ^{\cdot -}$. At this point, the oxidation process is repeated with a second $CoQH_2$ molecule and, at the end of the process the partially reduced ubiquinone attached to b_H is fully reduced to $CoQH_2$, completing the cycle. To sum up, four protons are released to the intermembrane space through the reduction of two molecules of $CoQH_2$ at the b_L site, and two protons are taken from the matrix to complete the reduction of a CoQ at the b_H haem. The net product of a complete cycle is the oxidation of one $CoQH_2$, the reduction of two cytochrome c and the transference of four protons to the intermembrane space [115] (*Figure 4*).

The ultimate destination of electrons passed along the ETC is to take part in the reduction of molecular oxygen (O_2) into water (H_2O) in complex IV, also known as cytochrome C oxidase. The electrons delivered by the reduced cytochrome C, the mobile electron carrier linking complex III to complex IV, are accepted by the latter to catalyze O_2 reduction, while pumping protons to the intermembrane space [105]. Complex IV has a dimeric structure, each monomer composed by 14 subunits, even though only three of them comprise its functional core. Mechanistically, in each catalytical cycle four electrons are donated, one by one, by four cytochrome c molecules to the primary electron acceptor of complex IV, the copper center Cu_A. Electrons are passed down to haems *a* and a_3 to finally be transferred by the copper center Cu_B to a molecule of O_2 in the catalytical site, also known as the binuclear center. Simultaneously, two protons are taken from

the matrix to reduce O_2 into one water molecule, whereas two additional protons are pumped across the membrane. This process of oxygen consumption is known as mitochondrial respiration [116] (*Figure 4*).

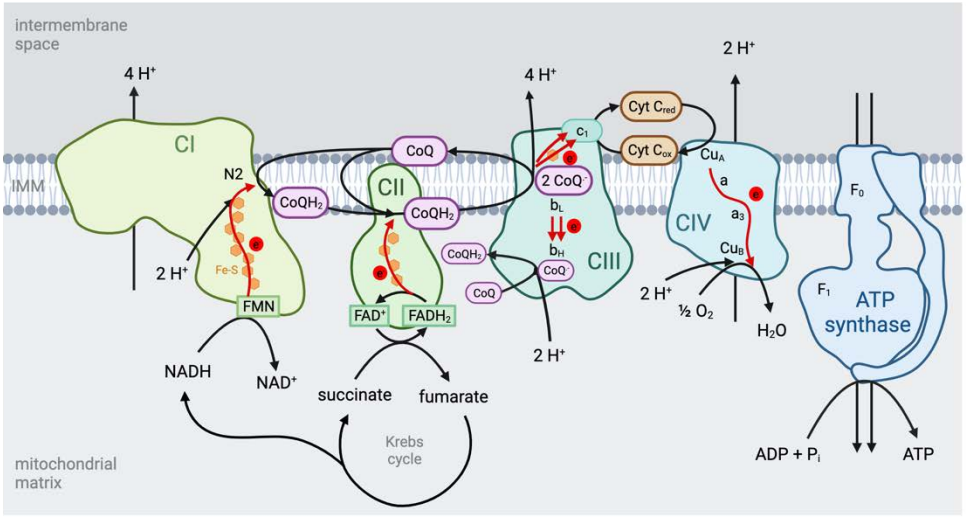

Figure 4: Overview of the ETC and ATP synthesis. Red arrows represent electron transference through the respiratory complexes. Electrons originated from the reducing equivalents NADH and $FADH_2$ are taken by complex I (CI) and II (CII), respectively, and transferred to Coenzyme Q (CoQ). Reduced CoQ ($CoQH_2$), then, donates the electrons to complex III (CIII), and subsequently to complex IV (CIV) via cytochrome C (Cyt C). In complex IV, electrons are used to reduce oxygen into water. This process is coupled with proton translocation to the intermembrane space by complex I, III and IV, generating the protomotive force to pump them back to the matrix through the ATP synthase, process that is coupled with ATP synthesis. Based on [112,437,438]. Created with Biorender.

All the potential energy built up by the ETC and stored as mitochondrial electrochemical gradient is then used by the ATP synthase. Also considered as the fifth complex of the ETC, or Complex V, it couples the return of those protons that were accumulating in the intermembrane space into the mitochondrial matrix with the synthesis of ATP in the final step of the OXPHOS process [106]. ATP synthase is a multi-subunit complex comprised of two main functional components, a lipophilic F_O domain embedded in the IMM, which contains the rotatory c-ring responsible for proton translocation, and the hydrophilic F_1 domain which projects towards the matrix and comprises the catalytic head responsible for ADP phosphorylation. Both domains are kept together by the central stalk. Under a normal membrane potential, the protonmotive force

powers the rotation of the c-ring through which protons are released into the matrix. C-ring rotatory energy is then transmitted to the F_1 domain, inducing a series of conformational changes which allow ATP synthesis [117–119]. In fact, ATP synthase is usually found in an oligomeric state, as dimers, which have been shown to be required for cristae structure formation [120,121]. Moreover, Complex V can function in the reverse direction as an ATPase, in situations such as ischemia [17] (*Figure 4*).

The organization of the respiratory complexes in the IMM has been extensively debated over the years and it is currently known that, in addition to its free existence, they gather into large supramolecular structures named supercomplexes. This structural and functional association increase the efficiency of electron transport, reduce electron leak and production of ROS, and stabilize the structure of the individual complexes. Special interest has been focused in the respirasome, which contains all those complexes required for electron transfer completion (Complexes I, III and IV), being the most abundant supercomplex [122–124]. Assembly and structural integrity of supercomplexes has been proved to be dependent, among other factors, on the phospholipid cardiolipin, present at the IMM [125]. Its oxidation during reperfusion induces complex IV dissociation from the respirosome, contributing to energetic disfunction and ROS generation [126].

1.2.5 EFFECTS OF ISCHEMIA ON MITOCHONDRIAL FUNCTION

As key regulators of cellular homeostasis, mitochondria are severely affected by the biochemical and metabolic perturbations brought by ischemia [127]. During the first minutes of oxygen deprivation, the ETC is halted and, therefore, mitochondrial membrane potential and proton gradient are lost. This situation leads to a switch from a metabolism based in OXPHOS to one based in anaerobic glycolysis. However, substrates are quickly exhausted which generates a state of bioenergetic insufficiency. It also induces an increase in lactate, the by-product of glucose anaerobic oxidation, hence acidifying intracellular pH. Furthermore, due to the close interconnection with the sarcoplasmic reticulum in the MAMs, Ca^{2+} overload is transferred into mitochondria [128].

With reperfusion, ATP and mitochondrial membrane potential are restored and mitochondrial Ca^{2+} overload is accentuated via the MCU, constituting one of the hallmarks of ischemia-reperfusion injury [128]. Moreover, the sudden restart of the ETC causes an excessive ROS production with numerous deleterious effects. As a result, mitochondrial fission is excessively increased [129] because, on the one hand, cytosolic Ca^{2+} activates calcineurin, which dephosphorylates and activates Drp1 [128], and, on the other hand, both Ca^{2+} overload and the increase in ROS induce Drp1 translocation to the outer mitochondrial membrane [130,131]. The acceleration of mitochondrial fragmentation, then, leads to an increased autophagy and cell death [128].

Simultaneously, Ca^{2+} accumulation and increased ROS production, together with pH normalization, favor the opening of the mPTP at the onset of reperfusion. In fact, the acidic pH that was present during the ischemic phase maintained the mPTP closed. However, this protection is lost when the physiological pH is restored during reperfusion [15,132]. The mPTP opening leads to the dissipation of mitochondrial membrane potential and ion gradients across the IMM and elicits the release of mitochondrial proteins and DNA into the cytosol. This phenomenon initiates a cascade of events such as mitochondrial swelling, induction of mitophagy, activation of the innate immune response, and activation of proteases, which lead to cardiomyocyte death and acute tissue failure [133].

1.2.6 OPENING OF THE mPTP

1.2.6.1 mPTP: Definition

The term permeability transition was first introduced in the late 1970s by Hunter and Haworth describing an unselective permeability increase of the IMM which occurs in the presence of Ca^{2+} [134–137]. It was later discovered that this increase in permeability is, in fact, due to the regulated opening of a non-specific channel located at the IMM, highly permeable to solutes with a molecular weight up to 15 kDa, which became known as the mitochondrial permeability transition pore (mPTP) [138,139]. Opening of the mPTP allows a variety of solutes and ions to be redistributed between the mitochondrial matrix and the cytosol, leading to an abrupt loss of mitochondrial metabolites and factors, including Ca^{2+}, cytochrome

C and other proapoptotic factors. It also elicits mitochondrial swelling, causing eventual rupture of the OMM, dissipation of mitochondrial membrane potential, loss of pH gradient, uncoupling of OXPHOS, halt of ATP synthesis, and irreversible mitochondrial homeostasis perturbations that can result in cell death [140].

1.2.6.2 Molecular identity of the mPTP

The molecular identity of the mPTP has been extensively investigated over the past 40 years but still has not been completely elucidated. However, several theories have been proposed in an attempt to shed light on the subject [139,141,142].

The earliest model for mPTP channel formation consisted in a multiprotein complex that included, as its core component, the adenine nucleotide translocase (ANT), the mitochondrial ADP/ATP carrier located at the IMM. Together with ANT, the complex was proposed to be formed by cyclophilin D (CypD) located at the mitochondrial matrix, the VDAC channel at the OMM, as well as a plethora of interacting, stabilizing and regulatory subunits, such as the translocator protein (TSPO), the inorganic phosphate carrier (PiC), the hexokinase II (HKII), and the mitochondrial creatine kinase (mCK) [143]. Although this model was supported by several studies that proved the sensitivity of the mPTP to ligands and inhibitors of these proteins and by data showing the copurification of several of its components [141], it was later questioned by genetic studies. Development of genetic deletion models of each of the putative components (ANT [144], VDAC [145] and TSPO [146]) demonstrated that none of them were essential for mPTP formation, downgrading its involvement in the complex from a structural role to a complex regulator.

Nevertheless, CypD has remained uncontested as an important part of the mPTP. Early studies demonstrated that the mPTP is extremely sensitive to the immunosuppressant cyclosporin A (CsA), a strong inhibitor of CypD [147–149]. In this case, transgenic mice studies [150,151] confirmed its importance in mPTP regulation and this discovery was instrumental in stablishing the pathogenic role of mPTP in ischemia-reperfusion injury [152,153].

While the initial structural model for mPTP has been now discarded, new candidates have emerged. Among these candidates, the ATP synthase quickly stood out and it has been the main focus of study in the past decade [133,154]. Two

currents of thought emerged around its possible involvement. The first one postulated that dimerization of ATP synthase is essential for pore formation. In this model, Ca^{2+}-induced activation would lead to the formation of a channel displaying mPTP properties, at the interface between the two ATP synthase monomers [155]. The second hypothesis proposed that the c-subunit of the ATP synthase monomer alone could form the mPTP channel. This last theory is known as the death finger hypothesis [156,157].

On the other hand, recent studies in which ablation of individual subunits of the ATP synthase was performed revealed that a pore with reduced conductance was still present, which could be inhibited by CsA or compounds targeting ANT, such as bongkrekic acid [158,159].

Therefore, the current emerging model is the product of the combination of previous theories and proposes the existence of 2 distinct pores, both of them being Ca^{2+} sensitive channels and modulated by CypD [160]. A low conductance pore, which could have a role in physiological responses, is likely to be formed by ANT. On the other hand, the channel with higher conductance is attributed to a pore originated within the ATP synthase, being induced by stressful situations like ischemia-reperfusion injury. In this case, the most recent hypothesis proposes that, upon Ca^{2+} activation, significant spatial rearrangements at the mPTP structure may occur. This would increase overall rigidity, a response in which the OSCP subunit of the ATP synthase is involved, in a process favored by CypD. The c-ring core would be affected by the conformational changes allowing the formation of the pore [133,160,161].

1.2.6.3 Regulation of mPTP opening

Opening of the mPTP is a highly regulated process, with elevated Ca^{2+} being the most well-known trigger for mPTP opening. However, the threshold of Ca^{2+} concentration required to elicit the event is highly dependent on the prevailing conditions within the cell and the concentrations of several endogenous modulators [162]. Other activators of mPTP include increased ROS and inorganic phosphate, as well as a low mitochondrial membrane potential. On the other hand, intracellular acidosis inhibits mPTP opening, together with elevated concentrations of ADP, ATP and AMP [133,139].

Interestingly, the conditions occurring during ischemia-reperfusion mimic those that are favorable for mPTP opening. During ischemia, Ca^{2+} concentration is increased due to the activity of the NCX in its reverse mode, and the impaired ATP synthesis leads to an increase in inorganic phosphate. However, despite the presence of these sensitizing conditions, acidic pH, originated from lactic acid accumulation as a by-product of anaerobic glucose oxidation, maintains the mPTP closed [134,141].

The situation changes dramatically upon reperfusion. Metabolite washout during blood flow restoration allows intracellular pH recovery [132]. In addition, ATP synthesis is restored, Ca^{2+} overload is increased, and reperfusion brings an extensive ROS production originating from several sources, including the ETC. These conditions are, as previously described, optimal for mPTP opening [138,147,163], event known to occur during myocardial ischemia-reperfusion injury from early studies [132].

Opening of the mPTP and development of hypercontracture during myocardial reperfusion are closely intertwined phenomena and are the main causes of cell death during ischemia-reperfusion injury. Both processes are inhibited during ischemia and are triggered by physiological pH recovery and increased Ca^{2+} at the onset of reperfusion. The additional release of Ca^{2+} from mitochondria brought by mPTP opening leads to a further increase in cytosolic Ca^{2+} oscillations, aggravating hypercontracture development. In fact, ischemia duration seems to play a critical role in establishing the contribution of mPTP opening in myocardial cell death during reperfusion. It has been described that whereas mPTP plays a key role in cell death after long ischemic periods, shorter episodes of oxygen deprivation would cause cell death mostly through hypercontracture [13,164].

1.3 MITOCHONDRIAL ROS PRODUCTION: ROLE OF REVERSE ELECTRON TRANSFER

ROS generation underlie many pathological processes in a wide range of conditions such as cancer, and neurological, psychiatric, and cardiovascular diseases [165]. However, and despite their detrimental consequences in some circumstances, low and controlled concentrations of reactive oxygen species are also known to be involved in several vital physiological processes as intracellular signaling molecules, playing an important role in cellular proliferation and differentiation, gene expression, control of inflammatory responses and cellular migration [166–168]. In a cardiac context, low levels of ROS have been shown to be involved in some cardioprotective mechanisms like that of cardiac preconditioning [169–171].

The critical involvement of ROS in ischemia-reperfusion injury has been widely demonstrated. ROS are massively released during the first minutes of reperfusion and act as a key mediator of injury [18,170]. They are highly reactive species derived from molecular oxygen and the most abundant and physiologically relevant are oxygen peroxide (H_2O_2), superoxide anion ($O_2^{-\cdot}$), and hydroxyl radical (OH^-) [172].

Oxidative stress is, in fact, the consequence of a disbalance between ROS generation and an insufficient antioxidant detoxification system. The subsequent accumulation of these reactive oxygen species elicits a plethora of deleterious events in cellular structure and function [172–174]. DNA can suffer oxidative damage leading to DNA breaks, degradation of bases, mutations, and crosslinking with proteins, and also the formation of 8-hydroxyguanosine, which can alter transcriptional factors and modify gene expression [175]. On the other hand, proteins are also affected by ROS, causing fragmentation of peptide chains, alterations in its electrical charge, and oxidation of specific amino acids, like cysteine and methionine, leading to conformational changes and an increased susceptibility to protein degradation [176]. ROS also induces disruption of lipidic bilayers by lipid peroxidation, whose products may lead to inactivation of proteins by crosslinking [177,178]. Cytokine activation and inflammation are also induced by ROS [173]. However, one of the most harmful consequences of ROS

production is opening of the mPTP, especially relevant during ischemia-reperfusion injury. As previously mentioned, together with Ca^{2+} overload and pH restoration, ROS production at the onset of reperfusion lead to mPTP opening which, added to hypercontracture, induce cardiomyocyte death [173].

In ischemia-reperfusion injury, ROS can be produced by several processes and in different locations within the cell [179]. Mitochondria are, with no doubt, the major intracardiac sources of ROS in the reperfused myocardium. However, before diving into the mechanisms of ROS generation by mitochondria, it is necessary to address the contribution of these other cardiac sources.

1.3.1 NON-MITOCHONDRIAL SOURCES OF ROS IN THE MYOCARDIUM

Several are the ROS sources that have been associated with the increased oxidative stress occurring during myocardial infarction. Whereas non-enzymatic sources of ROS include hemoglobin and myoglobin, released into the extracellular environment after trauma, enzymatic sources may include lipoxygenases, and cyclooxygenases. Nevertheless, most non-mitochondrial ROS sources comprise enzymes like xanthine oxidase, NADPH oxidase and nitric oxide synthase [126,180,181].

1.3.1.1 Xanthine oxidoreductases

Xanthine oxidoreductases (XOR) catabolize the hydroxylation of hypoxanthine to uric acid, the rate-limiting reaction within purine catabolism. These enzymes exist in two interconvertible forms, xanthine oxidase (XO) and xanthine dehydrogenase (XDH), the latter being the predominant form under physiological conditions. The electron acceptor of XDH is NAD^+ whereas XO utilizes O_2, thereby presenting susceptibility to produce ROS [126,182]. During ischemia, ATP exhaustion causes accumulation of hypoxanthine. Upon blood flow and O_2 restoration, hypoxanthine is metabolized to xanthine, while consuming O_2 and producing uric acid and superoxide as waste products. Superoxide is later converted to H_2O_2, OH^- and peroxynitrite ($ONOO^-$, a free radical formed by the reaction of oxygen with nitric oxide (NO)) [183,184] (*Figure 5*).

These reactive species, then, promote the activation of cytokine cascades and recruitment of leukocytes causing inflammation.

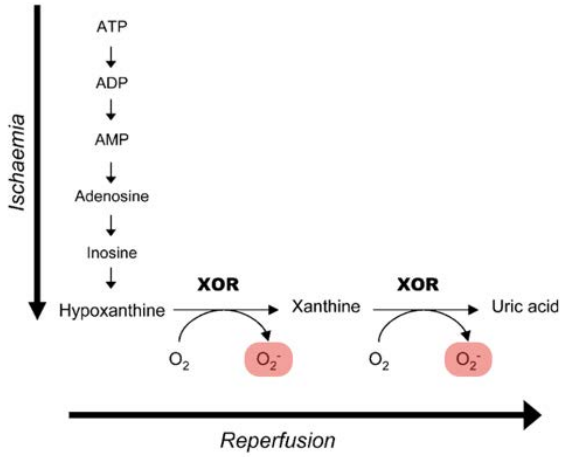

Figure 5: Mechanism of ROS production by XO during ischemia-reperfusion injury. Modified from [182].

Several inhibitors have been used to assess the role of XOR in ischemia-reperfusion, like allopurinol and oxypurinol, even though contradictory results have been reported [185–189]. Despite the scarce and conflicting results obtained in animal models, several clinical trials were designed to assess the efficacy of XOR inhibitors in ischemia reperfusion [182], with results being, according to a recent metanalysis, again not convincing [190]. One of the reasons for the described discrepancies could be the use, in some of those studies, of high doses of allopurinol, which may induce undesired effects [191].

1.3.1.2 NADPH oxidases

The NADPH oxidases (NOX) are major enzymatic sources of ROS and important redox regulators. To date, 7 members of this family of transmembrane multiprotein complexes have been identified, NOX1 to NOX5 and the dual oxidases, DUOX1 and 2. All these isoforms are differentially expressed between tissues, with NOX1, 2 and 4 expressed in the myocardium, whereas other isoforms are also present in other cardiac cell types, including endothelial, smooth muscle cells, fibroblasts and leucocytes [180,192]. Their main function is to produce ROS, while transferring electrons from NADPH to O_2 and synthetizing

superoxide. Actually, NOX1, 3 and 5 generate superoxide, but DUOX enzymes, along with NOX4, seem to predominantly produce hydrogen peroxide [192].

NOX enzymes have been proposed to be involved in ROS production during ischemia-reperfusion, as they are overexpressed and have a higher activity during this period [193–195]. The involvement of NOX in ischemia-reperfusion injury was demonstrated by the fact that inhibitors, such as apocynin and diphenylene iodonium, were able to reduce cell death after simulated ischemia-reperfusion injury in H9c2 cells [196–198]. However, these results should be interpreted with caution given the lack of specificity of these inhibitors and its intrinsic antioxidant properties. Despite this, studies in NOX-isoform specific knock-out models have shown that NOX2 and NOX4 deletion led to a reduction in ROS production, effect associated with lower myocardial infarct size [195,199–201]. This effect has been proposed to be organ and cell specific, given that the deletion of the different isoforms is protective depending on the cell type [202].

1.3.1.3 Nitric oxide synthases

The nitric oxide synthase (NOS) family of enzymes generate nitric oxide (NO) via the conversion of L-arginine to L-citrulline. It is comprised by four isoforms, neuronal NOS (nNOS), endothelial NOS (eNOS) and inducible NOS (iNOS), plus mitochondrial NOS, all of them being differentially expressed between cell types and subcellular locations and activated under different circumstances. Both eNOS and iNOS are located in cardiomyocytes [203,204]. Structurally, all isoforms are formed by an oxygenase domain, which contains a heme group and tetrahydrobiopterin (BH_4), and binds L-arginine, and a reductase domain which contains the flavin FAD and FMN, and binds NADPH. Electrons are donated by NADPH which, in a reaction mediated by the BH_4 cofactor, are transferred to the heme group, where O_2 binds and allows L-arginine oxidation and NO synthesis [203] (*Figure 6*). NO has anti-inflammatory and antioxidant properties and appears to be protective against ischemia-reperfusion injury [205–207]. However, enzymatic activity of NOS is highly controlled by the presence of its cofactors and substrates, whose concentration can be altered during ischemia, leading to NOS uncoupling and release of O_2 from the heme group as superoxide.

BH_4 concentration is a crucial limiting factor for NO production. During ischemia-reperfusion, oxidative stress induces BH_4 oxidation, reducing its levels and

dysregulating the BH_4/NOS ratio. This leads to NOS uncoupling and ROS production in a positive feedback loop [204]. The impact of BH_4 concentration in ROS production by NOS uncoupling has been assessed in *in vitro* and *in vivo* models of ischemia-reperfusion [208,209]. In addition, supplementation with BH_4 has been shown to exert protective effects against ischemia-reperfusion injury, ameliorating inflammation and tissue damage [180,208,210,211]. Furthermore, O_2^- can react with NO producing $ONOO^-$, the main source of nitrooxidative damage, which causes detrimental effects on mitochondrial respiration [212].

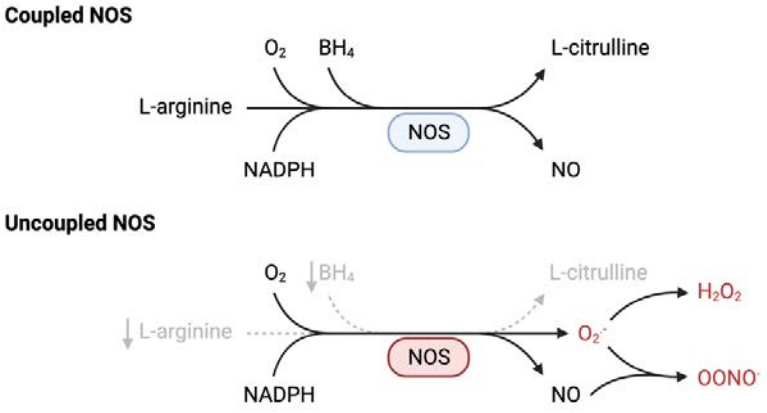

Figure 6: Reaction of coupled nitric oxide synthase (NOS), occurring under physiological conditions, and of uncoupled NOS, during ischemia-reperfusion, the last producing reactive oxygen species (ROS). Adapted from [439].

1.3.2 MITOCHONDRIAL SOURCES OF ROS

Mitochondria have been postulated to be the major myocardial source of ROS during reperfusion, something that has been confirmed in a wide range of tissues [213]. More than eleven ROS-producing sites have been identified within mitochondria, mainly linked to substrate catabolism, the ETC and OXPHOS [214]. Although most of these sites release superoxide and hydrogen peroxide into the mitochondrial matrix, some of them also deliver ROS into the intermembrane space [214]. For example, monoamine oxidases, located in the inner mitochondrial membrane, catalyze the oxidative deamination of neurotransmitters and other biological amines generating H_2O_2 as a byproduct of this reaction [215,216]. Pharmacological inhibition of monoamine oxidases has been shown to

ameliorate ischemia-reperfusion injury [217–219]. In addition, PDH and α-ketoglutarate dehydrogenase, structurally similar and dependent on NADPH/NADPH$^+$ ratio, are capable of producing ROS under some conditions [220]. Other enzymes of the Krebs cycle, particularly aconitase, have been used as oxidative stress markers and have been also proposed to be a source of ROS [221].

However, it is generally admitted that the most important source of ROS within the mitochondria is the ETC. Even in physiological conditions, during the course of normal OXPHOS, the movement of electrons through the different ETC complexes can result in some electron leakage, leading to an incomplete reduction of molecular O_2 to superoxide [214,221]. As mentioned above, organization of the ETC components into supercomplexes provides structural and functional links between them, increasing the efficiency of electron transfer and consequently reducing electron leak [122,222–225]. In this regard, oxidative damage of cardiolipin triggered by ischemia-reperfusion can destabilize supercomplex structural integrity and lead to disassociation of its components, which would increase the probability of ROS generation and subsequent amplification [122,222].

Overall, superoxide generation is favored when the protonmotive force across the IMM is increased or when, for various reasons, the rate of oxygen reduction to water is unable to match the transference of electrons through the ETC [226]. Studies in isolated mitochondria with specific inhibitors and substrates of individual complexes have been used to determine the sites of ROS production in the ETC [227]. Although all complexes have the potential for ROS production, based on these approaches complex I and complex III are believed to be the main sites for ROS production, at least during myocardial reperfusion [221,224,228,229].

Two sites of complex I are widely recognized to be responsible for superoxide generation. The interaction site between the FMN cofactor and NADH, the I_F site, has been suggested to be the first superoxide source within complex I, as a by-product of the reaction of reduced FMN with oxygen. In addition, ROS can also be produced at the site of CoQ reduction in complex I (I_Q site), where semiubiquinone can transfer electrons to oxygen. Both sites release superoxide into the matrix side of the IMM [228,230].

ROS production by forward transfer of electrons in complex I is low under physiological conditions [228,231]. This mechanism of ROS production is exacerbated

by a high NADH/NAD^+ ratio, which provides additional electrons to complex I, and especially when it is accompanied by a high degree of reduction of the carriers located downstream the ETC and/or increased mitochondrial membrane potential [226,228,230]. The addition of the CoQ-binding site inhibitor rotenone also increases superoxide production due to the accumulation of electrons at the FMN site, where superoxide will be generated [232].

In addition to this more conventional mechanism of ROS production by forward transfer of electrons, complex I can also operate in the reverse mode. This mechanism occurs when electrons entering the ETC from succinate oxidation are faced with a highly reduced CoQ pool and a high protonmotive force. Under this situation, electrons are forced back to complex I instead of advancing in the forward direction to complex III, in a process known as reverse electron transfer (RET). Once they have reached complex I, electrons would lead to reduction of NAD^+ to NADH and ROS production [228,230]. Under these conditions, complex I produces the largest amounts of ROS, which play a key role in both physiological and pathological situations, including during myocardial infarction [224]. In this case, rotenone addition prevents the access of electrons into complex I at the CoQ binding site and abolishes ROS production [233].

Even though some studies have postulated that complex II could also generate ROS on his own [234,235], the current consensus stablishes that the main role of this complex in ROS production is providing electrons for RET. In contrast, different studies have demonstrated that complex III is also an important source of ROS [236]. In this regard, inhibition of the Q_i site of complex III with antimycin together with the presence of a reduced CoQ pool blocks electron flow at the complex. Consequently, the reaction of O_2 with the unstable semiubiquinone bound to the Q_o site leads to ROS release to both sides of the IMM. ROS production by complex III might not be very relevant under physiological conditions, although it has been suggested that it may be involved in the cardioprotective effect of some maneuvers, such as ischemic preconditioning [171,237]. Moreover, the contribution of complex III to the detrimental burst of ROS occurring early during reperfusion is thought to be limited and lower than that of complex I [238–241].

It has to be taken into account that post-translational modifications may regulate ROS production by the different complexes forming the ETC. For instance, hyperphosphorylation of complex IV by protein kinase A (PKA) and protein kinase

C (PKC), occurring during ischemia, can compromise complex IV activity and lead to production of ROS [126,221,242].

1.3.3 CELLULAR RESPONSE TO ROS PRODUCTION

Myocardial cells are equipped with an endogenous antioxidant system responsible for the control of ROS levels and elimination of its excess when necessary. ROS scavengers neutralize the effect of ROS by reducing its reactivity with other molecules through the oxidation of the antioxidant compound itself. For this reason, oxidative stress is not solely determined by intracellular ROS production, but rather by the equilibrium between ROS generation and scavenging [167].

The antioxidant system is mainly located within the mitochondria and in the cytoplasm and includes several detoxifying enzymes implicated in the direct degradation of oxidant radicals [243]. Superoxide dismutase (SOD) catalyzes the conversion of superoxide into H_2O_2 which, in turn, can be reduced to water by catalase. This last reaction is also performed by glutathione peroxidase (GPx) via glutathione (GSH) oxidation into glutathione disulphide (GSSG) and by the peroxiredoxin (Prx) and thioredoxin (Trx) system [166,244]. Both of these thiol-based scavenging systems are dependent on a reducing environment maintained by a high $NADPH/NADP^+$ ratio. Alternatively, superoxide can react with NO to produce $ONOO^-$, whereas hydrogen peroxide can lead to the synthesis of OH^- through the Fenton reaction (*Figure 7*)[167,172].

The correct function of these detoxifying enzymes contributes to the low and regulated cellular levels of ROS found in physiological conditions. As previously mentioned, controlled concentrations of ROS mediate several important physiological processes [166–168]. However, the amount of ROS production can overwhelm the cellular antioxidant system leading to an enhanced oxidative stress, and this situation is precisely what happens during myocardial ischemia-reperfusion injury. On the one hand, the $NADPH/NADP^+$ ratio required for the maintenance of some of the scavenging machinery is lost during ischemia. On the other hand, during ischemia some of the antioxidant enzymes are released into the extracellular fluid, and then washed out upon blood flow restoration. As

a consequence, the remaining and damaged antioxidant system is not able to cope with the burst of oxidant radicals produced at the onset of reperfusion [245].

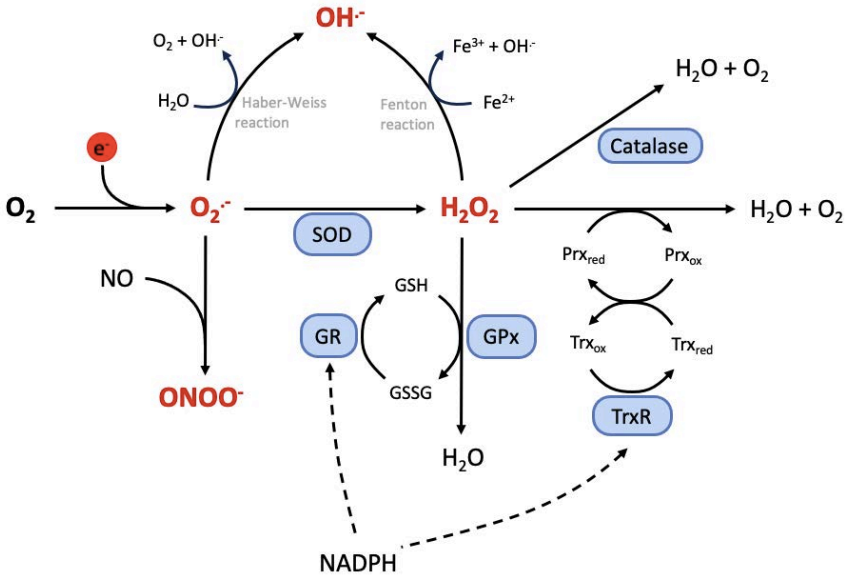

Figure 7: Overview of ROS formation and detoxification by the enzymes of the antioxidant system. GPx: glutathione peroxidase, GSH: glutathione, GSSG: glutathione disulfide, GR: glutathione reductase, Prx: peroxiredoxin Trx: thioredoxin TrxR: thioredoxin reductase, SOD: superoxide dismutase. Modified from [165,167].

1.3.4 REVERSE ELECTRON TRANSFER

1.3.4.1 Role or reverse electron transfer in physiological processes

The ability of complex I to generate ROS by RET was known since the 60s [246,247] and was tacitly assumed for decades to be an *in vitro* phenomenon of unknown relevance *in vivo* [228]. It was found in isolated mitochondria and cells from heart [228,248,249], brain [231,250,251] and liver [250], respiring on high concentrations of succinate. However, ROS production by RET was later proved to occur under substrate concentrations that mimic physiological conditions [252,253] and, in the last 15 years, accumulated evidence from several independent groups have demonstrated an important role of this mechanism in a plethora of physiological and pathological processes [254,255].

ROS generation by RET can function as redox signals in response to cellular stress or intervene in processes where cellular adaptation is required [254,256,257]. For example, RET is involved in sensing of arterial oxygen levels by the carotid body. When oxygen concentration declines, chemoreceptor cells located at the carotid body trigger a hypoxia-dependent response leading to hyperventilation. Activation of the carotid body cells has been found to be mediated in part by a metabolic shift leading to increased utilization of succinate, which enhances ROS production by RET via a highly reduced CoQ pool [258,259]. Lifespan extension in flies is also modulated by RET via the oxidative state of CoQ, as demonstrated by the fact that rotenone administration, a complex I inhibitor that decreases ROS production by RET, together with an induction of a decrease in mitochondrial membrane potential, were able to reduce ROS production and extended lifespan [260]. ROS production by RET is also essential for the inflammatory response induced by macrophages against a bacterial infection, characterized by pro-inflammatory cytokines production. Macrophage activation is mediated by a shift in mitochondrial energy production, enhanced succinate accumulation and oxidation, and increased mitochondrial membrane potential that helps drive ROS generation by RET. Moreover, suppression of ROS production by RET inhibited pro-inflammatory cytokines generation [261,262]. Recently, electron leak at the CoQ site in complex I has been found to be critical for oxygen sensing by the *ductus arteriosus*, which gets constricted and closed at birth by the increase in O_2 [263]. Even at the cardiac level, RET may have a physiological role. In this regard, RET has been also implicated in the differentiation of myoblasts into myotubes. ROS production by complex I has been shown to stimulate differentiation of H9c2 rat cardiac myoblasts, effect that was suppressed by the administration of ROS scavengers and rotenone [264]. Importantly, some studies pointed out that complex I-derived ROS production depends on the substrates used to feed the ETC. Fatty acid oxidation increases the percentage of $FADH_2$ used by the ETC, resulting in an over-reduced CoQ and leading to enhanced RET and ROS production [265]. In this case, the ratio of $CoQH_2$/CoQ would act as a sensor of the ETC efficiency and, through ROS production at complex I, it would reorganize the ETC and the degree of supercomplex assembly, together with its composition, in order to match the prevailing substrate profile [265]. For this reason, RET provides a sensitive mechanism for real-time feedback on ATP demand and electron supply to the ETC [266].

1.3.4.2 Role of reverse electron transfer during myocardial ischemia-reperfusion injury

The burst of ROS produced during tissue reperfusion following an episode of ischemia was, for many years, presumed to be a non-specific consequence of a dysfunctional and damaged respiratory chain, with electrons leaking at multiple non-specific sites [13,267–269]. However, it is now generally believed that the main source for ROS during reperfusion is the mitochondria, occurring specifically by RET at complex I of the respiratory chain, with this mechanism being especially important in the myocardium [58,270].

Consistent with this hypothesis, accumulated evidence demonstrated increased succinate concentrations during hypoxia and ischemia, something that was first proved in 1975 in diving mammals [271,272] and later confirmed in rabbit papillary muscles [273], isolated guinea pig heart [274], and isolated rat cardiomyocytes [249]. Succinate accumulation was seen, though, as a response to general Krebs cycle inhibition. It was also proved that succinate is abruptly lost from the tissue at reperfusion [275].

On the other hand, and as mentioned above, it has long been acknowledged that the most effective way for superoxide generation in isolated mitochondria is through RET [250,276,277], which is driven by succinate oxidation through the reverse action of SDH [273,278].

Chouchani and colleagues [279] connected these concepts and, in 2014, demonstrated that the accumulation of succinate occurring during ischemia results from the reverse action of SDH. Importantly, the increased levels of this metabolite stand out as a common ischemic signature across multiple tissues, including the myocardium. Moreover, they proved that SDH reverts to its forward catalytic mode at reperfusion and rapidly re-oxidizes succinate leading to superoxide generation by RET, suggesting it as the origin of the massive burst of ROS at the onset of reperfusion [279].

Accumulation of excessive succinate, thus, emerged as a critical driver for ROS production. Preventing its build-up, by administration of the reversible SDH inhibitor malonate before ischemia, in an in vivo mice model of transient coronary occlusion, was able to significantly reduce infarct size and to protect

against ischemia-reperfusion injury [279]. In addition, our group showed that protection by malonate was also present when administered at reperfusion. Under these conditions, malonate, instead of preventing succinate accumulation, would slow down its oxidation during flow restoration, thus reducing the rate of superoxide production [280]. Indeed, malonate administration at the onset of reperfusion to isolated mice hearts resulted in a reduction in infarct size, which correlated with a decrease in LDH release and improved functional recovery during reperfusion, and with reduced ROS production both in isolated mitochondria and in cardiac slices obtained at the end of the experiments [280]. Furthermore, these effects have been associated with a reduction in mPTP opening [280] that, as commented before, is one of the mechanisms of cell death during myocardial infarction. This approach opened the door for the utilization of malonate as a therapeutic tool, since patients arrive at the hospital with an already occluded artery, and thereby therapeutic interventions are only possible at the onset of reperfusion during the pPCI procedure. On top of that, these results were confirmed in a clinically relevant pig model, where intracoronary administration of malonate was carried out at reperfusion following transient coronary occlusion [281]. Notably, no undesirable effects of malonate were found neither in distant myocardial tissue nor in the appearance of reperfusion arrythmias [281].

Consistent with these findings, several studies have demonstrated that the blockade of ETC at complex I with other inhibitors is protective against ischemia-reperfusion injury, like amobarbital [282,283], rotenone [284], metformin [285,286] and Mito-SNO [287]. However, these approaches were not designed to diminish ROS by RET, but rather complex I general activity, and most of them were not reversible. Moreover, considerable additional evidence has suggested that inhibition of complex II, a crucial component of RET, can also decrease ROS production [288,289]. In addition, the crucial importance of ROS produced by RET in ischemia-reperfusion injury has been extended into other tissues, including kidney [290] and brain [291,292].

Therefore, a growing body of evidence on this topic has consolidated the current model for mitochondrial ROS generation at the onset of reperfusion, which is as follows [293] (*Figure 7*):

With ischemia, oxygen supply is interrupted and OXPHOS and the flow of electrons through the ETC stops. In an effort to preserve ATP synthesis, complex I continues to oxidize NADH and pump protons across the IMM to generate some mitochondrial membrane. However, due to the lack of the terminal electron acceptor oxygen, the rest of the ETC is halted. In this situation, SDH (or complex II), working in its reverse mode, takes the electrons from the highly reduced CoQ and reduces fumarate to succinate [294,295]. The mechanisms that maintain fumarate levels are not well known, but it has been proposed to originate from either the purine-nucleotide cycle (PNC), by conversion of aspartate to oxalacetate within the malate-aspartate shuttle (MAS) [279] or by the canonical citric acid cycle activity [296]. Anyway, fumarate reduction leads to an important accumulation of succinate during ischemia, which cannot be further metabolized. Simultaneously, the ATP/ADP ratio decreases, and AMP is subsequently metabolized in the PNC to xanthine and hypoxanthine [17,297].

Reintroduction of oxygen at reperfusion restarts the ETC and results in the rapid oxidation of succinate to fumarate by the forward mode of SDH. However, low ADP levels, which can take some time to recover, compromise ATP synthesis and the ETC is unable to function at its full capacity. Consequently, this leads to a near to maximum mitochondrial membrane potential and a highly reduced CoQ pool and, in these conditions, the excess of electrons is forced backwards, from complex II to complex I. Once in complex I, electrons flow into the FMN site where they react with oxygen to generate superoxide [294,295]. However, not all accumulated succinate is oxidized during reperfusion. In fact, part can be extruded from the mitochondria to the cytosol via the mitochondrial dicarboxylate carrier (DIC), and then released out of the cell by the monocarboxylate transporter 1 (MCT1). Importantly, the activity of the latter is facilitated by the acidic intracellular pH still present at the onset of reperfusion [298,299].

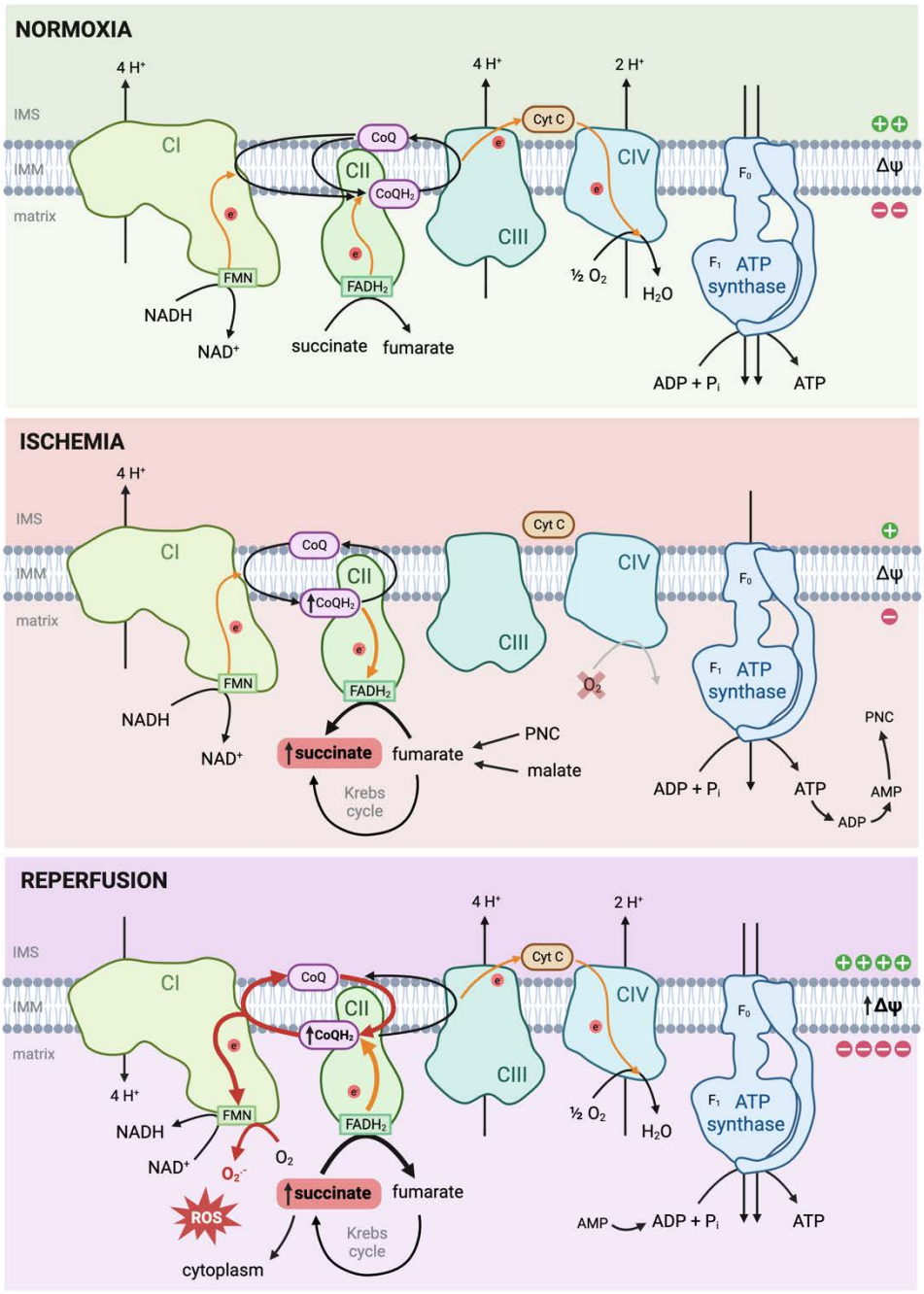

Figure 8: ROS production by succinate-driven RET during ischemia-reperfusion injury. Complete explanation in main text. Cyc C: cytochrome C; CI: complex I; CII: complex II; CIII: complex III; CIV: complex IV; IMM: inner mitochondria membrane; IMS: intermembrane space; PNC: purine nucleotide cycle; ROS: reactive oxygen species; Δψ: mitochondrial membrane potential. Adapted from [254,293,294].

1.4 UNRESOLVED ISSUES

1.4.1 EFFECTS OF THE COMBINATION OF SUCCINATE DEHYDROGENASE INHIBITION WITH MALONATE AND REMOTE ISCHEMIC CONDITIONING ON MYOCARDIAL ISCHEMIA-REPERFUSION INJURY

Discovery of isquemia-reperfusion injury opened a window of opportunity to explore new therapeutic approaches to reduce final infarct size. However, and despite the extensive body of work addressing this issue and the identification of several promising strategies with potential to reduce ischemia-reperfusion injury, none of them has been able to become part of the standard clinical care. Thus, further efforts are needed to identify new strategies that are able to mitigate ischemia-reperfusion injury in the clinical setting [300,301]. One of these promising candidates is, as discussed above, the inhibition of SDH at the onset of reperfusion with the reversible inhibitor malonate. This would lead to a reduction in succinate oxidation after ischemia, followed by a lower ROS production and mPTP opening and, consequently, by reduced cell death. In fact, and as mentioned previously, malonate has been shown to be protective against ischemia reperfusion injury in a clinically relevant pig model of transient coronary occlusion [281].

On the other hand, emerging evidence suggests that multitargeted approaches using a combination of therapies directed against several of the intracellular signaling pathways that are involved in reperfusion injury would be helpful to reduce infarct size in the clinical setting [301,302]. Indeed, some combination therapies have been previously demonstrated to exert additive effects against reperfusion injury in *in situ* pig hearts, as is the case of treatments targeting cardiac metabolism and remote ischemic conditioning (RIC) [303,304]. RIC is a non-pharmacological and safe maneuver, consisting of brief episodes of ischemia and reperfusion applied remotely, mainly to a limb, which activates a variety of endogenous mechanisms of cardioprotection [305–308]. It has been reported to exert protective effects in both experimental models [303,309,310] and in proof-of-concept clinical trials in STEMI patients [311,312]. Therefore, the question arises whether these two promising mechanisms, SDH inhibition by malonate and RIC,

would present additive effects in a combined therapy. Thus, the first objective of this thesis was to investigate the potential utility of the combination of RIC, applied during myocardial ischemia, with the SDH inhibitor malonate, given at the onset of reperfusion, to attenuate myocardial reperfusion injury and reduce infarct size in an *in situ* pig model of transient coronary occlusion.

1.4.2 UTILITY OF PLASMA SUCCINATE LEVELS AS A PROGNOSTIC BIOMARKER

Early application of reperfusion therapies is the most effective option for limiting infarct size in STEMI patients. However, the extent of the infarcted tissue is not easy to evaluate during the first hours or days following the event [313–315]. The gold standard technique to assess myocardial infarct size is cardiovascular magnetic imaging, which is only fully reliable 5-7 days after PCI [315,316]. On the other hand, release of cardiac biomarkers to serum, including cardiac troponin I and T, has been often used as a surrogate [314,317], but their kinetics and concentration depends on several factors other than infarct size itself, like the type and success of reperfusion therapy, the sensitivity of troponin assays and the presence of collateral flow [314,318,319]. Thus, further efforts are needed to identify new prognostic biomarkers that would allow early prediction of infarct size, in order to improve vital clinical decisions for patient prognosis.

Succinate has been demonstrated to be massively released into circulation during initial reperfusion and has been postulated to be a characteristic hallmark of ischemia-reperfusion [296,298,320]. Importantly, it can be detected in plasma from STEMI patients immediately after stent implantation, both in blood obtained from a peripheral vein or from the coronary sinus [320]. However, whether their levels correlate with infarct size or other clinical variables has not been previously investigated in detail. Thus, in this thesis we also aimed to evaluate the potential for succinate to become a biomarker of injury. To fulfil this objective, we analyzed plasma samples obtained from both the pigs included in the previous aim, and from STEMI patients submitted to pPCI, and enrolled in the COMBAT-MI study [316] in our hospital.

1.4.3 MODULATION OF RET BY INTERNAL FACTORS: ROLE OF Cx43

As discussed above, superoxide production by RET is a major contributor to the bust of ROS produced at reperfusion which drives mPTP opening and ischemia-reperfusion cellular damage. However, regulation of RET has not been characterized in detail. In addition to succinate concentrations, thermodynamic RET drivers include the CoQ redox status [321] and the electrochemical gradient or proton-motive force (Δp), including its major component, the mitochondrial membrane potential $\Delta\psi$ [322]. RET is facilitated by an enhanced degree of reduction of the CoQ pool and a high $\Delta\psi$, with the last providing the required energy to drive electrons in reverse direction [295,321]. In addition, single point mutation in the ND6 subunit of complex I render the complex unable to catalyze RET and thereby to generate ROS by this mechanism, even though forward electron transfer and proton translocation are not affected [323]. However, whether RET can be modulated by other intracellular endogenous factors is currently unknown.

In this regard, Cx43, a sarcolemmal protein that allows conduction of the electrical impulse [37], emerges as a potential candidate for RET regulation. Besides its primary location at the plasma membrane, where it forms gap junctional channels, Cx43 has also been found at the IMM of cardiomyocytes [324–327] and other cell types [328–331]. Although the exact functions of mitochondrial Cx43 remain largely obscure, it has been proposed that it may modulate the organelle ionic homeostasis [332]. In addition, it is well-established that mitochondrial Cx43 can impact ROS production under specific conditions, such as after treatment with diazoxide, an activator of mitochondrial K^+ channels [37,48,333]. Accordingly, the third aim of this thesis was to assess whether Cx43 modulates RET in the myocardium using mitochondria and isolated hearts obtained from inducible knock-out $Cx43^{Cre\text{-}ER(T)/fl}$ mice.

1.4.4 MODULATION OF RET BY EXTERNAL FACTORS: EFFECTS OF AIR POLLUTION

Ambient air pollution is the fourth major risk factor of death of any cause [334]. Most of the world population is exposed to it [335] and, among numerous other conditions, it is associated with cardiovascular diseases [336,337]. Air pollution is

formed by a heterogeneous mixture of gaseous pollutants and solid particles, including particulate matter (PM). PM is of especial concern, given its high toxicity and worldwide distribution. Particulate matter can be divided, depending on its diameter, in fine (<2.5 µm, PM2.5) and coarse (between 2 and 10 µm, PM10). Previous studies have demonstrated that inhalation of PM promotes cardiovascular events [338], and increases in PM2.5 and PM10 levels have been associated with enhanced daily cardiovascular mortality and with different cardiovascular disorders [339,340], including myocardial infarction, as shown previously for the city of Barcelona [340].

The mechanisms associated with the deleterious effects of air pollution in cardiovascular diseases are complex and interconnected, including inflammation, production of ROS, endothelial dysfunction, autonomic imbalance, and increased thrombogenesis [341,342]. Oxidative stress plays a prominent role in the pathogenic effects of air pollution in the vasculature, the lungs and the heart [343]. At the myocardial level, exposure to particulate matter reduces contractility of isolated cardiomyocytes exposed to diesel exhaust particles (DEP, often used in experimental models to mimic the effects of air pollution, as they are rich in PM), effect that is partially reversed by antioxidants [344]. Notably, some authors have shown that infarct size was increased in DEP-exposed mice submitted in vivo to transient [345] or permanent [346] coronary artery occlusion, as well as in isolated Langendorff-perfused mice hearts [345,347]. In accordance with the mechanisms described for air pollution, DEP exposure increased ROS in isolated hearts from DEP-treated animals [345]. Furthermore, previous studies have suggested that exposure to DEP induced mitochondrial dysfunction and ROS production [347–349]. Therefore, current data indicates that mitochondrial dysfunction and ROS production are important players in the deleterious effects brought by air pollution exposure. However, the specific origin of the ROS induced by air pollution is currently unknown as well as its potential modulation by RET. In the last part of this thesis, we explored whether air pollution influences RET in cardiac mitochondria isolated from rats exposed to DEP, and whether these potential effects modify infarct size after ischemia-reperfusion in isolated, Langendorff-perfused hearts from these animals.

2. HYPOTHESIS

HYPOTHESIS

The hypothesis of this thesis is as follows:

Inhibition of SDH at the onset of reperfusion and thus of RET exerts additive protective effects with RIC against myocardial ischemia-reperfusion injury, whereas succinate, the endogenous substrate of this enzyme, may be useful as a biomarker of myocardial damage. Regulation of RET is mediated by internal factors, such as Cx43, and external factors, such as air pollution.

3. OBJECTIVES

OBJECTIVES

Main objective:

To assess the role and regulation of RET in myocardial ischemia-reperfusion injury and its utility as a biomarker of myocardial damage.

Secondary objectives:

1. To investigate the potential benefits of the combination of RIC, applied during myocardial ischemia, and reversible SDH inhibition with malonate, given during initial reperfusion, to attenuate myocardial ischemia-reperfusion injury in a porcine model of transient coronary occlusion.

2. To evaluate the utility of plasma succinate as a prognostic biomarker of ischemic injury, using samples from both our pig model of transient coronary occlusion and from STEMI patients submitted to pPCI.

3. To assess whether Cx43 modulates RET in the myocardium using both mitochondria and isolated hearts from a Cx43 inducible knock-out mice.

4. To determine whether air pollution influences RET in cardiac mitochondria obtained from rats intratracheally instilled with DEP, and to assess its consequences on infarct size.

4. MATERIALS AND METHODS

4.1 EFFECTS OF THE COMBINATION OF SUCCINATE DEHYDROGENASE INHIBITION WITH MALONATE AND REMOTE ISCHEMIC CONDITIONING ON MYOCARDIAL ISCHEMIA-REPERFUSION INJURY

4.1.1 ANIMALS AND INSTRUMENTATION

This study complies with Directive 2010/63/EU of the European Parliament on the protection of animals used for scientific purposes and the NIH Guide for the Care and Use of Laboratory Animals (NIH publications No. 85-23, revised 1996, updated in 2011). The study was approved by the Ethics Committee of the Vall d'Hebron Institut de Recerca (reference number: CEEA 33/17).

Forty male farm pigs (25-30 kg, fasted for 12 h prior to surgery) were premedicated with tiletamine-zolazepam (4–6 mg/kg, intramuscular) and anesthetized with sodium thiopental (25 mg/kg, intravenous (IV), plus continuous infusion at 6–14 mg/kg*h) and fentanyl (5 µg/kg, IV, plus continuous infusion at 3–6 µg/kg*h). Following intubation and mechanical ventilation, a midsternotomy was performed and the pericardium opened, suturing its free margins to the borders of the sternotomy to cradle the heart. The left anterior descending (LAD) coronary artery was dissected free below the first diagonal branch, and an elastic snare was placed around the artery and used for coronary ligation and ischemia induction. A second dissection point, located one centimetre below the first, was used to measure coronary blood flow [281,303]. In addition, the left femoral artery and vein were cannulated to obtain the aortic pressure (AP) and to extract blood samples, respectively. The right femoral artery was also dissected and surrounded with an elastic snare to perform the remote RIC manoeuvre.

4.1.2 MONITORING

Heart rate and the presence of possible ventricular arrythmias was monitored by a conventional electrocardiogram (ECG). Internal defibrillation at 30 Jules was used to revert malignant arrythmias, like ventricular fibrillation, if necessary.

Arterial blood gases were monitored during the experimental procedure and maintained within normal limits.

Left ventricular (LV) pressure and its first derivate (dP/dt) were recorded with a *Millar SPR-350 Mikro-Tip®* pressure transducer (*Millar Instruments, Inc*, Texas, USA) inserted into the left ventricle through the cardiac apex. Aortic pressure was also monitored from the left femoral artery using a water-filled catheter connected to a pressure transducer (*Coulbourn Instruments,* Massachusetts, USA) [281,303].

Blood flow at the LAD coronary artery was monitored with an ultrasound flowmeter (*Transonic System Inc, model T206*, New York, USA) placed around the coronary artery in the distal dissection point [350,351].

Regional myocardial contractility was determined in a control region (remote LV myocardium supplied by the circumflex coronary artery) and in the area at risk (supplied by the LAD coronary artery). Two pairs of hemispherical polystyrene crystals were inserted into the midmyocardial layer, with 1 cm of separation, in the aforementioned regions and perpendicular to the LV long axis. Systolic segment shortening ratio (SS) was calculated as SS = (EDL − ESL)/EDL, where EDL is end-diastolic length and ESL corresponds to end-systolic length. End-diastolic measurements were taken at the point at which the positive dP/dt begins to rise, and end-systolic values were taken 20 ms before the lowest point of the negative dP/dt [22,281,303].

All parameters were digitized at 100 samples/second, amplified and recorded in a computer using a *ML119 PowerLab* interface connected to the software *Chart 5.0* (*ADInstruments*, Dunedin, New Zealand).

4.1.3 EXPERIMENTAL PROTOCOL

All animals were intravenously administered, through the femoral vein, with a bolus of sodium heparin (100 UI/kg). Immediately, the right carotid artery was dissected free and a Judkins 8F guiding catheter was inserted and advanced until the coronary ostium. Then, a 2.8/2.5F intracoronary infusion catheter (*TRANSIT, Cordis Neurovascular Inc.*, Miami, Florida, USA) was advanced through the

guiding catheter into the LAD coronary artery, until a position located distal to the dissection site selected for coronary occlusion [281].

To assess the effects of treatments on ischemia-reperfusion injury, pigs were then submitted to 40 min of LAD coronary artery occlusion, followed by 2 h of reperfusion (*Figure 9*). This time of ischemia (40 min) was selected based on previous publications from our group that demonstrated that this duration induced an infarct size of about 50% of the area at risk [281,303]. Myocardial ischemia was performed by occluding the LAD coronary artery around the infusion catheter using the elastic snare placed previously. Animals were randomly assigned to four different experimental groups (n = 10/group). Control pigs received intracoronary saline for 6 min, beginning at 39 min of ischemia and lasting for the first 5 min of reperfusion, at a flow rate of 15 mL/min (37°C). Malonate-treated animals received intracoronary saline containing disodium malonate at a concentration of 10 mmol/L during the same period. Conditioned animals (RIC) were submitted, in addition to intracoronary saline infusion, to a

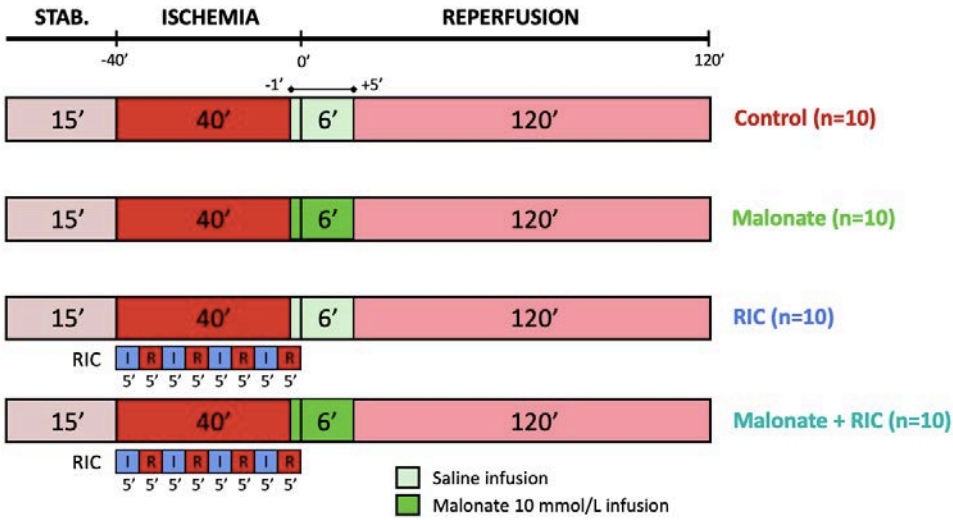

Figure 9: Study design. Open-chest pigs were submitted to 40 minutes of left anterior descending coronary artery occlusion followed by reperfusion and were distributed among four experimental groups: Control group, with intracoronary saline infusion beginning in the last minute of ischemia and lasting for the first 5 minutes of reperfusion; malonate-treated group, with malonate infusion at 10 mmol/L during the same period; remote ischemic conditioning (RIC) group, consisting of four cycles of 5 minutes of ischemia (I) in the femoral artery followed by 5 minutes of reperfusion (R); and Malonate + RIC, with a combination of both treatments.

protocol of remote ischemic conditioning consisting of four cycles of 5 min of right lower limb ischemia followed by 5 min of reperfusion, starting simultaneously with LAD coronary artery ligature, using the elastic snare placed around the right femoral artery. Finally, a fourth treatment group (Malonate + RIC) consisted in the combination of both treatments (*Figure 9*).

Blood samples were obtained in all cases at baseline and 1, 5, and 10 minutes after the onset of reperfusion, both from the great cardiac vein (or anterior interventricular vein), running parallel to the LAD coronary artery, and from the left femoral vein. An additional peripheral blood sample was obtained at the end of reperfusion (120 min). Blood was collected in heparinized tubes (BD *Vacutainer*, New Jersey, USA), centrifuged at 1500 g for 10 min (4ºC) to obtain plasma, and stored at −80ºC until analysis. At the end of the experiments, animals were euthanized by a pentobarbital overdose (100 mg/kg, IV).

4.1.4 AREA AT RISK AND INFARCT SIZE

Two hours after reperfusion, the LAD was reoccluded and 10 mL of 10% fluorescein (*SERB Pharmaceuticals*, Brussels, Belgium) was intravenously administered. After anesthetic overdose, the heart was rapidly excised, cooled down with 4ºC saline and sliced in six transversal sections (1-1,5 cm thickness), perpendicular to the long cardiac axis. Next, slices were weighted and photographed, together with a scale, under ultraviolet light, using a digital camera. Area at risk was determined as the area not stained by fluorescein.

Then, the slices were incubated with 1% 2,3,5-triphenyltetrazolium chloride (TTC) for 15 minutes, at 37ºC, and then photographed again, this time under white light, to quantify the area of infarction. After TTC staining, viable tissue adopts a vivid red color due to the reduction of this compound mediated by NADH, which is only present in cells whose sarcolemmal membrane is preserved. On the other hand, dead cells within necrotic areas lose the integrity of the sarcolemma and consequently intracellular NADH. Infarcted areas appear, thus, unstained, adopting a white color [46].

Area at risk and infarcted areas were measured from the images with the software *ImagePro® Plus* (*Media Cybernetics*, Rockville, Maryland, United

States). Area at risk was expressed as percentage of total ventricular weight and infarct size as percentage of area at risk.

4.1.5 INCIDENCE OF MALIGNANT REPERFUSION ARRYTHMIAS

ECG recordings were analyzed for the incidence of ventricular tachycardia (VT) and ventricular fibrillation (VF) during ischemia and the first 20 min of reperfusion. VT was defined as three or more consecutive premature beats of ventricular origin at a heart rate faster than 120 beats/min, and wide QRS durations (>120 ms). VF was defined as areas with chaotic and disorganized electric activity, without defined ECG waves, and associated with reduced aortic and ventricular pressure [303].

4.1.6 STATISTICAL ANALYSIS

All measurements were carried out by a researcher blinded to group allocation and analyzed with the software *IBM® SPSS® Statistics 20* (Armonk, New York, USA). Data are expressed as mean ± Standard Error of the Mean (SEM). Normal distribution was assessed by Kolmogorov–Smirnov test. Analysis of variance (ANOVA) and Tukey post-hoc test were used to assess differences in infarct size and area at risk. Changes in the time course of hemodynamic and contractility variables were assessed by repeated measures ANOVA and Tukey post-hoc tests. Non-parametric Kruskal-Wallis test was used to assess differences in the number of ventricular tachyarrhythmias. Incidence of VF was analyzed by the Pearson Chi-square test. Differences were considered significant when $p<0.05$.

4.2 ASSESSMENT OF THE POTENTIAL UTILITY OF PLASMA SUCCINATE LEVELS AS PROGNOSTIC BIOMARKER

4.2.1 TARGETED UPLC-MS/MS ANALYSIS OF CITRIC ACID CYCLE METABOLITES IN PORCINE PLASMA SAMPLES

Separation and detection of the citric acid cycle metabolites succinate, fumarate, malate, and citrate, together with lactate and malonate, in porcine plasma samples obtained in the previous experiments was performed on a *Waters® Acquity* Ultra Performance Liquid Chromatographic equipment coupled with a *Waters® Xevo™ TQ* MS triple quadrupole mass spectrometer (UPLC-MS/MS) (*Waters Corporation*, Milford, Massachusetts, USA).

Standard calibration curves for each analyte were freshly prepared by adding 5 µL of 7 different concentrations of the distinct metabolites to 200 µL of plasma. An additional blank sample lacking analytes was also prepared. Linearity for the standard calibration curves was obtained between 3.125 and 500 µmol/L for succinate, 0.1 and 20 µmol/L for fumarate, 0.5 and 40 µmol/L for malate, 7.8125 and 125 µmol/L for citrate, 0.005 and 2500 µmol/L for malonate, and 500 and 8000 µmol/L for lactate. Metabolites were then extracted with the methanol method [352] by adding 200 µL or 400 µL of methanol, containing 0.05 mmol/L succinic acid-2,2,3,3-d4 (*Merck KGaA*, Darmstadt, Germany) as an internal standard, to 100 µL of each sample or 200 µL of each calibration standard, respectively. Samples were vortexed, cooled at -20°C for 20 min, and centrifuged at 11000 rpm for 30 min, at 4°C. Supernatants containing metabolites were transferred to new 1.5 mL propylene tubes, lyophilized, and stored at -20°C until analysis.

Before injection to UPLC-MS/MS, the purified residues were reconstituted with 100 µL (for samples) or 200 µL (for calibration standards) of a mobile phase solution consisting of mobile phase A (formic acid 0.2% in acetonitrile) and mobile phase B (formic acid 0.2% in water) at 10:90 v/v. Samples and calibration standards were vortexed for 5 min and centrifuged again at 11000 rpm for 5 min, at 4°C.

Separation was achieved following injection of 4 µL of each sample on an *Acquity UPLC HSS* C18 column (2.1 × 100 mm, 1.8 µm particle size, *Waters® Corporation*, Milford, Massachusetts, USA). A gradient elution program was conducted for chromatographic separation with mobile phase A and mobile phase B as follows: 0-1.5 min hold for 10% eluent A, 1.5-5 min from 95% to 60% eluent A, 5-7 min hold for 60% eluent A, 7-7.5 min from 60% to 10% eluent A and 7.5-9 min hold for 10% eluent A to reequilibrate the column before next injection. Pump was operated at a flow rate of 0.3 mL/min with an overall run time of 9 min. The autosampler was held at 6°C and column oven was set up at 30°C. The mass spectrometer was operated in multiple reaction monitoring (MRM) using an electrospray (ESI) source in negative mode for all compounds, with a capillary voltage of 2.02 kV. Argon was used as collision gas and flow was 0.17 mL/min. Desolvation temperature was 450 °C with a gas flow of 1100 L/h. Ion transitions and optimal cone voltage and collision energy used for fragments detection are summarized in *Table 1*. System control and data analysis were carried out using the *MassLynx™* software (Version 4.1, *Waters® Corporation*, Milford, MA, USA) and processed using *TargetLynx™* program (*Waters® Corporation*, Milford, Massachusetts, USA). For each calibration standard, the ratio between the intermediate peak and the internal standard containing succinic acid-2,2,3,3-d4 was determined. Linear regressions describing the calibration curves were then calculated using a weighting factor of $1/x^2$, where x was concentration.

Table 1: Ion transitions and optimal cone voltage and collision energy used for fragments detection in UPLC-MS/MS analysis of citric acid cycle metabolites in porcine plasma samples.

Compound	**Precursor Ion** (m/z)	**Product Ion** (m/z)	**Cone Voltage** (V)	**Collision Energy** (V)
Succinate	117.10	73.00	16	11
Succinic acid-2,2,3,3-d_4 (IS)	121.10	76.50	15	9
Fumarate	115.09	71.01	13	6
Malate	133.04	115.02	20	10
Citrate	191.13	111.00	18	10
Malonate	103.09	59.00	12	8
Lactate	89.11	43.00	18	10

IS: internal standard.

4.2.2 PROGNOSTIC VALUE OF PLASMA SUCCINATE AND OTHER METABOLITES IN STEMI PATIENTS

4.2.2.1 Patient characteristics

Plasma concentration of succinate and other metabolites were analyzed in a subgroup of STEMI patients submitted to pPCI (n=111) and included in the COMBAT-MI clinical trial (registered at www.clinicaltrials.gov (NCT02404376) on 31/03/2015; EudraCT number 2015-001000-58) [316]. The COMBAT-MI trial was a prospective, randomized, multicentric, double blinded, clinical trial comparing the effects of sham procedure, intravenous exenatide, RIC, and their combination on infarct size measured by late gadolinium enhancement in cardiac magnetic resonance (CMR) in patients with STEMI undergoing pPCI (allocation ratio 1:1:1:1 via a web-based clinical support system accessible 24 h a day (W3NEXUS, Barcelona, Spain) [316], and main results were published in [316]. The study was conducted in accordance with the Declaration of Helsinki and the European Guidelines for Good Clinical Practice, and was approved by the Agencia Española de Medicamentos y Productos Sanitarios (AEMPS) and the Ethics Committee of participant institutions. All patients provided written informed consent before randomization.

Patients with diagnosis of STEMI, older than 18 years, presenting within 6 h of symptom onset were included in the original study [316]. STEMI was characterized by ischemic symptoms, including chest pain, and ≥1 mm ST elevation in 2 leads in the same territory or ≥2 mm ST elevation in ≥2 V1 through V4 leads or left bundle branch block with ≥1 mm concordant ST elevation. Exclusion criteria included TIMI flow grade at admission equal to 2 or 3 [316]. Patients eligible were recruited in Vall d'Hebron Hospital between March 2016 and June 2019 and enrolled in the emergency room or upon entering the catheterization laboratory.

A total of 378 patients were randomized in the original study. Following application of exclusion criteria, 222 remaining patients were included in the intention-to-treat analysis [316]. Plasma samples were available, in our center, from 111 patients.

4.2.2.2 Cardiac catheterization

Further details for study procedures can be found in [316]. PPCI followed guideline recommendations [353] and was performed by experienced operators without any delay. Stenting was performed in accordance with usual procedures and local practice. Thrombectomy and selection of antiplatelet and anticoagulant regimens were at operator discretion. Blood samples were obtained at the time of pPCI from 111 STEMI patients randomized in our center (in 102 patients who met the inclusion criteria (TIMI flow ≤1) within the first 10 minutes after revascularization, and in 9 additional patients with initial TIMI flow ≥ 2 during coronariography) and placed in EDTA tubes. Plasma was obtained after centrifugation at 1500 g for 10 min. The supernatant was then centrifuged again at 2500 g (15 min) and maintained at -80ºC until use. Samples and data from patients included in this study were provided by the Cardiology Bank of Vall d'Hebron University Hospital Biobank (PT17/0015/0047), integrated in the Spanish National Biobanks Network, and they were processed following standard operating procedures with the appropriate approval of the Ethical and Scientific Committees.

4.2.2.3 Cardiac magnetic resonance data

CMR data included, among others, myocardial infarct size determined by late gadolinium enhancement (LGE) 3-7 days after pPCI [316] (both as percentage of LV mass and in absolute weight), myocardial salvage index (ratio of LGE to the extent of myocardial edema, assessed by T2-weighted CMR), transmurality index (mass of myocardium showing LGE respect to the mass of the myocardial segment containing it), extent of edema, left ventricular ejection fraction (LVEF) measured by CMR imaging, and microvascular obstruction volume respect to infarct size on LGE sequences.

4.2.2.4 Analysis of plasma samples by nuclear magnetic resonance spectroscopy

Plasma metabolites were extracted using the methanol method also described in section 2.1 [352]. Briefly, methanol (300 µL) was added to 100 µL of plasma, vortexed, kept at -20ºC for 20 min, and centrifuged at 15000 rpm for 30 minutes at 4ºC. Supernatants were recovered, lyophilized and stored at -20ºC until

analysis. Dried samples were dissolved in 180 µL of deuterium oxide containing 0.5 mmol/L of the internal and chemical shift standard TSP (3-(trimethylsilyl)propionic-2,2,3,3-d4 acid sodium salt) (*Sigma*, Saint Louis, Missouri, USA). Nuclear magnetic resonance (^{1}H-NMR) spectra were acquired on a vertical bore 9.4T magnet interfaced to a *Bruker* Avance 400 spectrometer (*Bruker*, Billerica, Massachusetts, USA). Each spectrum consisted in the accumulation of 64 scans using a fully relaxed pulse-and-acquire pulse sequence with presaturation of the residual water signal. Spectrums were processed, submitted to Fourier transformation and phase was manually adjusted with the program XWINNMR (*Bruker*, Billerica, Massachusetts, USA). Peak allocation and quantification were achieved with the program *Chemomx* (*Chemomx* Inc, Edmonton, Canada) using data previously published and annexed to the program.

4.2.3 STATISTIC ANALYSIS

Data are expressed as Mean ± SEM. Analyses were performed using the software *IBM SPSS Statistics 20* (Armonk, New York, USA). Regarding data from the porcine model, changes in the time course of the different metabolites were assessed by repeated measures ANOVA and Tukey post-hoc tests. Student's t-test was used to compare metabolite concentrations at baseline between peripheral and great cardiac vein plasma samples. Differences were considered significant when $p<0,05$.

Regarding data from STEMI patients, differences in baseline characteristics and outcomes between patients with initial TIMI flow ≤1 and those with TIMI flow ≥ 2 were analyzed by Student's t-test. Linear regression analysis was used to assess the existence of correlations between metabolite concentrations and CMR variables. Predictors for myocardial infarct size, myocardial salvage index, transmurality index, left ventricular ejection fraction and microvascular obstruction volume, measured by CMR imaging, were determined by stepwise regression analysis. Differences were considered significant when $p<0.05$.

4.3 MODULATION OF RET BY INTERNAL FACTORS: ROLE OF Cx43.

4.3.1 ANIMAL MODEL: THE $Cx43^{Cre\text{-}ER(T)/fl}$ MICE

Experiments included in this study conform to the NIH Guide for the Care and Use of Laboratory Animals (NIH publications Nº. 85-23, revised 1996, updated in 2011), and were performed in accordance with European legislation (Directive 2010/63/UE). The study was approved by the Ethics Committee of the Vall d'Hebron Institut de Recerca (CEEA 22.20).

Animals were kept with undisturbed social interaction (5 animals per cage) in conventional cages and maintained in a temperature and humidity-controlled environment (22-24ºC, and 60-65%, respectively), on a 12h-light/dark cycle. All animals had *ad libitum* access to tap water and standard diet throughout the whole experimental period.

Experiments were performed in a mouse model of global conditional deletion of Cx43, an animal model previously developed by Eckardt and colleges [354] under a C57BL/6J genetic background. In these mice, the region coding for one of the Cx43 alleles was replaced by a fusion construct of the Cre recombinase and a mutated domain of the human estrogen receptor, which is insensitive to the natural ligand β-estradiol (Cre-ER(T)). Under no additional treatments, these animals express about 50% of normal Cx43 content. However, after treatment with 4-hydroxytamoxifen (4OHT), binding of the drug to the ER(T) domain induces Cre activity and, consequently, a global deletion of Cx43 after recognition of the loxP sites flanking the second Cx43 allele [39,355,356]. Therefore, 4OHT treatment would fully delete the only Cx43 allele present in the $Cx43^{Cre\text{-}ER(T)/fl}$ ($Cx43^{Cre/fl}$) mice and would not have any effect on their corresponding control animals ($Cx43^{fl/fl}$). $Cx43^{Cre\text{-}ER(T)/fl}$ mice and their corresponding control animals, were intraperitoneally injected with 3 mg/day of 4OHT, suspended in castor oil, for 5 consecutive days, and all posterior experiments were performed 13 days after start of the treatment.

4.3.1.1 Genotyping

4.3.1.1.1 Genomic DNA extraction

Genomic DNA was isolated from distal tail snips using the *Wizard*® SV Genomic DNA Purification System (*Promega*, Madison, Wisconsin, USA). Briefly, tail biopsies were digested overnight, at 55°C, with 275 µL of Digestion Solution Master Mix (200 µL of Nuclei Lysis Solution supplemented with 50 µL of EDTA 0.5 mol/L (pH 8), 20 µL of Proteinase K 20 mg/mL, and 5 µL of RNAse 4 mg/mL). Afterwards, samples were centrifuged at 2000 g to pellet undigested hair or cartilage, and supernatant were transferred to 1.5 mL microcentrifuge tubes. Then, 250 µL of *Wizard*® SV Lysis Buffer containing ethanol were added to the lysed samples and transferred to the *Wizard*® SV Minicolumn where they were centrifuged at 13000 g for 3 minutes to bind genomic DNA to the silica-membrane. Following nucleic acid binding, the columns were washed four times and centrifuged at 13000 g for 1 minute to ensure removal of any residual impurities from the membrane. Finally, DNA was eluted with nuclease-free water by centrifugation at 13000 g for 2 minutes.

Purified genomic DNA concentration was measured using a *Nanodrop™ 2000* spectrophotometer (*Thermofisher*, Whaltham, Massachussetts, USA). Samples with a 260/280 ratio ≥ 1.8 were accepted as pure and used for gene amplification.

4.3.1.1.2 DNA amplification by Polymerase Chain Reaction

Polymerase chain reaction (PCR) was performed to amplify the Cx43 and Cre gene fragments using the enzyme Platinum™ Taq DNA Polymerase (10966034, *Thermofisher*, Whaltham, Massachussetts, USA). Five µL of purified genomic DNA were added, in 0.2 mL tubes, to 20 µL of a PCR master mix (PCR Buffer 1x; $MgCl_2$ 1.5 mmol/L; dNTP mix 0.2 mmol/L; Platinum™ Taq DNA Polymerase 1U, and 0.2 µmol/L of each primer, (*Table 2*)). Final solutions were, then, incubated in an *iCycler* thermal cycler (*Bio-Rad*, Hercules, California, USA) using the following amplification protocol: 4 minutes at 95°C, followed by 34 cycles of 60 seconds at 95°C, 60 seconds at 55 °C, and 90 seconds at 72°C. A final step of 5 minutes at 72°C ensured that all gene sequences were at full length. The reaction was then stopped by cooling the samples to 4°C.

	Primer	Primer sequence (5'→3')
Cre	Cre26	CCT GGA AAA TGC TTC TGT CCG
	Cre36	CAG GGT GTT ATA AGC AAT CCC
LoxP	UMP	TCA TGC CCG GCA CAA GTG AGA C
	UMPR	TCA CCC CAA GCT GAC TCA ACC G

Table 2: Primers used for DNA amplification during genotyping of the $Cx43^{Cre\text{-}ER(T)/fl}$ mice.

4.3.1.1.3 Agarose gel electrophoresis

The amplified PCR products were separated by electrophoresis on a 1.5 % agarose gel prepared in 1x Tris-Acetate-EDTA (TAE) buffer (Trizma base 40 mmol/L, EDTA 1 mmol/L, glacial acetic acid 20 mmol/L, pH 8) that contained *SYBR® Safe* DNA gel stain (*Thermofisher*, Waltham, Massachusetts, USA). PCR products were diluted 10:1 in *TrackIt™ Cyan/Orange* Loading Buffer (*Thermofisher*, Waltham, Massachusetts, USA), to track electrophoresis progress and DNA migration. The electrophoresis procedure was performed at 90 V for 40 minutes in TAE 0.5x. DNA bands were visualized in a Molecular Imager® *Gel Doc™* (*Bio-Rad*, Hercules, California, USA) with ultraviolet light and processed with *Quantity One®* Analysis Software (*Bio-Rad*, Hercules, California, USA).

Control $Cx43^{fl/fl}$ mice showed a single amplicon of 1000 bp, corresponding to the loxP sequence. In contrast, $Cx43^{Cre\text{-}ER(T)/fl}$ presented two bands, one corresponding to the same 1000 bp amplicon, and an additional one at 900 bp corresponding to the Cre-recombinase allele, as shown in *Figure 10*.

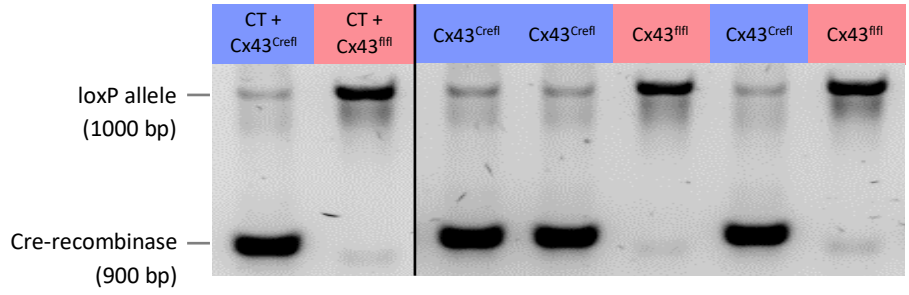

Figure 10: Representative image showing the results obtained after electrophoresis of amplified PCR products. The two first columns at the left show bands from pre-existing $Cx43^{Cre\text{-}ER(T)/fl}$ ($Cx43^{Crefl}$) and $Cx43^{flfl}$ controls, respectively. The five columns at the right show bands from experimental samples.

4.3.1.2 Confirmation of Cx43 gene deletion by Western Blot

Reduction of Cx43 expression after 4OHT administration was verified by Western Blot analysis of brain total homogenates 13 days after first induction [39,355]. Frozen tissue was homogenized with a Polytron (*Diax 600 homogenizer*, Heidolph, Gernamy) in RIPA buffer (Tris Base 50 mmol/L, NaCl 150 mmol/L, Triton™ X-100 1%, Na-deoxycholate 0.5%, SDS 0.1%, Tween20 0.1%, supplemented with NaF 5 mmol/L, Na_3VO_4 1 mmol/L, and Protease inhibitor cocktail (*Sigma*, Burlington, Massachusetts, USA) 1%, pH 8). The resulting homogenates were centrifuged at 1600 g for 10 minutes at 4°C, to discard nuclei and other tissue debris, and supernatants were stored at -80°C until analysis. Protein concentration was quantified with the Bradford method.

Proteins were separated by molecular weight under denaturizing conditions on a sodium dodecyl sulphate-polyacrylamide gel electrophoresis (SDS-PAGE). The running gel composition was acrylamide/bis-acrylamide 37.5:1 (10%), Tris-base (0.375 mmol/L), SDS (0.1%), ammonium persulphate (APS, 0.05%), and tetramethylethylenediamine (TEMED, 0.1%), pH 8.8 [355]. The stacking gel (4%) that was prepared above the running gel contained acrylamide/bis-acrylamide 37.5:1 (4%), Tris base (0.125 mmol/L), SDS (0.1%), APS (0.05%), and TEMED (0.1 %), pH 6.8. [355]. Samples (40 µg) were 1:1 diluted in Laemmli buffer 2x and loaded into the gel wells. Electrophoresis was run at a constant amperage of 20 mA per gel in electrophoresis buffer (Tris base 25 mmol/L, glycine 192 mmol/L, SDS 0.1%, pH 8.3).

Proteins were then transferred from the polyacrylamide gel to a nitrocellulose membrane (*Hyband ECL* membranes, *Amersham Biosciences*, Sweden) at a constant voltage of 100V for 60 minutes while immersed in transfer buffer (Tris base 25 mmol/L, glycine 20 mmol/L, methanol 20%). Membranes were then stained with Ponceau S for 5 minutes and imaged under white light. Next, membranes were washed with TBS and unspecific binding was blocked by incubation in 5% non-fat milk in Tris Buffered Saline-Tween (TBS-T, Tris-base 20 mmol/L, NaCl 150 mmol/L, Tween20 0.1%, pH 7.4) for 60 minutes at room temperature (RT). Then, membranes were incubated with a rabbit primary polyclonal antibody raised against Cx43 (#C6219, dilution 1:8000, *Sigma*, Burlington, Massachusetts, USA) diluted in blocking buffer, for 90 minutes. After washing, membranes were incubated with the secondary, peroxidase-

conjugated, anti-rabbit antibody (#31460 Goat anti-rabbit IgG (H+L) Secondary antibody HRP, Pierce (*Thermofisher*, Waltham, Massachusetts, USA)), diluted 1:50000 in blocking buffer, for 60 minutes at RT. Immunoreactive bands were detected using the *ECL™ Prime* Western Blotting Detection Reagent (*Amersham™ Biosciences*, Amersham, United Kingdom) and captured using an *Odyssey® FC* Imaging System (LI·COR, Lincoln, New England, USA). Band intensities were quantified by densitometry scanning using *Image Studio™ Lite* (LI·COR, Lincoln, New England, USA) software. Cx43 was normalized to GAPDH, that served as a loading control.

4.3.2 ANALYSIS OF MITOCHONDRIAL FUNCTION

4.3.2.1 Isolation of subsarcolemmal and interfibrillar mitochondria

Mouse subsarcolemmal (SSM) and interfibrillar (IFM) mitochondria were isolated from hearts of $Cx43^{flfl}$ and $Cx43^{Cre\text{-}ER(T)/fl}$ mice treated with 4OHT (both sexes, 50% each) by differential centrifugation according to the method initially described by Palmer et al. [55,280,357]. Mice were euthanized by anaesthetic overdose with sodium pentobarbital (1.5 g/kg, intraperitoneal (IP)). Immediately, the chest was opened, and the heart rapidly excised. After atrial removal, ventricular tissues were homogenized, using a glass-teflon Potter-Elvehjem tissue homogenizer, in cold sucrose buffer (sucrose 290 mmol/L; MOPS 5 mmol/L; EGTA 1 mmol/L; BSA 0.1%; pH 7.4). The homogenate was centrifuged for 5 minutes at 800 g (4°C) and the supernatant was centrifuged again, for 5 minutes at 5000 g (4°C), to obtain a pellet containing the crude fraction of SSM. The initial pellet obtained from the first centrifugation was resuspended in cold potassium buffer (KCl 100 mmol/L; MOPS 50 mmol/L; EGTA 1 mmol/L; BSA 0.1%; pH 7.4) containing 1 mg/mL of proteinase K (#P2308, *Sigma*, Burlington, Massachusetts, USA, P2308) and homogenized again with the glass-teflon Potter homogenizer. Following incubation for 1 min, samples were subsequently centrifuged, first for 5 minutes at 800 g (4°C), and the supernatant again for 5 minutes at 5000 g (4°C), to obtain a pellet containing a crude fraction of IFM. Both SSM and IFM pellets were resuspended in cold sucrose buffer and kept on ice until use.

4.3.2.2 Protein quantification

Protein quantification of mitochondrial homogenates was performed by the Bradford method. Samples were solubilized in 0.15% sodium deoxycholate, and a bovine serum albumin (BSA) standard curve was used, with concentrations ranging from 0 to 200 µg/mL. Bradford reagent was added to the samples and standards, and absorbance was determined with a spectrophotometer *iD3 SpectraMax®* (*Molecular Devices*, San Jose, California, USA) at 595 nm. Sample concentration was quantified from the standard curve adjusted to a linear regression. Mitochondrial Yield (MY) was calculated as mg of protein in the homogenate divided by wet cardiac weight.

4.3.2.3 Citrate synthase activity

To evaluate mitochondrial content at both SSM and IFM fractions, citrate synthase (CS) activity was quantified using a colorimetric assay. CS is a mitochondrial matrix enzyme which catalyzes the synthesis of citrate from the reaction of acetyl-CoA and oxalacetate (OAA), the first reaction of the citric acid cycle (*Figure 11*). The activity of this enzyme can be used as an indicator of the number of mitochondria present in the sample.

First, 30 µL of samples were lysed with 170 µL of 0.1% Triton-X100. Then, 2.5 µL of the lysate were mixed with 237.5 µL of TRIS-HCl buffer containing 0.3 µmol/L of acetyl-CoA and 0.1 µmol/L of dithiobis-(2-nitrobenzoic) acid (DTNB, Ellman's reagent), at pH 8. To start the reaction, 12.5 µL of oxalacetate 0.1 mmol/L were added, allowing DTNB to be converted into 2-nitro-5-thiobenzoate (TNB), whose absorbance at 405 nm was spectrophotometrically monitored for 5 minutes. Units of CS activity (UCS) were determined as µmol DTNB/min*mg of mitochondrial protein [280,357].

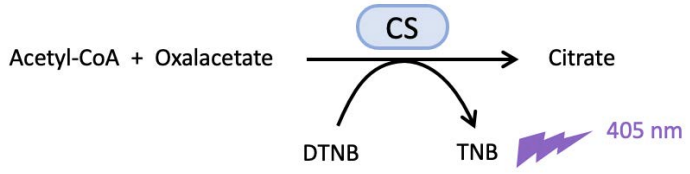

Figure 11: Citrate synthase (CS) reaction, using acetyl-CoA, oxalacetate and dithiobis-(2-nitrobenzoic) acid (DTNB) as substrates, and resulting in the production of citrate and 2-nitro-5-thiobenzoate (TNB).

4.3.2.4 Mitochondrial oxygen consumption

Mitochondrial respiration in both SSM and IFM was assessed using a Clark-type electrode (*Oxygraph*, *Hansatech Instruments*, Pentney, United Kingdom) at room temperature after addition of assay buffer (KCl 100 mmol/L, MOPS 50 mmol/L, KH_2PO_4 5 mmol/L, EGTA 1 mmol/L, $MgCl_2$ 1 mmol/L, pH 7.4) containing respiration substrates feeding complex I (malate 2 mmol/L and glutamate 5 mmol/L). Oxygen consumption measurements were performed in the absence or presence of ADP 250 µmol/L, in order to obtain state 2 (basal, non-ADP dependent O_2 consumption, S2) and state 3 (ADP-stimulated respiration, S3) oxygen consumption, respectively [280,357]. Oxygen consumption rates were expressed as nmols O_2/min*UCS. Respiratory control ratio (RCR) was defined as state 3/state 2 oxygen consumption.

4.3.2.5 Mitochondrial ROS production

ROS production by isolated SSM and IFM mitochondria was assessed with an Amplex™ Red assay. This reagent reacts with H_2O_2 when horseradish peroxidase (HRP) is present, to produce the highly fluorescent resorufin (*Figure 12*). To evaluate ROS production, mitochondria were resuspended in assay buffer supplemented with Amplex™ Red (10 µmol/L) and HRP (5 U/mL). Respiration substrates for complex I dependent ROS production (malate 2 mmol/L, glutamate 5 mmol/L) and for complex II-dependent ROS production (succinate 5 mmol/L), both with or without rotenone 0.5 µmol/L, were added and H_2O_2 production was determined using a multimode reader (*iD3 SpectraMax*, *Molecular Devices*, San Jose, California, USA) [280]. Changes in fluorescence were monitored at 590 nm during 10 min and H_2O_2 concentration was calculated using standard H_2O_2 curves. Rates were expressed, respect to baseline fluorescence, as nmols H_2O_2/min*mg protein. ROS production by RET was calculated as the

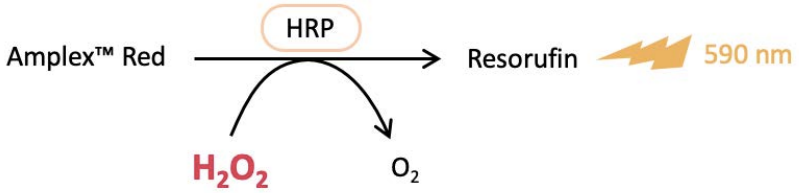

Figure 12: Principle of H_2O_2 quantification of resorufin formation from Amplex™ Red, in the presence of horseradish peroxidase (HRP).

difference between values obtained with succinate in the absence and presence of rotenone.

4.3.2.6 Mitochondrial membrane potential

Mitochondrial membrane potential was assessed using the fluorescent mitochondrial probe tetramethylrhodamine ethyl ester perchlorate (TMRE). This positively charged marker is taken up by active mitochondria in a membrane potential dependent manner. Mitochondria (0.125 µg protein/mL) were incubated for 10 minutes at RT in assay buffer containing TMRE 10 nmol/L, after addition of succinate 5 mmol/L with or without rotenone 0.5 mol/L. Samples were centrifuged at 5000 g for 2 min (4°C) to remove the TMRE not captured by mitochondria and resuspended with assay buffer containing the corresponding substrates without TMRE. Fluorescence was determined at 600 nm using a multimode reader (*iD3 SpectraMax*, *Molecular Devices*, San Jose, California, USA) (excitation wavelength 550 nm).

4.3.2.7 Quantification of CoQ and its redox state by UPLC-MS/MS in isolated mitochondria

4.3.2.7.1 CoQ extraction

CoQ was extracted from mitochondrial enriched preparations as previously described [321,323]. In brief, mitochondria (50 µg protein) were incubated, for 10 minutes, in assay buffer containing succinate 5 mmol/L. Samples were centrifuged at 5000 g for 2 min (4°C), resuspended in 200 µL of ice-cold methanol acidified in HCl 0.1% and vortexed. Hexane (200 µL) was then added, the suspension vortexed again and centrifuged at 17000 g for 5 min (4°C). After centrifugation, two phases were formed, and the upper hexane phase, containing the hydrophobic CoQ, was collected in another 1.5 mL eppendorf tube. The hexane phase was then dried down in a *SpeedVac®* Concentrator *Savant™ SPD111V* (*Thermofisher*, Waltham, Massachusetts, USA) for 10 minutes and stored at -20°C until analysis.

4.3.2.7.2 CoQ analysis by UPLC-MS/MS

CoQ pool concentration and its redox state [321,323,358] were determined by UPLC-MS/MS. Analyses were carried on a *Waters® Acquity* Ultra Performance Liquid

Chromatographic equipment coupled with a Waters® Xevo™ TQ MS triple quadrupole mass spectrometer (*Waters® Corporation*, Milford, Massachusetts, USA). Standard calibration curves for CoQ10, together with an additional blank sample, were freshly prepared, and linearity was obtained between 2 and 1000 µg/L. Before injection to UPLC-MS/MS, standards and samples were reconstituted in the mobile phase solution (2 mmol/L ammonium formate in methanol). Autosampler was hold at 8°C prior to injection of 4 µL of CoQ extracts into a 15 µL flow-through needle and separated by reverse-phase at 45 °C using a Waters® Acquity UPLC BEH C18 column (1.7 µm, 130 Å, 2.1 × 100 mm; *Waters® Corporation*, Milford, Massachusetts, USA). Mobile phase (isocratic 2 mmol/L ammonium formate in methanol) operated at a flow rate of 0.75 mL/min over 4 min. The injection of each sample was followed by a progressive gradient elution program performed to re-equilibrate the column before next injection, as shown in *Table 3*.

Table 3: Gradient elution program of each sample injected into the UPLS-MS/MS for CoQ analysis.

Time (min)	Flow rate (mL/min)	Solution A (%) (2mmol/L ammonium formate in water)	Mobile phase (%) (2 mmol/L ammonium formate in methanol)
0	0.75	0	100
4	0.75	0	100
5	0.4	0	100
6.5	0.4	50	50
7.5	0.4	50	50
8	0.4	0	100
9	0.75	0	100
9.5	0.75	0	100

For MS/MS analysis, electrospray ionization in positive ion mode was used with the following settings: capillary voltage 2 kV; cone voltage 43 V; ion source temperature 150°C; desolvatation temperature 450°C; desolvatation gas flow 1100 L/h; collision energy 30 V. MRM in positive ion mode was used for compound detection. Transitions used for quantification are listed in *Table 4*. Samples were quantified using *MassLynx™* software (Version 4.1, *Waters®*

Corporation, Milford, Massachusetts, USA) and processed using *TargetLynx™* program (*Waters® Corporation*, Milford, Massachusetts, USA)

Table 4: Ion transitions for the reduced and oxidized forms of CoQ9 and CoQ10 used for its detection in the UPLC-MS/MS analysis.

Molecule	**Precursor Ion** (m/z)	**Product Ion** (m/z)
CoQ9	812.9	197.2
$CoQ9H_2$	814.2	197.2
CoQ10	880.9	197.2
$CoQ10H_2$	882.8	197.2

4.3.3 MYOCARDIAL ISCHEMIA-REPERFUSION INJURY IN ISOLATED MICE HEARTS

4.3.3.1 Isolated, Langendorff-perfused, mice heart preparation

Myocardial ischemia-reperfusion injury was induced in isolated mice hearts using a Langendorff perfusion system, which enables monitoring of various cardiac parameters during the ischemia-reperfusion procedure, assessment of the effect of cardioprotective treatments, and quick harvest of the myocardium for subsequent analysis at any time point during the protocol.

Thirteen days after first intraperitoneal administration of 4OHT, adult male $Cx43^{Cre\text{-}ER(T)/fl}$ and $Cx43^{fl/fl}$ mice (25-35 g) were euthanized with sodium pentobarbital overdose (1.5 g/kg, IP) and submitted to a bilateral thoracotomy. Hearts were quickly removed and transferred into an ice-cold saline solution to remove the excess of blood. Immediately (less than 3 minutes), the aorta was cannulated and secured with a 3-0 suture, and the myocardium was retrogradely perfused with an oxygenated (95% O_2: 5% CO_2) Krebs solution at 37°C (NaCl 118 mmol/L, KCl 4.7 mmol/L, $MgSO_4$ 1.2 mmol/L, $CaCl_2$ 1.8 mmol/L, $NaHCO_3$ 25 mmol/L, KH_2PO_4 1.2 mmol/L, and glucose 11 mmol/L, pH 7.4) in a constant flow Langendorff system [280]. Baseline flow (about 3.5 mL/min) was adjusted to produce a perfusion pressure of 80-90 mmHg, measured with a pressure

transducer connected through a catheter to a side port located in the perfusion line. LV pressure was monitored with a water-filled latex balloon connected to another pressure transducer, placed in the left ventricle, and inflated to obtain a LV end-diastolic pressure (LVEDP) between 6 and 8 mmHg (*Figure 13*).

All signals were amplified and digitalized with a *ML119 PowerLab* interface (*PowerLab/8SP SP9150, ADInstruments*, Dunedin, New Zealand), and visualized and analyzed with the software *Chart 5.0* (*ADInstruments*, Dunedin, New Zealand).

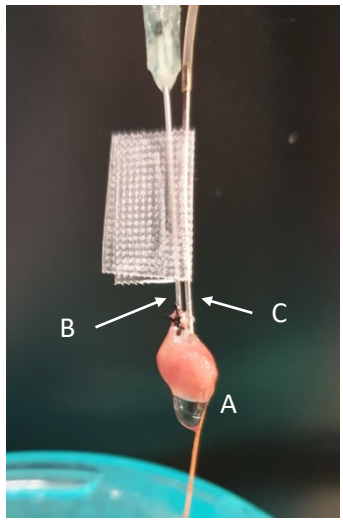

Figure 13: Langendorff system for retrograde perfusion of isolated mice hearts. The heart (**A**) is canulated through the aorta (**B**), and a latex balloon connected to a cannula (**C**) is inserted in the left ventricle to monitor the LV pressure.

4.3.3.2 Effect of Cx43 deficiency and malonate administration in ischemia-reperfusion injury

4.3.3.2.1 Study protocol

The effects of Cx43 deficiency and of malonate treatment on ischemia-reperfusion injury were assessed in 38 isolated mice hearts submitted, after a period of 30 min of equilibration, to 35 min of global ischemia followed by 60 min of reperfusion (*Figure 14*). During ischemia, hearts were immersed in hypoxic Krebs solution to maintain temperature at 37°C (NaCl 118 mmol/L; KCl 4.7 mmol/L; $MgSO_4$ 1.2 mmol/L; $CaCl_2$ 1.8 mmol/L; $NaHCO_3$ 25 mmol/L; KH_2PO_4 1.2 mmol/L; and sucrose 11 mmol/L; pH 7.4; bubbled with 95% N_2 : 5% CO_2). Hearts from both 4OHT-treated $Cx43^{Cre\text{-}ER(T)/fl}$ and $Cx43^{fl/fl}$ mice were infused or

not, during the first 15 min of reperfusion, with the succinate dehydrogenase reversible inhibitor malonate, added to the Krebs at 3 mmol/L, as previously described [280]. Results obtained were compared between both wild-type and Cx43-deficient animals, and between control and malonate-treated hearts.

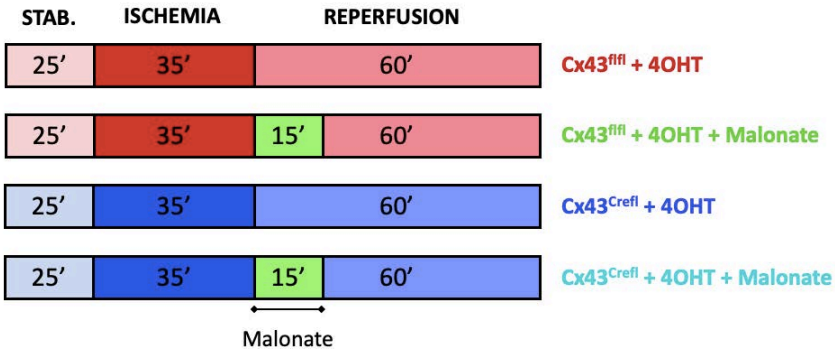

Figure 14: Experimental protocol of ischemia-reperfusion conducted in isolated hearts of $Cx43^{fl/fl}$ and $Cx43^{Cre\text{-}ER(T)/fl}$ ($Cx43^{Cre/fl}$) mice. Hearts were submitted, after 25 minutes of stabilization (Stab.) to 35 minutes of global ischemia and 60 minutes of reperfusion. Hearts of both genotypes were administered or not with malonate 3 mmol/L added to the Krebs solution during the first 15 minutes of reperfusion.

LV developed pressure (LVdevP) was calculated as the difference between systolic and telediastolic pressures. Functional recovery was expressed as percentage of baseline LVdevP value.

4.3.3.2.2 Lactate dehydrogenase release

Cell death at baseline and during reperfusion was evaluated by assessing lactate dehydrogenase (LDH) release. LDH, a cytoplasmatic enzyme, is rapidly released to the extracellular space, and to the coronary effluent, when the plasma membrane is ruptured due to cellular damage, and for this reason it is used as an indirect marker of cell injury. Thereby, coronary effluent was collected both during equilibration and at different timepoints during reperfusion, and LDH release was quantified by spectroscopy in a 96-well plate. The reaction (37°C) began when samples (10-20 µL) were added to phosphate buffer (0.1 mol/L, pH 7.4) containing NADH (310 µmol/L) and pyruvate (1 mmol/L). The decrease in NADH absorbance at 340 nm was then monitored for 5 minutes. LDH activity was

expressed as LDH units/minute of effluent*mg of dry tissue [280] (*Figure 15*). Dry myocardial tissue weight was obtained after 24-hour dehydration at 100°C.

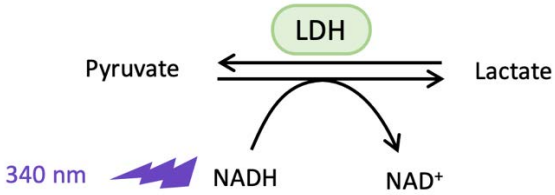

Figure 15: Reaction catalyzed by lactate dehydrogenase (LDH), showing the transformation of pyruvate to lactate and of NADH to NAD+. Consumption of NADH can be monitored at 340 nm, with the slope of its consumption correlating with the amount of LDH in the sample.

4.3.3.2.3 Infarct size

At the end of the 60 minutes of reperfusion, hearts were collected and cut into four 1-1.5 mm thick transversal slices, which were weighted and incubated with TTC at 37°C, for 15 minutes, as described in Section 1.4. Then, pictures of the stained slices were obtained, and infarct size was measured with the software *ImagePro® Plus* (*Media Cybernetics*, Rockville, Maryland, United States). In this case, as hearts were submitted to global ischemia, fluorescein was not needed to delineate area at risk, as the size of the area at risk correspond to the total slice area. Infarct size was expressed as percentage of total ventricular weight [280].

4.3.3.3 Succinate accumulation in ischemic myocardium

Succinate accumulation during ischemia was analysed in 16 additional hearts by ^{1}H-NMR [280]. Hearts from 4OHT-treated Cx43$^{Cre\text{-}ER(T)/fl}$ and Cx43$^{fl/fl}$ mice were submitted to 60 minutes of normoxic perfusion or to 25 minutes of stabilization followed by 35 minutes of global ischemia without reperfusion (*Figure 16*). Hearts were immediately collected and frozen in liquid nitrogen until analysis.

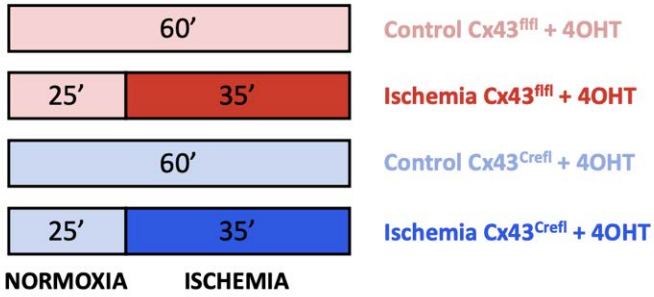

Figure 16: Experimental protocol conducted in isolated hearts from $Cx43^{fl/fl}$ and $Cx43^{Cre\text{-}ER(T)/fl}$ ($Cx43^{Cre/fl}$) mice to assess myocardial succinate concentrations. Hearts were submitted to 60 minutes of normoxic perfusion or to 25 minutes of stabilization followed by 35 minutes of ischemia.

Cardiac metabolites were, then, extracted using the methanol:chloroform method [280]. In this case, frozen tissue samples were pulverized and 2 mL of a methanol:chloroform (2:1) mixture was added. After 30 minutes of incubation at RT, 0.83 mL of chloroform and 1.25 mL of water were added, and the resulting suspension was thoroughly vortexed. Samples underwent centrifugation at 1200 g for 5 minutes (RT). Two distinct phases were then obtained: the upper one formed by methanol and water, which contains the hydrophilic metabolites, and the lower one, containing chloroform and the organic metabolites. The hydrophilic phase was set aside, and the extraction process was repeated with the intermediate phase formed by the residual tissue to improve the extraction efficiency. The resulting hydrophilic phases were grouped together. The methanol component was evaporated using a *SpeedVac*® Concentrator *Savant™ SPD111V* (*Thermofisher*, Waltham, Massachusetts, USA), while the water was lyophilized. Samples were again stored at -80°C until analysis.

For ^{1}H-NMR analysis, extracts were dissolved in 180 µL of deuterium oxide containing 0.5 mmol/L of TSP as a standard and ^{1}H-NMR spectra were acquired on a vertical bore 9.4T magnet interfaced to a *Bruker* Avance 400 spectrometer (*Bruker*, Billerica, Massachusetts, USA) as described above (chapter 2.2.4).

4.3.3.4 ROS production in cardiac tissue

To quantify ROS production in cardiac tissue, hearts from three additional 4OHT-treated $Cx43^{Cre\text{-}ER(T)/fl}$ and $Cx43^{fl/fl}$ mice were submitted to 65 min of normoxic perfusion or to 25 minutes of stabilization and 35 min of global ischemia followed by 5 min of reperfusion (*Figure 17*). Hearts were quickly removed, fixed in 4% paraformaldehyde, embedded in paraffin, and cut in sections (5 µm). Myocardial sections were incubated with dihydroethidium (DHE, 5 µmol/L, (#D23107 Invitrogen™, Waltham, Massachusetts, USA) for 30 min (at RT and darkness) to assess ROS production by confocal microscopy (Zeiss LMS 980 Airyscan 2 (Oberkochen, Germany)) as previously described (excitation wavelength 488 nm, emission wavelength 540-640 nm) [280]. Five representative images were obtained from each heart.

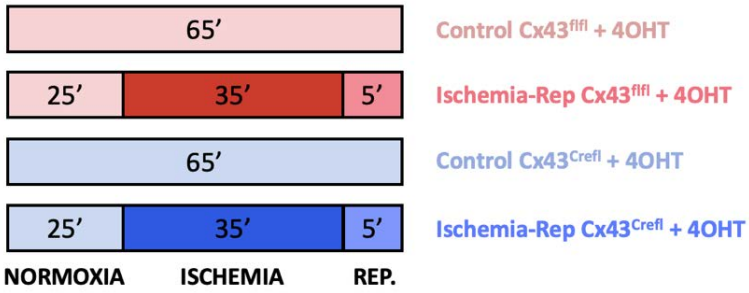

Figure 17: Experimental protocols conducted in isolated hearts from $Cx43^{fl/fl}$ and $Cx43^{Cre\text{-}ER(T)/fl}$ ($Cx43^{Cre/fl}$) mice to assess ROS production in cardiac tissue. Hearts were submitted to 65 minutes of normoxic perfusion or 25 minutes of stabilization followed by 35 minutes of ischemia and 5 min of reperfusion (REP.).

4.3.4 STATISTICAL ANALYSIS

Data are expressed as mean ± SEM. Normal distribution was assessed by Kolmogorov–Smirnov test. Differences were assessed by Student's t test (RCR in oxygen consumption experiments, CS activity, MY quantification, and CoQ levels and its redox state), Mann-Whitney U test (ROS production by RET), and ANOVA and Tukey post-hoc tests (oxygen consumption, ROS production in isolated mitochondria, membrane potential, infarct size, myocardial succinate levels, and ROS production in tissue). Changes in the time course of LDH release and

functional recovery were assessed by repeated measures-ANOVA and Tukey post-hoc test. Differences were considered significant when $p<0.05$.

4.4 MODULATION OF RET BY EXTERNAL FACTORS: EFFECTS OF AIR POLLUTION

4.4.1 RAT MODEL OF EXPOSURE TO DIESEL EXHAUST PARTICLES

The present study conforms to the Directive 2010/63/EU of the European Parliament on protection of animals used for scientific purposes and to the NIH Guide for the Care and Use of Laboratory Animals (NIH publications No. 85-23, revised 1996, updated in 2011). The study was approved by the Ethics Committee of the Vall d'Hebron Institut de Recerca (CEEA 49/20).

Animals were kept with undisturbed social interaction (2 animals per cage) in conventional cages and maintained in a temperature and humidity-controlled environment (22-24°C, and 60-65%, respectively), on a 12h-light/dark cycle. All animals had *ad libitum* access to tap water and standard diet throughout the whole experimental period.

Experiments were performed in Sprague-Dawley rats intratracheally instilled with saline containing or not diesel exhaust particles (DEP) to mimic air pollution exposure. Following an acclimatization period of 1 month, 10-week-old rats (both sexes, 50% each) were intratracheally instilled with saline, containing or not DEP (7,5 mg/kg, 0,375 mL/kg, 20 mg/mL), 3 days per week for a period of 3 weeks (*Figure 18*). Instillation was performed under general anaesthesia with ketamine (75 mg/kg, IP) and medetomidine (0,5 mg/kg, IP), while recovery was facilitated by the use of atipemazol (1 mg/kg, IP).

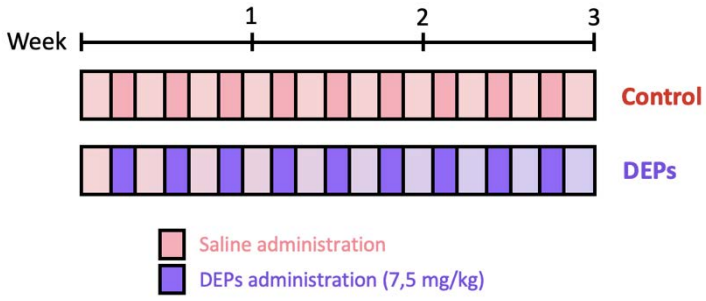

Figure 18: Schematic representation of the protocol used to expose rats to diesel exhaust particles (DEP), used as a surrogate of air pollution. Rats were intratracheally instilled with saline containing or not DEP, 3 times per week for 3 weeks.

Three weeks after exposure animals were euthanized by sodium pentobarbital overdose (1.5 g/Kg, IP) and the heart quickly removed and used for the different studies described below. In order to confirm exposure to DEP, lungs of all rats were also removed. A portion of the lungs was fixed and dehydrated in methanol for 48h and, afterwards, was incubated in a mixture of benzyl alcohol/benzyl benzoate (BA/BB, 2:1) for at least one week. BA/BB allows the tissue to become transparent, thus permitting to visualize DEP accumulation within it (*Figure 18*). In addition, another portion of the lungs was fixed in formaldehyde 4%, embedded in paraffin and cut into 4 µm sections. Slices were stained with picrosirius red (*Sigma-Aldrich*, Massachusetts, USA) and viewed under a microscope (*Eclipse Ts2R-FL, Nikon*, Tokyo, Japan) at 40x magnification to confirm DEP presence in the alveolar cavity (*Figure 19*).

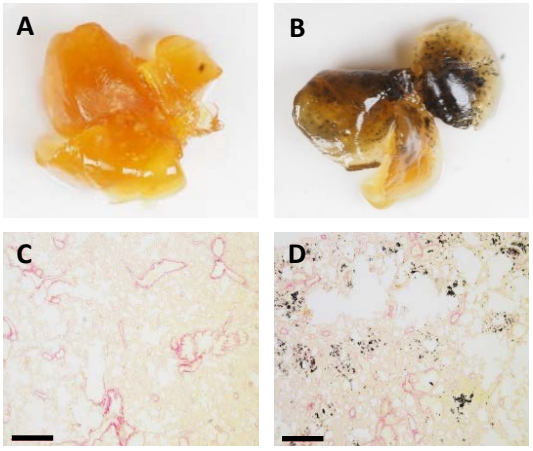

Figure 19: Representative lung images obtained from a saline-instilled rat (left) and from a DEP-instilled animal (right). Upper pictures (**A**, **B**) show macroscopic images after transparentation with BA/BB. Lower pictures (**C, D**) show microscopic analysis of the same lungs stained with picrosirius red (Bar indicates 500 µm).

4.4.2 ANALYSIS OF MITOCHONDRIAL FUNCTION

4.4.2.1 Isolation of subsarcolemmal and interfibrillar mitochondria

Rat SSM and IFM mitochondria were isolated, at the end of the DEP exposure period, from whole hearts by differential centrifugation according to the method initially described by Palmer et al. [55,280,357] and detailed in section 3.2.1. Protein

quantification of the mitochondrial homogenates was performed by the Bradford method (See section 3.2.2).

4.4.2.2 Citrate synthase activity

To evaluate mitochondrial content of the homogenates, CS activity was quantified by colorimetric analysis, as described in section 3.2.3.

4.4.2.3 Mitochondrial oxygen consumption

To evaluate the effect of DEP administration in mitochondrial function, mitochondrial respiration in both SSM and IFM was assessed as detailed in section 3.2.4, using substrates feeding complex I (malate 2 mmol/L and glutamate 5 mmol/L) or complex II (succinate 5 mmol/L plus rotenone 0.5 µmol/L) [280,357].

4.4.2.4 Mitochondrial ROS production

ROS production in isolated SSM and IFM mitochondria from saline and DEP exposed animals was assessed using the Amplex™ Red assay previously described in section 3.2.5. (15). H_2O_2 concentration was calculated using standard H_2O_2 curves and expressed, respect to baseline fluorescence, as nmols H_2O_2/min*UCS. In addition, basal ROS production was determined as Amplex™ Red fluorescence of mitochondrial preparations before substrate addition and divided by UCS.

4.4.3 MYOCARDIAL ISCHEMIA-REPERFUSION INJURY IN ISOLATED RAT HEARTS

4.4.3.1 Isolated, Langendorff-perfused, rat heart preparation

Myocardial ischemia-reperfusion injury was induced in isolated male rat hearts from saline and DEP-exposed animals using a Langendorff perfusion system, as described in section 3.3. Once the period of 3 weeks of intratracheal instillation was completed, control and DEP-instilled animals were euthanized with sodium pentobarbital overdose (1.5 g/kg, IP). At that time, rats had 13 weeks of age and weighted 400-500 g. All animals were submitted to a bilateral thoracotomy and

the hearts were quickly removed, transferred into ice-cold saline solution and immediately (under less than 3 minutes) cannulated through the aorta. The myocardium was retrogradely perfused with a Krebs solution at 37°C as described in section 3.3 [280]. Baseline flow (about 10 mL/min) was adjusted to produce, in this case, a perfusion pressure of 40-60 mmHg (*Figure 20*).

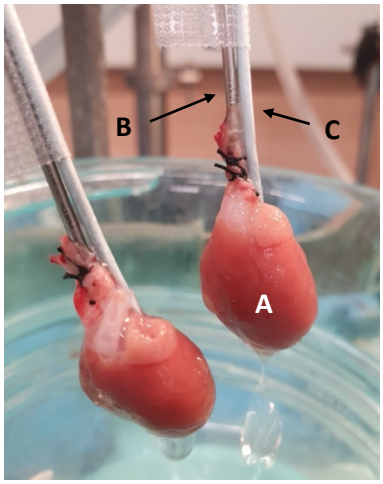

Figure 20: Langendorff system for retrograde perfusion of isolated rat hearts. The heart (**A**), canulated through the aorta (**B**), receives oxygenated Krebs buffer which is distributed via the coronary arteries throughout the myocardium. A latex balloon connected to a cannula (**C**) is inserted in the left ventricle to monitor ventricular pressure.

The effects of DEP administration on ischemia-reperfusion injury were assessed in 15 isolated rat hearts submitted, after a period of 25 min of equilibration, to 60 min of global ischemia followed by 90 min of reperfusion (*Figure 21*). During ischemia, hearts were immersed in hypoxic Krebs solution to maintain temperature at 37°C, as described in section 3.3. [280].

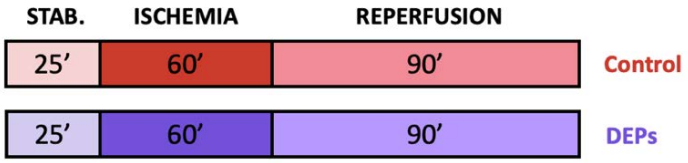

Figure 21: Experimental protocol of ischemia-reperfusion performed in isolated rat hearts from animals previously instilled, for three weeks, with saline containing or not DEP. Hearts were submitted to 25 minutes of stabilization (Stab.) followed by 60 minutes of ischemia and 90 minutes of reperfusion.

4.4.3.2 Lactate dehydrogenase release and infarct size

Cell death at baseline and during reperfusion was evaluated by LDH release measurements, as previously detailed in section 3.3.2 (15). Infarct size was determined at the end of reperfusion by TTC staining as described in section 3.3.3 [280].

4.4.4 STATISTICAL ANALYSIS

Data are expressed as mean ± SEM. Normal distribution was assessed by Kolmogorov–Smirnov test. Differences were assessed by Student's t test (infarct size, functional recovery, cumulative LDH release, CS activity and MY quantification) or two-way ANOVA and ANOVA followed by DMS post-hoc tests (oxygen consumption, ROS production in isolated mitochondria and basal ROS production). Changes in the time course of LDH release and functional recovery were assessed by repeated measures ANOVA and Tukey post-hoc test. Differences were considered significant when $p<0.05$.

5. RESULTS

5.1 EFFECTS OF THE COMBINATION OF SUCCINATE DEHYDROGENASE INHIBITION WITH MALONATE AND REMOTE ISCHEMIC CONDITIONING ON MYOCARDIAL ISCHEMIA-REPERFUSION INJURY

5.1.1 HEMODYNAMIC PARAMETERS, CORONARY BLOOD FLOW, AND REGIONAL MYOCARDIAL CONTRACTILITY

Ischemia-reperfusion injury after transient coronary occlusion was assessed in control pigs and in animals treated with either malonate 10 mmol/L, RIC or a combination of both treatments with the aim to evaluate the possible presence of additive effects. *Figure 22* depicts a representative recording obtained from a control animal which illustrate the changes induced by a 40-minute ischemic episode followed by 120 minutes of reperfusion in the analyzed variables.

Baseline values for heart rate, hemodynamic variables, coronary blood flow and SS were similar in all groups and are shown in *Table 5*. As expected, ischemia-reperfusion induced significant reductions in aortic pressure, LV systolic pressure and LV (+)dP/dt compared to baseline values, and increases in heart rate and LV (−)dP/dt. Coronary blood flow, which completely disappeared during ischemia, depicted a clear hyperemic reaction during initial reperfusion. However, the time course of all these changes was similar in all experimental groups (*Table 5, Figure 23*).

Systolic segment shortening in distant, control myocardium, assessed by ultrasonic piezoelectric crystals, was only slightly reduced during ischemia-reperfusion (*Table 5, Figure 23E*). In contrast, myocardial function in the area at risk was markedly depressed during ischemia, with no recovery during reperfusion (*Table 5, Figure 23F*). Neither intracoronary malonate, RIC, nor combined treatment, led to an improvement in myocardial function in this region throughout the 2 h reperfusion period (*Table 5, Figure 23F*).

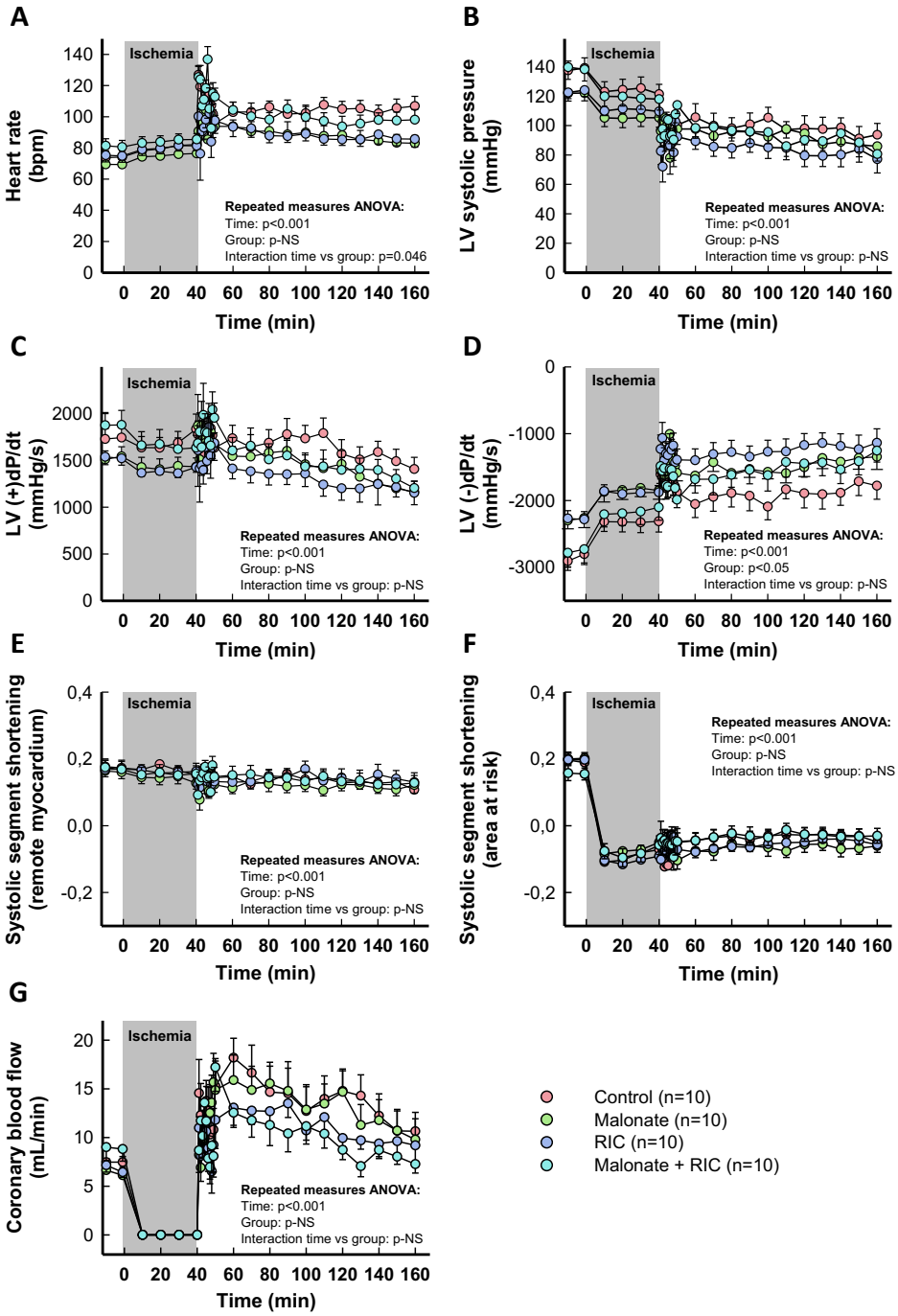

Figure 23: Effects of intracoronary malonate, given at the onset of reperfusion, remote ischemic conditioning (RIC), or combined treatment, on heart rate (**A**), left ventricular (LV) systolic pressure (**B**), LV (+)dP/dt (**C**), LV (−)dP/dt (**D**), systolic segment shortening in remote myocardium (**E**) and area at risk (**F**), and coronary blood flow (**G**) in pigs submitted to 40 min of LAD coronary artery occlusion followed by 2 h of reperfusion.

5.1.2 INFARCT SIZE

Infarct size was determined with TTC staining, as shown in *Figure 24A*. Control pigs submitted to 40 min of LAD coronary artery occlusion followed by reperfusion had an average infarct size of 46.47 ± 14.21% of the area at risk, which was significantly reduced by both 10 mmol/L of intracoronary malonate, given during initial reperfusion, and RIC (*Figure 24B*). However, combined treatment (malonate + RIC) did not induce any additive effect, with infarct size being similar to individual treatments (*Figure 24A, B*).

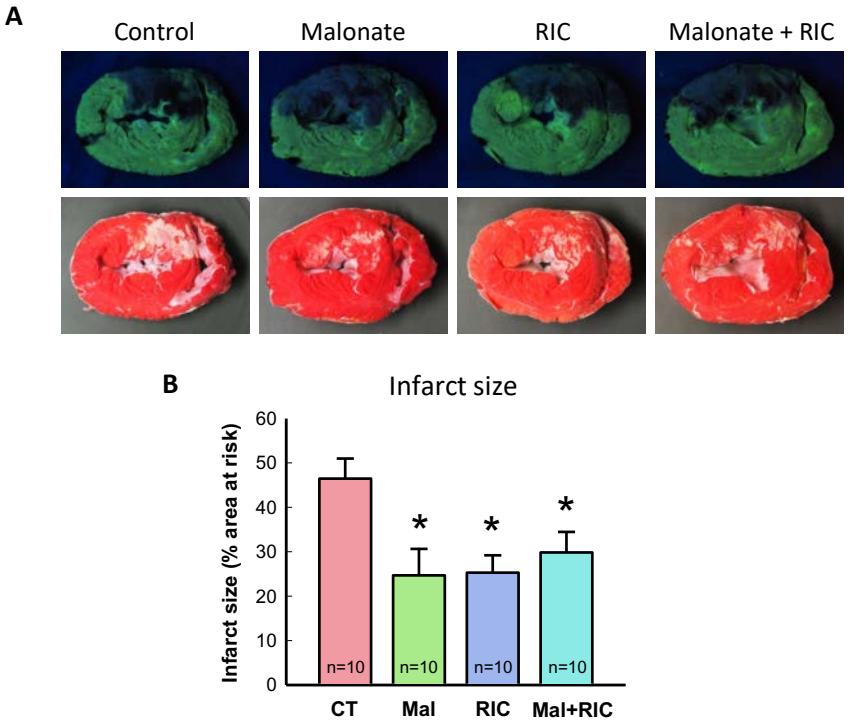

Figure 24: Representative images of porcine cardiac cross sections depicting the area at risk, in black, contrasted with the rest of the heart stained with fluorescein (upper pictures), and infarct size, in white, contrasted with the living tissue stained with 1% 2,3,5-triphenyltetrazolium chloride (TTC) (lower pictures) (**A**), and infarct size quantification expressed as percentage of area at risk (**B**), in pigs submitted to 40 minutes of left anterior descending (LAD) coronary artery occlusion followed by 2 h of reperfusion and treated with saline (control group), intracoronary malonate, remote ischemic conditioning (RIC), and the combination of both (Mal+RIC). *($p < 0.05$) indicates significant differences vs. control animals.

No differences were observed between experimental groups in the size of the area at risk (*Figure 25A*) or body temperature during ischemia, both factors potentially having great influence on final infarct size (*Figure 25B*).

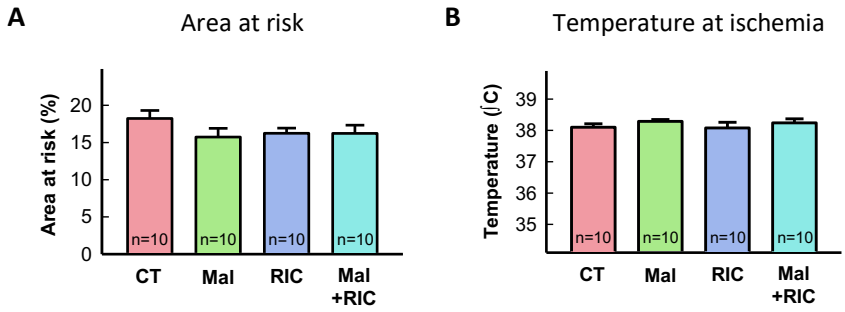

Figure 25: Area at risk expressed as percentage of total ventricular weight (**A**) and body temperature during ischemia (**B**) in pigs submitted to 40 minutes of left anterior descending (LAD) coronary artery occlusion followed by 2 h of reperfusion and treated with saline, intracoronary malonate (Mal) given at the onset of reperfusion, remote ischemic conditioning (RIC), or the combination of both.

5.1.3 INCIDENCE OF MALIGNANT REPERFUSION ARRYTHMIAS

To assess the possibility of deleterious effects of the analyzed treatments, the incidence of ventricular malignant reperfusion arrythmias was assessed. No significant differences were observed in the total number of ventricular tachyarrhythmias (VT + VF) during the first 20 min of reperfusion (*Figure 26A, B*). However, the incidence of VF during initial reperfusion was significantly higher in animals treated with malonate (8 out of 10 animals developed VF) and RIC (10 out of 10) as compared with controls (2 out of 10, $p<0.01$) (*Figure 26A*). This enhancement was associated with a trend towards a lower number of VT in these two groups, which reaches significance in malonate-treated pigs ($p<0.05$).

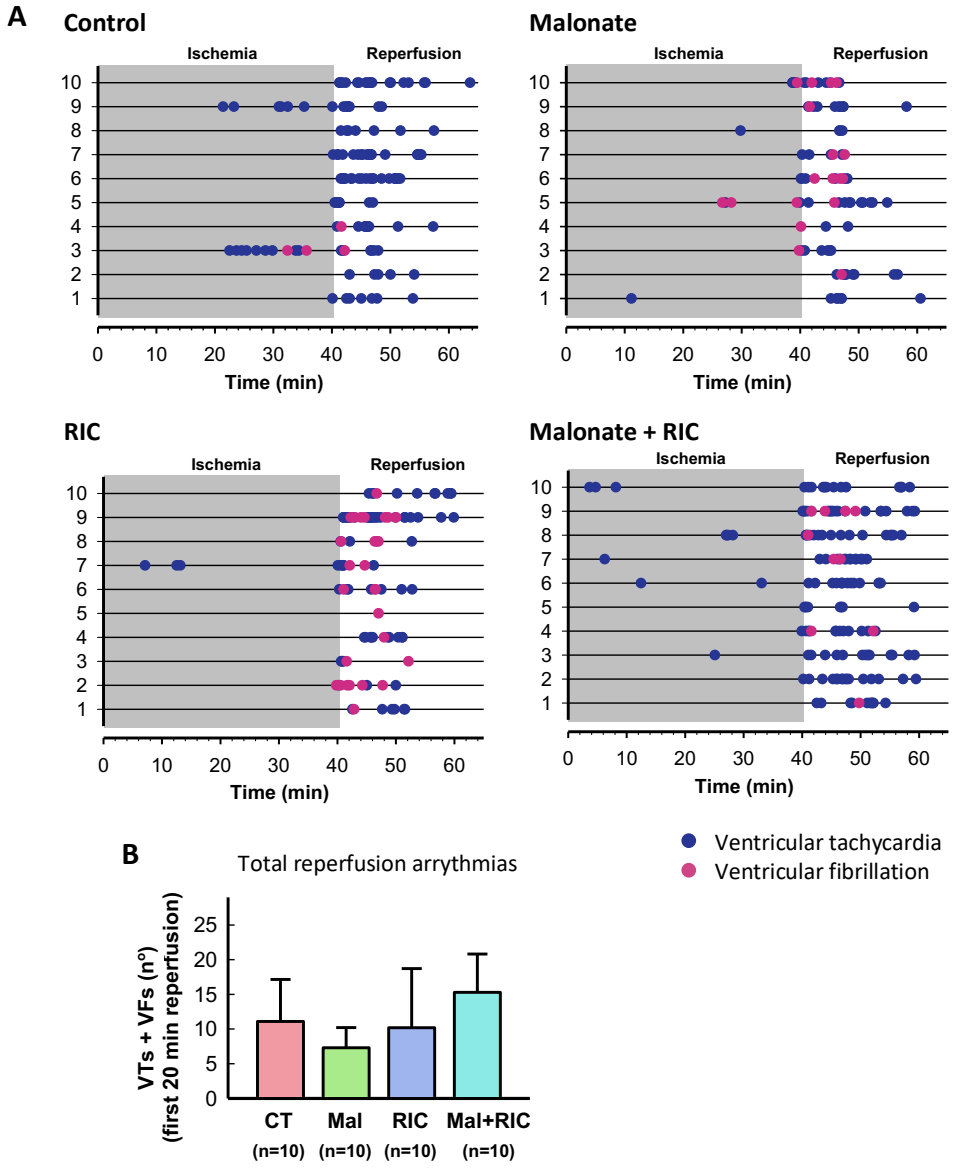

Figure 26: Incidence of ventricular tachyarrhythmias (ventricular tachycardias (VTs) and ventricular fibrillations (VFs)) during ischemia and the first 20 min of reperfusion in control pigs submitted to 40 min LAD coronary artery occlusion followed by reperfusion, and in animals treated with intracoronary malonate, given at the onset of reperfusion, remote ischemic conditioning (RIC), or its combination. (**A**): Detailed incidence of VTs and VFs in each animal of each experimental group. (**B**) Total number of ventricular tachyarrhythmias during the first 20 min of reperfusion.

5.2 ASSESSMENT OF THE POTENTIAL UTILITY OF PLASMA SUCCINATE LEVELS AS PROGNOSTIC BIOMARKER

5.2.1 ANALYSIS OF CITRIC ACIC CYCLE METABOLITES IN PORCINE PLASMA SAMPLES

To investigate the potential utility of succinate and other citric acid cycle intermediates as biomarkers of injury, we first tried to correlate plasma levels of these metabolites, as assessed in blood samples obtained from our pig model of transient coronary occlusion, with the degree of irreversible injury.

Analysis of peripheral blood samples obtained from control pigs submitted to transient coronary occlusion did not show any significant change in plasma concentrations for succinate, fumarate, malate, or lactate during the first 10 min of reperfusion (*Figure 27A-C, E*), whereas a slight and continuous increase in citrate was observed in these samples following ischemia (*Figure 27D*). Only modest enhancements in fumarate (from 0.80 ± 0.50 µmol/L at baseline to 1.97 ± 1.93 at the end of the experiment, Student's t test, p=0.039) and malate (from 2.45 ± 0.75 µmol/L to 4.89 ± 3.49, Student's t test, p=0.031) were noticeable 2 h after reperfusion.

In contrast, plasma samples obtained from the great cardiac vein depicted, in this group of animals, a marked increase in all analyzed metabolites, peaking, in most cases, at 5 min of reperfusion (*Figure 27A-E*). Small differences in baseline values between peripheral and great cardiac vein samples were apparent for succinate, fumarate, and especially, lactate, with higher concentrations in the peripheral blood in all cases. Malonate was not detected in these animals at any time.

As these results demonstrate that citric acid cycle metabolites are only enhanced in plasma samples obtained from the great cardiac vein, we decided to assess the influence of malonate, RIC, or combined treatment only in blood from this source. Accordingly, repeated measures ANOVA analysis demonstrated significantly enhanced levels of succinate during reperfusion in all experimental groups, but with no differences between treatments (*Figure 28A*). In contrast, the increase in fumarate and malate detected during initial reperfusion in control

animals was significantly attenuated by cardioprotective maneuvers, especially malonate and malonate + RIC. Indeed, repeated measures ANOVA demonstrated

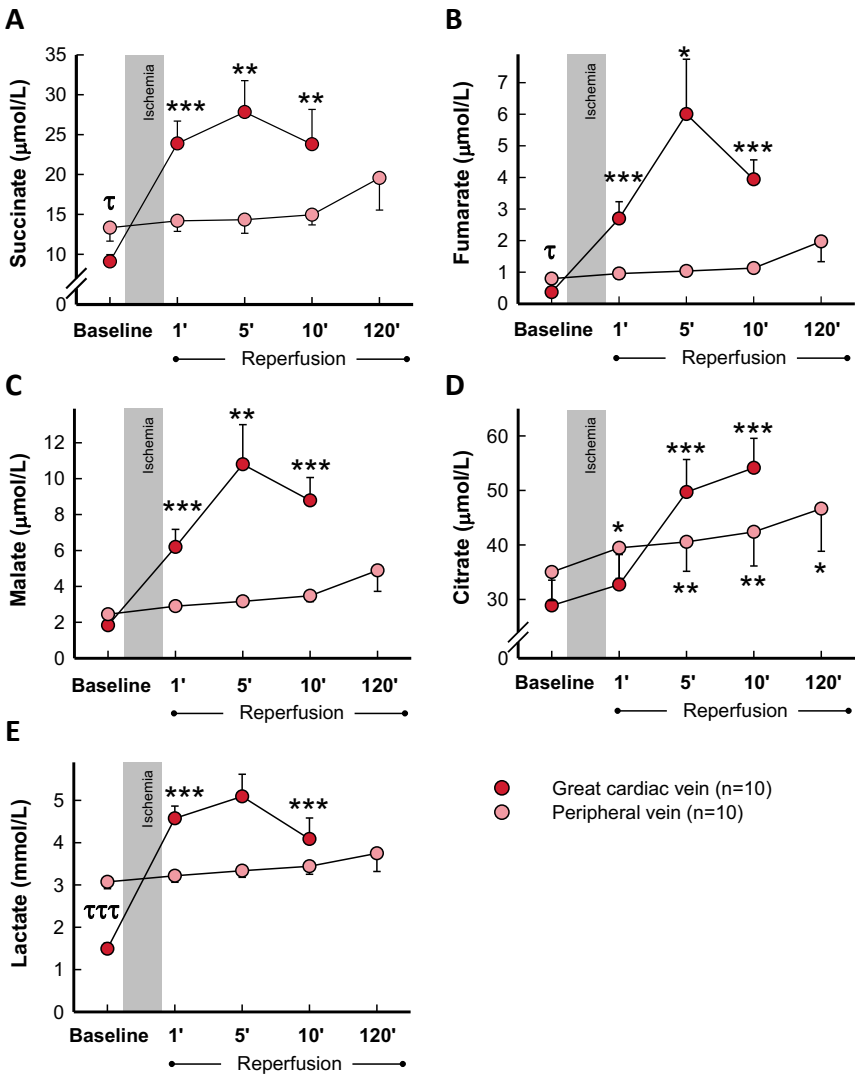

Figure 27: Concentrations of the citric acid cycle metabolites succinate (**A**), fumarate (**B**), malate (**C**), and citrate (**D**), together with lactate (**E**), assessed by UPLC-MS/MS, in plasma samples obtained from the great cardiac and femoral veins in control pigs submitted to 40 min of left anterior descending (LAD) coronary artery occlusion followed by 2 h of reperfusion. * ($p < 0,05$), ** ($p<0.01$) and *** ($p<0.001$) indicate significant differences vs. the corresponding baseline value (repeated measures ANOVA and Tukey tests). τ ($p<0.05$) and ττ ($p<0.001$) indicate significant differences between both baseline values (Student's t test).

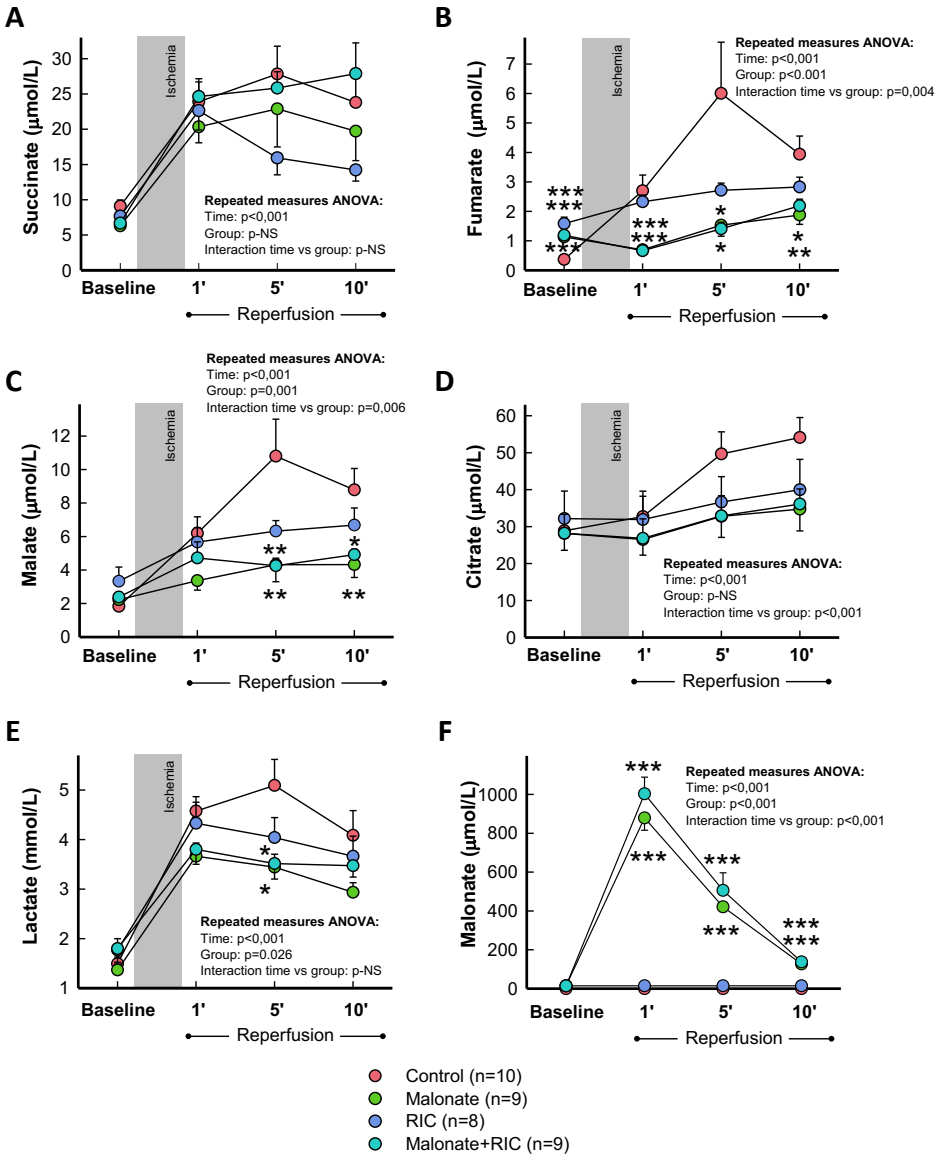

Figure 28: Concentrations of the citric acid cycle metabolites succinate (**A**), fumarate (**B**), malate (**C**), and citrate (**D**), together with lactate (**E**) and malonate (**F**) assessed by UPLC-MS/MS, in plasma samples obtained from the great cardiac vein in control pigs, submitted to 40 min of left anterior descending (LAD) coronary artery occlusion followed by 2 h of reperfusion, and in animals treated with intracoronary malonate, given at the onset of reperfusion, remote ischemic conditioning (RIC), or malonate + RIC. * ($p < 0,05$), ** ($p<0.01$) and *** ($p<0.001$) indicate significant differences vs. the corresponding value in the control group (ANOVA and Tukey tests).

a significant effect of group allocation for both fumarate and malate, together with positive interactions between group allocation and the time course of concentration changes (*Figure 28B, C*). In addition, the enhancement in citrate levels observed in control animals was also attenuated in all treated groups (*Figure 28D*). Regarding lactate, a marginally significant effect of group allocation was detected, with significant differences at 5 minutes in malonate and malonate + RIC treatments (*Figure 28E*). Measurement of malonate, used as a positive control, demonstrated an increase in its plasma concentration only in animals treated with this reversible SDH inhibitor (*Figure 28F*).

When analyzed independently of the control group, pooled samples from the two groups receiving malonate showed a trend to have higher succinate concentrations than those receiving RIC alone (repeated measures ANOVA, $p=0.051$ for interaction), and significantly reduced levels of fumarate (repeated measures ANOVA, $p=0.014$ for interaction and $p<0.001$ for group allocation) and malate (repeated measures ANOVA, $p=0.019$ for group allocation).

Interestingly, concentrations of succinate, fumarate, malate, and lactate, obtained 5 min after reperfusion from the great cardiac vein, significantly correlated with infarct size, expressed as percentage of ventricular weight, with good correlation coefficients, particularly for succinate levels (*Figure 29A-D*). Similar data were obtained when infarct size was expressed in grams (not shown). In contrast, only succinate and lactate concentrations correlated with the size of the area at risk, although in these cases correlation coefficients were slightly lower (*Figure 29E, F*).

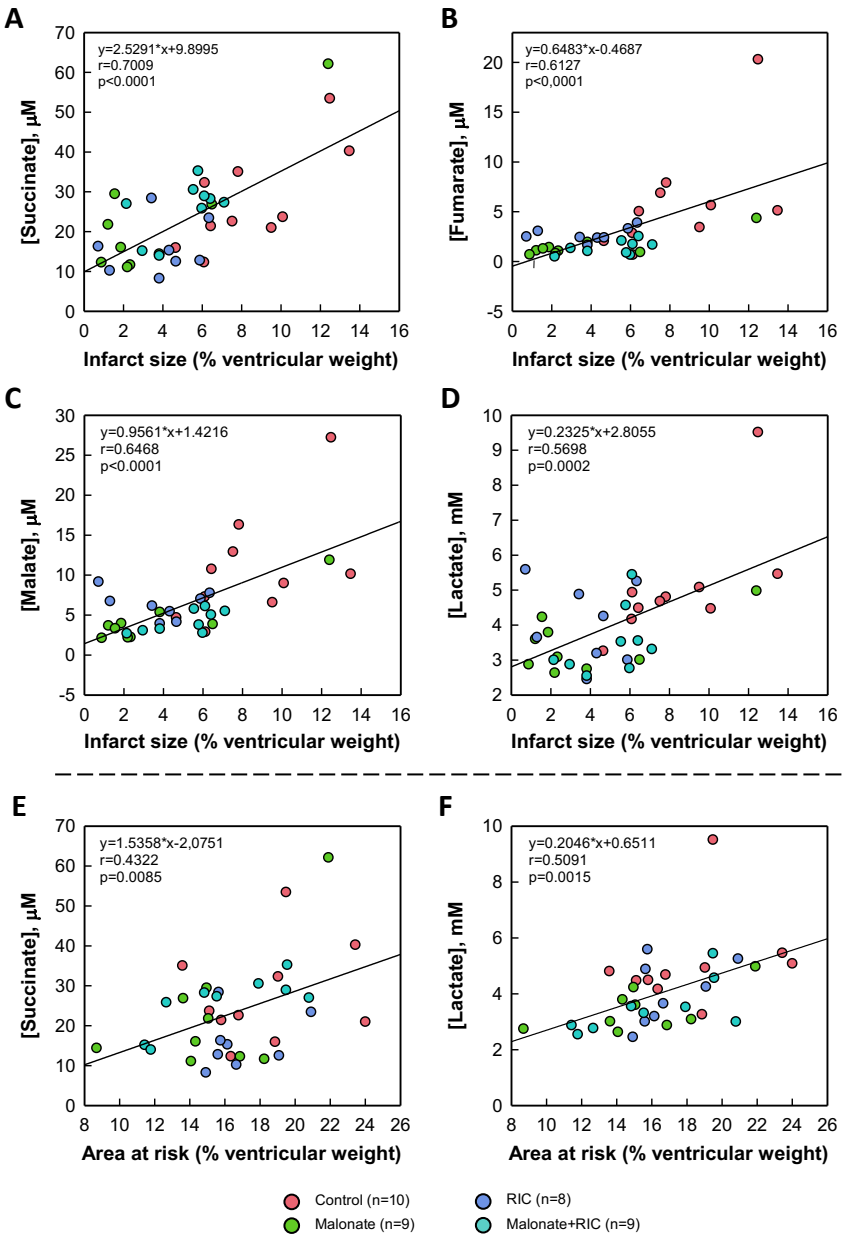

Figure 29: Correlations between infarct size (upper panels), expressed as percentage of total cardiac weight, and succinate (**A**), fumarate (**B**), malate (**C**), and lactate (**D**) concentrations, together with correlations between area at risk (lower panels), calculated as percentage of ventricular weight, and succinate (**E**) and lactate (**F**) concentrations. All metabolites were measured 5 min after reperfusion in plasma obtained from the great cardiac vein in pigs from the four experimental groups.

5.2.2 PROGNOSTIC VALUE OF PLASMA SUCCINATE AND OTHER METABOLITES IN STEMI PATIENTS

Our previous data in the porcine model suggest that plasma levels of succinate and other citric acid intermediates are enhanced in the blood obtained from the great cardiac vein 5 min after reperfusion, and that their concentrations are reduced by protective maneuvers and correlates with final infarct size. However, obtaining blood from the coronary sinus is not included in the routine practice, is not always feasible and is not without risks. As most STEMI patients have a peripheral via, and as succinate concentration is also enhanced in blood from this origin [320], here we assessed whether the concentration of succinate and other metabolites, obtained during the coronary procedure, correlates with myocardial edema or infarct size, as determined by CMR, in patients undergoing emergency primary percutaneous coronary intervention in our center and included in the COMBAT-MI clinical trial [316].

5.2.2.1 Patient characteristics

Plasma samples, obtained from a peripheral via, were available for a total of 102 out of the original 222 STEMI patients undergoing emergency pPCI included in the COMBAT-MI clinical trial (TIMI flow ≤ 1), and for 9 additional patients with TIMI flow ≥ 2. From the 102 analyzed samples from patients with TIMI flow ≤ 1, 30 belong to the Sham + Placebo group, 30 to the Sham + Exenatide, 24 to the RIC + Placebo, and 18 to the RIC + Exenatide. Baseline characteristics and comorbidities were similar between patients, either when compared between the four treatment groups (*Table 6*) or between TIMI flow ≤ 1 and TIMI flow ≥ 2 (*Table 7*).

Table 6: Baseline characteristics and comorbidities of patients included in the Sham + Placebo, Sham + Exenatide, RIC + Placebo, and RIC + Exenatide groups.

Baseline characteristics:		**Sham + Placebo (n=30)**	**Sham + Exenatide (n=30)**	**RIC + Placebo (n=24)**	**RIC + Exenatide (n=18)**	**p value**
Male, nº (%)		27 (90.00)	24 (80.00)	22 (91.67)	14 (77.78)	NS
Age (years)		59.00±2.28	61.10±1.84	65.42±2.21	62.83±3.03	NS
Body weight (kg)		79.73±2.16	81.33±2.25	75.92±2.49	76.92±3.14	NS
Height (cm)		169.50±1.44	169.97±1.39	167.79±1.57	168.06±2.09	NS
BMI (kg/m^2)		27.67±0.54	28.08±0.61	27.01±0.90	27.14±0.87	NS
Body surface area (m^2)		1.93±0.03	1.96±0.03	1.88±0.03	1.89±0.05	NS
Comorbidities:						
Smoking. nº (%)	Active	14 (46.67)	12 (40.00)	12 (50.00)	6 (33.33)	NS
	Ex-smoker	13 (43.33)	9 (30.00)	6 (25.00)	6 (33.33)	
Hypertension. nº (%)		14 (46.67)	12 (40.00)	11 (45.83)	7 (38.89)	NS
Dyslipidemia. nº (%)		16 (53.33)	18 (60.00)	15 (62.50)	10 (55.56)	NS
Diabetes. nº (%)	With diet	2 (6.67)	0 (0.00)	2 (8.33)	1 (5.56)	NS
	Insulin	0 (0.00)	1 (3.33)	3 (12.50)	0 (0.00)	
	OAD	3 (10.00)	6 (20.00)	6 (25.00)	2 (11.11)	
	Insulin+OAD	0 (0.00)	1 (3.33)	0 (0.00)	0 (0.00)	
Killip class	1	26 (86.67)	25 (83.33)	18 (75.00)	14 (77.78)	NS
	2	3 (10.00)	2 (6.67)	2 (8.33)	4 (2.22)	
	3	0 (0.00)	0 (0.00)	1 (4.17)	0 (0.00)	
	4	0 (0.00)	2 (6.67)	2 (8.33)	0 (0.00)	

BMI: body mass index; OAD: oral antidiabetic drugs; RIC: remote ischemic conditioning.
Data are shown as mean ± SEM.

***Table 7**:* Baseline characteristics and comorbidities of patients with initial TIMI flow ≤1 vs. those with TIMI flow at admission ≥ 2.

Baseline characteristics:		**TIMI ≤ 1 (n=102)**	**TIMI ≥ 2 (n=9)**	**p value**
Male. nº (%)		87 (85.29%)	9 (100%)	NS
Age (years)		61.80±1.15	56.89±2.09	NS
Body weight (kg)		78.81±1.22	83.89±4.08	NS
Height (cm)		168.98±0.78	174.33±2.62	NS
BMI (kg/m²)		27.54±0.35	27.77±1.71	NS
Body surface area (m²)		1.92±0.02	2.01±0.05	NS
Comorbidities:				
Smoking. nº (%)	Active	44 (43.14)	6 (66.67)	NS
	Ex-smoker	34 (33.33)	1 (11.11)	
Hypertension. nº (%)		44 (43.14)	5 (55.55)	NS
Dyslipidemia. nº (%)		59 (55.84)	6 (66.67)	NS
Diabetes. nº (%)	With diet	5 (4.90)	0 (0.00)	NS
	Insulin	4 (3.92)	0 (0.00)	
	OAD	17 (16.67)	2 (22.22)	
	Insulin+OAD	1 (0.98)	0 (0.00)	
Killip class	1	83 (81.37)	8 (88.89)	NS
	2	11 (10.78)	1 (11.10)	
	3	1 (9.80)	0 (0.00)	
	4	4 (3.92)	0 (0.00)	

BMI: body mass index; OAD: oral antidiabetic drugs.
Data are shown as mean ± SEM.

Similarly, procedural details and CMR outcomes were also similar between patients in all four treatment groups (*Table 8*) or between initial TIMI ≤ 1 and TIMI ≥ 2 (*Table 9*). The mean age of the pooled population was 61.41 ± 1.07 years, and 96 (85.5%) of the patients were male. The culprit vessel was the right coronary artery in 52 patients (46.9%), the left anterior descending coronary artery in 48 patients (43.2%) and the circumflex coronary artery in 11 patients (9.9%).

Table 8: Procedural details of the pPCI procedure and CMR outcomes in patients of all four treatment groups.

Procedural details		Sham + Placebo (n=30)	Sham + Exenatide (n=30)	RIC + Placebo (n=24)	RIC + Exenatide (n=18)	p value
Infarct –related artery	RCA	14 (46.70)	15 (50.00)	12 (50.00)	7 (38.90)	NS
	LDA	12 (40.00)	13 (43.30)	10 (41.70)	9 (50.00)	
	LCX	3 (10.00)	3 (10.00)	2 (8.30)	2 (11.10)	
Symptom-to-door (min)		151.9±13.7	149.3±13.6	154.9±12.1	148.7±19.1	NS
Symptom-to-ballon (min)		163.1±13.1	168.5±13.6	172.3±11.8	171.2±19.9	NS
TIMI flow (admission)	TIMI=1, nº(%)	30 (100.00)	30 (100.00)	24 (100.00)	18 (100.00)	NS
Nº of RIC cycles at rep.		2.87±0.16	2.70±0.17	2.63±0.16	3.06±0.17	NS
Sum of ST-seg. elevation		3.23±0.32	3.62±0.34	3.71±0.67	5.93±1.36 *	0.034
Systolic pres. (mmHg)		131.03±4.85	129.43±5.23	126.58±4.11	144.61±6.07	NS
Diastolic pres. (mmHg)		79.57±3.57	77.43±2.99	73.42±2.42	84.06±3.21	NS
Heart rate (beats/min)		72.00±2.38	71.93±3.19	70.25±3.15	75.17±3.81	NS
TIMI flow (post-proced.)	TIMI=1, nº(%)	0 (0.00)	0 (0.00)	0 (0.00)	1 (5.56)	NS
	TIMI=3, nº(%)	2 (6.67)	2 (6.67)	2 (12.5)	1 (5.56)	
	TIMI=4, nº(%)	27 (90.00)	28 (93.33)	22 (91.67)	16 (88.89)	
Outcomes						
CMR (days post-pPCI)		8.70±2.98	7.03±1.64	5.67±0.50	6.50±0.85	NS
Infarct size (% of LV mass)		20.21±1.94	24.55±1.99	22.60±2.15	28.51±3.29	NS
Infarct size (g)		27.33±3.13	30.64±3.10	28.04±2.71	35.15±4.25	NS
Myocardial salvage index (%)		12.51±1.71	6.15±0.86 *	9.02±1.28	7.79±1.25	0.006
Transmurality index		45.85±2.26	48.77±2.21	45.82±2.46	51.39±2.95	NS
Heart rate (beats/min)		65.21±2.42	63.67±1.93	68.71±2.70	66.61±2.18	NS
LVEDV (mL)		147.54±6.45	141.14±8.08	144.59±6.83	146.18±10.87	NS
LVEDV/BSA		76.10±2.98	71.95±3.74	77.09±3.38	77.06±5.06	NS
LVESV (mL)		79.81±5.71	79.69±5.85	81.54±6.20	85.36±7.96	NS
LVESV/BSA		40.96±2.66	40.46±2.76	43.46±3.22	44.82±3.82	NS
LVEF (%)		47.30±1.93	44.45±1.70	44.68±2.25	42.49±1.98	NS
Extent of edema (g)		41.07±3.96	35.62±3.21	36.31±2.78	42.03±4.88	NS
MVO (%)		0.95±0.35	1.04±0.35	0.58±0.25	0.58±0.17	NS
Cardiac mass (g)		127.80±4.54	122.20±5.28	125.89±5.57	122.80±8.02	NS
Cardiac mass/BSA		66.23±2.36	62.24±2.29	67.13±2.62	64.49±3.29	NS
Stroke volume (mL)		68.63±3.28	61.50±3.27	63.04±3.25	60.89±4.63	NS
Cardiac output (L/min)		4.34±0.18	3.83±0.19	4.26±0.23	3.97±0.24	NS

BSA: body surface area; CMR: cardiac magnetic resonance; LCX: left circumflex coronary artery; LDA: left descending coronary artery; LV: left ventricular; LVEDV: left ventricular end diastolic volume; LVEF: left ventricular ejection fraction; LVESV: left ventricular end systolic volume; MVO: relative microvascular obstruction; post-proced.: post-procedure; PCI: primary percutaneous coronary intervention; pres.: pressure; RCA: right coronary artery; rep.: reperfusion; RIC: remote ischemic conditioning; seg.: segment.

Data are shown as mean ± SEM. * ($p<0.05$) indicate significant differences vs. sham+placebo.

Table 9: Procedural details of the pPCI procedure and CMR outcomes in patients with TIMI ≤ 1 and TIMI ≥ 2.

Procedural details		TIMI ≤ 1 (n=102)	TIMI ≥ 2 (n=9)	p value
Infarct-related artery	RCA	48 (47.06)	4 (44.44)	NS
	LDA	44 (43.14)	4 (44.44)	
	LCX	10 (9.80)	1 (11.11)	
Symptom-to-door (min)		151.29±7.09	134.44±13.92	NS
Symptom-to-balloon (min)		168.25±7.01	153.33±14.29	NS
TIMI flow (admission)	TIMI=1, nº (%)	102 (100.00)	0 (0.00)	
	TIMI=2, nº (%)	0 (0.00)	9 (100.00)	
Nº of RIC cycles at rep.		2.79±0.09	2.56±0.24	NS
Sum of ST-seg. elevation		3.93±0.33	4.71±0.92	NS
Systolic pres. (mmHg)		131.91±2.58	136.22±5.09	NS
Diastolic pres. (mmHg)		78.28±1.60	89.00±4.92	NS
Heart rate (beats/min)		72.13±1.53	83.67±4.21	NS
TIMI flow (post-proced.)	TIMI=1, nº (%)	1 (0.98)	0 (0.00)	NS
	TIMI=3, nº (%)	7 (6.86)	2 (22.22)	
	TIMI=4, nº (%)	93 (91.18)	7 (77.78)	
Outcomes:				
CMR (days post-pPCI)		7.11±1.01	4.11±0.51	NS
Infarct size (% of LV mass)		23.60±1.14	22.99±3.48	NS
Infarct size (g)		29.88±1.62	30.09±4.95	NS
Myocardial salvage index (%)		9.09±.073	7.46±1.46	NS
Transmurality index		47.70±1.21	44.93±3.47	NS
Heart rate (beats/min)		65.83±1.17	72.11±7.49	NS
LVEDV (mL)		144.70±3.89	146.69±12.57	NS
LVEDV/BSA		75.28±1.83	72.46±5.23	NS
LVESV (mL)		81.18±3.10	86.98±13.71	NS
LVESV/BSA		42.09±1.50	42.09±1.50	NS
LVEF (%)		45.00±0.99	42.89±3.90	NS
Extent of edema (g)		38.56±1.85	37.56±4.86	NS
MVO (%)		0.82±0.16	0.81±0.60	NS
Cardiac mass (g)		124.79±2.79	129.48±6.11	NS
Cardiac mass/BSA		64.59±1.28	64.56±2.93	NS
Stroke volume (mL)		63.85±1.77	59.67±4.65	NS
Cardiac output (L/min)		4.11±0.10	4.14±0.32	NS

BSA: body surface area; CMR: cardiac magnetic resonance; LCX: left circumflex coronary artery; LDA: left descending coronary artery; LV: left ventricular; LVEDV: left ventricular end diastolic volume; LVEF: left ventricular ejection fraction; LVESV: left ventricular end systolic volume; MVO: relative microvascular obstruction; post-proced.: post-procedure; PCI: primary percutaneous coronary intervention; pres.: pressure; RCA: right coronary artery; rep.: reperfusion; RIC: remote ischemic conditioning; seg.: segment.
Data are shown as mean ± SEM.

5.2.2.2 Metabolic profile of plasma samples from STEMI patients by nuclear magnetic resonance spectroscopy.

Figure 30 shows a representative ^{1}H-NMR spectra obtained from plasma extracts from a STEMI patient with initial TIMI flow ≤1 and included in the COMBAT-MI clinical trial. In addition to succinate, other quantified metabolites were lactate, 3-hydroxybutirate, acetate, glucose, alanine, creatine, creatinine, threonine, and tyrosine.

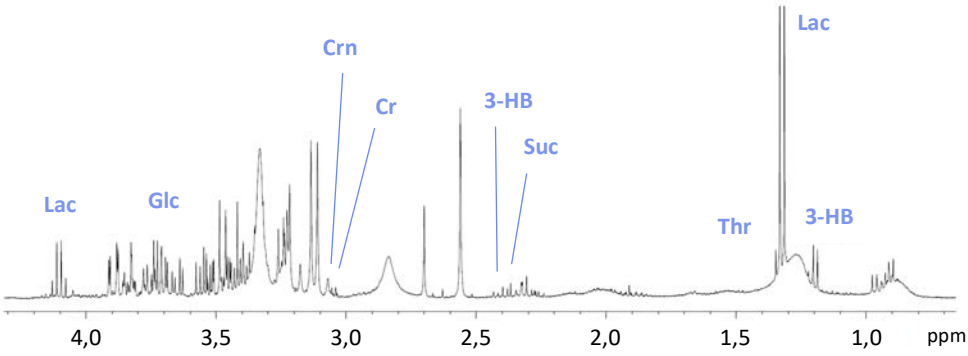

Figure 30: Representative ^{1}H-NMR spectra of a plasma sample obtained from a STEMI patient. Cr: Creatine; Crn; Creatinine; Glc: Glucose; Lac: Lactate; Suc; succinate; Thr: Threonine; 3-HB: 3-hydroxybutirate.

Succinate concentrations averaged 0.0882 ± 0.0188 mmol/L in the control group (Placebo + Sham), which was in the range found in previous studies in patients [359,360], and were not modified by the different treatments, either when applied individually or in combination (*Figure 31A*). Similar findings were obtained with remaining metabolites (*Figure 31B-J*).

In patients with TIMI flow ≤ 1, succinate concentration averaged 0.069 ± 0.0073 mmol/L, and was significantly enhanced in the 9 additional patients with TIMI flow ≥ 2 (*Figure 32*). Other metabolites, especially creatine, presented similar trends (*Figure 32*).

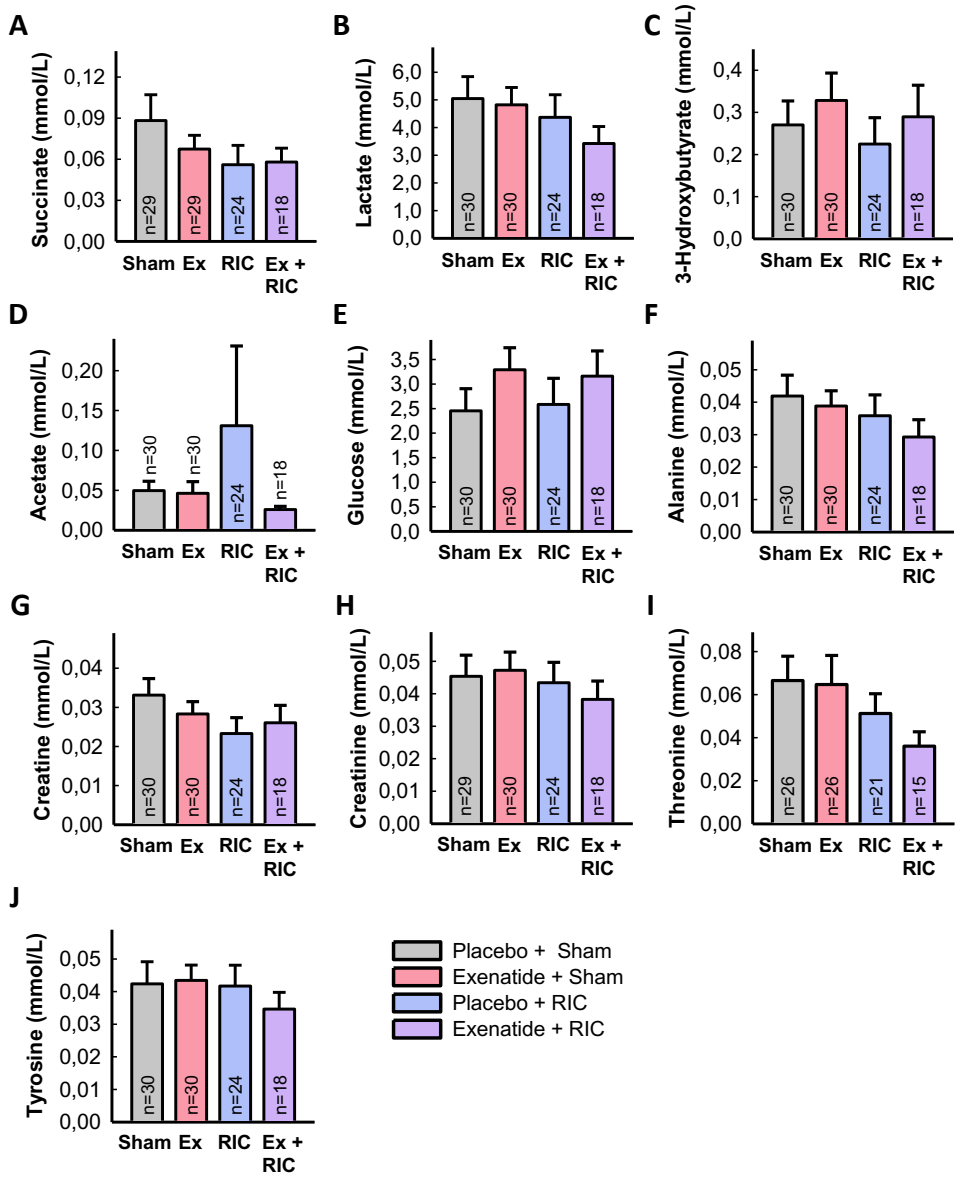

Figure 31: Concentration of selected metabolites (mmol/L) analyzed by ^{1}H NMR spectroscopy in plasma extracts obtained from peripheral blood samples in STEMI patients included in the COMBAT-MI clinical trial and randomized to four treatment groups, Sham + Placebo, Sham + Exenatide, RIC + Placebo, and RIC + Exenatide. Ex: Exenatide; RIC: Remote Ischemic Conditioning.

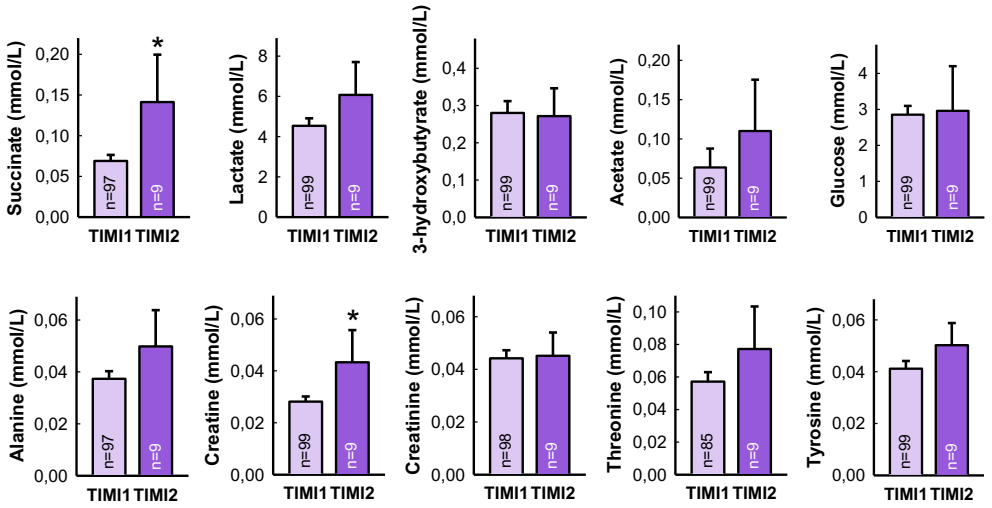

Figure 32: Concentration of selected metabolites (mmol/L) analyzed by ^{1}H-NMR spectroscopy in plasma extracts obtained from peripheral blood samples in STEMI patients with initial TIMI flow ≤ 1 (TIMI1) as compared with data from those with initial TIMI flow ≥ 2 (TIMI2). * ($p<0.05$) indicates significant differences vs. TIMI 1 group (Student's t-test).

5.2.2.3 Correlations between metabolite concentrations in peripheral plasma and CMR variables

Unfortunately, regression analysis did not reveal any significant correlation between the concentration of the different analyzed metabolites, including succinate, and infarct size (determined as percentage of left ventricular mass or as absolute weight), myocardial salvage index, transmurality index, extent of edema, left ventricular ejection fraction (LVEF) or microvascular obstruction volume. Furthermore, with the exception of creatine for myocardial salvage index ($p = 0.008$) and transmurality index ($p = 0.039$), stepwise regression analysis did not identify any metabolite as predictor of any of the analyzed variables. Taken together, these data point against the use of this metabolite as a non-invasive prognostic biomarker in STEMI patients, at least, when analyzed in peripheral blood.

5.3 MODULATION OF RET BY INTERNAL FACTORS: ROLE OF Cx43

5.3.1 EFFECTS OF Cx43 DEFICIENCY ON MITOCHONDRIAL FUNCTION

5.3.1.1 Effects of Cx43 deficiency on mitochondrial respiration

To elucidate whether Cx43 modulates mitochondrial ROS production by RET, both SSM and IFM were isolated, 13 days after 4OHT treatment, from hearts obtained from $Cx43^{fl/fl}$ wild-type mice ($Cx43^{fl/fl}$+4OHT) and from Cx43-deficient mice ($Cx43^{Cre\text{-}ER(T)/fl}$+4OHT) ($Cx43^{Cre/fl}$+4OHT).

Cx43 deficiency did not modify CS activity (*Figure 33A, C*) or mitochondrial yield (*Figure 33B,D*) in any mitochondrial subpopulation, indicating similar amount of these organelles in both mitochondrial preparations.

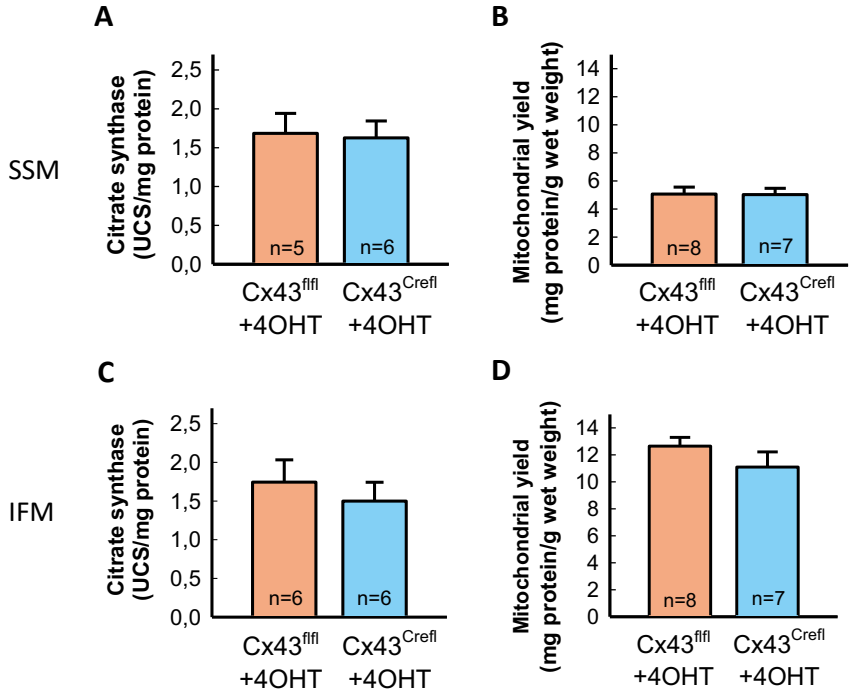

Figure 33: Citrate synthase activity (**A, C**) and mitochondrial yield (**B, D**) in SSM and IFM obtained from hearts from $Cx43^{fl/fl}$+4OHT wild-type mice and from 4OHT-treated $Cx43^{Cre\text{-}ER(T)/fl}$ animals (Cx43-deficient, $Cx43^{Crefl}$+4OHT).

Oxygen consumption was determined after incubation with malate and glutamate as substrates feeding complex I. As expected, basal, ADP-independent, oxygen consumption (state 2) was low, both for SSM and IFM, in mitochondria from wild-type animals ($Cx43^{flfl}$ mice treated with 4OHT), but was markedly enhanced following addition of ADP (state 3) (*Figure 34A, C*). Cx43 deficiency did not modify neither state 2 nor state 3 respiration in cardiac mitochondria from $Cx43^{Cre\text{-}ER(T)/fl}$ mice treated with 4OHT (*Figure 34A, C*). Accordingly, no changes were observed in the corresponding respiratory control ratios in any mitochondrial subpopulation (*Figure 34B, D*).

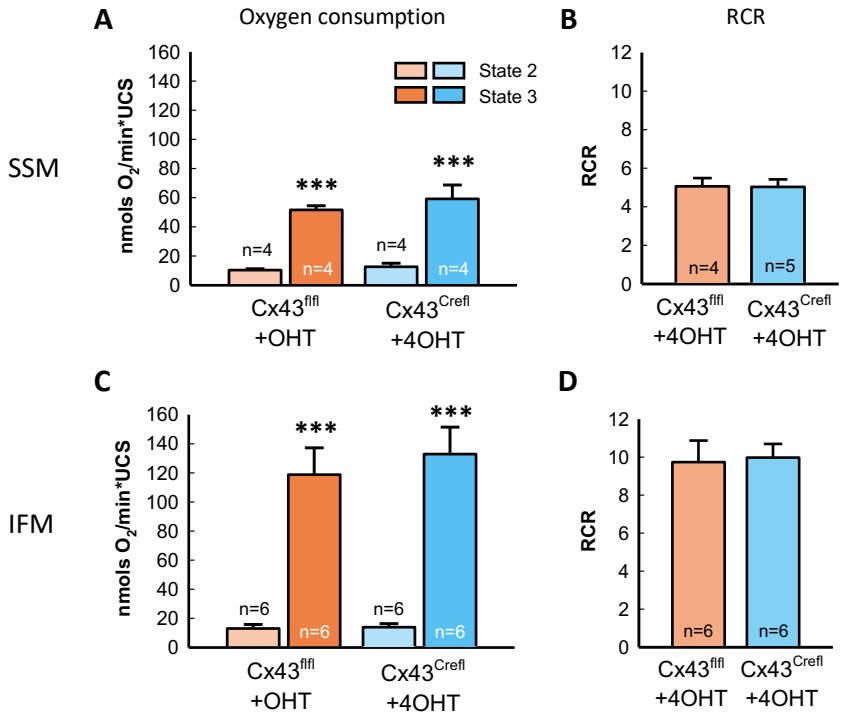

Figure 34: Baseline (state 2) and ADP-stimulated (state 3) oxygen consumption in cardiac SSM (**A**) and IFM (**C**) from $Cx43^{fl/fl}$ and 4OHT-treated $Cx43^{Cre\text{-}ER(T)/fl}$ animals ($Cx43^{Cre/fl}$+4OHT) animals fueled with malate and glutamate, as substrates of respiratory complex I. **B** and **D** depict the corresponding respiratory control ratio (RCR), determined as state 3/state 2. ***($p<0.001$) indicates significant differences when compares with its corresponding values without ADP.

5.3.1.2 Effects of Cx43 deficiency on mitochondrial ROS production

Mitochondrial ROS production was initially evaluated in SSM isolated from hearts from Cx43$^{fl/fl}$ wild-type mice and from Cx43$^{Cre\text{-}ER(T)/fl}$-deficient animals. ROS production in the presence of malate and glutamate, used as substrates feeding complex I, was low in all cases, with no differences between both genotypes (*Figure 35A*). In contrast, incubation with succinate (feeding complex II) induced a considerable and significant ($p<0.001$) increase in ROS production in cardiac SSM from Cx43$^{fl/fl}$ wild-type mice, which was largely prevented by addition of rotenone (*Figure 35B*), suggesting that it originates from RET in complex I. Remarkably, Cx43 deficiency significantly attenuated succinate-dependent ROS production in SSM (*Figure 35B*). Accordingly, ROS production by RET, calculated as the difference between values obtained in the absence and presence of rotenone was significantly reduced in SSM from Cx43-deficient mice (Mann-Whitney U test, $p=0.035$) (*Figure 35C*).

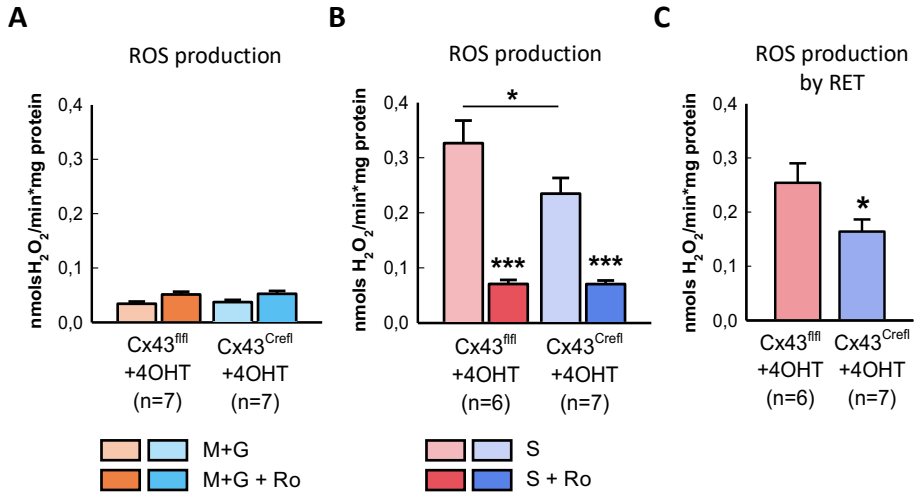

Figure 35: Rates of H_2O_2 production in SSM obtained from hearts from 4OHT-injected Cx43$^{fl/fl}$ mice (wild-type, Cx43^{flfl}+4OHT) and from 4OHT-treated Cx43$^{Cre\text{-}ER(T)/fl}$ animals (Cx43-deficient, Cx43^{Crefl}+4OHT) after incubation with substrates feeding complex I (malate and glutamate (M+G)) (**A**), or complex II (succinate (S)) (**B**), both with or without rotenone (Ro). ROS production by RET (**C**) was calculated as the difference between values obtained with succinate in the absence and presence of rotenone. ***($p<0.001$) indicates significant differences when compared with its corresponding values without rotenone and *($p<0.05$) when compared with Cx43$^{fl/fl}$+4OHT animals.

Similar to SSM, ROS production in cardiac IFM from wild-type animals was low after incubation with malate and glutamate (complex I) (*Figure 36A*) but was markedly and significantly (p<0.001) increased after incubation with succinate (complex II), in a rotenone-dependent manner (*Figure 36B*). However, and contrary to SSM, Cx43 deficiency did not modify neither complex I nor complex II-dependent ROS production (*Figure 36A-B*). Therefore, ROS production by RET was not modified in cardiac IFM from Cx43-deficient mice (*Figure 36C*).

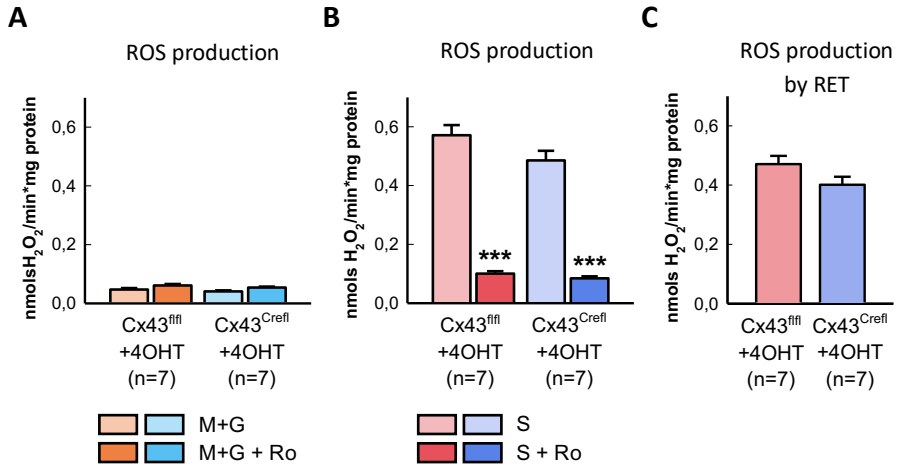

Figure 36: Rates of H_2O_2 production in IFM obtained from hearts from 4OHT-injected $Cx43^{fl/fl}$ mice (wild-type, $Cx43^{flfl}$+4OHT) and from 4OHT-treated $Cx43^{Cre\text{-}ER(T)/fl}$ animals (Cx43-deficient, $Cx43^{Crefl}$+4OHT) after incubation with substrates feeding complex I (malate and glutamate (M+G)) (**A**) or complex II (succinate (S)) (**B**), both with or without rotenone (Ro). ROS production by RET (**C**) was calculated as the difference between values obtained with succinate in the absence and presence of rotenone. ***(p<0.001) indicates significant differences when compared with its corresponding values without rotenone.

5.3.1.3 Effects of Cx43 deficiency on mitochondrial membrane potential

Our previous data demonstrate that Cx43 deficiency results in a reduction in ROS production by RET in SSM, but not in IFM. ROS production by RET can be modulated by its thermodynamic drivers, the mitochondrial membrane potential $\Delta\psi$ and by the CoQ redox state, in addition to succinate concentration [295]. In order to assess whether the reduction in ROS production by RET could be

explained by changes in these parameters, we started by measuring $\Delta\psi$ by TMRE fluorescence.

As depicted in *Figure 37*, Cx43 deficiency in $Cx43^{Cre\text{-}ER(T)/fl}$ mice treated with 4OHT did not modify TMRE fluorescence, neither in SSM (*Figure 37A*) nor in IFM (*Figure 37B*) fed with succinate, neither in the absence or presence of rotenone.

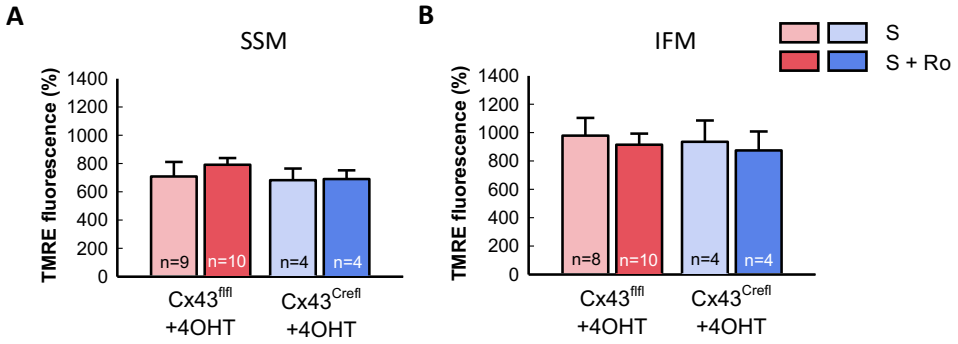

Figure 37: Mitochondrial membrane potential assessed by TMRE fluorescence in SSM (**A**) and IFM (**B**) from 4OHT-injected $Cx43^{fl/fl}$ mice (wild-type, $Cx43^{fl/fl}$+4OHT) and from 4OHT-treated $Cx43^{Cre\text{-}ER(T)/fl}$ (Cx43-deficient, $Cx43^{Cre/fl}$+4OHT) animals. Mitochondrial preparations were fed with succinate in the absence or presence of rotenone. Data are expressed respect to baseline values before substrate addition. No significant differences were observed in any case.

5.3.1.4 Effects of Cx43 deficiency on coenzyme Q pool quantification and redox state

CoQ pool concentration and its redox state were quantified by UPLC-MS/MS to evaluate the second thermodynamic driver of ROS production by RET. *Figure 38* depicts representative chromatograms of CoQ9, $CoQ9H_2$, CoQ10 and $CoQ19H_2$. The most abundant form of the CoQ family in our mice hearts was CoQ9, with CoQ10 representing about 15% of total CoQ pool in both SSM (*Figure 39A*) and IFM (*Figure 39B*), with no differences between groups and being in the range of previous publications [361].

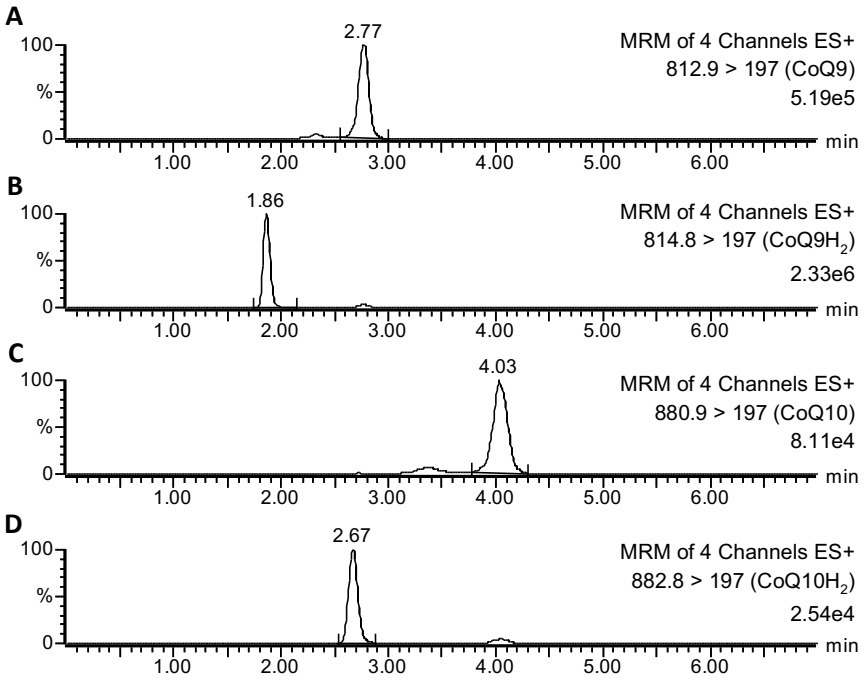

Figure 38: Representative UPLC-MS/MS chromatograms the ion transitions used for CoQ9 (A), CoQ9H2 (B), CoQ10 (C) and CoQ10H2 (D) detection. MRM: multiple reaction monitoring; ES+: electrospray ionization in positive ion mode.

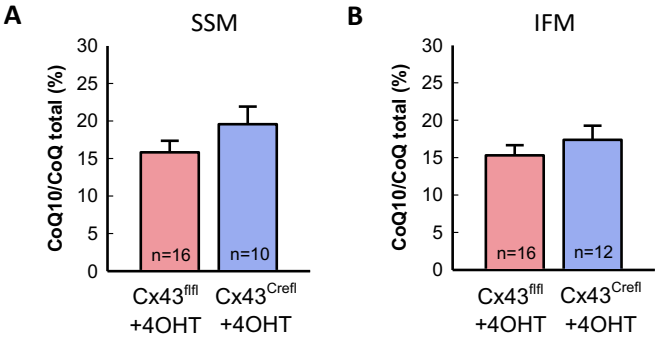

Figure 39: Percentage of coenzyme Q10 (CoQ10) out of total CoQ pool present in SSM (**A**) and IFM (**B**) obtained from hearts from 4OHT-injected $Cx43^{fl/fl}$ mice (wild-type, $Cx43^{fl/fl}$+4OHT) and from 4OHT-treated $Cx43^{Cre\text{-}ER(T)/fl}$ (Cx43-deficient, $Cx43^{Cre/fl}$+4OHT) animals.

Notably, peak quantification demonstrated a significant decrease in the total CoQ9 pool in SSM from Cx43-deficient mice, as compared with the amount found in $Cx43^{fl/fl}$+4OHT animals, but not in IFM (*Figure 40A, B*). In addition, Cx43 deficiency was also associated with a decrease in the abundance of the reduced form of CoQ9, $CoQ9H_2$, in SSM (from 73.94 ± 1.18% of total CoQ9 pool in $Cx43^{fl/fl}$ animals to 60.98 ± 3.70% in Cx43-deficient mice, p=0.002) (*Figure 41A*), a difference that, again, was not observed in IFM (*Figure 41B*).

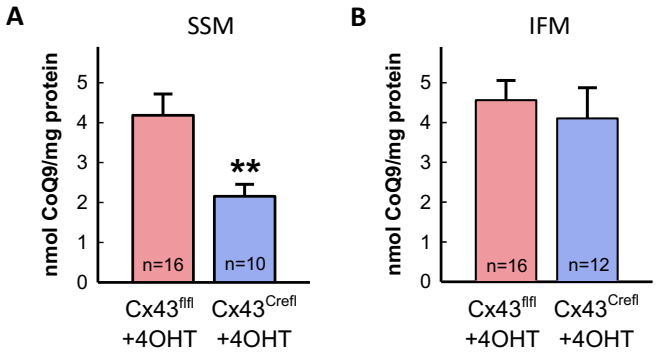

Figure 40: Coenzyme Q9 (CoQ9) quantification in SSM (**A**) and IFM (**B**) obtained from hearts from 4OHT-injected $Cx43^{fl/fl}$ (wild-type, $Cx43^{fl/fl}$+4OHT) mice and from 4OHT-treated $Cx43^{Cre-ER(T)/fl}$ (Cx43-deficient, $Cx43^{Cre/fl}$+4OHT) animals. **(p<0.01) indicates significant differences when compared with values found in $Cx43^{fl/fl}$+4OHT mice.

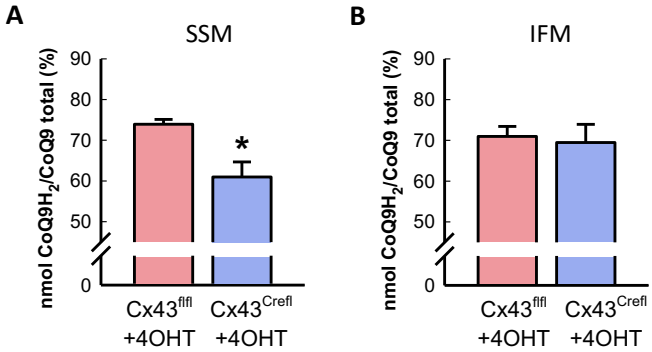

Figure 41: Abundance of the reduced form of coenzyme Q9 ($CoQ9H_2$), expressed as percentage of total Coenzyme Q9 (CoQ) pool, in SSM (**A**) and IFM (**B**) obtained from hearts from 4OHT-injected $Cx43^{fl/fl}$ (wild-type, $Cx43^{fl/fl}$+4OHT) mice and from 4OHT-treated $Cx43^{Cre-ER(T)/fl}$ (Cx43-deficient, $Cx43^{Cre/fl}$+4OHT) animals. *(p<0.05) indicates significant differences when compared with values found in $Cx43^{fl/fl}$+4OHT mice.

5.3.2 EFFECTS OF Cx43 DEFICIENCY ON SUCCINATE LEVELS IN ISCHEMIC MYOCARDIUM

Differences in succinate accumulation during ischemia might explain, together with alterations in $\Delta\psi$ and the CoQ pool, the reduction in ROS production by RET observed in isolated cardiac SSM from Cx43-deficient mice. Therefore, succinate concentration was determined in myocardial samples obtained from isolated hearts from $Cx43^{fl/fl}$ and $Cx43^{Cre\text{-}ER(T)/fl}$ mice, both treated with 4OHT, and submitted in the Langendorff system to normoxic perfusion or to 35 minutes of ischemia. As can be seen in *Figure 42*, ischemia induced a massive increase in succinate concentrations in isolated hearts from both wild-type animals and from Cx43-deficient mice, with no differences between both genotypes.

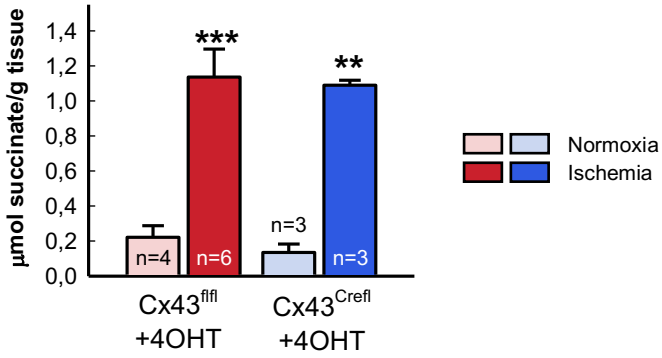

Figure 42: Succinate concentrations, assessed by ^{1}H-NMR spectroscopy, in myocardial extracts obtained from hearts from 4OHT-injected $Cx43^{fl/fl}$ mice (wild-type) and from 4OHT-treated $Cx43^{Cre\text{-}ER(T)/fl}$ (Cx43-deficient) animals perfused under normoxic conditions or submitted to 35 min of global ischemia. ***($p<0.001$), **($p<0.01$) indicates significant differences when compared with the respective normoxic hearts.

5.3.3 EFFECTS OF Cx43 DEFICIENCY ON ISCHEMIA-REPERFUSION INJURY AND ON CARDIOPROTECTION BY MALONATE IN ISOLATED MICE HEARTS

Isolated hearts from $Cx43^{fl/fl}$ mice and $Cx43^{Cre\text{-}ER(T)/fl}$ mice treated with 4OHT were submitted to 35 minutes of ischemia followed by 60 minutes of reperfusion and treated or not with malonate during the first 15 minutes of reperfusion. *Figure 43* depicts a representative recording obtained from a $Cx43^{fl/fl}$ control isolated perfused mouse.

LVdevP was markedly reduced during ischemia in all hearts, reaching a minimum 2-3 minutes later. Ischemic rigor contracture, detected as an abrupt increase in LVEDP, occurred during the first minutes of ischemia, with no differences between groups (*Figure 44A*). Reperfusion induced a new increase in LVEDP, corresponding to hypercontracture, which tended to be higher in hearts from $Cx43^{flfl}$ mice not treated with malonate, although differences did not reach statistical significance. (*Figure 44B*).

Functional recovery during reperfusion, expressed as percentage of baseline LVdevP, was negligible in isolated hearts from 4OHT-injected $Cx43^{flfl}$ wild-type mice (*Figure 45A,B*). In contrast, repeated measures ANOVA demonstrated a significant effect of group allocation, with a trend towards a better functional recovery both in hearts treated with malonate and in those from Cx43-deficient animals. These differences reached significance at several time points after treatment with malonate in hearts from both genotypes (*Figure 45A,B*). Similarly, a separate analysis of functional recovery at the end of reperfusion by ANOVA revealed an almost significant trend ($p=0.054$) for an improved function in $Cx43^{fl/fl}$ animals treated with malonate and in Cx43-deficient mice (*Figure 45B*).

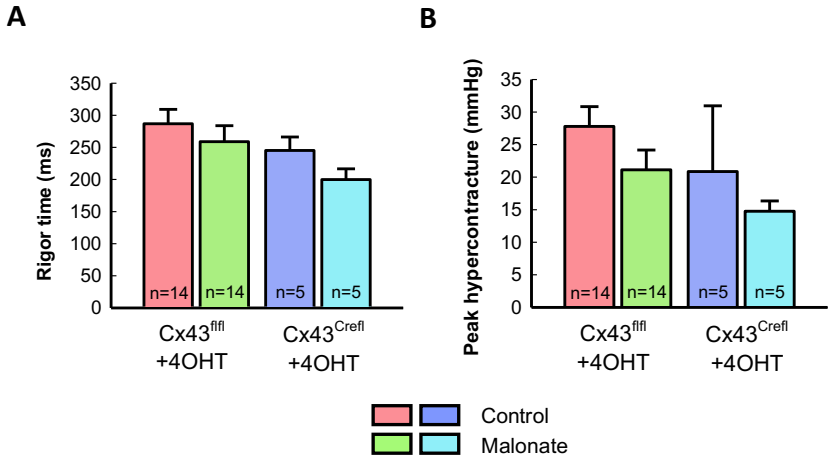

Figure 44: Ischemic rigor (**A**) and peak hypercontracture during initial reperfusion (**B**) in isolated hearts from 4OHT-injected $Cx43^{fl/fl}$ ($Cx43^{flfl}$+4OHT) and $Cx43^{Cre\text{-}ER(T)/fl}$ ($Cx43^{Crefl}$+4OHT) animals submitted to 35 minutes of ischemia followed by reperfusion, and treated or not with malonate at the onset of reflow.

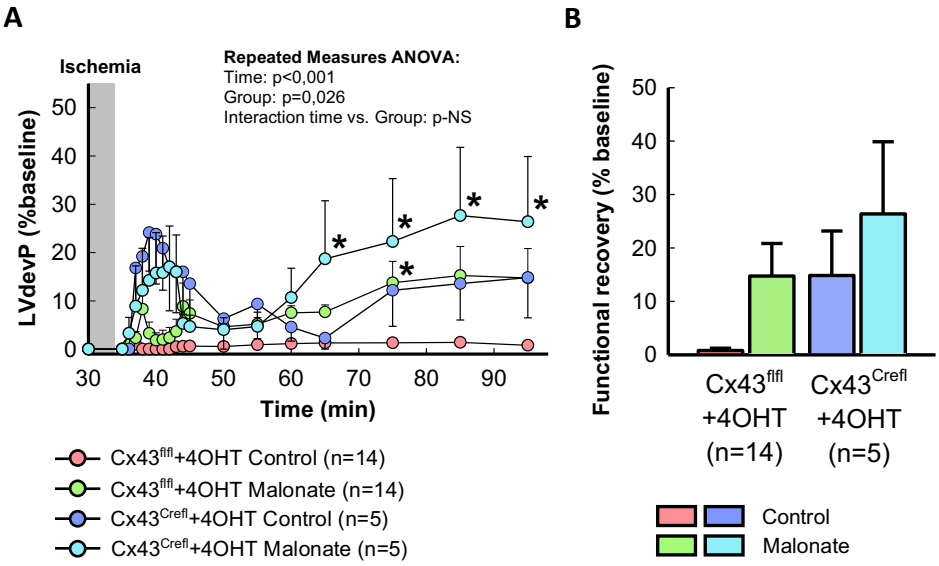

Figure 45: Left ventricular developed pressure (LVdevP) during reperfusion (**A**) and functional recovery at the end of reperfusion (**B**) in isolated hearts from 4OHT-injected $Cx43^{fl/fl}$ ($Cx43^{flfl}$+4OHT) and $Cx43^{Cre\text{-}ER(T)/fl}$ animals ($Cx43^{Crefl}$+4OHT), submitted to 35 minutes of ischemia followed by reperfusion, and treated or not with malonate during the first minutes of reflow. * ($p<0.05$) indicates significant differences when compared with respective time values in control $Cx43^{fl/fl}$ mice.

Figure 46A depicts representative images of cardiac slices stained with TTC and obtained from isolated hearts from 4OHT-injected $Cx43^{fl/fl}$ and $Cx43^{Cre\text{-}ER(T)/fl}$ mice submitted to 35 minutes of ischemia followed by reperfusion and treated or not with malonate during the first 15 minutes of reflow. As previously published, Cx43 deletion led to a marked and significant reduction in infarct size as compared with hearts from $Cx43^{fl/fl}$ wild-type animals [47] (*Figure 46B*). Malonate, given at the onset of reperfusion, was able to reduce infarct size in hearts from wild-type $Cx43^{fl/fl}$ mice but did not present any additional protective effect in hearts from Cx43-deficient animals (*Figure 46B*).

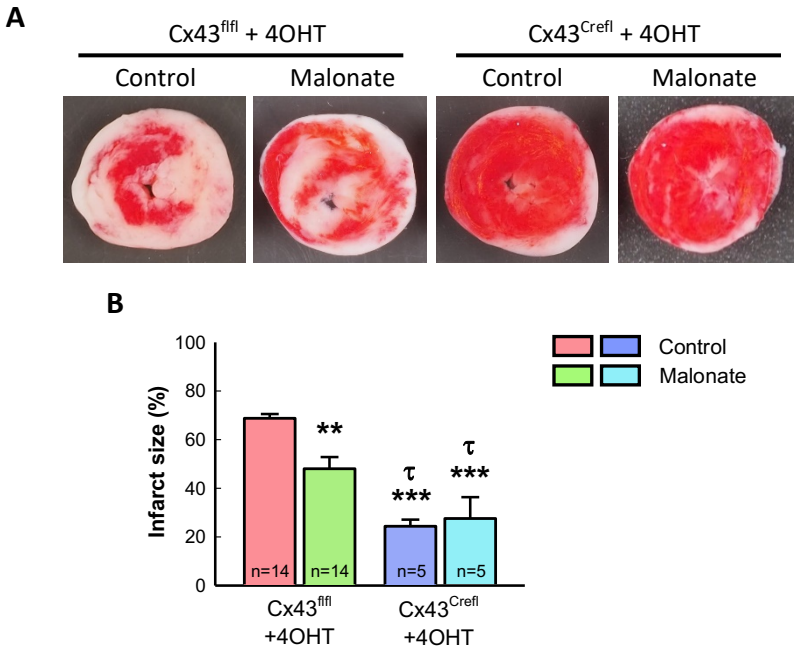

Figure 46: Representative images of cardiac slices stained with TTC (showing infarcted areas in white) (**A**) and infarct size quantification, as percentage of ventricular weight (**B**), in 4OHT-injected $Cx43^{fl/fl}$ ($Cx43^{flfl}$+4OHT) and $Cx43^{Cre\text{-}ER(T)/fl}$ ($Cx43^{Crefl}$+4OHT) animals submitted to 35 minutes of ischemia followed by reperfusion and treated or not with malonate at the onset of reflow. **($p<0.01$), ***($p<0.001$) indicate significant differences when compared with hearts from control, untreated, $Cx43^{fl/fl}$+4OHT animals. τ ($p<0.05$) indicates differences with hearts from $Cx43^{fl/fl}$+4OHT mice treated with malonate.

Data on infarct size correlated with LDH release to the coronary effluent during reperfusion, an indirect indicator of cell death. Indeed, repeated measures-ANOVA revealed a significant effect of time and group allocation on LDH release and a significant interaction between both variables, with those curves corresponding to malonate-treated hearts or Cx43-deficient animals running below that of malonate-untreated, wild-type, $Cx43^{flfl}$ mice (*Figure 47A*). In fact, cumulative LDH during the 60 minutes of reperfusion was significantly reduced both by Cx43 deficiency and malonate treatment as compared with that obtained in hearts from malonate-untreated, wild-type mice (ANOVA $p<0.001$) (*Figure 47B*).

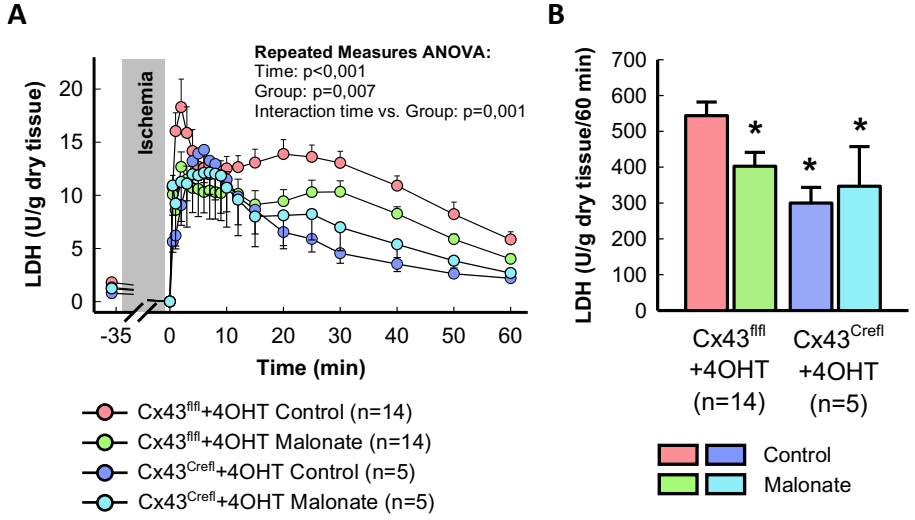

Figure 47: LDH release in the coronary effluent during reperfusion (**A**) and cumulative LDH release during the 60 minutes of reperfusion (**B**) in 4OHT-injected $Cx43^{fl/fl}$ ($Cx43^{flfl}$+4OHT) and $Cx43^{Cre\text{-}ER(T)/fl}$ ($Cx43^{Crefl}$+4OHT) animals treated or not with malonate at the onset of reperfusion following 35 minutes of ischemia. *($p<0.05$) indicates significant differences when compared with $Cx43^{fl/fl}$+4OHT mice.

5.3.4 EFFECTS OF Cx43 DEFICIENCY ON ROS PRODUCTION IN ISCHEMIC CARDIAC TISSUE

Isolated hearts from $Cx43^{fl/fl}$+4OHT and $Cx43^{Cre\text{-}ER(T)/fl}$+4OHT mice were submitted to normoxic perfusion or 35 minutes of ischemia followed by 5 minutes of reperfusion to assess ROS production in tissue by DHE staining. Hearts from $Cx43^{fl/fl}$ wild-type animals submitted to ischemia and 5 min of reperfusion

depicted a significantly enhanced DHE fluorescence, as compared with those perfused under normoxic conditions (*Figure 48*). In contrast, confocal fluorescence microscopy was not able to detect any increase in DHE staining after ischemia in hearts from Cx43-deficient mice (*Figure 48*).

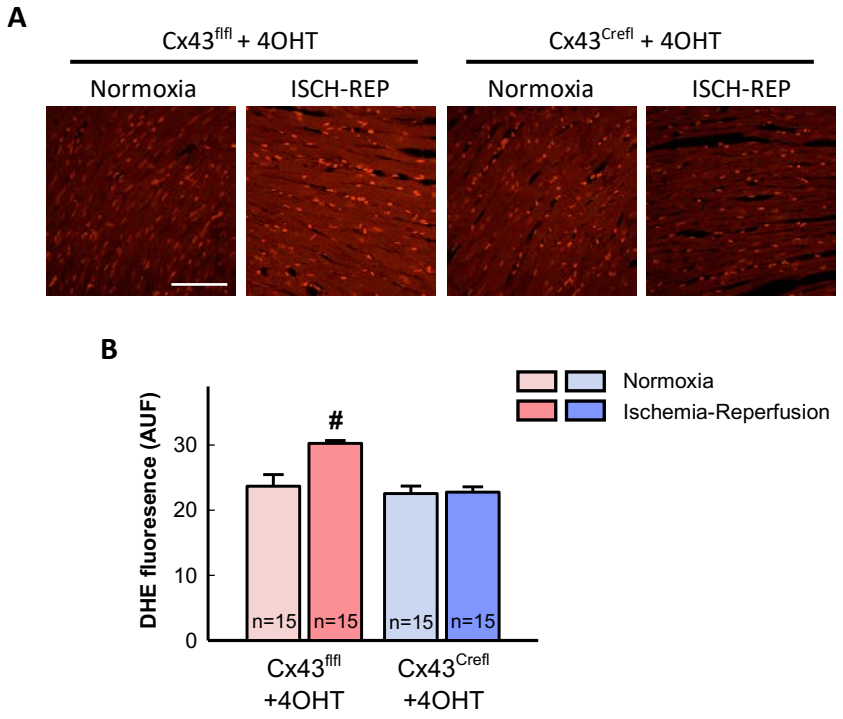

Figure 48: Upper panels depict representative images of DHE staining (**A**) in cardiac samples from 4OHT-treated Cx43$^{fl/fl}$ mice (wild-type, Cx43$^{fl/fl}$+4OHT) and from 4OHT-treated Cx43$^{Cre\text{-}ER(T)/fl}$ (Cx43-deficient, Cx43^{Crefl}+4OHT) animals, either perfused under normoxic conditions or submitted to ischemia (35 min) and 5 min of reperfusion (ISCH-REP). Lower graph shows DHE staining quantification (**B**) in the same samples, measured in AUF (arbitrary units of fluorescence). Data were obtained, in each group, from five different sections of three distinct hearts. # ($p<0.05$) indicates significant differences when compared to all the other three groups. White bar in **A** represents 100 µm.

5.4 MODULATION OF RET BY EXTERNAL FACTORS: EFFECTS OF AIR POLLUTION

5.4.1 EFFECTS OF DEP EXPOSURE ON MITOCHONDRIAL FUNCTION

5.4.1.1 Effects of DEP exposure on mitochondrial respiration

To evaluate the effect of particulate matter exposure on mitochondrial function, cardiac SSM and IFM mitochondria were isolated from control and DEP-treated rats. CS activity of mitochondrial homogenates was quantified as an indicator, as previously described, of the number of mitochondria present in the homogenate. DEP intratracheal instillation induced a reduction in CS activity both in SSM (1.69 ± 0.15 UCS in control rats vs. 1.23 ± 0.06 UCS in DEP-treated animals, Student's t-test, p=0.009) (*Figure 49A*) and IFM (1.98 ± 0.30 UCS vs. 1.38 ± 0.11, Student's t-test, p=0.049) (*Figure 49B*), suggesting some degree of mitochondrial damage after DEP exposure. However, MY, which indicates the quality of the mitochondrial preparation, was not modified my DEP exposure, neither in SSM nor in IFM.

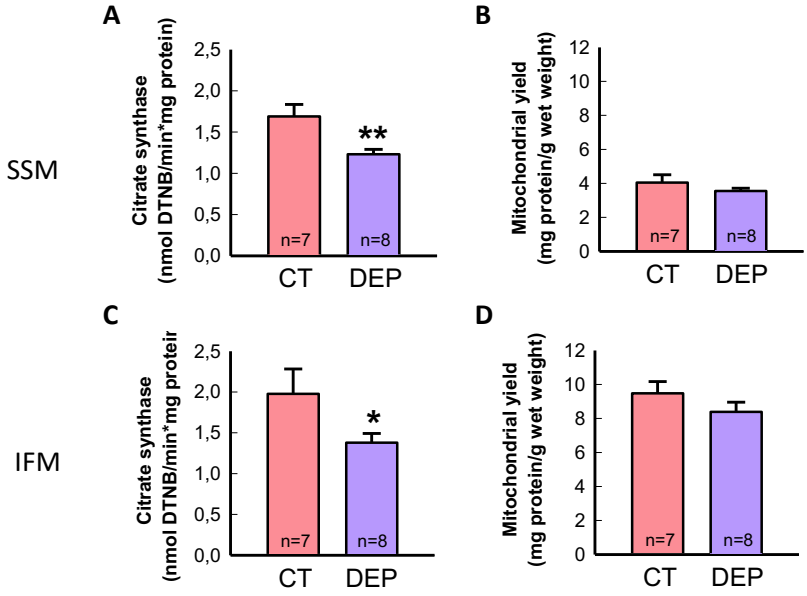

Figure 49: Citrate synthase activity, expressed in units of citrate synthase (UCS) per mg of protein, in SSM (**A**) and IFM (**C**), and mitochondrial yield, expressed as mg of mitochondrial protein per g of wet weight, in SSM (**B**) and IFM (**D**) from control (CT) and DEP-treated animals (DEP). *(p<0.05) and ** (p<0.01) indicates significant differences between both groups.

Oxygen consumption was determined after addition of either substrates feeding complex I (malate and glutamate) or complex II (succinate plus rotenone, the last used to avoid any influence of complex I).

Both SSM and IFM from control rats, fed with malate and glutamate (complex I), depicted a low basal, ADP-independent, oxygen consumption (state 2), that was markedly enhanced following addition of ADP (state 3) (*Figure 50A, C*). DEP exposure did not alter neither state 2 nor state 3 respiration in none of these mitochondrial subpopulations (*Figure 50A, C*). Accordingly, no changes were observed in the corresponding respiratory control ratios (*Figure 50B, D*).

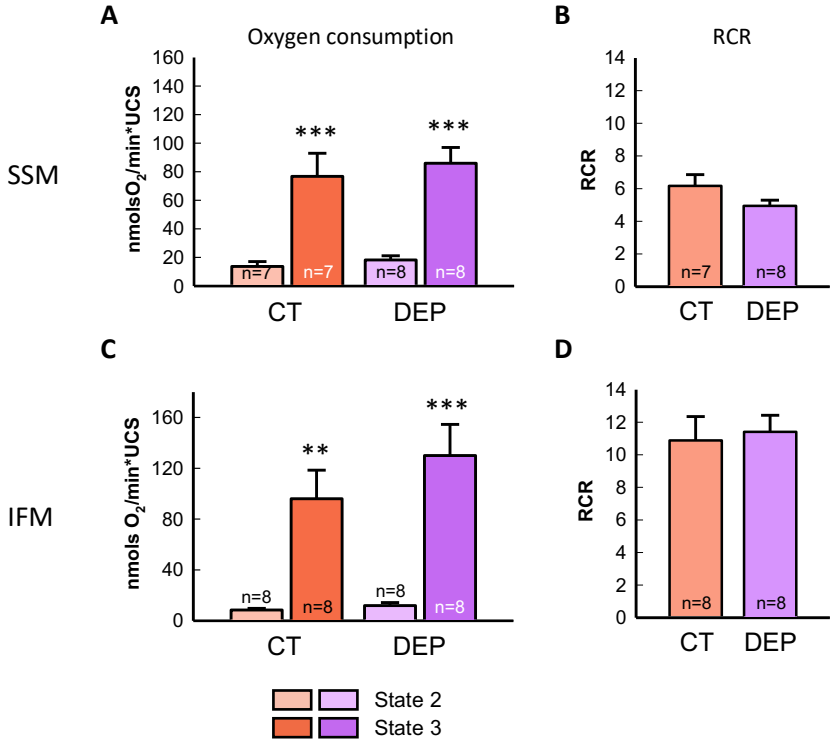

Figure 50: Baseline (state 2) and ADP-stimulated (state 3) oxygen consumption in cardiac SSM (**A**) and IFM (**C**) from control (CT) and DEP-exposed rats (DEP), fueled with malate and glutamate as substrates of respiratory complex I. (**B**) and **(D**) depict the corresponding respiratory control ratio (RCR), determined as state 3/state 2. **(p<0.01), ***(p<0.001) indicates significant differences with the corresponding state 2 respiration values.

As in the case of complex I-driven mitochondrial respiration, complex II-dependent oxygen consumption (in the presence of succinate and rotenone) was also low in both cardiac SSM and IFM from control rats in the absence of ADP, but significantly enhanced after its addition (*Figure 51A, C*). Again, DEP exposure did not influence mitochondrial respiration in any case (*Figure 51A, C*), nor the corresponding respiratory control ratios (*Figure 51B, D*).

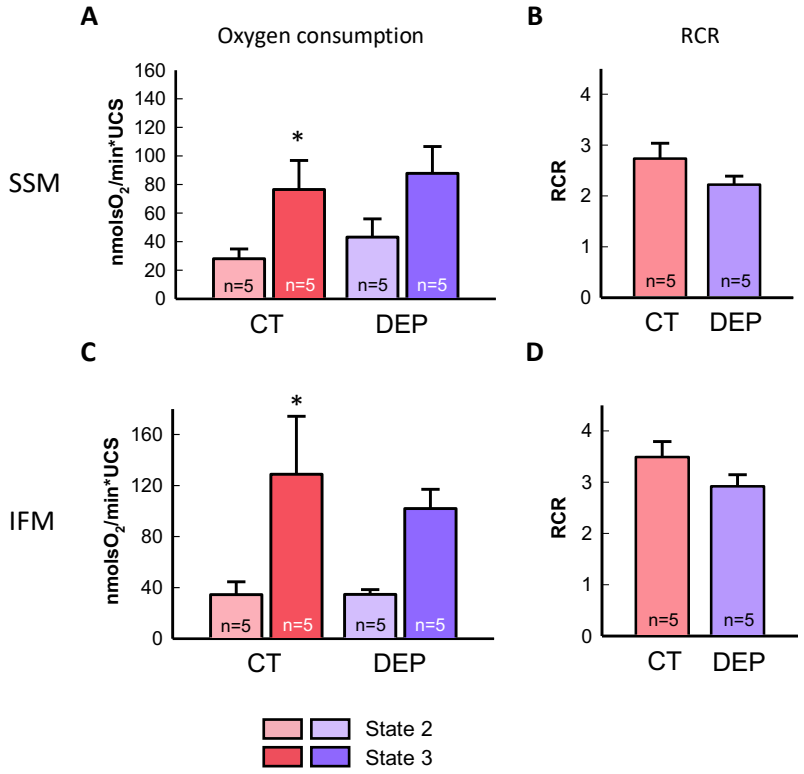

Figure 51: Baseline (state 2) and ADP-stimulated (state 3) oxygen consumption in cardiac SSM (**A**) and IFM (**C**) from control and DEP-exposed rats, fueled with succinate (plus rotenone) as substrate of respiratory complex II. (**B**) and (**D**) show the corresponding respiratory control ratio (RCR), determined as state 3/state 2. *($p<0.05$) indicates significant differences with the corresponding state 2 respiration values.

5.4.1.2 Effects of DEP exposure on mitochondrial ROS production

Mitochondrial ROS production was quantified in cardiac rat SSM after incubation with malate and glutamate, as substrates feeding complex I. ROS production, as normalized by CS activity, was significantly enhanced both by rotenone and DEP instillation in this mitochondrial subpopulation (*Figure 52A*). Remarkably, two-way ANOVA analysis demonstrated a significant effect of both DEP instillation and rotenone in ROS production in SSM after incubation with malate and glutamate, together with a significant interaction between both variables.

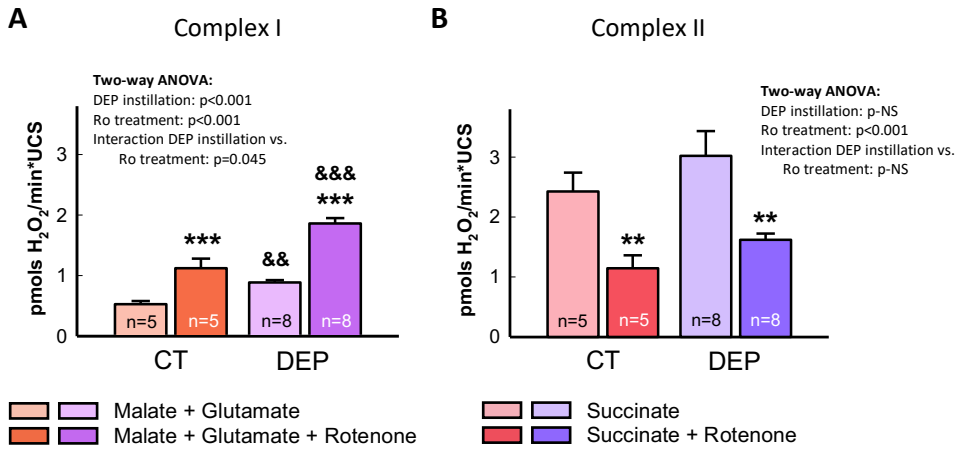

Figure 52: ROS production in the absence or presence of rotenone (Ro) in isolated cardiac SSM obtained from control (CT) and DEP-instilled rats (DEP) and fueled with glutamate and malate as substrates of complex I (**A**), and with succinate as substrate of complex II (**B**). *** (p<0,001) indicate significant differences when compared with its corresponding values without rotenone. &&(p<0.01) &&&(p<0.001) indicate significant differences when compared with the corresponding values in the control group.

Complex II-driven ROS production was evaluated, in the same mitochondrial subpopulation, by incubation of mitochondria with succinate. As expected, in SSM from control animals, ROS production with succinate was higher than with complex I substrates (*Figure 52B*). Remarkably, it was significantly attenuated by rotenone, suggesting that most ROS production under these conditions was due to RET. However, and although there was a trend towards an increase in ROS production in mitochondria from DEP-instilled animals, these differences did not

reach statistical significance (*Figure 52B*). Accordingly, two-way ANOVA analysis only was able to detect a significant effect of rotenone treatment.

IFM showed similar behaviour to that depicted by SSM. After incubation with complex I substrates, ROS production was significantly increased by rotenone, especially in DEP-treated animals. Again, two-way ANOVA analysis demonstrated a significant effect of both DEP instillation and rotenone in ROS production in this mitochondrial subpopulation (*Figure 53A*). In contrast, when incubated with succinate, ROS production was markedly enhanced compared to that occurring with complex I substrates, and this increase was attenuated by rotenone, suggesting RET (two-way ANOVA p<0.001). However, as happened with SSM, previous exposure of rats to DEP did not result in any change in ROS production (*Figure 53B*).

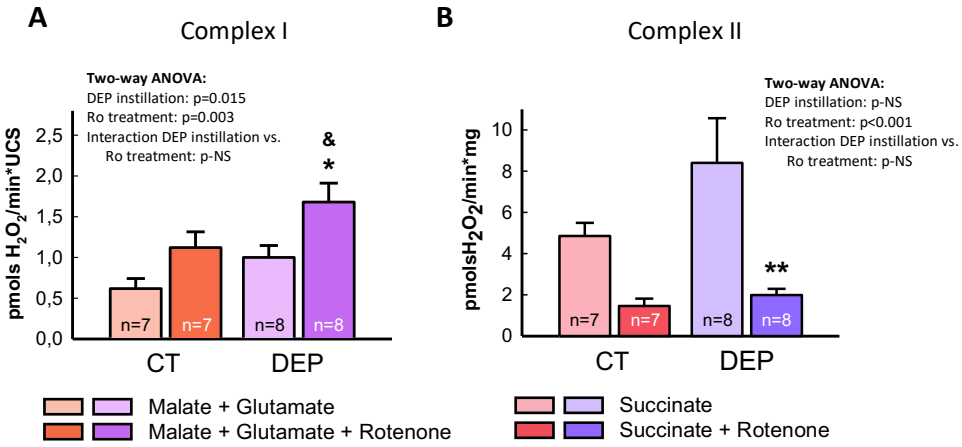

Figure 53: ROS production in the absence or presence of rotenone (Ro) in isolated cardiac IFM obtained from control (CT) and DEP-instilled rats (DEP) and fueled with glutamate and malate as substrates of complex I (**A**), and with succinate as substrate of complex II (**B**). **(p<0.01), *(p<0.05) indicate significant differences when compared with its corresponding value without rotenone. &(p<0.05) indicate significant differences when compared with its corresponding value in the control group.

In addition to ETC-dependent ROS production, Amplex™ Red fluorescence before substrate addition allowed us to determine baseline ROS production. As can be seen in *Figure 54*, two-way ANOVA analysis revealed a significant effect of group allocation (p=0.026), indicating that basal ROS production was significantly enhanced in DEP-exposed animals, both in SSM and IFM (*Figure 54*).

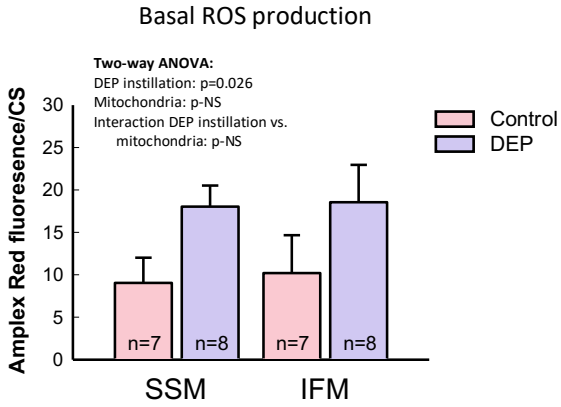

Figure 54: Basal ROS production, in the absence of respiratory substrates, in isolated cardiac SSM and IFM obtained from control and DEPs-instilled rats.

5.4.2 EFFECTS OF DEP EXPOSURE ON MYOCARDIAL ISCHEMIA-REPERFUSION INJURY IN ISOLATED RAT HEARTS

Isolated hearts from control and DEP-instilled rats were retrogradely perfused in a Langendorff perfusion system to evaluate the effects of previous particulate matter exposure on ischemia-reperfusion injury. *Figure 55* depicts a representative recording obtained from a control isolated perfused rat heart submitted to 60 minutes of ischemia followed by 90 minutes of reperfusion. Baseline LVdevP values ranged between 100 and 130 mmHg in all hearts. Perfusion pressure and heart rate were between 40 and 55 mmHg and 250 and 290 bpm, respectively.

Ischemic rigor appeared around minute 16 of ischemia and was detected as a sudden increase in EDLVP, with no differences between hearts from control and DEPs-exposed animals (*Figure 56A*). Reperfusion induced a new increase in EDLVP, known as hypercontracture, which was also not modified by DEPs administration (*Figure 56B*).

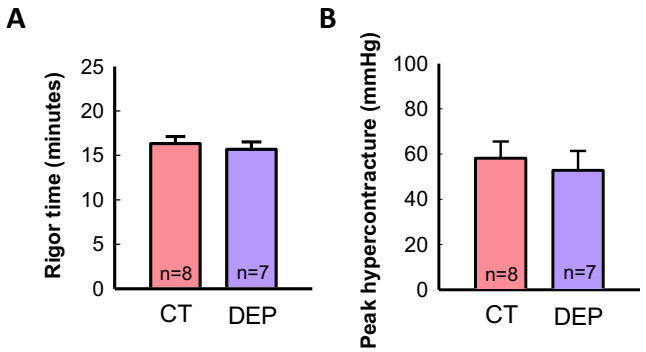

Figure 56: Ischemic rigor contracture (**A**) and peak hypercontracture during reperfusion (**B**) in isolated hearts from control (CT) and DEP-instilled (DEP) rats submitted to 60 minutes of ischemia followed by 90 minutes of reperfusion.

Functional recovery during reperfusion was low in both groups of animals, with no significant differences between them (*Figure 57*).

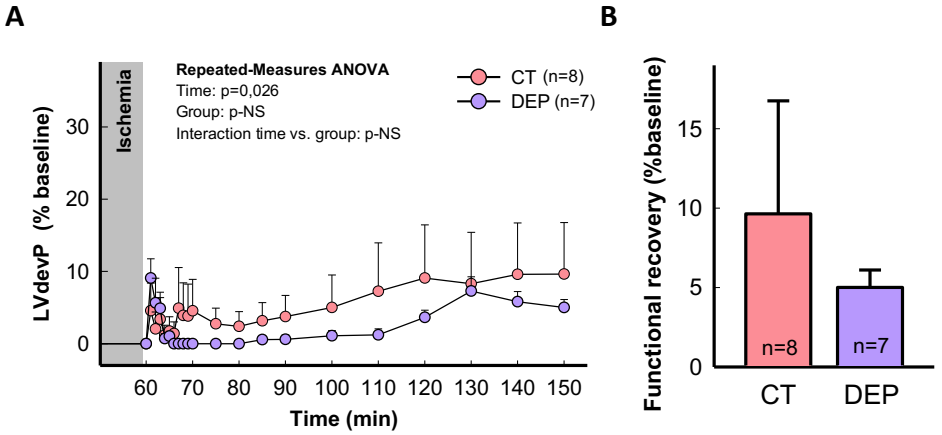

Figure 57: Changes in left ventricular developed pressure (LVdevP) during the 90 minutes of reperfusion (**A**) and functional recovery, expressed as percentage of baseline LVdevP, at the end of reperfusion (**B**), in isolated hearts from control (CT) and DEP-instilled (DEP) rats, submitted to 60 minutes of ischemia followed by reperfusion.

Infarct size averaged 49.79 ± 6.94 % of ventricular weight in hearts from control animals, and was not significantly modified by DEP administration (53.77 ± 3.21 %) (*Figure 58A, B*). LDH release in the coronary effluent was negligible during the stabilization period but markedly and similarly increased during reperfusion in

both groups of animals, with a peak during the first minutes of reflow (*Figure 58C*). Cumulative LDH release during the 90 minutes of reperfusion was also similar in both groups of hearts (*Figure 58D*).

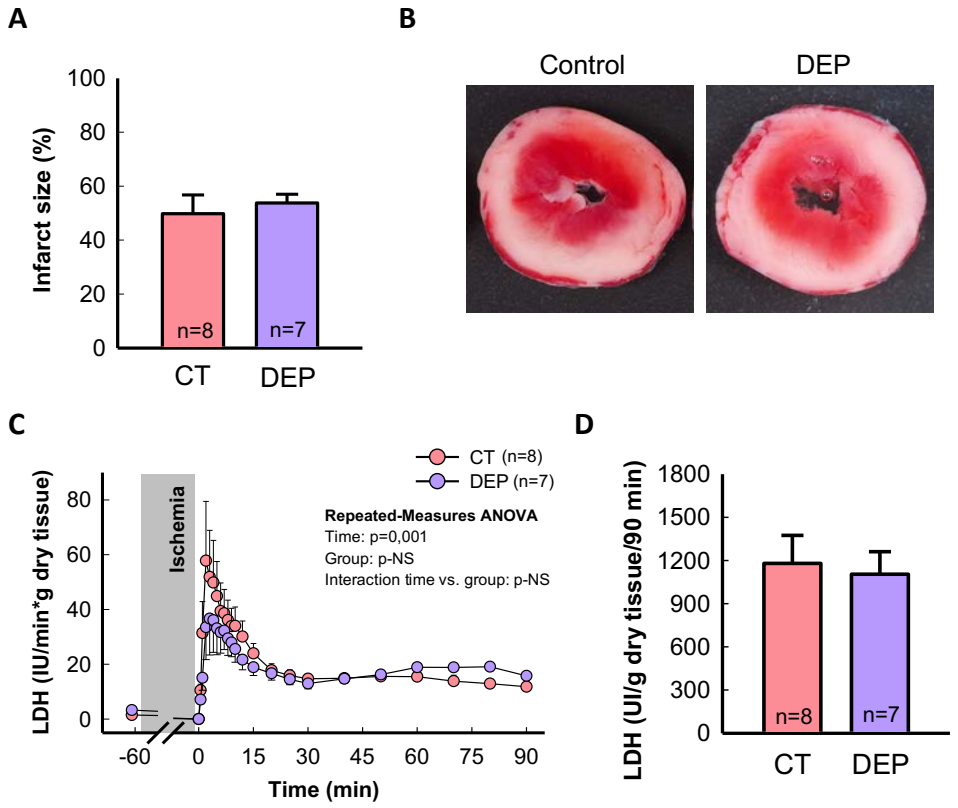

Figure 58: Quantification of cell death in control hearts (CT) and in hearts from animals intratracheally instilled with DEP (DEP). Isolated hearts were submitted to 60 minutes of global ischemia followed by 90 min of reperfusion. (**A**) Infarct size, expressed as percentage of ventricular weight. (**B**) Representative images of cardiac slices, stained with TTC (showing infarcted areas in white), from a control and a DEP-exposed rat. (**C**) LDH release during the entire reperfusion. (**D**) Cumulative LDH release to the coronary effluent during the 90 minutes of reperfusion.

6. DISCUSSION

6.1 EFFECTS OF THE COMBINATION OF SUCCINATE DEHYDROGENASE INHIBITION WITH MALONATE AND REMOTE ISCHEMIC CONDITIONING ON MYOCARDIAL ISCHEMIA-REPERFUSION INJURY

In this study, we investigated whether the combination of RIC, applied during myocardial ischemia, with intracoronary administration of the SDH inhibitor malonate, given at the onset of reperfusion, could result in additive protection against ischemia-reperfusion injury, compared with that provided by the individual treatments alone. Unfortunately, our results demonstrate that the combination of RIC and intracoronary malonate administration exerts non-additive cardioprotective effects in pigs submitted to transient coronary occlusion.

Prevention of succinate accumulation during ischemia by pretreatment with the reversible SDH inhibitor malonate was demonstrated in previous studies to reduce myocardial infarct size in several animal models [279,362,363]. It was also shown that accumulated succinate is rapidly oxidized during reperfusion by forward SDH activity, which, in turn, induces a massive ROS production by reverse electron transfer from mitochondrial complex II to complex I [279,280]. This oxidative stress is associated with mPTP opening and cell death [279,280]. Furthermore, it has been demonstrated that administration of the SDH inhibitor malonate at the onset of reperfusion reduces myocardial infarct size in several, independent, experimental models, including the Langendorff-perfused isolated mice heart preparation [280], the *in-situ* mice model of myocardial ischemia-reperfusion injury [362], and the porcine model of transient coronary occlusion [281]. In all these models, the protective effect of malonate was associated with reduced oxidation of succinate during the first minutes of reperfusion, less ROS production, preserved mitochondrial function, and increased calcein retention in isolated mitochondria, suggestive of reduced mPTP opening [280]. Notably, it has been recently proposed that malonate entry into cardiomyocytes via MCT1 is facilitated by the acidic environment present in the cell at the onset of reperfusion, suggesting that this drug would be selectively taken up by cardiomyocytes within the area at risk during an episode of myocardial infarction [364]. Our present results thus support the cardioprotective effects of SDH

inhibition when applied at the onset of reperfusion, revealed as a reduction in infarct size comparable to that observed in previous works [281].

RIC activates a variety of endogenous mechanisms of cardioprotection [305,308,310] and has been shown to exert protective effects in both experimental models [304,309,310], and in proof-of-concept clinical trials in STEMI patients [307,311,312]. Experimental studies have demonstrated that the cardioprotective signal is transferred from the remote conditioned organ or tissue to the heart, either through the release of humoral factors or through activation of neuronal pathways [308,365]. In the heart, RIC causes activation of intracellular transduction cascades similar to those of classic, local, ischemic pre or postconditioning, including the RISK and SAFE pathways [306,308,365–367], being the mitochondria the end-effectors [306,308,368,369]. Our present results confirm previous data obtained by our group in the same animal model [303,304], and support the cardioprotective effect of RIC against myocardial infarction. Unfortunately, however, two recently published randomized clinical trials have not been able to find any effect of RIC on clinical outcomes or on infarct size, evaluated by cardiac biomarkers or NMR, in STEMI patients [316,317]. Different reasons have been proposed to explain the failure of translation of cardioprotective strategies, including presence of comorbidities, such as aging, diabetes, or hypertension, which may alter the efficacy of cardioprotective maneuvers [370], the routine use of different comedications, such as P2Y12 antagonists, which may have protective effects [371], or the lack of uniformity in the method used to quantify infarct size [316]. Optimization of conditioning protocols in the clinical setting may help to improve efficacy of RIC in STEMI patients [316].

Under this situation, emerging evidence suggests that a multitargeted approach using two or more therapies, directed against different signaling pathways or cell targets involved in ischemia-reperfusion injury, would be advantageous in STEMI patients in order to reduce final infarct size [301]. Additive protection may be reached when the mechanisms of action of the combined interventions are different and would be especially interesting when the efficacy of the individual treatments is expected to be reduced by comorbidities or comedications. To date, some of the combined strategies that have demonstrated additive protection are addressed to different cell targets, such as coronary circulation or microvascular obstruction vs. cardiomyocytes [372]. This is the case of the combination of the antiplatelet cangrelor (a P2Y12 receptor antagonist) and

cariporide (a NHE inhibitor) or hypothermia, the last two acting mostly on cardiomyocytes, which has been shown to exert additive protection in open-chest rats submitted to transient coronary occlusion [373]. Other strategies have used treatment combinations acting on different signaling pathways within cardiomyocytes, including those targeting ischemic and reperfusion injury separately. In this regard, additive protection was found between RIC and local ischemic postconditioning in an in vivo rat model of ischemia-reperfusion [374], a finding that was later extended to STEMI patients [375]. Similarly, our group has previously demonstrated additive effects between treatments modulating myocardial energy metabolism (glucose-insulin-potassium (GIK) or exenatide, a mimetic of the incretin glucagon-like peptide-1 (GLP-1)), and RIC [303,304]. Furthermore, synergistic effects of inhibition of succinate accumulation and oxidation with hypothermia have been also described in rabbits [376]. However, not all treatment combinations are equally effective. Thus, protection by long-term nitroglycerine and RIC was shown to be abrogated when both individual treatments were combined in rats [377]. Similarly, no additive effects were found between aminooxyacetate, a malate-aspartate shuttle inhibitor, and local ischemic preconditioning in isolated rat hearts [378]. Unfortunately, our present results demonstrate that the addition of the SDH inhibitor malonate to RIC does not exert additive cardioprotective effects in pigs submitted to transient coronary occlusion. Lack of additive effects in our study can be due to the fact that both strategies share part of their mechanisms of action, as RIC was previously demonstrated to reduce, as occurred with malonate, oxidative stress [303]. Despite the antioxidant effects of RIC do not seem to rely on RET modulation [379–381], it might be enough to prevent the possibility of additive effects with RET inhibition with malonate.

As conduction arrhythmias may severely affect cardiac performance during reperfusion, we assessed whether our two individual treatments and the combination of both was able to modify the incidence of ventricular tachyarrhythmias during initial reperfusion. Accordingly, we observed that none of the three treatments were able to modify the total number of ventricular tachyarrhythmias following ischemia. However, the incidence of VF during initial reperfusion was significantly higher in animals treated with malonate and RIC as compared with controls, although this enhancement was, in part, compensated with a trend towards a lower number of VTs in these two groups. In contrast to these findings, we have previously demonstrated that neither malonate [280], nor

RIC [304], were able to modify the incidence of VFs in the same animal model. These discrepancies could be explained by the possibility that smaller but patchier infarctions in malonate and RIC-treated animals in the present study would create the ideal substrate for VF to evolve, at the expense of a lower number of VTs. Nevertheless, the higher incidence of VFs in these two groups in the present study would not modify our main conclusion, as defibrillation, performed after the occurrence of each VF, has been associated with higher infarctions in the pig model [382]. Therefore, even smaller infarctions would be expected in these two groups in the absence of VF, thus magnifying its protective action. On the contrary, the incidence of VF in pigs receiving the treatment combination was not modified, thereby supporting the fact that both treatments have no additive effect on infarct size.

6.2 ASSESSMENT OF THE POTENTIAL UTILITY OF PLASMA SUCCINATE LEVELS AS PROGNOSTIC BIOMARKER

6.2.1 Analysis of citric acid cycle metabolites in porcine plasma samples

Previous studies have shown, as discussed above, that succinate accumulates in ischemic tissues, including the myocardium [274,279,280,383,384]. However, the mechanisms of succinate accumulation are still not fully stablished [385]. Most studies have proposed that succinate accumulates as consequence of a reverse action of SDH, leading to reduction of fumarate into succinate [279,294]. In this situation, both the malate/aspartate shuttle and the PNC pathways would lead to enhanced fumarate production during ischemia, which is then converted to succinate by SDH reversal. However, some reports, using stable-isotope-resolved metabolomics, have suggested that succinate primarily originates from canonical citric acid cycle activity, partially supported by aminotransferase anaplerosis and glycolysis from glycogen [296]. In addition, a recent computational model of complex II behavior in ischemia supported the idea that SDH reverse action cannot be the only source of the high concentration of succinate observed during ischemia [386].

Regardless of the mechanism by which succinate increases during myocardial ischemia, part of the accumulated succinate is released into the bloodstream after flow restoration [296,298,320]. In fact, the rapid decay in succinate occurring

during reperfusion [280] might not be due only to reoxidation during RET, but also by its efflux from the myocardial tissue [387]. Indeed, Prag and coworkers have recently suggested that succinate release upon reperfusion of the ischemic heart is mediated by the MCT1, in a process that is facilitated by ischemic acidification of the myocardium [298]. Therefore, the rapid decay of succinate occurring during reperfusion [279,280] has been attributed to both mechanisms, with about two-thirds being released into the perfusate within the first 5 minutes of reperfusion, while one-third is metabolized [296].

Supporting the existence of this efflux, succinate, together with other citric acid cycle metabolites including fumarate, malate and citrate, have been found to accumulate in the interstitial space of isolated rat hearts during ischemia and initial reperfusion [378]. Similar findings were obtained in the right ventricular interstitial space of newborn pigs submitted to 10 cycles of 3 minutes of ischemia followed by 3 min of reperfusion, as determined using microdialysis catheters [388]. However, analysis of interstitial metabolite concentrations in newborn animals in the last study might not be directly translated to changes occurring in adult hearts, as a gradual switch in cardiac energy generation from glycolysis to fatty acid oxidation occurs over the first postnatal weeks [388]. Furthermore, short episodes of ischemia in that study [388] may not completely reflect changes occurring after myocardial infarction.

Several studies have characterized the plasma metabolome in patients with STEMI. Using a non-targeted liquid chromatography tandem mass spectroscopy (LC-MS/MS) approach in 27 STEMI patients who underwent pPCI, it was demonstrated that the largest cohort of molecules undergoing significant changes, from 2 to 48 h after pPCI, were lipid metabolites, although citric acid intermediates, and especially succinate, were also increased [389]. In contrast, others found a decrease in succinate, fumarate, and citrate in serum obtained 1 hour after symptom onset in 20 STEMI patients [390]. Significantly, in the aforementioned studies samples were taken at different timepoints, which could partially explain these discrepancies. In addition, samples were obtained from peripheral blood, which might not be the most appropriate to analyze these changes. Indeed, it was demonstrated in STEMI patients, and in a porcine model of transient coronary occlusion, that the greatest increase in succinate concentrations occurred when blood was taken, immediately after reperfusion, from the coronary sinus [298,320]. Importantly, succinate was the metabolite

released in greater quantity from the myocardium [320]. Consistent with this observation, our present results obtained in the porcine model indicate that citric acid cycle metabolites like succinate, fumarate and malate are markedly increased in blood from the great cardiac vein, but not in peripheral blood. In the latter, only a modest increase in metabolite concentrations was observed two hours after reperfusion.

However, whether release of succinate and other citric acid cycle intermediates to the bloodstream during reperfusion can be modified by protective maneuvers was until now unknown. Our present results demonstrate that the enhanced levels of fumarate, malate, and citrate, detected in the plasma from the great cardiac vein in control animals during initial reperfusion, were reduced by both individual treatments and by the combination of RIC with malonate.

The increase in citric acid cycle intermediates seen after reperfusion can be due to two different mechanisms that may work simultaneously. On the one hand, membrane rupture would cause a massive release of intracellular metabolites, and in this sense, our present results may merely reflect differences in the amount of cell death. On the other hand, however, it may also reflect differences in the metabolic profile of cardiac cells and in the active release of metabolites. Accordingly, our present data demonstrate that groups receiving malonate had higher succinate plasma concentrations as compared with those receiving RIC alone. As these groups of animals have similar infarctions, these differences can only be ascribed to the effect of malonate on SDH activity [279,280]. Furthermore, these differences seem to extend to fumarate and malate.

In addition, it was unknown whether citric acid cycle metabolite concentrations might have a prognostic value during myocardial ischemia-reperfusion. In the study by Kohlhauer et al. including STEMI and non-STEMI patients, a modest correlation between coronary sinus succinate concentrations and edema volume, but not irreversible myocardial injury (i.e., final myocardial infarct size at 6 months, as measured by cardiac magnetic resonance, or troponins, determined during the first 48 h), was found [320]. Edema volume was quantified, in the aforementioned study, by T2-weighted nuclear magnetic resonance imaging performed 2 days after pPCI, a supposed surrogate of area at risk and acute injury [320]. However, it has been suggested that T2-weighted edema might not constitute an accurate surrogate for the area at risk [391], especially when it is

not determined in a time window ranging between 4 and 7 days post myocardial infarction [392] and when cardioprotective therapies are applied [393]. Our present results using a targeted UPLC-MS/MS approach demonstrate that not only succinate, but also fumarate and malate, are significantly enhanced during initial reperfusion in blood from the great cardiac vein. Our data also confirm a moderate correlation between succinate (and lactate) concentrations measured 5 min after reperfusion with the size of the area at risk, and suggest positive correlations between succinate, fumarate, and malate and myocardial infarct size. These data are suggestive that citric acid metabolite concentrations obtained in blood samples from the coronary sinus might constitute a new prognosis tool to predict final infarct size in STEMI patients.

6.2.2 Prognostic value of plasma succinate and other metabolites in STEMI patients

As is apparent from our previous data obtained in the pig model of myocardial infarction, the potential utility of citric acid cycle intermediates as biomarkers would be higher in blood from the coronary sinus. However, obtaining blood from this origin is not included in the routine practice, is not always feasible and is not without risks. Notably, previous studies have suggested that succinate is also increased in blood obtained from a peripheral vein in STEMI patients immediately after stent implantation [320]. Therefore, given that most STEMI patients have a peripheral via, here we aimed to assess whether the concentration of succinate and other metabolites in peripheral plasma, obtained during the coronary procedure, correlates with myocardial edema or infarct size, as determined by CMR, in patients undergoing emergency primary percutaneous coronary intervention (pPCI) in our center (Vall d'Hebron Hospital Universitari, Barcelona, Spain) and included in the randomized COMBAT-MI clinical trial [316].

Our present study shows that the presence of restituted blood flow at the culprit vessel before pPCI in STEMI patients with TIMI flow ≥ 2 upon arrival (i.e., having experienced spontaneous reperfusion before the procedure), had increased levels of succinate as compared with patients with TIMI ≤ 1. This observation may indicate that the concentration of this metabolite achieved in the peripheral blood of STEMI patients undergoing successful reperfusion increases over time, and that a delay before blood sampling might be needed to attain higher levels of this metabolite. In fact, our results in the porcine model also support this

hypothesis, since no modification in the plasma concentrations of succinate or other metabolites was observed in peripheral blood during initial reperfusion and a modest increase was observed only after 2 hours of reflow.

As previously mentioned, Kohlhauer and coworkers found increased concentrations of succinate in the blood of STEMI patients obtained from a peripheral vein or the coronary sinus immediately after stent implantation [320]. Furthermore, our results reported above showed a similar increase in succinate levels during initial reperfusion in the blood of the great cardiac vein in the pig model of transient coronary occlusion. Remarkably, whereas in the first study succinate plasma concentration at the coronary sinus correlated with edema volume but did not correlate with irreversible myocardial injury [320], our results obtained in the porcine model demonstrate that succinate concentrations at the great cardiac vein correlated with infarct size, measured 2 hours after reperfusion, and were reduced by protective maneuvers. Unfortunately, however, and in contrast with these previous observations, our present analysis shows that succinate concentrations in peripheral blood, obtained early after pPCI, do not correlate with the degree of irreversible injury (i.e., infarct size) or the size of the area at risk in STEMI patients undergoing pPCI, limiting the applicability of this metabolite as a non-invasive prognostic biomarker in STEMI patients.

As stated above, a possible explanation for the lack of correlation in our present study is that metabolite concentrations were measured in blood of a peripheral origin, as we intended to mimic the clinical situation in which a peripheral via is available in most, if not all, STEMI patients. In contrast, previous studies measured succinate concentrations at the coronary sinus [320], where a better picture of the metabolic changes occurring in the area at risk might be represented. Indeed, succinate was found to be the only metabolite significantly increased in blood from the coronary sinus compared with peripheral blood in STEMI patients [320]. Whether its concentrations at the coronary sinus correlate with the area at risk (acute ischemic injury) or final infarct size deserves, thus, further investigation. Given that succinate concentrations increase over time during reperfusion, as we have demonstrated in the pig model and in patients with TIMI flow ≥ 2, another possible explanation for the lack of correlation between succinate levels and infarct size or area at risk would be that peripheral blood samples were taken too early after the pPCI. For this reason, the existence

of potential correlations between succinate concentration in peripheral plasma at longer time intervals after pPCI and CMR variables should be explored in the future.

Lack of correlations in our present study in STEMI patients might be also explained by methodological differences when compared with previous works. Whereas in our current analysis CMR data were obtained 3–7 days after pPCI [316], in the study by Kohlhauer and coworkers edema volume was quantified by T2-weighted CMR 2 days after pPCI [320] which, as explained above, may not constitute an accurate surrogate for the area at risk [391,392]. Similarly, in our previous study in pigs, infarct size was measured by TTC staining soon after coronary occlusion, an experimental methodology notably different to that used in the clinical context.

Succinate concentrations in plasma seem to have a great variability between studies. In the work by Sadagopan [394], serum succinate concentrations, as measured by LC-MS/MS, in samples from hypertensive or diabetic patients, ranged between 1 and 8 µmol/L, values similar to those found by Kohlhauer in patients with angina or acute myocardial infarction [320]. However, others have found, using the same technique, values around 1–3 mmol/L in patients with acute myocardial infarction or coronary artery disease, and undetectable levels in healthy controls [395]. No clear explanation is currently available for these discrepancies, apart from methodological errors. But even within the same work, huge variations have been described. D'Alessandro et al., also using LC-MS/MS, found mean values or 10.1 ± 22.7 µmol/L in plasma of a control population with traumatic injuries that was increased to 96.1 ± 144.2 µmol/L in deceased patients, but values ranged from below 5 to more than 200 µmol/L (40x fold) [360]. Similarly, patients with aortic diseases had a median of 35.15 µmol/L, significantly higher than healthy controls (15.30 µmol/L), but again values ranged from about 10 to near 200 µmol/L (20x fold) [396], whereas Osuna-Prieto and coworkers showed that succinate plasma levels ranged from 11 to 130 µmol/L in young adults (11x fold) [359]. In our present study in STEMI patients we measured succinate concentrations by ^{1}H-NMR spectroscopy in plasma, and our values were in the range of some of those previous studies (about 69 ± 7 µmol/L in TIMI 1 and 141 ± 58 µmol/L in TIMI 2 patients), and near to those we found in our pig model of transient coronary occlusion (from 9.1 ± 0.9 to 27.8 ± 3.9 µmol/L) in blood from the great cardiac vein, but also presenting a high variability (from 40

to 423 µmol/L, 10x fold). Reasons for this high variability are unknown but may be due, in part, to the different conditions within each individual patient, to the analytical technique (^{1}H-NMR vs. LC-MS/MS), to the extraction method, or to the use of plasma vs. serum.

6.3 MODULATION OF RET BY INTERNAL FACTORS: ROLE OF CX43

Despite the extensive body of work regarding ROS production by RET [293], there is currently no available information on endogenous RET modulators. Given the location of Cx43 at the inner mitochondrial membrane of cardiomyocyte SSM and its role in regulating ROS production under specific circumstances, this protein emerges as a promising candidate to modulate RET. Our results demonstrate that Cx43 ablation attenuates ROS production by RET in cardiac SSM isolated from Cx43$^{Cre\text{-}ER(T)/fl}$ mice hearts. This effect is associated with a decrease in the amount of CoQ9 and in its reduced state, but not with changes in mitochondrial membrane potential or with distinct accumulation of succinate during global ischemia in isolated mice hearts. The lower ROS production occurring under conditions mimicking those found during initial reperfusion might explain, at least in part, the marked protection these animals have against ischemia-reperfusion injury, and the fact that transient, reversible, inhibition of SDH with malonate during initial reperfusion, does not exert additional protection.

6.3.1 Effects of Cx43 deficiency on mitochondrial function and ROS production by RET

Cx43 is the most ubiquitous member of the connexin family, which consists of 20 and 21 isoforms in mice and humans, respectively [37]. All connexins are transmembrane proteins primarily located in the sarcolemma, where they form channels known as connexons or hemichannels through the oligomerization of six individual molecules [37,397]. In the heart three main isoforms are expressed, Cx43, Cx40 and Cx45, with Cx43 being the most abundant in the ventricular myocardium. All of these isoforms play a critical role in cardiac physiology by facilitating the proper propagation of the electrical impulse between contiguous cardiomyocytes through the formation of intercellular channels. These channels result from the juxtaposition of two hemichannels from the two connected cells

and, as previously mentioned in this thesis, within a structure known as gap junction [37,398].

Besides its primary location at the plasma membrane, Cx43 has also been found at the inner mitochondrial membrane of cardiomyocyte mitochondria [324–327]. This unique location is shared by other cell types or tissues, including endothelial cells [330], brain [328], astrocytes [329] or bone marrow stem cells [331]. Remarkably, Cx43 has been demonstrated to be almost exclusively located at SSM, with IFM presenting little to no expression [399].

While the exact functions of mitochondrial Cx43 remain largely unknown, previous studies have suggested that mitochondrial Cx43 may have an impact on complex I respiration and oxygen consumption. SSM from rat hearts were shown to depict a reduction in ADP-stimulated respiration, when incubated with substrates feeding complex I, or after treatment with the gap junction uncoupler 18α-glycyrrhetinic acid or the mimetic inhibitory peptide Gap27 [400]. Similarly, mitochondria from $Cx43^{Cre\text{-}ER(T)/fl}$ mice treated with 4OHT, and thus lacking Cx43 expression, also showed a decrease in ADP-stimulated complex I respiration, but not in complex II respiration [400]. In contrast, our present study does not reveal any differences in either baseline respiration or ADP-stimulated complex I respiration. On the other hand, others have shown that inhibition or knockdown of Cx43 improves palmitic acid-induced mitochondrial dysfunction and oxidative phosphorylation in macrophages [401]. Unfortunately, there is no available explanation for these discrepancies.

It also has been proposed that mitochondrial Cx43 may modulate the ionic homeostasis of the organelle. Thus, mitochondrial K^+ influx was shown to be reduced in permeabilized cardiomyocytes from Cx43 deficient mice, and in wild-type animals treated with 18α-glycyrrhetinic acid or Gap19, [326,332]. These studies suggest that mitochondrial Cx43 impact in K^+ fluxes in this organelle. Mitochondrial Cx43 might also contribute to mitochondrial Ca^{2+} entry and cell death in the heart [402]. In addition, it is well-established that mitochondrial Cx43 can impact ROS production under specific circumstances. Several studies addressing this matter have used diazoxide, an opener of mitoK_{ATP} channels which induces cardioprotection by enhancing ROS production and generates pharmacological preconditioning [333]. In this regard, diazoxide cardioprotection is no longer present in cardiomyocytes from $Cx43^{+/-}$ mice and this drug is unable to

increase both ROS formation and cell viability [333]. Similar findings were observed in isolated hearts from Cx43-deficient animals [47,48]. This effect on Cx43-deficient cardiomyocytes seems to be specific for diazoxide, as other drugs inducing ROS through different mechanisms remained effective in these cells [333]. Therefore, these findings collectively support the role of mitochondrial Cx43 in preconditioning protection, particularly in those pathways involving ROS production by these organelles [403].

However, in addition to the controlled ROS formation induced by diazoxide and other preconditioning maneuvers, superoxide is, as discussed previously, massively produced during reperfusion by RET [279,280]. Unfortunately, there is currently no available information on endogenous RET modulators. As Cx43 is located at the inner mitochondrial membrane of cardiomyocyte SSM, where it modulates ROS production, as described above, we hypothesized that this protein could be an endogenous modulator of RET. Notably, some studies have indicated that a significant pharmacological overlap exists between complex II inhibitors (which attenuate RET) and mitoK_{ATP} channel agonists, as diazoxide, whose actions are not present in Cx43-deficient mice. For instance, the effects of diazoxide have been suggested to involve inhibition of SDH activity, a crucial component of RET [289]. On top of that, interaction between complex II and mitochondrial Cx43 has been proved [327]. On the other hand, certain complex II inhibitors, like atpenin A5 and even malonate, have been shown to act as potent mitoK_{ATP} activators [288,404]. In our present data, we observed a reduction of ROS production by RET in Cx43-deficient mice specifically in SSM from cardiomyocytes, but not in IFM, which correlates with the presence of the protein in the former and its absence in the latter. Therefore, our results provide evidence that Cx43 play a role in modulating ROS production RET.

RET is facilitated by factors such as increased degree of reduction of the CoQ pool, high $\Delta\psi$, and elevated succinate levels [321,322]. Thus, after our results suggesting a role of Cx43 in RET modulation in SSM, we sought to investigate whether Cx43 deficiency in $Cx43^{Cre\text{-}ER(T)/fl}$ mice treated with 4OHT might have any influence in any of these RET thermodynamic drivers. Our findings indicate that Cx43 deficiency did not alter $\Delta\psi$, in either isolated SSM or IFM, nor did it affect succinate levels at the end of ischemia in isolated mice hearts. As detailed previously, these two parameters are key factors that determine whether

electrons would flow back to complex I by RET, and neither of them appear to be involved in the reduction of ROS production by RET induced by Cx43 deficiency.

Regarding CoQ, and in contrast with the two previously analyzed factors, we observed that Cx43 deficiency was associated with a reduction in total CoQ9 levels, specifically in SSM, as assessed by UPLC-MS/MS analysis. It is important to note that the decrease of CoQ9 concentration observed in Cx43 deficient mice was not due to an alteration in the mitochondrial abundance in the mitochondrial preparation, since both citrate synthase activity and the mitochondrial yield were similar in both genotypes. Importantly, the CoQ9 levels that we have found in our mitochondrial preparations are in the range of previous publications [405,406].

Only few studies have addressed the question of how CoQ mitochondrial levels may influence mitochondrial ROS production [407]. Mitochondria isolated from mice hearts containing about 10% of normal CoQ content depicted lower ROS production in all ROS production sites, including the ones located at complex I from where ROS by RET is produced [408]. Similarly, lung mitochondria obtained from endurance trained rats showed a reduced mitochondrial CoQ pool size which was associated with a decrease in ROS production and with a lower degree of reduction of the CoQ pool [409]. One mechanism by which low CoQ levels might be able to reduce mitochondrial ROS production in our model is by induction of supercomplex assembly, which have been demonstrated to increase electron transport efficiency from one complex to another [410,411].

Furthermore, our data showed that deletion of Cx43 also induced a decrease in the percentage of $CoQ9H_2$, the reduced form of CoQ9, only in the SSM mitochondrial subpopulation. It is widely accepted that CoQ reduction state is critical in determining the levels of ROS production in mitochondria, and specially via RET [299]. In this regard, increased levels of ROS release have been associated with an enhanced degree of reduction of the CoQ pool when mitochondria were incubated under non-phosphorylating conditions (in the absence of ADP) [406]. Moreover, in isolated mitochondria from *Acanthamoeba castellanii* incubated with increasing concentration of different modulators of the ETC, the more degree of reduction of the CoQ pool, the higher mitochondrial ROS production was detected [412]. Importantly, ROS production by RET at complex I was

demonstrated to be favored, in isolated heart mitochondria, by a high degree of reduction of the CoQ pool, together with a high $\Delta\psi$ [266].

Therefore, and given that no changes were observed in $\Delta\psi$ and succinate concentrations, the most plausible explanation for the attenuated ROS production by RET observed in Cx43 deficient animals is the combined reduction in both total CoQ9 pool and in its reduced state.

6.3.2 Effects of Cx43 deficiency on ischemia-reperfusion injury and cardioprotection.

As a decrease in RET may lead to significant consequences in myocardial ischemia-reperfusion injury, we proceeded to evaluate the effects of both Cx43 deficiency and malonate treatment in isolated mice hearts submitted to transient global ischemia. Consistent with previous reports [47,413], we observed a notable reduction in infarct size and LDH release in hearts from $Cx43^{Cre\text{-}ER(T)/fl}$ mice treated with 4OHT, compared to hearts from wild-type $Cx43^{fl/fl}$ animals. While part of this protective effect might be attributed to a reduction in propagation of injury through gap junctional channels in these hearts [44,47,414], the extent of protection may suggest the involvement of additional mechanisms. Given that a reduction in ROS production by RET has been linked to reduced infarctions [279–281,362,364], it is tempting to speculate that at least part of this protection arises from this second mechanism.

On the other hand, malonate, administered during initial reperfusion, exhibited a moderate, yet significant, protective effect against infarction in hearts from wild-type mice, thus confirming previous findings in various species [279–281,362,364]. In contrast, malonate's efficacy was no longer observed in hearts from Cx43-deficient mice. The small magnitude myocardial infarction has in $Cx43^{Cre\text{-}ER(T)/fl}$ mice treated with 4OHT might have hindered the attainment of further protection in these animals. This situation was analogous to the case of ischemic preconditioning, which failed to confer protection against infarction in Cx43-deficient mice, as a consequence of the inability of their mitochondria to produce ROS in response to preconditioning stimuli [47,333]. Nonetheless, this was not the case for other cardioprotective strategies, such as ischemic postconditioning, which was shown to be able to reduce infarct size in Cx43-deficient mice [413,415], suggesting that additional avenues for protection still exist. Our current data

would suggest, thus, that malonate fails to induce protection in these animals due to their attenuated ROS production by RET, similar to what was described for ischemic preconditioning and diazoxide [413,415]. Notably, the reduction in ROS production was not limited to isolated mitochondria, but it was also confirmed by DHE staining in cardiac samples.

6.4 MODULATION OF RET BY EXTERNAL FACTORS: EFFECTS OF AIR POLLUTION

The study of the role of RET as a source of ROS in physiopathological conditions has been carried out by several groups over the last decade, but there is still a plethora of conditions where its involvement has not been addressed. Air pollution is an external factor that has emerged as a leading risk factor in human health and specially in cardiovascular diseases [334,337] and, among the multiple mechanisms that mediate the deleterious cardiovascular consequences induced by air pollution exposure, ROS production has been reported as one of the most relevant [348,349]. Several studies have associated PM exposure with increased oxidative stress, as suggested by data showing either an enhanced ROS production in the tissue [345] or in cultured cells [416], or a depletion of proteins included in the antioxidant system [347,417–419]. Furthermore, such increased oxidative stress has been shown to be manifested as enhanced lipid peroxidation [418,420], and administration of antioxidants has been demonstrated to reduce cellular damage induced by PM exposure [421]. However, the origin of this increased oxidative stress and ROS production, and how the last are generated, has not been investigated in detail. Therefore, our aim in the last section of this thesis was to investigate the role of ROS production by RET in the cardiovascular effects of air pollution.

Mitochondrial dysfunction has been demonstrated to play an important role in the deleterious consequences of PM exposure in several tissues, including the myocardium [348]. Our present results demonstrate that DEP exposure is associated with a decreased CS activity in both SSM and IFM, as compared with that found in hearts from control animals. Whereas CS is commonly used as a quantitative marker of the presence of intact mitochondria in the preparation [422], a depleted CS activity may indicate either a reduced initial mitochondrial content in the original tissue or a diminished survival of mitochondria during the

extraction process. However, MY measurements were not modified in cardiac mitochondria from exposed animals, which would rule out a defective mitochondrial extraction. Therefore, our data demonstrates that intratracheal instillation of DEP induces a reduction in the number of viable mitochondria in hearts from exposed animals, both in the case of SSM and IFM. Others have also found a decreased mitochondrial DNA copy number in the myocardium of rats instilled with diesel particulate matter for 21 days, thus supporting our data [347,423]. Furthermore, mitochondrial morphology abnormalities, including swelling and cristae disruption, have been found in cardiac mitochondria from mice exposed to urban air for 16 weeks [424].

Exposure to DEP did not induce, in the present study, any change in baseline (state 2) or ADP-stimulated (state 3) mitochondrial oxygen consumption, neither in isolated cardiac SSM, nor IFM, fuelled with substrates feeding complex I or complex II. These results are in contrast with the ones obtained in previous reports, which showed a general decrease in oxygen consumption after PM exposure. Marchini and colleges reported a decreased oxygen uptake by left ventricular tissue cubes obtained from mice exposed to urban air for 12 weeks [424]. Moreover, whereas freshly isolated cardiac mitochondria obtained from these hearts depicted a conserved oxygen consumption under state 2 conditions, they showed a reduction in mitochondrial respiration after addition of ADP (state 3) [424]. Similarly, state 3 respiration was decreased in permeabilized cardiac fibres from rats exposed to diesel exhaust for 3 weeks, while acute exposure did not modify these parameters. The effects of diesel exhaust on mitochondrial function might be more prominent in complex I activity, as demonstrated in left ventricular homogenates, whereas no changes were observed in complex III or IV activities [425]. Finally, in another study, cardiac samples obtained from mice 3 hours after acute instillation with residual oil fly ash (the inorganic residue resulting from the incomplete oxidation of motor vehicle emissions and fossil fuel combustion), presented a reduction in oxygen consumption, whereas isolated cardiac mitochondrial showed a decreased respiration under state 2 and 3 conditions [426]. One reason for the discrepancies between our present results and those previously reported could be the different sources of PM used in these studies, together with the wide range of exposure times, ranging from acute exposure to continuous, for even 3 months.

As described above, oxidative stress induced by PM has been generally determined by indirect or general approaches [345,416,418,420], or attributed to a decreased activity of the antioxidant system, including SOD and catalase, or to a reduction in the GSH/GSSG ratio [347,418,423,427]. Few reports have explored deeper into the source of ROS by PM. Shukla and co-workers showed how intact mitochondria from endothelial cells incubated, for 1 hour, with pyruvate and the air pollutant BP-1,6-Q, presented an increase in ROS production, which was partially reverted by addition of rotenone or antimycin, inhibitors of Complex I and III, respectively [349]. In another study, isolated cardiac mitochondria from mice exposed to urban air for 12 weeks presented an enhanced ROS production, as measured by MitoSOX and Amplex Red, when compared with those from control animals, finding that was associated with a decreased CII activity [424]. Therefore, the few available reports on the origin of the enhanced ROS production after exposure to air pollution or PM point to the ETC as an important source.

In our present study, we observed a significant increase in ROS production in cardiac mitochondria isolated from animals intratracheally instilled with DEP, as compared with those from controls mice. This enhanced ROS production was apparent both in SSM and IFM when fuelled with complex I substrates, with a similar trend observed when fuelled with the complex II substrate succinate. Remarkably, ROS production by RET, determined as the difference between values obtained with succinate in the absence and presence of rotenone, were not different between cardiac mitochondria from DEP-exposed animals and control mice in any mitochondrial subpopulation. Therefore, our results support the idea that the ETC in involved in the increase in ROS production brought by PM exposure, but by a mechanism independent of RET.

Moreover, we found that isolated cardiac mitochondria from DEP-exposed animals have an already enhanced ROS production under baseline conditions, before addition of respiratory substrates. This fact points to the possibility that other mitochondrial sources, beyond the ETC, also play a role in the enhanced oxidative stress occurring after PM exposure. Recent results obtained in the lab by other researchers have demonstrated an increased expression, after DEP exposure, of the ROS-producing enzyme NADPH oxidase 4 (NOX4) (personal communication), which is expressed in the mitochondria [428,429]. Furthermore, several other sources of ROS have been described within the mitochondria,

including monoamine oxidases, which may play a role in such baseline production [430]. In addition, reductions in the expression of the antioxidant enzyme thioredoxin reductase, also located in this organelle, have been also observed by our group after DEP instillation (personal communication). How this enhanced baseline ROS production might contribute to the increased levels detected after incubation with respiratory substrates is currently unknown.

As an enhanced ROS production may impact on infarct size, we evaluated whether DEP intratracheal instillation had any effect on myocardial ischemia-reperfusion injury. In this regard, previous reports showed that PM exposure worsens the outcome of ischemia-reperfusion. For instance, hearts from rats exposed to diesel particulate matter submitted to global ischemia in the Langendorff system, exhibited an impaired functional recovery during reperfusion, together with an increased infarct size [347]. The same authors also described an increased infarct size in a rat model of isoproterenol-induced myocardial infarction [423]. Similarly, an increased myocardial infarction was observed in mice submitted in vivo to ischemia-reperfusion, 12 weeks after respiring urban air [424], or after acute instillation of residual oil fly ash in a model of permanent coronary ligature [346]. In contrast to these previous reports, McIntosh-Kastrinsky et al [431] demonstrated that isolated hearts from mice exposed to multipollutant mixtures for 4 h depicted a reduction in infarct size, 8 h later, when submitted to global transient ischemia. In our present study, we have been unable to detect any effect of previous DEP exposure on infarct size or functional recovery in our rat model. We do not have any explanation for these discrepancies, beyond differences between the protocols of exposure and the contaminant used. However, and given that we were not able to observe changes in ROS production by RET, these data might support an essential role for RET in myocardial infarction.

Contrary to what happened with myocardial infarction, recent unpublished results from our group reveal an increase, after DEP exposure, in the incidence and duration of sustained ventricular tachyarrhythmias after application of a protocol on programmed electrical stimulation to isolated rat hearts. This would be in agreement with previous reports, showing that PM exposure enhanced ventricular tachyarrhythmias, effect associated with an increased oxidative stress and calcium calmodulin kinase II activation [432].

In summary, our data suggest that DEP exposure reduces the number of viable mitochondria and enhances mitochondrial ROS production, both under baseline conditions and after incubation with respiration substrates, but this effect is independent of RET. No effects on infarct size were observed in isolated rat hearts submitted to transient global ischemia.

7. CONCLUSIONS

CONCLUSIONS

The results of this thesis lead to the following conclusions:

1. The combination of RIC, applied during myocardial ischemia, and transient SDH inhibition with malonate, given during initial reperfusion, exert non-additive cardioprotective effects in a porcine model of transient coronary occlusion.

2. Succinate levels in plasma obtained from the great cardiac vein significantly correlates with infarct size in our porcine model of transient coronary occlusion. Unfortunately, however, succinate concentrations in peripheral blood do not correlate with CMR variables in STEMI patients, limiting the applicability of this metabolite as a non-invasive prognostic biomarker in this population.

3. The presence of restituted blood flow at the culprit vessel before pPCI increases succinate concentrations in the peripheral blood of STEMI patients. This data may suggest that succinate levels increase over time following myocardial infarction in blood from a peripheral origin.

4. Cx43 deficiency attenuates ROS production by RET in isolated cardiac subsarcolemmal mitochondria from $Cx43^{Cre\text{-}ER(T)/fl}$ mice, effect associated with a decrease in the CoQ pool and in its reduction state. This fact may explain, at least in part, the marked protection these animals have against myocardial ischemia-reperfusion injury, and that transient, reversible inhibition of SDH with malonate does not exert additional protection.

5. DEP exposure reduces the number of viable mitochondria and enhances mitochondrial ROS production, both under baseline conditions and after incubation with respiration substrates, but this effect is independent of RET. No effects on infarct size were observed in isolated rat hearts submitted to transient global ischemia.

8. FUTURE DIRECTIONS

FUTURE DIRECTIONS

Although our present findings do not support an additive effect between RIC and SDH inhibition with malonate, this should not discourage us to find other solutions. A consortium of several research groups included in the UE Cost Action on Cardioprotection has recently proposed to test, in a multicentric approach, the combination of acid malonate, acting on cardiomyocytes, with angiopoietin-like-4 [433], acting on endothelial cells. This combination has been considered promising and experiments will we carried in the consortium formed in the Cost Action in the near future.

In the second aim of this thesis, we have demonstrated that succinate concentrations in the great cardiac vein correlate with infarct size in a porcine model of coronary occlusion. However, this was not the case in peripheral blood samples, neither in pigs submitted to transient coronary occlusion, nor in samples from STEMI patients obtained just after reperfusion. Our data also suggest that concentrations of this metabolite increase over time during reperfusion. This finding should be explored in more detail, and the possible correlation between succinate concentrations in peripheral plasma from STEMI patients obtained with some delay after reperfusion and CMR outcomes could be addressed in future studies.

Our data also demonstrates that ROS production by RET is attenuated by Cx43 deficiency, which is associated with a decrease in CoQ pool levels and in the amount of its reduced form. However, we did not address the exact mechanism by which Cx43 influences CoQ concentration and redox state, and more work would be needed to further investigate this question. One aspect to consider could be whether the interaction of Cx43 with components of the respiratory chain like complex I or complex II could have an effect on CoQ redox state, as well as whether Cx43 may influence the formation of supercomplexes. Additionally, the possible effect of Cx43 in the CoQ synthesis pathway should be explored in the future, since the last steps of this process occur within the IMM [434].

Notably, this thesis already has continuity with a project that has recently started in our group, evaluating the effects of particulate matter exposure in the myocardium. Although our present results demonstrate that ROS production by

RET is not modified by particulate matter exposure, we also observed that ROS production is, indeed, increased in isolated mitochondria. Therefore, the origin and consequences of this oxidative stress in our model of DEP instillation should be explored in more detail. In this regard, other sources of oxidative stress have been investigated in our group and we have recently demonstrated that DEP-exposed rats present an increased expression of the ROS-producing enzyme NOX4 and a decreased presence of the antioxidant enzyme thioredoxin reductase. Whether these alterations in oxidative stress are reflected in tissue as well could be assessed in future works.

On the other hand, we were unable to observe any effect of DEP exposure on infarct size in isolated hearts. One possible explanation could be that alterations in the autonomous nervous system or in humoral regulators play a key role in the possible effect of DEP on ischemia-reperfusion injury. Despite some studies have demonstrated an increase in infarct size in isolated hearts [347,416], most previous works were done *in vivo* [345,346,424]. To test the possible involvement of humoral or nervous factors, additional studies would be needed *in vivo* in rats submitted to transient coronary occlusion. In case any effect is detected, this would drive us to analyze the mechanisms involved by use of specific inhibitors of the sympathetic or parasympathetic nervous system.

In this last aim, we focused on the consequences of PM exposure on mitochondrial ROS production and on myocardial ischemia-reperfusion injury. However, how DEP instillation might also influence the development of heart failure, including that secondary to a previous myocardial infarction, is currently unknown. New studies in animals with post-infarction heart failure could provide more detailed insights into the effects of PM exposure on prognosis of patients with an already established cardiovascular condition, thus allowing a better understanding of the complex pathologies faced by doctors in clinical practice. Therefore, with a new *in vivo* rat model of myocardial infarction followed by three weeks of DEP-instillation, the consequences of DEP exposure on scar development and cardiac remodeling could be evaluated. In addition, the arrhythmogenic effect of PM demonstrated in previous experiments could be compared with the possible alteration of ventricular arrythmias in previously infarcted animals, exposed or not to DEP. Future studies should be addressed also to evaluate the role of oxidative stress and mitochondria under these conditions.

9. BIBLIOGRAPHY

1. Tsao, C. W. *et al.* Heart Disease and Stroke Statistics-2022 Update: A Report from the American Heart Association. *Circulation* **145**, E153–E639 (2022).

2. World Health Organization Fact Sheet-Top 10 causes of death. https://www.who.int/news-room/fact-sheets/detail/the-top-10-causes-of-death (2020).

3. Roth, G. A. *et al.* Global Burden of Cardiovascular Diseases and Risk Factors, 1990-2019: Update From the GBD 2019 Study. *J Am Coll Cardiol* **76**, 2982–3021 (2020).

4. Bueno, H. & Pérez-Gómez, B. Global Rounds: Cardiovascular Health, Disease, and Care in Spain. *Circulation* **140**, 13–15 (2019).

5. Malakar, A. K. *et al.* A review on coronary artery disease, its risk factors, and therapeutics. *J Cell Physiol* **234**, 16812–16823 (2019).

6. Severino, P. *et al.* Ischemic heart disease pathophysiology paradigms overview: From plaque activation to microvascular dysfunction. *Int J Mol Sci* **21**, 1–30 (2020).

7. Smith, J. N., Negrelli, J. M., Manek, M. B., Hawes, E. M. & Viera, A. J. Diagnosis and management of acute coronary syndrome: An evidence-based update. *Journal of the American Board of Family Medicine* **28**, 283–293 (2015).

8. Reimer, K. A., Lowe, J. E., Rasmussen, M. M. & Jennings, R. B. The Wavefront Phenomenon of Ischemic Cell Death 1. Myocardial Infarct Size vs Duration of Coronary Occlusion in Dogs. 786–794 (1977).

9. Garcia-Dorado, D., Theroux, P., Elizaga, J., Galinanes, M. & Fernandez Aviles, F. Myocardial reperfusion in the pig heart model: infarct size and duration of coronary occlusion. *Cardiovasc Res* **21**, 537–544 (1987).

10. Hausenloy, D. J. *et al.* Translating cardioprotection for patient benefit: Position paper from the Working Group of Cellular Biology of the Heart of the European Society of Cardiology. *Cardiovasc Res* **98**, 7–27 (2013).

11. Ibanez, B. *et al.* 2017 ESC Guidelines for the management of acute myocardial infarction in patients presenting with ST-segment elevation. *Eur Heart J* **39**, 119–177 (2018).

12. Garcia-Dorado, D., Rodríguez-Sinovas, A., Ruiz-Meana, M. & Inserte, J. Protección contra el daño miocárdico por isquemia-reperfusión en la práctica clínica. *Rev Esp Cardiol* **67**, 394–404 (2014).

13. Hausenloy, D. J. & Yellon, D. M. Myocardial ischemia-reperfusion injury: A neglected therapeutic target. *Journal of Clinical Investigation* **123**, 92–100 (2013).

14. Piper, H. M., Garcıa-Dorado, D. & Ovize, M. A fresh look at reperfusion injury 1. *Cardiovasc Res* **38**, 291–300 (1998).

15. Inserte, J. *et al.* Effect of acidic reperfusion on prolongation of intracellular acidosis and myocardial salvage. *Cardiovasc Res* **77**, 782–790 (2008).

16. Bowers, K. C. *et al.* Bioluminescent Measurement in Single Cardiomyocytes of Sudden Cytosolic ATP Depletion Coincident with Rigor. *J Mol Cell Cardiol* **24**, 213–218 (1992).

17. Grover, G. J. *et al.* Excessive ATP hydrolysis in ischemic myocardium by mitochondrial F 1 F 0-ATPase: effect of selective pharmacological inhibition of mitochondrial ATPase hydrolase activity. *American Journal of Physiology* **287**, 1747–1755 (2004).

18. Murphy, E. & Steenbergen, C. Mechanisms Underlying Acute Protection From Cardiac Ischemia-Reperfusion Injury. *Physiology Reviews* **88**, 581–609 (2008).

19. Piper, H. M., Abdallah, Y. & Schäfer, C. The first minutes of reperfusion: A window of opportunity for cardioprotection. *Cardiovasc Res* **61**, 365–371 (2004).

20. Miyazaki, S. *et al.* Quantitative analysis of contraction band and coagulation necrosis after ischemia and reperfusion in the porcine heart. *Circulation* **75**, 1074–1082 (1987).

21. Ganote, C. E. Contraction Band Necrosis and Irreversible Myocardial Injury*. *Cardiology* **15**, 67–80 (1983).

22. Garcia-Dorado, D. *et al.* Selective Inhibition of the Contractile Apparatus A New Approach to Modification of Infarct Size, Infarct Composition, and Infarct Geometry During Coronary Artery Occlusion and Reperfusion. *Circulation* **85**, 1160–1175 (1992).

23. Inserte, J., Garcia-Dorado, D., Hernando, V. & Soler-Soler, J. Calpain-mediated impairment of Na+/K+-ATPase activity during early reperfusion contributes to cell death after myocardial ischemia. *Circ Res* **97**, 465–473 (2005).

24. Inserte, J. *et al.* E ffect of inhibition of Na / Ca exchanger at the time of myocardial reperfusion on hypercontracture and cell death. *Cardiovasc Res* **55**, 739–748 (2002).

25. Piper, H. M., Kasseckert, S. & Abdallah, Y. The sarcoplasmic reticulum as the primary target of reperfusion protection. *Cardiovasc Res* **70**, 170–173 (2006).

26. Ruiz-Meana, M., Fernandez-Sanz, C. & Garcia-Dorado, D. The SR-mitochondria interaction: A new player in cardiac pathophysiology. *Cardiovasc Res* **88**, 30–39 (2010).

27. Marban, E. & Kusuoka, H. Maximal Ca2+-activated Force and Myofilament Ca 2+ Sensitivity in Intact Mammalian Hearts Differential Effects of Inorganic Phosphate and Hydrogen Ions. *Journal of General Physiology* **9**, 609–623 (1987).

28. Priori, S. G., Mantica, M., Napolitano, C., Schwartz, P. J. & Di, C. Early Afterdepolarizations Induced In Vivo by Reperfusion of Ischemic Myocardium A Possible Mechanism for Reperfusion Arrhythmias. *Circulation* **81**, 1911–1920 (1990).

29. Garcia-Dorado, D., Andres-Villarreal, M., Ruiz-Meana, M., Inserte, J. & Barba, I. Myocardial edema: A translational view. *J Mol Cell Cardiol* **52**, 931–939 (2012).

30. Inserte, J., Hernando, V. & Garcia-Dorado, D. Contribution of calpains to myocardial ischaemia/reperfusion injury. *Cardiovasc Res* **96**, 23–31 (2012).

31. Liu, X. & Schnellmann, R. G. Calpain mediates progressive plasma membrane permeability and proteolysis of cytoskeleton-associated paxillin, talin, and vinculin during renal cell death. *Journal of Pharmacology and Experimental Therapeutics* **304**, 63–70 (2003).

32. Armstrong, S. C., Latham, C. A., Shivell, C. L. & Ganote, C. E. Ischemic loss of sarcolemmal dystrophin and spectrin: Correlation with myocardial injury. *J Mol Cell Cardiol* **33**, 1165–1179 (2001).

33. Takamure, M., Murata, K. Y., Tamada, Y., Azuma, M. & Ueno, S. Calpain-dependent α-fodrin cleavage at the sarcolemma in muscle diseases. *Muscle Nerve* **32**, 303–309 (2005).

34. Barta, J. *et al.* Calpain-1-sensitive myofibrillar proteins of the human myocardium. *Mol Cell Biochem* **278**, 1–8 (2005).

35. Müller, A. L., Hryshko, L. V. & Dhalla, N. S. Extracellular and intracellular proteases in cardiac dysfunction due to ischemia-reperfusion injury. *Int J Cardiol* **164**, 39–47 (2013).

36. Nielsen, M. S. *et al.* Gap junctions. *Compr Physiol* **2**, 1981–2035 (2012).

37. Rodríguez-Sinovas, A., Sánchez, J. A., Valls-Lacalle, L., Consegal, M. & Ferreira-González, I. Connexins in the heart: Regulation, function and involvement in cardiac disease. *Int J Mol Sci* **22**, 4413 (2021).

38. Kleber, A. G. & Saffitz, J. E. Role of the intercalated disc in cardiac propagation and arrhythmogenesis. *Front Physiol* **5**, 404 (2014).

39. Sánchez, J. A., Rodríguez-Sinovas, A., Fernández-Sanz, C., Ruiz-Meana, M. & García-Dorado, D. Effects of a reduction in the number of gap junction channels or in their conductance on ischemia-reperfusion arrhythmias in isolated mouse hearts. *Am J Physiol Heart Circ Phys-iol* **301**, 2442–2453 (2011).

40. Liu, S. *et al.* A structural basis for the unequal sensitivity of the major cardiac and liver gap junctions to intracellular acidification: The carboxyl tail length. *Biophys J* **64**, 1422–1433 (1993).

41. Rodriguez-Sinovas, A., García-Dorado, D., Ruiz-Meana, M. & Soler-Soler, J. Enhanced effect of gap junction uncouplers on macroscopic electrical properties of reperfused myocardium. *Journal of Physiology* **559**, 245–257 (2004).

42. Ruiz-Meana, M. *et al.* Persistence of gap junction communication during myocardial ischemia. *Am J Physiol Heart Circ Physiol* **280**, 2563–2571 (2001).

43. Ruiz-Meana, M., Garcia-Dorado, D., Hofstaetter, B., Piper, H. M. & Soler-Soler, J. Propagation of Cardiomyocyte Hypercontracture by Passage of Na Through Gap Junctions. *Circ Res* **85**, 280–287 (1999).

44. García-Dorado, D., Rodríguez-Sinovas, A. & Ruiz-Meana, M. Gap junction-mediated spread of cell injury and death during myocardial ischemia-reperfusion. *Cardiovasc Res* **61**, 386–401 (2004).

45. Garcia-Dorado, D. *et al.* Cell-to-cell interaction: a mechanism to explain wave-front progression of myocardial necrosis. *American Journal of Physiology: Heart and Circulation Physiology* **256**, 1266–1273 (1989).

46. Garcia-Dorado, D. *et al.* Gap junction uncoupler heptanol prevents cell-to-cell progression of hypercontracture and limits necrosis during myocardial reperfusion. *Circulation* **96**, 3579–3586 (1997).

47. Sánchez, J. A. *et al.* Activation of RISK and SAFE pathways is not involved in the effects of Cx43 deficiency on tolerance to ischemia-reperfusion injury and preconditioning protection. *Basic Res Cardiol* **108**, (2013).

48. Rodríguez-Sinovas, A. *et al.* Effects of substitution of Cx43 by Cx32 on myocardial energy metabolism, tolerance to ischaemia and preconditioning protection. *Journal of Physiology* **588**, 1139–1151 (2010).

49. Lane, N. & Martin, W. The energetics of genome complexity. *Nature* **467**, 929–934 (2010).

50. Friedman, J. R. & Nunnari, J. Mitochondrial form and function. *Nature* **505**, 335–343 (2014).

51. Osellame, L. D., Blacker, T. S. & Duchen, M. R. Cellular and molecular mechanisms of mitochondrial function. *Best Pract Res Clin Endocrinol Metab* **26**, 711–723 (2012).

52. Annesley, S. J. & Fisher, P. R. Mitochondria in health and disease. *Cells* **8**, (2019).

53. Schaper, J., Meiser, E. & Stammler, G. Ultrastructural Morphometric Analysis of Myocardium from Dogs, Rats, Hamsters, Mice, and from Human Hearts. *Circulation Reseacrh* **56**, 377–391 (1985).

54. Hoppel, C. L., Tandler, B., Fujioka, H. & Riva, A. Dynamic organization of mitochondria in human heart and in myocardial disease. *International Journal of Biochemistry and Cell Biology* **41**, 1949–1956 (2009).

55. Palmer, J. W., Tandler, B. & Hoppel, C. L. Biochemical properties of subsarcolemmal and interfibrillar mitochondria isolated from rat cardiac muscle. *Journal of Biological Chemistry* **252**, 8731–8739 (1977).

56. Chakrabarty, R. P. & Chandel, N. S. Beyond ATP, new roles of mitochondria. (2022).

57. Doenst, T., Nguyen, T. D. & Abel, E. D. Cardiac metabolism in heart failure: Implications beyond atp production. *Circ Res* **113**, 709–724 (2013).

58. Murphy, M. P. Understanding and preventing mitochondrial oxidative damage. *Biochem Soc Trans* **44**, 1219–1226 (2016).

59. Lopaschuk, G. Regulation of carbohydrate metabolism in ischemia and reperfusion. *Am Heart J* **139**, s115–s119 (2000).

60. Zuurbier, C. J. *et al.* Cardiac metabolism as a driver and therapeutic target of myocardial infarction. *J Cell Mol Med* **24**, 5937–5954 (2020).

61. Honka, H. *et al.* Therapeutic Manipulation of Myocardial Metabolism: JACC State-of-the-Art Review. *J Am Coll Cardiol* **77**, 2022–2039 (2021).

62. Aerni-Flessner, L., Abi-Jaoude, M., Koenig, A., Payne, M. & Hruz, P. W. GLUT4, GLUT1, and GLUT8 are the dominant GLUT transcripts expressed in murine left ventricle. *Cardiovasc Diabetol* **11**, 1–10 (2012).

63. Dale Abel, E. Glucose transport in the heart. *Frontiers in Bioscience* **9**, 201–215 (2004).

64. Kolwicz, S. C. Ketone Body Metabolism in the Ischemic Heart. *Front Cardiovasc Med* **8**, (2021).

65. Karwi, Q. G. & Lopaschuk, G. D. Branched-Chain Amino Acid Metabolism in the Failing Heart. *Cardiovasc Drugs Ther* (2022) doi:10.1007/s10557-022-07320-4.

66. Czibik, G., Steeples, V., Yavari, A. & Ashrafian, H. Citric acid cycle intermediates in cardioprotection. *Circ Cardiovasc Genet* **7**, 711–719 (2014).

67. Des Rosiers, C., Labarthe, F., Lloyd, S. G. & Chatham, J. C. Cardiac anaplerosis in health and disease: Food for thought. *Cardiovasc Res* **90**, 210–219 (2011).

68. Nolfi-Donegan, D., Braganza, A. & Shiva, S. Mitochondrial electron transport chain: Oxidative phosphorylation, oxidant production, and methods of measurement. *Redox Biol* **37**, (2020).

69. Garbincius, J. F., Luongo, T. S. & Elrod, J. W. The debate continues – What is the role of MCU and mitochondrial calcium uptake in the heart? *J Mol Cell Cardiol* **143**, 163–174 (2020).

70. Garbincius, J. F. & Elrod, J. W. Mitochondrial calcium exchange in physiology and disease. *Physiol Rev* **102**, 893–992 (2022).

71. Bravo-Sagua, R. *et al.* Calcium transport and signaling in mitochondria. *Compr Physiol* **7**, 623–634 (2017).

72. Luongo, T. S. *et al.* The mitochondrial Na+/Ca2+ exchanger is essential for Ca2+ homeostasis and viability. *Nature* **545**, 93–97 (2017).

73. Giorgi, C., Marchi, S. & Pinton, P. The machineries, regulation and cellular functions of mitochondrial calcium. *Nat Rev Mol Cell Biol* **19**, 713–730 (2018).

74. Cao, J. L. *et al.* Role of mitochondrial Ca 2+ homeostasis in cardiac muscles. *Arch Biochem Biophys* **663**, 276–287 (2019).

75. Squire, J. Special issue: The actin-myosin interaction in muscle: Background and overview. *Int J Mol Sci* **20**, (2019).

76. Bers, D. M. Cardiac excitation-contraction coupling. *Nature* **415**, 198–205 (2002).

77. Zhang, D., Wang, F., Li, P. & Gao, Y. Mitochondrial Ca2+ Homeostasis: Emerging Roles and Clinical Significance in Cardiac Remodeling. *Int J Mol Sci* **23**, (2022).

78. Williams, G. S. B., Boyman, L. & Lederer, W. J. Mitochondrial calcium and the regulation of metabolism in the heart. *J Mol Cell Cardiol* **78**, 35–45 (2015).

79. Ruiz-Meana, M., Fernandez-Sanz, C. & Garcia-Dorado, D. The SR-mitochondria interaction: A new player in cardiac pathophysiology. *Cardiovasc Res* **88**, 30–39 (2010).

80. Gao, P., Yan, Z. & Zhu, Z. Mitochondria-Associated Endoplasmic Reticulum Membranes in Cardiovascular Diseases. *Front Cell Dev Biol* **8**, (2020).

81. Cao, Y. L. *et al.* MFN1 structures reveal nucleotide-triggered dimerization critical for mitochondrial fusion. *Nature* **542**, 372–376 (2017).

82. Mishra, P., Carelli, V., Manfredi, G. & Chan, D. C. Proteolytic cleavage of Opa1 stimulates mitochondrial inner membrane fusion and couples fusion to oxidative phosphorylation. *Cell Metab* **19**, 630–641 (2014).

83. Chan, D. C. Mitochondrial Dynamics and Its Involvement in Disease. *Annual Review of Pathology: Mechanisms of Disease* **15**, 235–259 (2019).

84. Friedman, J. R. *et al.* ER Tubules Mark Sites of Mitochondrial Division. *Science (1979)* **334**, 358–362 (2011).

85. Bravo-San Pedro, J. M., Kroemer, G. & Galluzzi, L. Autophagy and Mitophagy in Cardiovascular Disease. *Circ Res* **120**, 1812–1824 (2017).

86. Vásquez-Trincado, C. *et al.* Mitochondrial dynamics, mitophagy and cardiovascular disease. *Journal of Physiology* **594**, 509–525 (2016).

87. Bai, Y. *et al.* Mitochondrial quality control in cardiac ischemia/reperfusion injury: new insights into mechanisms and implications. *Cell Biol Toxicol* **39**, 33–51 (2022).

88. D'Arcy, M. S. Cell death: a review of the major forms of apoptosis, necrosis and autophagy. *Cell Biol Int* **43**, 582–592 (2019).

89. Kiraz, Y., Adan, A., Kartal Yandim, M. & Baran, Y. Major apoptotic mechanisms and genes involved in apoptosis. *Tumor Biology* **37**, 8471–8486 (2016).

90. Li, K., Delft, M. F. & Dewson, G. Too much death can kill you: inhibiting intrinsic apoptosis to treat disease. *EMBO J* **40**, (2021).

91. Peña-Blanco, A. & García-Sáez, A. J. Bax, Bak and beyond — mitochondrial performance in apoptosis. *FEBS Journal* **285**, 416–431 (2018).

92. Hsu, Y.-T., Wolter, K. G. & Youle, R. J. Cytosol-to-membrane redistribution of Bax and Bcl-X L during apoptosis (programmed cell deathBcl-2Baxdiphtheria toxin). **94**, 3668–3672 (1997).

93. Garrido, C. *et al.* Mechanisms of cytochrome c release from mitochondria. *Cell Death Differ* **13**, 1423–1433 (2006).

94. Cai, J., Yang, J. & Jones, D. P. Mitochondrial control of apoptosis: the role of cytochrome c. *Biochimica et Biophysika Acta* **1366**, 139–149 (1998).

95. Hill, M. M., Adrain, C., Duriez, P. J., Creagh, E. M. & Martin, S. J. Analysis of the composition, assembly kinetics and activity of native Apaf-1 apoptosomes. *EMBO Journal* **23**, 2134–2145 (2004).

96. Suzuki, Y. *et al.* A Serine Protease, HtrA2, Is Released from the Mitochondria and Interacts with XIAP, Inducing Cell Death. *Mol Cell* **8**, 613–621 (2001).

97. Du, C., Fang, M., Li, Y., Li, L. & Wang, X. Smac, a Mitochondrial Protein that Promotes Cytochrome c-Dependent Caspase Activation by Eliminating IAP Inhibition Hid, and Grim in terms of IAP neutralization and is the. *Cell* **102**, 33–42 (2000).

98. Verhagen, A. M. *et al.* Identification of DIABLO, a Mammalian Protein that Promotes Apoptosis by Binding to and Antagonizing IAP Proteins. *Cell* **102**, 43–53 (2000).

99. Bahi, N. *et al.* Switch from caspase-dependent to caspase-independent death during heart development: Essential role of endonuclease G in ischemia-induced DNA processing of differentiated cardiomyocytes. *Journal of Biological Chemistry* **281**, 22943–22952 (2006).

100. Inserte, J. *et al.* Studies on the role of apoptosis after transient myocardial ischemia: genetic deletion of the executioner caspases-3 and -7 does not limit infarct size and ventricular remodeling. *Basic Res Cardiol* **111**, 1–10 (2016).

101. Robichaux, D. J., Harata, M., Murphy, E. & Karch, J. Mitochondrial permeability transition pore-dependent necrosis. *J Mol Cell Cardiol* **174**, 47–55 (2023).

102. Seidlmayer, L. K. *et al.* Distinct mPTP activation mechanisms in ischaemia-reperfusion: Contributions of Ca2+, ROS, pH, and inorganic polyphosphate. *Cardiovasc Res* **106**, 237–248 (2015).

103. García-Dorado, D. Myocardial reperfusion injury: A new view. *Cardiovasc Res* **61**, 363–364 (2004).

104. Mitchell, P. Chemiosmotic coupling in oxidative and photosynthetic phosphorylation. *Biochim Biophys Acta Bioenerg* **1807**, 1507–1538 (2011).

105. Rich, P. R. & Maréchal, A. The mitochondrial respiratory chain. *Essays Biochem* **47**, 1–23 (2010).

106. Vercellino, I. & Sazanov, L. A. The assembly, regulation and function of the mitochondrial respiratory chain. *Nat Rev Mol Cell Biol* **23**, 141–161 (2022).

107. Kravchuk, V. *et al.* A universal coupling mechanism of respiratory complex I. *Nature* **609**, 808–814 (2022).

108. Kampjut, D. & Sazanov, L. A. The coupling mechanism of mammalian respiratory complex I. *Science (1979)* **370**, (2020).

109. Sousa, J. S., D'Imprima, E. & Vonck, J. Mitochondrial respiratory chain complexes. in *Subcellular Biochemistry* vol. 87 167–227 (Springer New York, 2018).

110. Du, Z. *et al.* Structure of the human respiratory complex II. *Proceedings of the National Academy of Sciences* **120**, (2023).

111. Lenaz, G. & Genova, M. L. Mobility and function of Coenzyme Q (ubiquinone) in the mitochondrial respiratory chain. *Biochim Biophys Acta Bioenerg* **1787**, 563–573 (2009).

112. Wang, Y. & Hekimi, S. Understanding Ubiquinone. *Trends Cell Biol* **26**, 367–378 (2016).

113. Ramsay, R. R. Electron carriers and energy conservation in mitochondrial respiration. *ChemTexts* **5**, (2019).

114. Trumpower, B. L. & Gennis, R. B. Energy Transduction by Cytochrome Complexes in Mitochondrial and Bacterial Respiration: The Enzymology of Coupling Electron Transfer Reactions to Transmembrane Proton Translocation. *Annu Rev Biochem* **63**, 675–716 (1994).

115. Banerjee, R., Purhonen, J. & Kallijärvi, J. The mitochondrial coenzyme Q junction and complex III: biochemistry and pathophysiology. *FEBS Journal* **289**, 6936–6958 (2022).

116. Rich, P. R. Mitochondrial cytochrome c oxidase: Catalysis, coupling and controversies. *Biochem Soc Trans* **45**, 813–829 (2017).

117. Zharova, T. V., Grivennikova, V. G. & Borisov, V. B. F1·Fo ATP Synthase/ATPase: Contemporary View on Unidirectional Catalysis. *Int J Mol Sci* **24**, 5417 (2023).

118. Nesci, S., Pagliarani, A., Algieri, C. & Trombetti, F. Mitochondrial F-type ATP synthase: multiple enzyme functions revealed by the membrane-embedded FO structure. *Crit Rev Biochem Mol Biol* **55**, 309–321 (2020).

119. Beutner, G., Alavian, K. N., Jonas, E. A. & Porter, G. A. The mitochondrial permeability transition pore and ATP synthase. in *Handbook of Experimental Pharmacology* vol. 240 21–46 (Springer New York LLC, 2017).

120. Blum, T. B., Hahn, A., Meier, T., Davies, K. M. & Kühlbrandt, W. Dimers of mitochondrial ATP synthase induce membrane curvature and self-assemble into rows. *Proc Natl Acad Sci U S A* **116**, 4250–4255 (2019).

121. Cogliati, S. *et al.* Mitochondrial cristae shape determines respiratory chain supercomplexes assembly and respiratory efficiency. *Cell* **155**, 160–171 (2013).

122. Genova, M. L. & Lenaz, G. Functional role of mitochondrial respiratory supercomplexes. *Biochim Biophys Acta Bioenerg* **1837**, 427–443 (2014).

123. Guan, S., Zhao, L. & Peng, R. Mitochondrial Respiratory Chain Supercomplexes: From Structure to Function. *Int J Mol Sci* **23**, (2022).

124. Letts, J. A. & Sazanov, L. A. Clarifying the supercomplex: The higher-order organization of the mitochondrial electron transport chain. *Nat Struct Mol Biol* **24**, 800–808 (2017).

125. Mileykovskaya, E. & Dowhan, W. Cardiolipin-dependent formation of mitochondrial respiratory supercomplexes. *Chem Phys Lipids* **179**, 42–48 (2014).

126. Granger, D. N. & Kvietys, P. R. Reperfusion injury and reactive oxygen species: The evolution of a concept. *Redox Biol* **6**, 524–551 (2015).

127. Ramachandra, C. J. A., Hernandez-Resendiz, S., Crespo-Avilan, G. E., Lin, Y. H. & Hausenloy, D. J. Mitochondria in acute myocardial infarction and cardioprotection. *EBioMedicine* **57**, (2020).

128. Marin, W., Marin, D., Ao, X. & Liu, Y. Mitochondria as a therapeutic target for cardiac ischemia-reperfusion injury (Review). *Int J Mol Med* **47**, 485–499 (2021).

129. Sharp, W. W. *et al.* Dynamin-related protein 1 (Drp1)-mediated diastolic dysfunction in myocardial ischemia-reperfusion injury: Therapeutic benefits of Drp1 inhibition to reduce mitochondrial fission. *FASEB Journal* **28**, 316–326 (2014).

130. Ong, S. B. *et al.* Inhibiting mitochondrial fission protects the heart against ischemia/reperfusion injury. *Circulation* **121**, 2012–2022 (2010).

131. Hom, J., Yu, T., Yoon, Y., Porter, G. & Sheu, S. S. Regulation of mitochondrial fission by intracellular Ca2+ in rat ventricular myocytes. *Biochim Biophys Acta Bioenerg* **1797**, 913–921 (2010).

132. Griffiths, E. J. & Halestrapt, A. P. Mitochondrial non-specific pores remain closed during cardiac ischaemia, but open upon reperfusion. *Biochem. J* **307**, 93–98 (1995).

133. Bonora, M., Giorgi, C. & Pinton, P. Molecular mechanisms and consequences of mitochondrial permeability transition. *Nat Rev Mol Cell Biol* **23**, 266–285 (2022).

134. Haworth2, R. A. & Hunter, D. R. The Ca2+-induced Membrane Transition in Mitochondria II. Nature of the Caz+ Trigger Site'. *Arch Biochem Biophys* **195**, 460–506 (1979).

135. Hunter, D. R. & Haworth, R. A. The Ca2+-Induced Membrane Transition in Mitochondria I. The Protective Mechanism+'. *Arch Biochem Biophys* **195**, 453–459 (1979).

136. Hunter, D. R., Haworth, R. A. & Southard, J. H. Relationship between configuration, function, and permeability in calcium treated mitochondria. *Journal of Biological Chemistry* **251**, 5069–5077 (1976).

137. Hunter, D. R. & Haworth, R. A. The Ca2+-Induced Membrane Transition in Mitochondria III. Transitional Ca2+ Release'. *Arch Biochem Biophys* **195**, 468–477 (1979).

138. Crompton, M., Costi, A. & Hayat, L. Evidence for the presence of a reversible Ca2+-dependent pore activated by oxidative stress in heart mitochondria. *Biochemical Journal* **245**, 915 (1987).

139. Halestrap, A. P. What is the mitochondrial permeability transition pore? *J Mol Cell Cardiol* **46**, 821–831 (2009).

140. Morciano, G. *et al.* The mitochondrial permeability transition pore: an evolving concept critical for cell life and death. *Biological Reviews* **96**, 2489–2521 (2021).

141. Morciano, G. *et al.* Molecular identity of the mitochondrial permeability transition pore and its role in ischemia-reperfusion injury. *J Mol Cell Cardiol* **78**, 142–153 (2015).

142. Halestrap, A. P. & Richardson, A. P. The mitochondrial permeability transition: A current perspective on its identity and role in ischaemia/reperfusion injury. *J Mol Cell Cardiol* **78**, 129–141 (2015).

143. Ong, S. B., Samangouei, P., Kalkhoran, S. B. & Hausenloy, D. J. The mitochondrial permeability transition pore and its role in myocardial ischemia reperfusion injury. *J Mol Cell Cardiol* **78**, 23–34 (2015).

144. Kokoszka, J. E. *et al.* The ADP/ATP translocator is not essential for the mitochondrial permeability transition pore. *Nature* **427**, 461–465 (2004).

145. Baines, C. P., Kaiser, R. A., Sheiko, T., Craigen, W. J. & Molkentin, J. D. Voltage-dependent anion channels are dispensable for mitochondrial-dependent cell death. *Nat Cell Biol* **9**, 550–555 (2007).

146. Šileikyte, J. *et al.* Regulation of the mitochondrial permeability transition pore by the outer membrane does not involve the peripheral benzodiazepine receptor (translocator protein of 18 kDa (TSPO)). *Journal of Biological Chemistry* **289**, 13769–13781 (2014).

147. Crompton, M., Ellinger, H. & Costi, A. Inhibition by cyclosporin A of a Ca2+-dependent pore in heart mitochondria activated by inorganic phosphate and oxidative stress. *Biochem. J* **255**, 357–360 (1988).

148. Nicolli, A., Basso, E., Petronilli, V., Wenger, R. M. & Bernardi, P. Interactions of cyclophilin with the mitochondrial inner membrane and regulation of the permeability transition pore, a cyclosporin A-sensitive channel. *Journal of Biological Chemistry* **271**, 2185–2192 (1996).

149. Halestrap, A. P. & Davidson, A. M. Inhibition of Ca2+-induced large-amplitude swelling of liver and heart mitochondria by cyclosporin is probably caused by the inhibitor binding to mitochondrial-matrix peptidyl-prolyl cis-trans isomerase and preventing it interacting with the adenine nucleotide translocase. *Biochem. J* **268**, 153–160 (1990).

150. Basso, E. *et al.* Properties of the permeability transition pore in mitochondria devoid of cyclophilin D. *Journal of Biological Chemistry* **280**, 18558–18561 (2005).

151. Baines, C. P. *et al.* Loss of Cyclophilin D reveals a critical role for mitochondrial permeability transition in cell death. *Nature* **434**, 658–662 (2005).

152. Duchen, M. R., Mcguinness, O., Brown, L. A. & Crompton, M. ViewPoint On the involvement of a cyclosporin A sensitive mitochondrial pore in myocardial reperfusion injury. *Cardiovasc Res* **27**, 1790–1794 (1993).

153. Griffiths, E. J. & Halestrap, A. P. Protection by cyclosporin A of ischemia/reperfusion induced damage in isolated rat hearts. *Journal of Molecular Cell Cardiology* **24**, 1461–1469 (1993).

154. Giorgio, V. *et al.* Cyclophilin D modulates mitochondrial F0F1-ATP synthase by interacting with the lateral stalk of the complex. *Journal of Biological Chemistry* **284**, 33982–33988 (2009).

155. Giorgio, V. *et al.* Dimers of mitochondrial ATP synthase form the permeability transition pore. *Proc Natl Acad Sci U S A* **110**, 5887–5892 (2013).

156. Alavian, K. N. *et al.* An uncoupling channel within the c-subunit ring of the F1F O ATP synthase is the mitochondrial permeability transition pore. *Proc Natl Acad Sci U S A* **111**, 10580–10585 (2014).

157. Bonora, M. *et al.* Role of the c subunit of the FO ATP synthase in mitochondrial permeability transition. *Cell Cycle* **12**, 674–683 (2013).

158. Neginskaya, M. A. *et al.* ATP Synthase C-Subunit-Deficient Mitochondria Have a Small Cyclosporine A-Sensitive Channel, but Lack the Permeability Transition Pore. *Cell Rep* **26**, 11-17.e2 (2019).

159. He, J. *et al.* Persistence of the mitochondrial permeability transition in the absence of subunit c of human ATP synthase. *Proc Natl Acad Sci U S A* **114**, 3409–3414 (2017).

160. Bernardi, P., Carraro, M. & Lippe, G. The mitochondrial permeability transition: Recent progress and open questions. *FEBS Journal* **289**, 7051–7074 (2022).

161. Gerle, C. Mitochondrial F-ATP synthase as the permeability transition pore. *Pharmacol Res* **160**, (2020).

162. Giorgio, V., Guo, L., Bassot, C., Petronilli, V. & Bernardi, P. Calcium and regulation of the mitochondrial permeability transition. *Cell Calcium* **70**, 56–63 (2018).

163. CROMPTON, M. & COSTI, A. Kinetic evidence for a heart mitochondrial pore activated by Ca2+, inorganic phosphate and oxidative stress: A potential mechanism for mitochondrial dysfunction during cellular Ca2+ overload. *Eur J Biochem* **178**, 489–501 (1988).

164. Ruiz-Meana, M. *et al.* The role of mitochondrial permeability transition in reperfusion-induced cardiomyocyte death depends on the duration of ischemia. *Basic Res Cardiol* **106**, 1259–1268 (2011).

165. Brieger, K., Schiavone, S., Miller, F. J. & Krause, K. H. Reactive oxygen species: From health to disease. *Swiss Med Wkly* **142**, (2012).

166. Brown, D. I. & Griendling, K. K. Regulation of signal transduction by reactive oxygen species in the cardiovascular system. *Circ Res* **116**, 531–549 (2015).

167. Dubois-Deruy, E., Peugnet, V., Turkieh, A. & Pinet, F. Oxidative stress in cardiovascular diseases. *Antioxidants* **9**, 1–15 (2020).

168. Krylatov, A. V. *et al.* Reactive Oxygen Species as Intracellular Signaling Molecules in the Cardiovascular System. *Curr Cardiol Rev* **14**, 290–300 (2018).

169. Chen, W., Gabel, S., Steenbergen, C. & Murphy, E. A redox-based mechanism for cardioprotection induced by ischemic preconditioning in perfused rat heart. *Circ Res* **77**, 424–429 (1995).

170. Cadenas, S. ROS and redox signaling in myocardial ischemia-reperfusion injury and cardioprotection. *Free Radic Biol Med* **117**, 76–89 (2018).

171. Otani, H. Reactive Oxygen Species as Mediators of Signal Transduction in Ischemic Preconditioning. *https://home-liebertpub-com.are.uab.cat/ars* **6**, 449–469 (2004).

172. Birben, E., Sahiner, U. M., Sackesen, C., Erzurum, S. & Kalayci, O. Oxidative stress and antioxidant defense. *World Allergy Organization Journal* **5**, 9–19 (2012).

173. Zhou, T., Chuang, C. C. & Zuo, L. Molecular Characterization of Reactive Oxygen Species in Myocardial Ischemia-Reperfusion Injury. *Biomed Res Int* **2015**, (2015).

174. Daiber, A., Andreadou, I., Oelze, M., Davidson, S. M. & Hausenloy, D. J. Discovery of new therapeutic redox targets for cardioprotection against ischemia/reperfusion injury and heart failure. *Free Radic Biol Med* **163**, 325–343 (2021).

175. Cadet, J. & Richard Wagner, J. DNA base damage by reactive oxygen species, oxidizing agents, and UV radiation. *Cold Spring Harb Perspect Biol* **5**, (2013).

176. Stadtman, E. R. & Berlett, B. S. Reactive Oxygen-Mediated Protein Oxidation in Aging and Disease. *http://dx.doi.org.are.uab.cat/10.3109/03602539808996310* **30**, 225–243 (2008).

177. Gaschler, M. M. & Stockwell, B. R. Lipid peroxidation in cell death. *Biochem Biophys Res Commun* **482**, 419–425 (2017).

178. Yin, H., Xu, L. & Porter, N. A. Free radical lipid peroxidation: Mechanisms and analysis. *Chem Rev* **111**, 5944–5972 (2011).

179. Heusch, G. *et al.* Health position paper and redox perspectives on reactive oxygen species as signals and targets of cardioprotection. *Redox Biol* **67**, (2023).

180. Wu, M. Y. *et al.* Current Mechanistic Concepts in Ischemia and Reperfusion Injury. *Cellular Physiology and Biochemistry* **46**, 1650–1667 (2018).

181. Xiang, M. *et al.* Role of Oxidative Stress in Reperfusion following Myocardial Ischemia and Its Treatments. *Oxid Med Cell Longev* **2021**, (2021).

182. Berry, C. E. & Hare, J. M. Xanthine oxidoreductase and cardiovascular disease: Molecular mechanisms and pathophysiological implications. *Journal of Physiology* **555**, 589–606 (2004).

183. Houston, M., Chumley, P., Radi, R., Rubbo, H. & Freeman, B. A. Xanthine Oxidase Reaction with Nitric Oxide and Peroxynitrite. *Arch Biochem Biophys* **355**, 1–8 (1998).

184. Kehrer, J. P. The Haber-Weiss reaction and mechanisms of toxicity. *Toxicology* **149**, 43–50 (2000).

185. Tan, Z. *et al.* Preservation of cardiac contractility after long-term therapy with oxypurinol in post-ischemic heart failure in mice. *Eur J Pharmacol* **621**, 71–77 (2009).

186. Werns, S. W. *et al.* Xanthine oxidase inhibition does not limit canine infarct size. *Circulation* **83**, 995–1005 (1991).

187. Kinsman, J. M., Murry, C. E., Richard, V. J., Jennings, R. B. & Reimer, K. A. The xanthine oxidase inhibitor oxypurinol does not limit infarct size in a canine model of 40 minutes of ischemia with reperfusion. *J Am Coll Cardiol* **12**, 209–217 (1988).

188. Chung, H. Y. *et al.* Xanthine dehydrogenase/xanthine oxidase and oxidative stress. *Age (Omaha)* **20**, 127 (1997).

189. Cantu-Medellin, N. & Kelley, E. E. Xanthine oxidoreductase-catalyzed reactive species generation: A process in critical need of reevaluation. *Redox Biol* **1**, 353–358 (2013).

190. Bredemeier, M. *et al.* Xanthine oxidase inhibitors for prevention of cardiovascular events: A systematic review and meta-analysis of randomized controlled trials. *BMC Cardiovasc Disord* **18**, 1–11 (2018).

191. Stamp, L. K. *et al.* Myeloperoxidase and oxidation of uric acid in gout: implications for the clinical consequences of hyperuricaemia. *Rheumatology (Oxford)* **53**, 1958–1965 (2014).

192. Lassègue, B., San Martín, A. & Griendling, K. K. Biochemistry, physiology, and pathophysiology of NADPH oxidases in the cardiovascular system. *Circ Res* **110**, 1364–1390 (2012).

193. Krijnen, P. A. J. *et al.* Increased Nox2 expression in human cardiomyocytes after acute myocardial infarction. *J Clin Pathol* **56**, 194–199 (2003).

194. Siu, K. L., Lotz, C., Ping, P. & Cai, H. Netrin-1 abrogates ischemia/reperfusion-induced cardiac mitochondrial dysfunction via nitric oxide-dependent attenuation of NOX4 activation and recoupling of NOS. *J Mol Cell Cardiol* **78**, 174–185 (2014).

195. Matsushima, S. *et al.* Broad suppression of NADPH oxidase activity exacerbates ischemia/reperfusion injury through inadvertent downregulation of hypoxia-inducible factor-1α and upregulation of peroxisome proliferator-activated receptor-α. *Circ Res* **112**, 1135–1149 (2013).

196. Meischl, C. *et al.* Ischemia induces nuclear NOX2 expression in cardiomyocytes and subsequently activates apoptosis. *Apoptosis* **11**, 913–921 (2006).

197. Borchi, E. *et al.* Role of NADPH oxidase in H9c2 cardiac muscle cells exposed to simulated ischaemia-reperfusion. *J Cell Mol Med* **13**, 2724 (2009).

198. Chen, H., Song, Y. S. & Chan, P. H. Inhibition of NADPH oxidase is neuroprotective after ischemia-reperfusion. *J Cereb Blood Flow Metab* **29**, 1262 (2009).

199. Braunersreuther, V. *et al.* Role of NADPH oxidase isoforms NOX1, NOX2 and NOX4 in myocardial ischemia/reperfusion injury. *J Mol Cell Cardiol* **64**, 99–107 (2013).

200. Yu, Q. *et al.* Elimination of NADPH oxidase activity promotes reductive stress and sensitizes the heart to ischemic injury. *J Am Heart Assoc* **3**, (2014).

201. Matsushima, S. & Sadoshima, J. Yin and Yang of NADPH Oxidases in Myocardial Ischemia-Reperfusion. *Antioxidants* **11**, (2022).

202. Kleikers, P. W. M. *et al.* NADPH oxidases as a source of oxidative stress and molecular target in ischemia/reperfusion injury. *J Mol Med* **90**, 1391–1406 (2012).

203. Förstermann, U. & Sessa, W. C. Nitric oxide synthases: Regulation and function. *Eur Heart J* **33**, (2012).

204. Rochette, L. *et al.* Nitric oxide synthase inhibition and oxidative stress in cardiovascular diseases: Possible therapeutic targets? *Pharmacol Ther* **140**, 239–257 (2013).

205. Schulz, R., Kelm, M. & Heusch, G. Nitric oxide in myocardial ischemia/reperfusion injury. *Cardiovasc Res* **61**, 402–413 (2004).

206. Roberts, B. W., Mitchell, J., Kilgannon, J. H., Chansky, M. E. & Trzeciak, S. Nitric oxide donor agents for the treatment of ischemia/reperfusion injury in human subjects: a systematic review. *Shock* **39**, 229–239 (2013).

207. Duranski, M. R. *et al.* Cytoprotective effects of nitrite during in vivo ischemia-reperfusion of the heart and liver. *Journal of Clinical Investigation* **115**, 1232 (2005).

208. De Pascali, F., Hemann, C., Samons, K., Chen, C. A. & Zweier, J. L. Hypoxia and Reoxygenation Induce Endothelial Nitric Oxide Synthase Uncoupling in Endothelial Cells through Tetrahydrobiopterin Depletion and S-Glutathionylation. *Biochemistry* **53**, 3679 (2014).

209. Dumitrescu, C. *et al.* Myocardial ischemia results in tetrahydrobiopterin (BH4) oxidation with impaired endothelial function ameliorated by BH4. *Proc Natl Acad Sci U S A* **104**, 15081 (2007).

210. Tratsiakovich, Y. *et al.* Myocardial protection by co-administration of L-arginine and tetrahydrobiopterin during ischemia and reperfusion. *Int J Cardiol* **169**, 83–88 (2013).

211. Masano, T. *et al.* Beneficial effects of exogenous tetrahydrobiopterin on left ventricular remodeling after myocardial infarction in rats: the possible role of oxidative stress caused by uncoupled endothelial nitric oxide synthase. *Circ J* **72**, 1512–1519 (2008).

212. Lalu, M. M., Wang, W. & Schulz, R. Peroxynitrite in Myocardial Ischemia-Reperfusion Injury. *Heart Fail Rev* **7**, 359–369 (2002).

213. Bugger, H. & Pfeil, K. Mitochondrial ROS in myocardial ischemia reperfusion and remodeling. *Biochim Biophys Acta Mol Basis Dis* **1866**, (2020).

214. Brand, M. D. Mitochondrial generation of superoxide and hydrogen peroxide as the source of mitochondrial redox signaling. *Free Radic Biol Med* **100**, 14–31 (2016).

215. Kaludercic, N., Mialet-Perez, J., Paolocci, N., Parini, A. & Di Lisa, F. Monoamine oxidases as sources of oxidants in the heart. *J Mol Cell Cardiol* **73**, 34–42 (2014).

216. Mialet-Perez, J. & Parini, A. Cardiac monoamine oxidases: at the heart of mitochondrial dysfunction. *Cell Death Dis* **11**, (2020).

217. Inagaki, T. *et al.* Monoamine oxidase-induced hydroxyl radical production and cardiomyocyte injury during myocardial ischemia-reperfusion in rats. *Free Radic Res* **50**, 645–653 (2016).

218. Bianchi, P. *et al.* Oxidative Stress by Monoamine Oxidase Mediates Receptor-Independent Cardiomyocyte Apoptosis by Serotonin and Postischemic Myocardial Injury. *Circulation* **112**, 3297–3305 (2005).

219. Pchejetski, D. *et al.* Oxidative stress-dependent sphingosine kinase-1 inhibition mediates monoamine oxidase A-associated cardiac cell apoptosis. *Circ Res* **100**, 41–49 (2007).

220. Quinlan, C. L. *et al.* The 2-oxoacid dehydrogenase complexes in mitochondria can produce superoxide/hydrogen peroxide at much higher rates than complex I. *Journal of Biological Chemistry* **289**, 8312–8325 (2014).

221. Chen, Y. R. & Zweier, J. L. Cardiac mitochondria and reactive oxygen species generation. *Circ Res* **114**, 524–537 (2014).

222. Maranzana, E., Barbero, G., Falasca, A. I., Lenaz, G. & Genova, M. L. Mitochondrial respiratory supercomplex association limits production of reactive oxygen species from complex i. *Antioxid Redox Signal* **19**, 1469–1480 (2013).

223. Paradies, G. *et al.* Decrease in Mitochondrial Complex I Activity in Ischemic/Reperfused Rat Heart. *Circ Res* **94**, 53–59 (2004).

224. Hernansanz-Agustín, P. & Enríquez, J. A. Generation of reactive oxygen species by mitochondria. *Antioxidants* **10**, 1–18 (2021).

225. Calvo, E. *et al.* Functional role of respiratory supercomplexes in mice: SCAF1 relevance and segmentation of the Q pool. *Sci Adv* **6**, (2020).

226. Chenna, S., Koopman, W. J. H., Prehn, J. H. M. & Connolly, N. M. C. Mechanisms and mathematical modeling of ROS production by the mitochondrial electron transport chain. *Am J Physiol Cell Physiol* **323**, C69–C83 (2022).

227. Quinlan, C. L., Perevoshchikova, I. V., Hey-Mogensen, M., Orr, A. L. & Brand, M. D. Sites of reactive oxygen species generation by mitochondria oxidizing different substrates. *Redox Biol* **1**, 304–312 (2013).

228. Murphy, M. P. How mitochondria produce reactive oxygen species. *Biochemical Journal* **417**, 1–13 (2009).

229. Antonucci, S., Di Lisa, F. & Kaludercic, N. Mitochondrial reactive oxygen species in physiology and disease. *Cell Calcium* **94**, (2021).

230. Hirst, J., King, M. S. & Pryde, K. R. The production of reactive oxygen species by complex I. *Biochem Soc Trans* **36**, 976–980 (2008).

231. Votyakova, T. V. & Reynolds, I. J. ΔΨm-Dependent and -independent production of reactive oxygen species by rat brain mitochondria. *J Neurochem* **79**, 266–277 (2001).

232. Lambert, A. J. & Brand, M. D. Inhibitors of the quinone-binding site allow rapid superoxide production from mitochondrial NADH:ubiquinone oxidoreductase (complex I). *Journal of Biological Chemistry* **279**, 39414–39420 (2004).

233. Brand, M. D. *et al.* Suppressors of Superoxide-H2O2 Production at Site IQ of Mitochondrial Complex I Protect against Stem Cell Hyperplasia and Ischemia-Reperfusion Injury. *Cell Metab* **24**, 582–592 (2016).

234. Siebels, I. & Dröse, S. Q-site inhibitor induced ROS production of mitochondrial complex II is attenuated by TCA cycle dicarboxylates. *Biochim Biophys Acta Bioenerg* **1827**, 1156–1164 (2013).

235. Quinlan, C. L. *et al.* Mitochondrial complex II can generate reactive oxygen species at high rates in both the forward and reverse reactions. *Journal of Biological Chemistry* **287**, 27255–27264 (2012).

236. Bleier, L. & Dröse, S. Superoxide generation by complex III: From mechanistic rationales to functional consequences ☆. *Biochim Biophys Acta* **1827**, 1320–1331 (2013).

237. Ludwig, L. M. *et al.* Preconditioning by isoflurane is mediated by reactive oxygen species generated from mitochondrial electron transport chain complex III. *Anesth Analg* **99**, 1308–1315 (2004).

238. Quinlan, C. L., Gerencser, A. A., Treberg, J. R. & Brand, M. D. The mechanism of superoxide production by the antimycin-inhibited mitochondrial Q-cycle. *Journal of Biological Chemistry* **286**, 31361–31372 (2011).

239. Turrens, J. F., Alexandre, A. & Lehninger, A. L. Ubisemiquinone is the electron donor for superoxide formation by complex III of heart mitochondria. *Arch Biochem Biophys* **237**, 408–414 (1985).

240. Cadenas, E., Boveris, A., Ragan, C. I. & Stoppani, A. O. M. Production of superoxide radicals and hydrogen peroxide by NADH-ubiquinone reductase and ubiquinol-cytochrome c reductase from beef-heart mitochondria. *Arch Biochem Biophys* **180**, 248–257 (1977).

241. Zorov, D. B., Juhaszova, M. & Sollott, S. J. Mitochondrial Reactive Oxygen Species (ROS) and ROS-Induced ROS Release. *Physiol Rev* **94**, 909–950 (2014).

242. Prabu, S. K. *et al.* Protein kinase A-mediated phosphorylation modulates cytochrome c oxidase function and augments hypoxia and myocardial ischemia-related injury. *Journal of Biological Chemistry* **281**, 2061–2070 (2006).

243. Nimse, S. B. & Pal, D. Free radicals, natural antioxidants, and their reaction mechanisms. *RSC Adv* **5**, 27986–28006 (2015).

244. Netto, L. E. S. & Antunes, F. The Roles of Peroxiredoxin and Thioredoxin in Hydrogen Peroxide Sensing and in Signal Transduction. *Mol. Cells* **39**, 65–71 (2016).

245. Venardos, K. M. & Kaye, D. M. Myocardial Ischemia-Reperfusion Injury, Antioxidant Enzyme Systems, and Selenium: A Review. *Curr Med Chem* **14**, 1539–1549 (2007).

246. Chance, B. The Interaction of Energy and Electron Transfer Reactions in Mitochondria II. General Properties of Adenosine triphosphate-linked Oxidation of Cytochrome and Reduction of Pyridine Nucleotide. *THE JOURNAL OF BIOLOQICAL CHEMISTRY* **236**, (1961).

247. Chance, B. & Hollunger, G. The Interaction of Energy and Electron Transfer Reactions in Mitochondria I. General Properties and Nature of the Products of Succinate-linked Reduction of Pyridine Nucleotide. *THE JOURNAL OF BIOLOQICAL CHEMISTRY* **236**, (1961).

248. Kussmaul, L. & Hirst, J. The mechanism of superoxide production by NADH:ubiquinone oxidoreductase (complex I) from bovine heart mitochondria. *Proc Natl Acad Sci U S A* **103**, 7607–7612 (2006).

249. Hohl, C. *et al.* Evidence for Succinate Production by Reduction of Fumarate during Hypoxia in isolated Adult Rat Heart Cells. *Arch Biochem Biophys* **259**, 52–59 (1987).

250. Liu, Y., Fiskum, G. & Schubert, D. Generation of reactive oxygen species by the mitochondrial electron transport chain. *J Neurochem* **80**, 780–787 (2002).

251. Stepanova, A. *et al.* Reverse electron transfer results in a loss of flavin from mitochondrial complex I: Potential mechanism for brain ischemia reperfusion injury. *Journal of Cerebral Blood Flow and Metabolism* **37**, 3649–3658 (2017).

252. Dröse, S., Bleier, L. & Brandt, U. A common mechanism links differently acting complex II inhibitors to cardioprotection: Modulation of mitochondrial reactive oxygen species production. *Mol Pharmacol* **79**, 814–822 (2011).

253. Zoccarato, F., Cavallini, L., Bortolami, S. & Alexandre, A. Succinate modulation of H 2 O 2 release at NADH:ubiquinone oxidoreductase (Complex I) in brain mitochondria. *Biochem. J* **406**, 125–129 (2007).

254. Scialò, F., Fernández-Ayala, D. J. & Sanz, A. Role of mitochondrial reverse electron transport in ROS signaling: Potential roles in health and disease. *Front Physiol* **8**, (2017).

255. Pell, V. R., Chouchani, E. T., Murphy, M. P., Brookes, P. S. & Krieg, T. Moving forwards by blocking back-flow the yin and yang of MI therapy. *Circ Res* **118**, 898–906 (2016).

256. Onukwufor, J. O., Berry, B. J. & Wojtovich, A. P. Physiologic implications of reactive oxygen species production by mitochondrial complex I reverse electron transport. *Antioxidants* **8**, (2019).

257. Bottje, W. G. Oxidative metabolism and efficiency: The delicate balancing act of mitochondria. *Poult Sci* **98**, 4223–4230 (2019).

258. Fernández-Agüera, M. C. *et al.* Oxygen Sensing by Arterial Chemoreceptors Depends on Mitochondrial Complex I Signaling. *Cell Metab* **22**, 825–837 (2015).

259. Arias-Mayenco, I. *et al.* Acute O 2 Sensing: Role of Coenzyme QH 2 /Q Ratio and Mitochondrial ROS Compartmentalization Article Acute O 2 Sensing: Role of Coenzyme QH 2 /Q Ratio and Mitochondrial ROS Compartmentalization. *Cell Metab* **28**, 145-158.e4 (2018).

260. Scialò, F. *et al.* Mitochondrial ROS Produced via Reverse Electron Transport Extend Animal Lifespan. *Cell Metab* **23**, 725–734 (2016).

261. Garaude, J. *et al.* Mitochondrial respiratory-chain adaptations in macrophages contribute to antibacterial host defense. *Nature Immunology 2016 17:9* **17**, 1037–1045 (2016).

262. Mills, E. L. *et al.* Succinate Dehydrogenase Supports Metabolic Repurposing of Mitochondria to Drive Inflammatory Macrophages. *Cell* **167**, 457-470.e13 (2016).

263. Read, A. D. *et al.* Electron Leak From the Mitochondrial Electron Transport Chain Complex I at Site I Q Is Crucial for Oxygen Sensing in Rabbit and Human Ductus Arteriosus. *Journal of the American Heart Association J Am Heart Assoc* **12**, 29131 (2023).

264. Lee, S. *et al.* Mitochondrial H 2 O 2 generated from electron transport chain complex I stimulates muscle differentiation. *Nature Publishing Group* **21**, 817–834 (2011).

265. Guarás, A. *et al.* The CoQH2/CoQ Ratio Serves as a Sensor of Respiratory Chain Efficiency. *Cell Rep* **15**, 197–209 (2016).

266. Robb, E. L. *et al.* Control of mitochondrial superoxide production by reverse electron transport at complex I. *Journal of Biological Chemistry* **293**, 9869–9879 (2018).

267. Zweier, J. L., Flaherty, J. T. & Weisfeldt, M. L. Direct measurement of free radical generation following reperfusion of ischemic myocardium. *Proc Natl Acad Sci U S A* **84**, 1404–1407 (1987).

268. Loor, G. *et al.* Mitochondrial oxidant stress triggers cell death in simulated ischemia–reperfusion. *Biochimica et Biophysica Acta (BBA) - Molecular Cell Research* **1813**, 1382–1394 (2011).

269. Hess, M. L. & Manson, N. H. Molecular oxygen: Friend and foe. The role of the oxygen free radical system in the calcium paradox, the oxygen paradox and ischemia/reperfusion injury. *J Mol Cell Cardiol* **16**, 969–985 (1984).

270. Vujic, A., Koo, A. N. M., Prag, H. A. & Krieg, T. Mitochondrial redox and TCA cycle metabolite signaling in the heart. *Free Radic Biol Med* **166**, 287–296 (2021).

271. Hochachka, P. W. & Storey, K. B. Metabolic consequences of diving in animals and man. *Science (1979)* **187**, 613–621 (1975).

272. Hochachka, P. W., Owen, T. G., Allen, J. F. & Whittow, G. C. Multiple end products of anaerobiosis in diving vertebrates. *Comp Biochem Physiol B* **50**, 17–22 (1975).

273. Taegtmeyer, H. Metabolic responses to cardiac hypoxia. Increased production of succinate by rabbit papillary muscles. *Circ Res* **43**, 808–815 (1978).

274. Pisarenko, O., Studneva, I., Khlopkov, V., Solomatina, E. & Ruuge, E. An assessment of anaerobic metabolism during ischemia and reperfusion in isolated guinea pig heart. *Biochimica et Biophysica Acta (BBA) - Bioenergetics* **934**, 55–63 (1988).

275. Ashrafian, H. *et al.* Fumarate is cardioprotective via activation of the Nrf2 antioxidant pathway. *Cell Metab* **15**, 361–371 (2012).

276. Boveris, A., Oshino, N. & Chance, B. The cellular production of hydrogen peroxide. *Biochem J* **128**, 617–630 (1972).

277. Adam-Vizi, V. & Chinopoulos, C. Bioenergetics and the formation of mitochondrial reactive oxygen species. *Trends Pharmacol Sci* **27**, 639–645 (2006).

278. Niatsetskaya, Z. V. *et al.* The oxygen free radicals originating from mitochondrial complex I contribute to oxidative brain injury following hypoxia-ischemia in neonatal mice. *Journal of Neuroscience* **32**, 3235–3244 (2012).

279. Chouchani, E. T. *et al.* Ischaemic accumulation of succinate controls reperfusion injury through mitochondrial ROS. *Nature* **515**, 431–435 (2014).

280. Valls-Lacalle, L. *et al.* Succinate dehydrogenase inhibition with malonate during reperfusion reduces infarct size by preventing mitochondrial permeability transition. *Cardiovasc Res* **109**, 374–384 (2016).

281. Valls-Lacalle, L. *et al.* Selective Inhibition of Succinate Dehydrogenase in Reperfused Myocardium with Intracoronary Malonate Reduces Infarct Size. *Sci Rep* **8**, (2018).

282. Chen, Q., Moghaddas, S., Hoppel, C. L. & Lesnefsky, E. J. Reversible blockade of electron transport during ischemia protects mitochondria and decreases myocardial injury

following reperfusion. *Journal of Pharmacology and Experimental Therapeutics* **319**, 1405–1412 (2006).

283. Chen, Q., Hoppel, C. L. & Lesnefsky, E. J. Blockade of electron transport before cardiac ischemia with the reversible inhibitor amobarbital protects rat heart mitochondria. *Journal of Pharmacology and Experimental Therapeutics* **316**, 200–207 (2006).

284. Lesnefsky, E. J. *et al.* Blockade of Electron Transport during Ischemia Protects Cardiac Mitochondria*. *J Biol Chem* **279**, 47961–47967 (2004).

285. Mohsin, A. A. *et al.* Mitochondrial complex I inhibition by metformin limits reperfusion injury. *Journal of Pharmacology and Experimental Therapeutics* **369**, 282–290 (2019).

286. Calvert, J. W. *et al.* Acute metformin therapy confers cardioprotection against myocardial infarction via AMPK-eNOS mediated signaling. *Diabetes* **57**, 696–705 (2008).

287. Chouchani, E. T. *et al.* Cardioprotection by S-nitrosation of a cysteine switch on mitochondrial complex i. *Nat Med* **19**, 753–759 (2013).

288. Wojtovich, A. P. & Brookes, P. S. The complex II inhibitor atpenin A5 protects against cardiac ischemia-reperfusion injury via activation of mitochondrial KATP channels. *Basic Res Cardiol* **104**, 121–129 (2009).

289. Anastacio, M. M. *et al.* Cardioprotective mechanism of diazoxide involves the inhibition of succinate dehydrogenase. *Annals of Thoracic Surgery* **95**, 2042–2050 (2013).

290. Beach, T. E. *et al.* Targeting succinate dehydrogenase with malonate ester prodrugs decreases renal ischemia reperfusion injury. *Redox Biol* **36**, (2020).

291. Xu, J. *et al.* Inhibiting Succinate Dehydrogenase by Dimethyl Malonate Alleviates Brain Damage in a Rat Model of Cardiac Arrest. *Neuroscience* **393**, 24–32 (2018).

292. Chavda, V. & Lu, B. Reverse Electron Transport at Mitochondrial Complex I in Ischemic Stroke, Aging, and Age-Related Diseases. *Antioxidants* **12**, 895 (2023).

293. Prag, H. A., Murphy, M. P. & Krieg, T. Preventing mitochondrial reverse electron transport as a strategy for cardioprotection. *Basic Res Cardiol* **118**, 34 (2023).

294. Pell, V. R., Chouchani, E. T., Frezza, C., Murphy, M. P. & Krieg, T. Succinate metabolism: A new therapeutic target for myocardial reperfusion injury. *Cardiovasc Res* **111**, 134–141 (2016).

295. Chouchani, E. T. *et al.* A unifying mechanism for mitochondrial superoxide production during ischemia-reperfusion injury. *Cell Metab* **23**, 254–263 (2016).

296. Zhang, J. *et al.* Accumulation of Succinate in Cardiac Ischemia Primarily Occurs via Canonical Krebs Cycle Activity. *Cell Rep* **23**, 2617–2628 (2018).

297. Kinugasa, Y. *et al.* Allopurinol Improves Cardiac Dysfunction After Ischemia-Reperfusion via Reduction of Oxidative Stress in Isolated Perfused Rat Hearts. *Circulation Journal* **67**, 781–787 (2003).

298. Prag, H. A. *et al.* Mechanism of succinate efflux upon reperfusion of the ischaemic heart. *Cardiovasc Res* **117**, 1188–1201 (2021).

299. Murphy, M. P. & Chouchani, E. T. Why succinate? Physiological regulation by a mitochondrial coenzyme Q sentinel. *Nat Chem Biol* **18**, 461–469 (2022).

300. Dirksen, M. T., Laarman, G. J., Simoons, M. L. & Duncker, D. J. G. M. Reperfusion injury in humans: A review of clinical trials on reperfusion injury inhibitory strategies. *Cardiovasc Res* **74**, 343–355 (2007).

301. Davidson, S. M. *et al.* Multitarget Strategies to Reduce Myocardial Ischemia/Reperfusion Injury: JACC Review Topic of the Week. *J Am Coll Cardiol* **73**, 89–99 (2019).

302. San-Martín-Martínez, D., Serrano-Lemus, D., Cornejo, V., Gajardo, A. I. J. & Rodrigo, R. Pharmacological Basis for Abrogating Myocardial Reperfusion Injury Through a Multi-Target Combined Antioxidant Therapy. *Clinical Pharmacokinetics 2022 61:9* **61**, 1203–1218 (2022).

303. Alburquerque-Béjar, J. J. *et al.* Combination therapy with remote ischaemic conditioning and insulin or exenatide enhances infarct size limitation in pigs. *Cardiovasc Res* **107**, 246–254 (2015).

304. Alburquerque-Béjar, J. J. *et al.* Additive Effects of Exenatide, Glucose-insulin-potassium, and Remote Ischemic Conditioning Against Reperfusion Ventricular Arrhythmias in Pigs. *Revista Española de Cardiología (English Edition)* **69**, 620–622 (2016).

305. Heusch, G., Bøtker, H. E., Przyklenk, K., Redington, A. & Yellon, D. Remote Ischemic Conditioning. *Journal of the American Association of Cardiology* **65**, (2015).

306. Schmidt, M. R., Redington, A. & Bøtker, H. E. Remote conditioning the heart overview: translatability and mechanism. *Br J Pharmacol* **172**, 1947–1960 (2014).

307. Schmidt, M. R., Rasmussen, M. E. & Bøtker, H. E. Remote Ischemic Conditioning for Patients with STEMI. *J Cardiovasc Pharmacol Ther* **22**, 302–309 (2017).

308. Hausenloy, D. J. & Yellon, D. M. Ischaemic conditioning and reperfusion injury. *Nat Rev Cardiol* **13**, 193–209 (2016).

309. Przyklenk, K., Bauer, B., Ovize, M., Kloner, R. A. & Whittaker, P. Regional ischemic 'preconditioning' protects remote virgin myocardium from subsequent sustained coronary occlusion. *Circulation* **87**, 893–899 (1993).

310. Schmidt, M. R. *et al.* Intermittent peripheral tissue ischemia during coronary ischemia reduces myocardial infarction through a KATP-dependent mechanism: First demonstration of remote ischemic perconditioning. *Am J Physiol Heart Circ Physiol* **292**, (2007).

311. Bøtker, H. E. *et al.* Remote ischaemic conditioning before hospital admission, as a complement to angioplasty, and effect on myocardial salvage in patients with acute myocardial infarction: a randomised trial. *The Lancet* **375**, 727–734 (2010).

312. Crimi, G. *et al.* Remote Ischemic Post-Conditioning of the Lower Limb During Primary Percutaneous Coronary Intervention Safely Reduces Enzymatic Infarct Size in Anterior Myocardial Infarction: A Randomized Controlled Trial. *JACC Cardiovasc Interv* **6**, 1055–1063 (2013).

313. Bøtker, H. E. *et al.* Practical guidelines for rigor and reproducibility in preclinical and clinical studies on cardioprotection. *Basic Res Cardiol* **113**, (2018).

314. Vogel, B. *et al.* ST-segment elevation myocardial infarction. *Nat Rev Dis Primers* **5**, (2019).

315. Ibanez, B. *et al.* Cardiac MRI Endpoints in Myocardial Infarction Experimental and Clinical Trials: JACC Scientific Expert Panel. *J Am Coll Cardiol* **74**, 238–256 (2019).

316. García del Blanco, B. *et al.* Effect of COMBinAtion therapy with remote ischemic conditioning and exenatide on the Myocardial Infarct size: a two-by-two factorial randomized trial (COMBAT-MI). *Basic Res Cardiol* **116**, 1–12 (2021).

317. Hausenloy, D. J. *et al.* Effect of remote ischaemic conditioning on clinical outcomes in patients with acute myocardial infarction (CONDI-2/ERIC-PPCI): a single-blind randomised controlled trial. *The Lancet* **394**, 1415–1424 (2019).

318. Katus, H. A., Remppis, A., Scheffold, T., Diederich, K. W. & Kuebler, W. Intracellular compartmentation of cardiac troponin T and its release kinetics in patients with reperfused and nonreperfused myocardial infarction. *Am J Cardiol* **67**, 1360–1367 (1991).

319. Thygesen, K. *et al.* How to use high-sensitivity cardiac troponins in acute cardiac care. *Eur Heart J* **33**, (2012).

320. Kohlhauer, M. *et al.* Metabolomic profiling in acute ST-segment-elevation myocardial infarction identifies succinate as an early marker of human ischemia-reperfusion injury. *J Am Heart Assoc* **7**, (2018).

321. Burger, N. *et al.* A sensitive mass spectrometric assay for mitochondrial CoQ pool redox state in vivo. *Free Radic Biol Med* **147**, 37–47 (2020).

322. Nicholls, D. G. & Ferguson, S. *Bioenergetics: Fourth Edition*. *Bioenergetics: Fourth Edition* (Elsevier Ltd, 2013). doi:10.1016/C2010-0-64902-9.

323. Yin, Z. *et al.* Structural basis for a complex I mutation that blocks pathological ROS production. *Nat Commun* **12**, (2021).

324. Boengler, K. *et al.* Connexin 43 in cardiomyocyte mitochondria and its increase by ischemic preconditioning. *Cardiovasc Res* **67**, 234–244 (2005).

325. Rodriguez-Sinovas, A. *et al.* Translocation of connexin 43 to the inner mitochondrial membrane of cardiomyocytes through the heat shock protein 90-dependent TOM pathway and its importance for cardioprotection. *Circ Res* **99**, 93–101 (2006).

326. Miro-Casas, E. *et al.* Connexin43 in cardiomyocyte mitochondria contributes to mitochondrial potassium uptake. *Cardiovasc Res* **83**, 747–756 (2009).

327. Rodríguez-Sinovas, A., Ruiz-Meana, M., Denuc, A. & García-Dorado, D. Mitochondrial Cx43, an important component of cardiac preconditioning. *Biochim Biophys Acta Biomembr* **1860**, 174–181 (2018).

328. Azarashvili, T. *et al.* Calcium-induced permeability transition in rat brain mitochondria is promoted by carbenoxolone through targeting connexin43. *Am J Physiol Cell Physiol* **300**, 707–720 (2011).

329. Kozoriz, M. G., Church, J., Ozog, M. A., Naus, C. C. & Krebs, C. Temporary Sequestration of Potassium by Mitochondria in Astrocytes. *J Biol Chem* **285**, 31107 (2010).

330. Li, H. *et al.* Paradoxical overexpression and translocation of connexin43 in homocysteine-treated endothelial cells. *Am J Physiol Heart Circ Physiol* **282**, 2124–2133 (2002).

331. Lu, G., Haider, H. K., Porollo, A. & Ashraf, M. Mitochondria-specific transgenic overexpression of connexin-43 simulates preconditioning-induced cytoprotection of stem cells. *Cardiovasc Res* **88**, 277 (2010).

332. Boengler, K., Ungefug, E., Heusch, G., Leybaert, L. & Schulz, R. Connexin 43 impacts on mitochondrial potassium uptake. *Front Pharmacol* **4 JUN**, (2013).

333. Heinzel, F. R. *et al.* Impairment of diazoxide-induced formation of reactive oxygen species and loss of cardioprotection in connexin 43 deficient mice. *Circ Res* **97**, 583–586 (2005).

334. Murray, C. J. L. *et al.* Global burden of 87 risk factors in 204 countries and territories, 1990–2019: a systematic analysis for the Global Burden of Disease Study 2019. *The Lancet* **396**, 1223–1249 (2020).

335. Gupta, A. K. Jaha spotlight on air pollution and cardiovascular disease: A call for urgent action. *J Am Heart Assoc* **10**, (2021).

336. Schraufnagel, D. E. *et al.* Air Pollution and Noncommunicable Diseases: A Review by the Forum of International Respiratory Societies' Environmental Committee, Part 2: Air Pollution and Organ Systems. *Chest* **155**, 417–426 (2019).

337. Brauer, M. *et al.* Taking a stand against air pollution - The impact on cardiovascular disease a joint opinion from the world heart federation, American college of cardiology, American Heart Association, and the european society of cardiology. *Glob Heart* **16**, (2021).

338. Tofler, G. H. & Muller, J. E. Triggering of acute cardiovascular disease and potential preventive strategies. *Circulation* **114**, 1863–1872 (2006).

339. Liu, C. *et al.* Ambient Particulate Air Pollution and Daily Mortality in 652 Cities. *New England Journal of Medicine* **381**, 705–715 (2019).

340. Bañeras, J. *et al.* Short-term exposure to air pollutants increases the risk of ST elevation myocardial infarction and of infarct-related ventricular arrhythmias and mortality. *Int J Cardiol* **250**, 35–42 (2018).

341. Fiordelisi, A. *et al.* The mechanisms of air pollution and particulate matter in cardiovascular diseases. *Heart Fail Rev* **22**, 337–347 (2017).

342. Lederer, A. M. *et al.* Cardiovascular effects of air pollution: Current evidence from animal and human studies. *Am J Physiol Heart Circ Physiol* **320**, H1417–H1439 (2021).

343. Miller, M. R. Oxidative stress and the cardiovascular effects of air pollution. *Free Radic Biol Med* **151**, 69–87 (2020).

344. Gorr, M. W. *et al.* In vitro particulate matter exposure causes direct and lung-mediated indirect effects on cardiomyocyte function. *Am J Physiol Heart Circ Physiol* **309**, 53–62 (2015).

345. Robertson, S. *et al.* Pulmonary diesel particulate increases susceptibility to myocardial ischemia/reperfusion injury via activation of sensory TRPV1 and β1 adrenoreceptors. *Part Fibre Toxicol* **11**, 1–10 (2014).

346. Marchini, T. *et al.* Acute exposure to air pollution particulate matter aggravates experimental myocardial infarction in mice by potentiating cytokine secretion from lung macrophages. *Basic Res Cardiol* **111**, 1–14 (2016).

347. Sivakumar, B. & Kurian, G. A. Diesel particulate matter exposure deteriorates cardiovascular health and increases the sensitivity of rat heart towards ischemia reperfusion injury via suppressing mitochondrial bioenergetics function. *Chem Biol Interact* **351**, (2022).

348. Daiber, A. *et al.* Effects of air pollution particles (ultrafine and fine particulate matter) on mitochondrial function and oxidative stress – Implications for cardiovascular and neurodegenerative diseases. *Arch Biochem Biophys* **696**, (2020).

349. Shukla, H. *et al.* Reactive oxygen species production by BP-1,6-quinone and its effects on the endothelial dysfunction: Involvement of the mitochondria. *Toxicol Lett* **322**, 120–130 (2020).

350. Rodríguez-Sinovas, A. *et al.* Pre-treatment with the Na+/H+ exchange inhibitor cariporide delays cell-to-cell electrical uncoupling during myocardial ischemia. *Cardiovasc Res* **58**, 109–117 (2003).

351. Rodríguez-Sinovas, A. *et al.* Intracoronary acid infusion as an alternative to ischemic postconditioning in pigs. *Basic Res Cardiol* **104**, 761–771 (2009).

352. Lema, C. *et al.* 1H NMR serum metabolomic profiling of patients at risk of cardiovascular diseases performing stress test. *Sci Rep* **10**, (2020).

353. Ibañez, B. *et al.* 2017 ESC Guidelines for the management of acute myocardial infarction in patients presenting with ST-segment elevation. *Eur Heart J* **39**, 119–177 (2018).

354. Eckardt, D. *et al.* Functional role of connexin43 gap junction channels in adult mouse heart assessed by inducible gene deletion. *J Mol Cell Cardiol* **36**, 101–110 (2004).

355. Valls-Lacalle, L. *et al.* Opposite effects of moderate and extreme Cx43 deficiency in conditional Cx43-deficient mice on angiotensin II-induced cardiac fibrosis. *Cells* **8**, (2019).

356. Van Rijen, H. V. M. *et al.* Slow Conduction and Enhanced Anisotropy Increase the Propensity for Ventricular Tachyarrhythmias in Adult Mice With Induced Deletion of Connexin43. *Circulation* **109**, 1048–1055 (2004).

357. Bou-Teen, D. *et al.* Defective dimerization of FoF1-ATP synthase secondary to glycation favors mitochondrial energy deficiency in cardiomyocytes during aging. *Aging Cell* **21**, (2022).

358. Hahn, S. H., Kerfoot, S. & Vasta, V. Assay to measure oxidized and reduced forms of CoQ by LC-MS/MS. *Methods in Molecular Biology* **837**, 169–179 (2012).

359. Osuna-Prieto, F. J. *et al.* Elevated plasma succinate levels are linked to higher cardiovascular disease risk factors in young adults. *Cardiovasc Diabetol* **20**, (2021).

360. D'Alessandro, A. *et al.* Plasma succinate is a predictor of mortality in critically injured patients. *Journal of Trauma and Acute Care Surgery* **83**, 491–495 (2017).

361. Turunen, M., Olsson, J. & Dallner, G. Metabolism and function of coenzyme Q. *Biochim Biophys Acta* **1660**, 171–199 (2004).

362. Prag, H. A. *et al.* Ester Prodrugs of Malonate with Enhanced Intracellular Delivery Protect Against Cardiac Ischemia-Reperfusion Injury In Vivo. *Cardiovasc Drugs Ther* **36**, (2020).

363. Jespersen, N. R. *et al.* Cardioprotective effect of succinate dehydrogenase inhibition in rat hearts and human myocardium with and without diabetes mellitus. *Sci Rep* **10**, (2020).

364. Prag, H. A. *et al.* Ischemia-Selective Cardioprotection by Malonate for Ischemia/Reperfusion Injury. *Circ Res* **131**, 528–541 (2022).

365. Kleinbongard, P., Skyschally, A. & Heusch, G. Cardioprotection by remote ischemic conditioning and its signal transduction. *Pflügers Archiv - European Journal of Physiology 2016 469:2* **469**, 159–181 (2016).

366. Breivik, L., Helgeland, E., Aarnes, E. K., Mrdalj, J. & Jonassen, A. K. Remote postconditioning by humoral factors in effluent from ischemic preconditioned rat hearts is mediated via PI3K/Akt-dependent cell-survival signaling at reperfusion. *Basic Res Cardiol* **106**, 135–145 (2011).

367. Hausenloy, D. J. *et al.* Investigating the signal transduction pathways underlying remote ischemic conditioning in the porcine heart. *Cardiovasc Drugs Ther* **26**, 87–93 (2012).

368. Turrell, H. E., Thaitirarot, C., Crumbie, H. & Rodrigo, G. C. Remote ischemic preconditioning of cardiomyocytes inhibits the mitochondrial permeability transition pore independently of reduced calcium-loading or sarcKATP channel activation. *Physiol Rep* **2**, e12231 (2014).

369. Wu, Y.-N. *et al.* Noninvasive Delayed Limb Ischemic Preconditioning Attenuates Myocardial Ischemia-Reperfusion Injury in Rats by a Mitochondrial K ATP Channel-Dependent Mechanism. *Physiol. Res* **60**, 271–279 (2011).

370. Kleinbongard, P. *et al.* Co-morbidities and co-medications as confounders of cardioprotection-Does it matter in the clinical setting? *Br J Pharmacol* **177**, 5252–5269 (2019).

371. Yang, X. M. *et al.* Platelet P2Y12 blockers confer direct postconditioning-like protection in reperfused rabbit hearts. *J Cardiovasc Pharmacol Ther* **18**, 251–262 (2013).

372. Hausenloy, D. J. *et al.* The coronary circulation in acute myocardial ischaemia/reperfusion injury: a target for cardioprotection. *Cardiovasc Res* **115**, 1143 (2019).

373. Yang, X. M., Cui, L., Alhammouri, A., Downey, J. M. & Cohen, M. V. Triple therapy greatly increases myocardial salvage during ischemia/reperfusion in the in situ rat heart. *Cardiovasc Drugs Ther* **27**, 403–412 (2013).

374. Xin, P. *et al.* Combined local ischemic postconditioning and remote perconditioning recapitulate cardioprotective effects of local ischemic preconditioning. *Am J Physiol Heart Circ Physiol* **298**, 1819–1831 (2010).

375. Stiermaier, T. *et al.* Combined intrahospital remote ischemic perconditioning and postconditioning improves clinical outcome in st-elevation myocardial infarction: Long-term results of the lipsia conditioning trial. *Circ Res* **124**, 1482–1491 (2019).

376. Kohlhauer, M. *et al.* Protection against cardiac ischemia-reperfusion injury by hypothermia and by inhibition of succinate accumulation and oxidation is additive. *Basic Res Cardiol* **114**, (2019).

377. Hauerslev, M. *et al.* Influence of long-term treatment with glyceryl trinitrate on remote ischemic conditioning. *Am J Physiol Heart Circ Physiol* **315**, H150–H158 (2018).

378. Støttrup, N. B. *et al.* Inhibition of the malate–aspartate shuttle by pre-ischaemic aminooxyacetate loading of the heart induces cardioprotection. *Cardiovasc Res* **88**, 257–266 (2010).

379. Sun, Y. Y. *et al.* Remote ischemic conditioning attenuates oxidative stress and inflammation via the Nrf2/HO-1 pathway in MCAO mice. *Redox Biol* **66**, 102852 (2023).

380. Bystrom, P., Foley +, N., Toledo-Pereyra, L. & Quesnelle, K. Ischemic preconditioning modulates ROS to confer protection in liver ischemia and reperfusion. *EXCLI J* **16**, 483–496 (2017).

381. Li, H. *et al.* Mediation of exogenous hydrogen sulfide in recovery of ischemic post-conditioning-induced cardioprotection via down-regulating oxidative stress and up-regulating PI3K/Akt/GSK-3β pathway in isolated aging rat hearts. *Cell Biosci* **5**, (2015).

382. Skyschally, A., Amanakis, G., Neuhäuser, M., Kleinbongard, P. & Heusch, G. Impact of electrical defibrillation on infarct size and no-reflow in pigs subjected to myocardial ischemia-reperfusion without and with ischemic conditioning. *Am J Physiol Heart Circ Physiol* **313**, H871–H878 (2017).

383. Krebs, H. A. Rate control of the tricarboxylic acid cycle. *Adv Enzyme Regul* **8**, 335–353 (1970).

384. Goldberg, N. D., Passonneau, J. V. & Lowry, O. H. Effects of Changes in Brain Metabolism on the Levels of Citric Acid Cycle Intermediates. *Journal of Biological Chemistry* **241**, 3997–4003 (1966).

385. Chinopoulos, C. Succinate in ischemia: Where does it come from? *International Journal of Biochemistry and Cell Biology* **115**, (2019).

386. Markevich, N. I. & Markevich, L. N. Computational Modeling Analysis of Kinetics of Fumarate Reductase Activity and ROS Production during Reverse Electron Transfer in Mitochondrial Respiratory Complex II. *Int J Mol Sci* **24**, (2023).

387. Andrienko, T. N., Pasdois, P., Pereira, G. C., Ovens, M. J. & Halestrap, A. P. The role of succinate and ROS in reperfusion injury – A critical appraisal. *J Mol Cell Cardiol* **110**, 1–14 (2017).

388. Hyldebrandt, J. A. *et al.* Citric Acid Cycle Metabolites Predict the Severity of Myocardial Stunning and Mortality in Newborn Pigs. *Pediatr Crit Care Med* **17**, e567–e574 (2016).

389. Surendran, A., Aliani, M. & Ravandi, A. Metabolomic characterization of myocardial ischemia-reperfusion injury in ST-segment elevation myocardial infarction patients undergoing percutaneous coronary intervention. *Sci Rep* **9**, (2019).

390. Gundogdu, G. *et al.* Serum metabolite profiling of ST-segment elevation myocardial infarction using liquid chromatography quadrupole time-of-flight mass spectrometry. *Biomedical Chromatography* **34**, (2020).

391. Croisille, P., Kim, H. W. & Kim, R. J. Controversies in Cardiovascular MR Imaging: T2-weighted Imaging Should Not Be Used to Delineate the Area at Risk in Ischemic Myocardial Injury. *Radiology* **265**, 12–22 (2012).

392. Fernández-Jiménez, R. *et al.* Dynamic edematous response of the human heart to myocardial infarction: Implications for assessing myocardial area at risk and salvage. *Circulation* **136**, 1288–1300 (2017).

393. Fernández-Jiménez, R. *et al.* Effect of Ischemia Duration and Protective Interventions on the Temporal Dynamics of Tissue Composition after Myocardial Infarction. *Circ Res* **121**, 439–450 (2017).

394. Sadagopan, N. *et al.* Circulating Succinate is Elevated in Rodent Models of Hypertension and Metabolic Disease. *Am J Hypertens* **20**, 1209–1215 (2007).

395. Aguiar, C. J. *et al.* Succinate causes pathological cardiomyocyte hypertrophy through GPR91 activation. *Cell Commun Signal* **12**, (2014).

396. Cui, H. *et al.* Untargeted metabolomics identifies succinate as a biomarker and therapeutic target in aortic aneurysm and dissection. *Eur Heart J* **42**, 4373–4385 (2021).

397. Sosinsky, G. E. & Nicholson, B. J. Structural organization of gap junction channels. *Biochimica et Biophysica Acta (BBA) - Biomembranes* **1711**, 99–125 (2005).

398. Kléber, A. G. & Jin, Q. Coupling between cardiac cells—An important determinant of electrical impulse propagation and arrhythmogenesis. *Biophys Rev* **2**, 31301 (2021).

399. Boengler, K. *et al.* Presence of connexin 43 in subsarcolemmal, but not in interfibrillar cardiomyocyte mitochondria. *Basic Res Cardiol* **104**, 141–147 (2009).

400. Boengler, K. *et al.* Mitochondrial connexin 43 impacts on respiratory complex i activity and mitochondrial oxygen consumption. *J Cell Mol Med* **16**, 1649–1655 (2012).

401. Zhou, Q. *et al.* Cx43 acts as a mitochondrial calcium regulator that promotes obesity by inducing the polarization of macrophages in adipose tissue. *Cell Signal* **105**, 110606 (2023).

402. Gadicherla, A. K. *et al.* Mitochondrial Cx43 hemichannels contribute to mitochondrial calcium entry and cell death in the heart. *Basic Res Cardiol* **112**, 1–21 (2017).

403. Ruiz-Meana, M. *et al.* Mitochondrial connexin43 as a new player in the pathophysiology of myocardial ischaemia-reperfusion injury. *Cardiovasc Res* **77**, 325–333 (2008).

404. Wojtovich, A. P. & Brookes, P. S. The endogenous mitochondrial complex II inhibitor malonate regulates mitochondrial ATP-sensitive potassium channels: Implications for ischemic preconditioning. *Biochim Biophys Acta Bioenerg* **1777**, 882–889 (2008).

405. Lass, A., Agarwal, S. & Sohal, R. S. Mitochondrial Ubiquinone Homologues, Superoxide Radical Generation, and Longevity in Different Mammalian Species*. *Journal of Biological Chemistry* **272**, 19199–19204 (1997).

406. Dominiak, K. & Jarmuszkiewicz, W. The Relationship between Mitochondrial Reactive Oxygen Species Production and Mitochondrial Energetics in Rat Tissues with Different Contents of Reduced Coenzyme Q. *Antioxidants 2021, Vol. 10, Page 533* **10**, 533 (2021).

407. Jarmuszkiewicz, W., Dominiak, K., Budzinska, A., Wojcicki, K. & Galganski, L. Mitochondrial Coenzyme Q Redox Homeostasis and Reactive Oxygen Species Production. *Front. Biosci. (Landmark Ed) 2023;* **28**, 61 (2023).

408. Wang, Y., Oxer, D. & Hekimi, S. Mitochondrial function and lifespan of mice with controlled ubiquinone biosynthesis. *Nature Communications 2015 6:1* **6**, 1–14 (2015).

409. Jarmuszkiewicz, W. *et al.* Lung mitochondria adaptation to endurance training in rats. *Free Radic Biol Med* **161**, 163–174 (2020).

410. Cogliati, S., Cabrera-Alarcón, J. L. & Enriquez, J. A. Regulation and functional role of the electron transport chain supercomplexes. *Biochem Soc Trans* **49**, 2655 (2021).

411. Hernansanz-Agustín, P. & Enríquez, J. A. Functional segmentation of CoQ and cyt c pools by respiratory complex superassembly. *Free Radic Biol Med* **167**, 232–242 (2021).

412. Dominiak, K., Koziel, A. & Jarmuszkiewicz, W. The interplay between mitochondrial reactive oxygen species formation and the coenzyme Q reduction level. *Redox Biol* **18**, 256–265 (2018).

413. Diez, E. R. *et al.* Ischemic postconditioning reduces reperfusion arrhythmias by adenosine receptors and protein kinase C activation but is independent of KATP channels or connexin 43. *Int J Mol Sci* **20**, (2019).

414. Rodríguez-Sinovas, A. *et al.* The modulatory effects of connexin 43 on cell death/survival beyond cell coupling. *Prog Biophys Mol Biol* **94**, 219–232 (2007).

415. Heusch, G., Büchert, A., Feldhaus, S. & Schulz, R. No loss of cardioprotection by postconditioning in connexin 43-deficient mice. *Basic Res Cardiol* **101**, 354–356 (2006).

416. Holland, N. A. *et al.* Ultrafine Particulate Matter Increases Cardiac Ischemia/Reperfusion Injury via Mitochondrial Permeability Transition Pore. *Cardiovasc Toxicol* **17**, 441–450 (2017).

417. Bhargava, A. *et al.* Ultrafine particulate matter impairs mitochondrial redox homeostasis and activates phosphatidylinositol 3-kinase mediated DNA damage responses in lymphocytes. *Environmental Pollution* **234**, 406–419 (2018).

418. Sivakumar, B., AlAsmari, A. F., Ali, N., Waseem, M. & Kurian, G. A. Consequential Impact of Particulate Matter Linked Inter-Fibrillar Mitochondrial Dysfunction in Rat Myocardium Subjected to Ischemia Reperfusion Injury. *Biology (Basel)* **11**, 1811 (2022).

419. Hatzis, C., Godleski, J. J., González-Flecha, B., Wolfson, J. M. & Koutrakis, P. Ambient particulate matter exhibits direct inhibitory effects on oxidative stress enzymes. *Environ Sci Technol* **40**, 2805–2811 (2006).

420. Liu, J. *et al.* Fine particulate matters induce apoptosis via the ATM/P53/CDK2 and mitochondria apoptosis pathway triggered by oxidative stress in rat and GC-2spd cell. *Ecotoxicol Environ Saf* **180**, 280–287 (2019).

421. Soberanes, S. *et al.* Metformin Targets Mitochondrial Electron Transport to Reduce Air-Pollution-Induced Thrombosis. *Cell Metab* **29**, 335–347 (2019).

422. Larsen, S. *et al.* Biomarkers of mitochondrial content in skeletal muscle of healthy young human subjects. *J Physiol* **590**, 3349 (2012).

423. Sivakumar, B. & Kurian, G. A. Inhalation of PM2.5 from diesel exhaust promote impairment of mitochondrial bioenergetics and dysregulate mitochondrial quality in rat heart: implications in isoproterenol-induced myocardial infarction model. *Inhal Toxicol* **34**, 107–119 (2022).

424. Marchini, T. *et al.* Chronic exposure to polluted urban air aggravates myocardial infarction by impaired cardiac mitochondrial function and dynamics ☆. *Environmental Pollution* **295**, (2022).

425. Karoui, A. *et al.* An integrated functional and transcriptomic analysis reveals that repeated exposure to diesel exhaust induces sustained mitochondrial and cardiac dysfunctions. *Environmental Pollution* **246**, 518–526 (2018).

426. Marchini, T. *et al.* Impaired cardiac mitochondrial function and contractile reserve following an acute exposure to environmental particulate matter. *Biochim Biophys Acta* **1830**, 2545–2552 (2012).

427. Sivakumar, B. & Kurian, G. A. PM2.5 Exposure Lowers Mitochondrial Endurance During Cardiac Recovery in a Rat Model of Myocardial Infarction. *Cardiovasc Toxicol* **22**, 545–557 (2022).

428. Kuroda, J. *et al.* NADPH oxidase 4 (Nox4) is a major source of oxidative stress in the failing heart. *Proc Natl Acad Sci U S A* **107**, 15565–15570 (2010).

429. Block, K., Gorin, Y. & Abboud, H. E. Subcellular localization of Nox4 and regulation in diabetes. *Proc Natl Acad Sci U S A* **106**, 14385–14390 (2009).

430. Wang, F. *et al.* Effects of volatile organic compounds and carbon monoxide mixtures on learning and memory, oxidative stress, and monoamine neurotransmitters in the brains of mice. *Toxicol Ind Health* **34**, 178–187 (2018).

431. Mcintosh-Kastrinsky, R. *et al.* Photochemically Altered Air Pollution Mixtures and Contractile Parameters in Isolated Murine Hearts before and after Ischemia. *Environ Health Perspect* **121**, 1344–1348 (2013).

432. Kim, J. B. *et al.* Particulate air pollution induces arrhythmia via oxidative stress and calcium calmodulin kinase II activation. *Toxicol Appl Pharmacol* **259**, 66–73 (2012).

433. Gomez Perdiguero, E. *et al.* ANGPTL4–αvβ3 interaction counteracts hypoxia-induced vascular permeability by modulating Src signalling downstream of vascular endothelial growth factor receptor 2. *J Pathol* **240**, 461–471 (2016).

434. Acosta, M. J. *et al.* Coenzyme Q biosynthesis in health and disease. *Biochimica et Biophysica Acta (BBA) - Bioenergetics* **1857**, 1079–1085 (2016).

435. Gunata, M. & Parlakpinar, H. A review of myocardial ischaemia/reperfusion injury: Pathophysiology, experimental models, biomarkers, genetics and pharmacological treatment. *Cell Biochem Funct* **39**, 190–217 (2021).

436. Dambrova, M., Zuurbier, C. J., Borutaite, V., Liepinsh, E. & Makrecka-Kuka, M. Energy substrate metabolism and mitochondrial oxidative stress in cardiac ischemia/reperfusion injury. *Free Radic Biol Med* **165**, 24–37 (2021).

437. Raimondi, V., Ciccarese, F. & Ciminale, V. Oncogenic pathways and the electron transport chain: a dangeROS liaison. *British Journal of Cancer 2019 122:2* **122**, 168–181 (2019).

438. Mazat, J. P., Devin, A. & Ransac, S. Modelling mitochondrial ROS production by the respiratory chain. *Cellular and Molecular Life Sciences* **77**, 455–465 (2020).

439. Katusic, Z. S. Vascular endothelial dysfunction: Does tetrahydrobiopterin play a role? *Am J Physiol Heart Circ Physiol* **281**, (2001).

10. ANNEXES

10.1 PUBLICATION 1

Citric Acid Cycle Metabolites Predict Infarct Size in Pigs Submitted to Transient Coronary Artery Occlusion and Treated with Succinate Dehydrogenase Inhibitors or Remote Ischemic Perconditioning.

Consegal M, Núñez N, Barba I, Benito B, Ruiz-Meana M, Inserte J, Ferreira-González I, Rodríguez-Sinovas A.

Int J Mol Sci. 2021 Apr 16;22(8):4151. doi: 10.3390/ijms22084151. PMID: 33923786; PMCID: PMC8072915.

Impact factor (2021): 6.208

International Journal of
Molecular Sciences

MDPI

Article

Citric Acid Cycle Metabolites Predict Infarct Size in *Pigs* Submitted to Transient Coronary Artery Occlusion and Treated with Succinate Dehydrogenase Inhibitors or Remote Ischemic Perconditioning

Marta Consegal [1,2,3], Norberto Núñez [4], Ignasi Barba [1,2,3,5], Begoña Benito [1,2,3], Marisol Ruiz-Meana [1,2,3], Javier Inserte [1,2,3], Ignacio Ferreira-González [1,2,6,*] and Antonio Rodríguez-Sinovas [1,2,3,*]

1 Cardiovascular Diseases Research Group, Department of Cardiology, Vall d'Hebron Institut de Recerca (VHIR), Vall d'Hebron Hospital Universitari, Vall d'Hebron Barcelona Hospital Campus, Passeig Vall d'Hebron 119-129, 08035 Barcelona, Spain; marta.consegal@vhir.org (M.C.); ignasibarba@gmail.com (I.B.); begona.benito@vhir.org (B.B.); mruizmeana@gmail.com (M.R.-M.); javier.inserte@vhir.org (J.I.)
2 Departament de Medicina, Universitat Autònoma de Barcelona, 08193 Bellaterra, Spain
3 Centro de Investigación Biomédica en Red (CIBER) de Enfermedades Cardiovasculares (CIBERCV), Instituto de Salud Carlos III, 28029 Madrid, Spain
4 Unit of High Technology, Vall d'Hebron Institut de Recerca (VHIR), Vall d'Hebron Hospital Universitari, Vall d'Hebron Barcelona Hospital Campus, Passeig Vall d'Hebron 119-129, 08035 Barcelona, Spain; norberto.nunez@vhir.org
5 Faculty of Medicine, University of Vic-Central University of Catalonia (UVicUCC), Can Baumann. Ctra. de Roda, 70, 08500 Vic, Spain
6 Centro de Investigación Biomédica en Red (CIBER) de Epidemiología y Salud Pública (CIBERESP), Instituto de Salud Carlos III, 28029 Madrid, Spain
* Correspondence: nachoferreira@secardiologia.es (I.F.-G.); antonio.rodriguez.sinovas@vhir.org (A.R.-S.); Tel.: +34-93-489-4184 (A.R.-S.)

check for updates

Citation: Consegal, M.; Núñez, N.; Barba, I.; Benito, B.; Ruiz-Meana, M.; Inserte, J.; Ferreira-González, I.; Rodríguez-Sinovas, A. Citric Acid Cycle Metabolites Predict Infarct Size in *Pigs* Submitted to Transient Coronary Artery Occlusion and Treated with Succinate Dehydrogenase Inhibitors or Remote Ischemic Perconditioning. *Int. J. Mol. Sci.* **2021**, *22*, 4151. https://doi.org/10.3390/ijms22084151

Academic Editor: Christian Jung

Received: 3 March 2021
Accepted: 14 April 2021
Published: 16 April 2021

Publisher's Note: MDPI stays neutral with regard to jurisdictional claims in published maps and institutional affiliations.

Abstract: Succinate dehydrogenase (SDH) inhibition with malonate during reperfusion reduced myocardial infarction in animals, whereas its endogenous substrate, succinate, is detected in plasma from STEMI patients. We investigated whether protection by SDH inhibition is additive to that of remote ischemic perconditioning (RIC) in *pigs* submitted to transient coronary artery occlusion, and whether protective maneuvers influence plasma levels of citric acid cycle metabolites. Forty *pigs* were submitted to 40 min coronary occlusion and reperfusion, and allocated to four groups (controls, sodium malonate 10 mmol/L, RIC, and malonate + RIC). Plasma was obtained from femoral and great cardiac veins and analyzed by LC-MS/MS. Malonate, RIC, and malonate + RIC reduced infarct size (24.67 ± 5.98, 25.29 ± 3.92 and 29.83 ± 4.62% vs. 46.47 ± 4.49% in controls, $p < 0.05$), but no additive effects were detected. Enhanced concentrations of succinate, fumarate, malate and citrate were observed in controls during initial reperfusion in the great cardiac vein, and most were reduced by cardioprotective maneuvers. Concentrations of succinate, fumarate, and malate significantly correlated with infarct size. In conclusion, despite the combination of SDH inhibition during reperfusion and RIC did not result in additive protection, plasma concentrations of selected citric acid cycle metabolites are attenuated by protective maneuvers, correlate with irreversible injury, and might become a prognosis tool in STEMI patients.

Keywords: succinate dehydrogenase; malonate; remote ischemic conditioning; myocardial infarction; ischemia-reperfusion

1. Introduction

Early diagnosis and immediate application of reperfusion therapies are the most effective ways to preserve viability of the ischemic myocardium and limit infarct size in

patients with ST-segment elevation myocardial infarction (STEMI). Preventive measures and advances in reperfusion therapies have greatly contributed to the reductions in mortality and morbidity observed in STEMI patients in the last decades [1]. However, the risk of cardiovascular events has been shown to remain high beyond the first year post-myocardial infarction [2]. Despite appropriate and timely application of reperfusion therapies, a high proportion of STEMI patients end up with extensive areas of myocardial necrosis, that would compromise cardiac function, leading to heart failure and arrhythmias, and eventually death. This is in part due to the existence of reperfusion injury triggered by blood flow restoration itself, a phenomenon consisting of an additional cell death to that induced by ischemia [3]. Indeed, it has been proposed that lethal reperfusion injury may account for about half of the final infarct size [4]. However, the discovery of reperfusion injury opened a window of opportunity to explore new therapeutic approaches to reduce final infarct size. Experimental studies have allowed us to identify a number of strategies able to attenuate reperfusion injury in different animal models [5]. Nevertheless, none of these studies have become part of standard clinical care. This is probably due to their limited protective effects in STEMI patients, which are often influenced by comorbidities, concomitant medications, and other factors, such as age [6]. Thus, further efforts are needed to identify new strategies that are able to mitigate reperfusion injury in the clinical setting.

Among these is the inhibition of mitochondrial succinate dehydrogenase (SDH) [7–9]. SDH or mitochondrial respiratory chain complex II is the enzyme that catalyzes oxidation of succinate to fumarate within the citric acid cycle, in a process that results in the donation of electrons to the mitochondrial respiratory chain via reduction of FAD to $FADH_2$. However, under some circumstances, SDH may work in the reverse direction, reducing fumarate and leading to succinate accumulation [9–11]. In this regard, previous studies have demonstrated that succinate accumulates in ischemic tissues due to the reversal action of the enzyme [7]. Resumption of forward SDH activity upon reperfusion leads to rapid oxidation of accumulated succinate, a process coupled with reverse electron transfer from mitochondrial complex II to complex I and reactive oxygen species production by the latter, thus contributing to cell death [7]. Interestingly, preventing succinate accumulation during ischemia using the competitive inhibitor malonate, given before transient coronary occlusion, has been shown to reduce infarct size in mice [7]. Furthermore, malonate was demonstrated to be also effective against reperfusion injury, as it was able to reduce infarct size, when given at the onset of blood flow restoration, both in isolated mice hearts and in *pigs* submitted to transient myocardial ischemia [8,12].

Emerging evidence suggests that multitargeted approaches using a combination of therapies directed against several of the intracellular signaling pathways that are involved in reperfusion injury would be helpful to reduce infarct size in the clinical setting [13]. Indeed, some combination therapies have been previously demonstrated to exert additive effects against reperfusion injury in in situ *pig* hearts, as is the case of treatments targeting cardiac metabolism and remote ischemic conditioning (RIC) [14,15]. RIC is a non-pharmacological and safe maneuver, consisting of brief episodes of ischemia and reperfusion applied remotely, mainly to a limb, that activates a variety of endogenous mechanisms of cardioprotection [16–18], and has been reported to exert protective effects in both experimental models [14,19,20] and in proof-of-concept clinical trials in STEMI patients [21,22]. However, the effects of a combination therapy with malonate and RIC have not been previously explored.

Thus, in this study we investigated the potential usefulness of the combination of RIC, applied during myocardial ischemia, with the SDH inhibitor malonate, given at the onset of reperfusion, to attenuate reperfusion injury and reduce infarct size in *pigs* submitted to transient coronary occlusion. Furthermore, because part of the succinate that accumulates during ischemia is released into the circulation during reperfusion [23–25], we also aimed to explore whether protective maneuvers may influence plasma levels of this and other citric acid cycle metabolites, with the ultimate goal of identifying a metabolic signature that may have prognostic value in the context of myocardial ischemia-reperfusion injury.

2. Results

2.1. Ischemia-Reperfusion Injury

Ischemia-reperfusion injury after transient coronary occlusion was assessed in control *pigs* and in animals treated with either malonate 10 mmol/L, RIC or a combination of both treatments, as depicted in Figure 1.

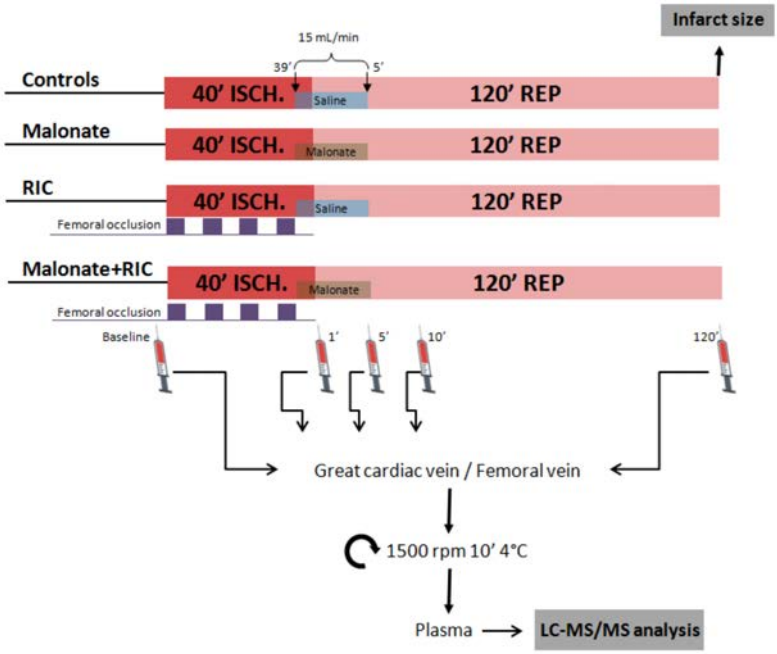

Figure 1. Study design. Open-chest *pigs* were submitted to 40 min of left anterior descending coronary artery occlusion followed by reperfusion and were treated with either malonate 10 mmol/L during the first 5 min of reperfusion, with 4 cycles of femoral artery occlusion (5 min each) followed by reperfusion (5 min each), applied during myocardial ischemia, or with a combination of both treatments. At the end of the experiment, infarct size was analyzed by TTC staining. Targeted LC-MS/MS analysis was performed in blood samples obtained from the great cardiac vein and a femoral vein.

2.1.1. Hemodynamic Variables, LAD Coronary Blood Flow and Regional Myocardial Contractility

Baseline values for heart rate, hemodynamics, coronary blood flow and systolic segment shortening are shown in Table 1. As expected, ischemia-reperfusion induced significant reductions in aortic pressure, LV systolic pressure and LV (+)dP/dt, and increases in heart rate and LV (−)dP/dt, whereas coronary blood flow depicted a clear hyperemic reaction during initial reperfusion. However, the time course of these changes was similar in all experimental groups (Table 1, Figure 2).

Table 1. Values at baseline and at the end of ischemia (40 min) and reperfusion (2 h) for heart rate, aortic pressure, left ventricular (LV) systolic and end-diastolic pressure, LV (+) and (−)dP/dt, coronary blood flow at the LAD, and systolic shortening (SS) in the control and ischemic areas, in control *pigs* and in *pigs* receiving intracoronary malonate, remote ischemic conditioning (RIC), or malonate + RIC. Data are shown as mean ± SD.

		Heart Rate (Beats/min)	Aortic Pressure (mm Hg)	LV Systolic Pressure (mm Hg)	LV End-Diastolic Pressure (mm Hg)	LV (+)dP/dt (mm Hg/s)	LV (–)dP/dt (mm Hg/s)	LAD Coronary Blood Flow (mL/min)	SS (Control)	SS (Ischemic)
Control	Baseline	74.17 ± 12.29	114.97 ± 14.73	139.14 ± 12.59	6.09 ± 3.242	1743 ± 337	−2803 ± 491	7.63 ± 1.72	0.17 ± 0.04	0.19 ± 0.08
(*n* = 10)	40′ isch	82.24 ± 13.06 *	101.97 ±1 3.67 *	121.39 ± 21.01 *	5.51 ± 4.07	1834 ± 506	−2312 ± 507 *	0.00 ± 0.00 *	0.15 ± 0.05	−0.07 ± 0.02 *
	2 h reperf	106.86 ± 19.70 *	81.39 ± 20.35 *	93.72 ± 24.52 *	4.21 ± 3.57	1407 ± 397 *	−1778 ± 644 *	8.18 ± 5.83	0.11 ± 0.03 *	−0.05 ± 0.08 *
Malonate	Baseline	69.35 ± 12.21	104.76 ± 10.60	122.17 ± 16.18	4.28 ± 3.33 τ	1543 ± 310	–2263 ± 431	6.12 ± 2.57	0.16 ± 0.06	0.20 ± 0.05
(*n* = 10)	40′ isch	76.46 ± 13.54 *	90.38 ± 14.69 *	105.36 ± 19.52 *	3.81 ± 4.06	1432 ± 282 *	−1852 ± 387 *	0.00 ± 0.00 *	0.13 ± 0.05	−0.05 ± 0.05 *
	2 h reperf	82.98 ± 14.95 *	76.64 ± 23.35 *	85.90 ± 25.49 *	3.06 ± 3.50	1164 ± 346 *	−1347 ± 563 *	9.79 ± 6.76	0.12 ± 0.07	−0.06 ± 0.06 *
RIC	Baseline	74.85 ± 12.72	102.56 ± 8.74	124.06 ± 13.61	8.20 ± 1.29 τ	1522 ± 232	−2283 ± 374	6.45 ± 1.67	0.17 ± 0.08	0.20 ± 0.07
(*n* = 10)	40′ isch	81.35 ± 9.84	93.19 ± 7.42 *	109.55 ± 11.73 *	7.11 ± 1.72	1428 ± 175	−1878 ± 286 *	0.00 ± 0.00 *	0.16 ± 0.05	−0.09 ± 0.08 *
	2 h reperf	85.66 ± 16.47	63.95 ± 23.00 *	77.17 ± 29.59 *	4.85 ± 2.11 *	1152 ± 401 *	−1137 ± 664 *	9.19 ± 5.69	0.13 ± 0.09	−0.06 ± 0.08 *
Malonate	Baseline	80.59 ± 13.34	112.80 ± 23.53	138.18 ± 25.03	5.13 ± 2.52	1879 ± 492	−2730 ± 646	8.82 ± 3.93	0.17 ± 0.08	0.16 ± 0.06
+ RIC	40′ isch	85.40 ± 11.96	98.16 ± 18.86 *	117.95 ± 23.52 *	5.09 ± 4.93	1636 ± 415 *	−2102 ± 611 *	0.00 ± 0.00 *	0.16 ± 0.10	−0.06 ± 0.09 *
(*n* = 10)	2 h reperf	98.10 ± 20.61	69.41 ± 14.26 *	80.62 ± 14.91 *	3.77 ± 3.06	1204 ± 229 *	−1254 ± 539 *	7.27 ± 2.91	0.13 ± 0.07	−0.03 ± 0.07 *

* ($p < 0.05$) indicates significant differences vs. the corresponding baseline value (repeated measures ANOVA); τ ($p < 0.05$) indicates significant differences between malonate and RIC baseline values (ANOVA and Tukey tests).

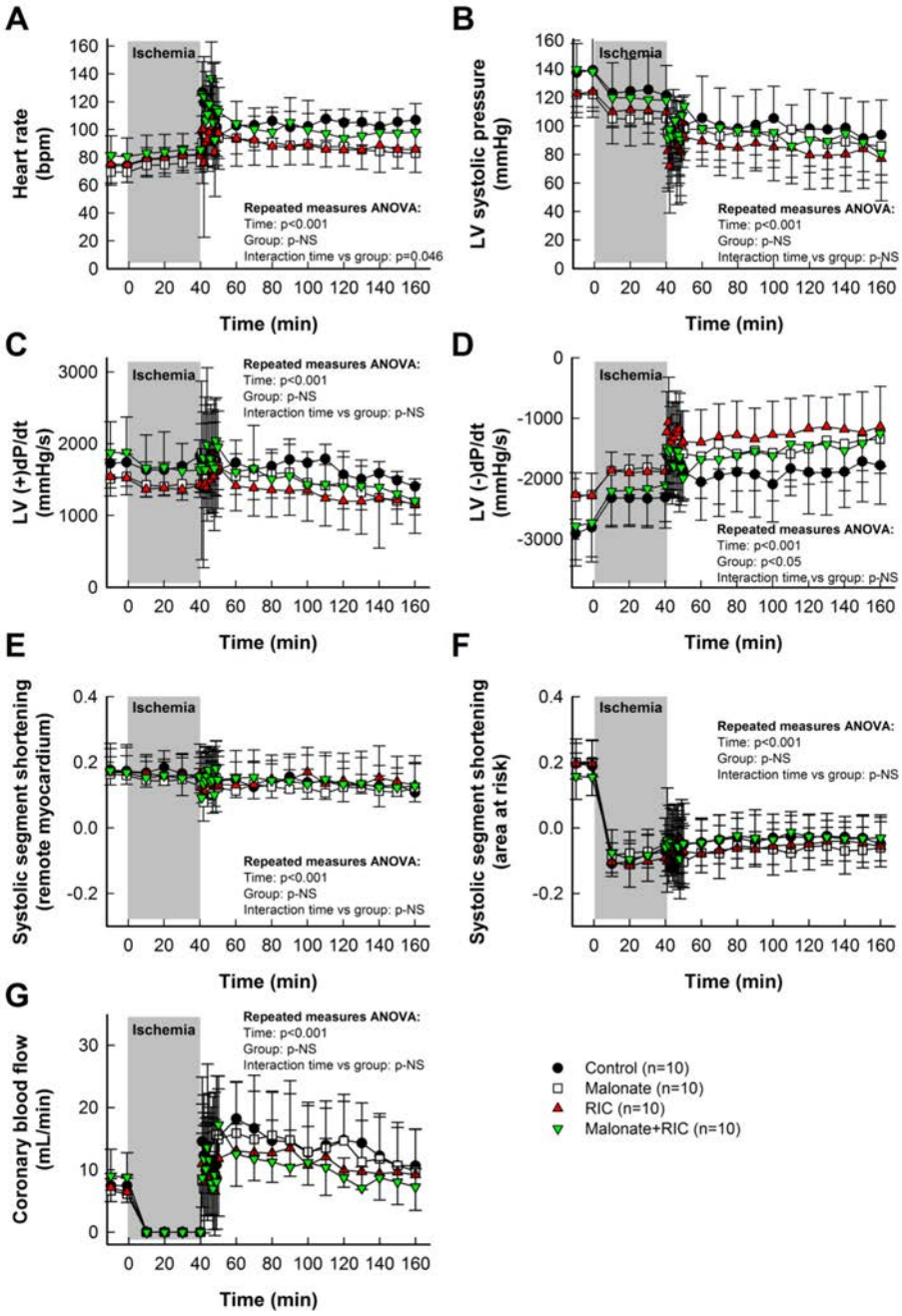

Figure 2. Effects of intracoronary malonate, given at the onset of reperfusion, remote ischemic conditioning (RIC), or combined treatment, on heart rate (**A**), left ventricular (LV) systolic pressure (**B**), LV (+)dP/dt (**C**), LV (−)dP/dt (**D**), systolic segment shortening in remote myocardium (**E**) and area at risk (**F**), and coronary blood flow (**G**) in pigs submitted to 40 min of LAD coronary artery occlusion followed by 2 h of reperfusion. No differences between groups were observed in the time course of any variable.

Systolic segment shortening in distant, control myocardium, assessed by ultrasonic piezoelectric crystals, was only slightly reduced during ischemia-reperfusion (Table 1, Figure 2E). In contrast, myocardial function in the area at risk was markedly depressed during ischemia, with no recovery during reperfusion (Table 1, Figure 2F). Neither intracoronary malonate, RIC, nor combined treatment, led to an improvement in myocardial function in this region throughout the 2 h reperfusion period (Table 1, Figure 2F).

2.1.2. Infarct Size

Control *pigs* submitted to 40 min of LAD coronary artery occlusion followed by reperfusion had an averaged infarct size of 46.47 ± 14.21% of the area at risk, which was significantly reduced by both 10 mmol/L of intracoronary malonate, given during initial reperfusion, and RIC (Figure 3A). However, combined treatment did not induce any additive effect, the infarct size being similar to individual treatments (Figure 3A). No differences were observed between experimental groups in the size of the area at risk or body temperature during ischemia (Figure 3B,C).

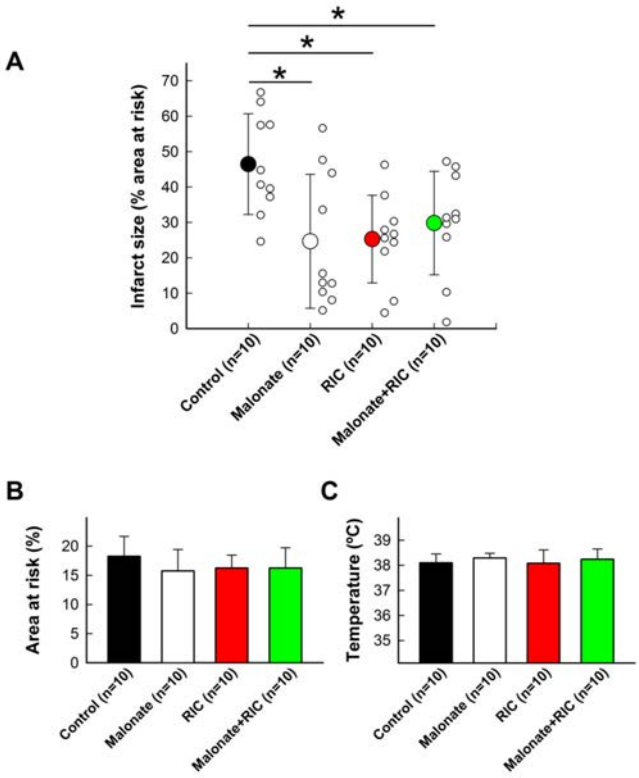

Figure 3. Effects of intracoronary malonate (white symbols or column), given at the onset of reperfusion, remote ischemic conditioning (RIC, red), or combined treatment (green), on infarct size (**A**) in pigs submitted to 40 min of LAD coronary artery occlusion followed by 2 h of reperfusion. Controls are shown in black. * ($p < 0.05$) indicates significant differences vs. control animals ($n = 10$/group). No differences were observed in the size of area at risk (**B**) or body temperature (**C**).

2.1.3. Reperfusion Arrhythmias

No significant differences were observed in the total number of ventricular tachyarrhythmias (ventricular tachycardias (VT) + ventricular fibrillations (VF)) during the first 20 min of reperfusion (Figure 4). However, the incidence of ventricular fibrillation

during initial reperfusion was significantly higher in animals treated with malonate (8 out of 10 animals developed FV) and RIC (10 out of 10) as compared with controls (2 out of 10, $p < 0.01$) (Figure 4). This enhancement was associated with a trend towards a lower number of ventricular tachycardias in these two groups, which reaches significance in malonate-treated *pigs* ($p < 0.05$).

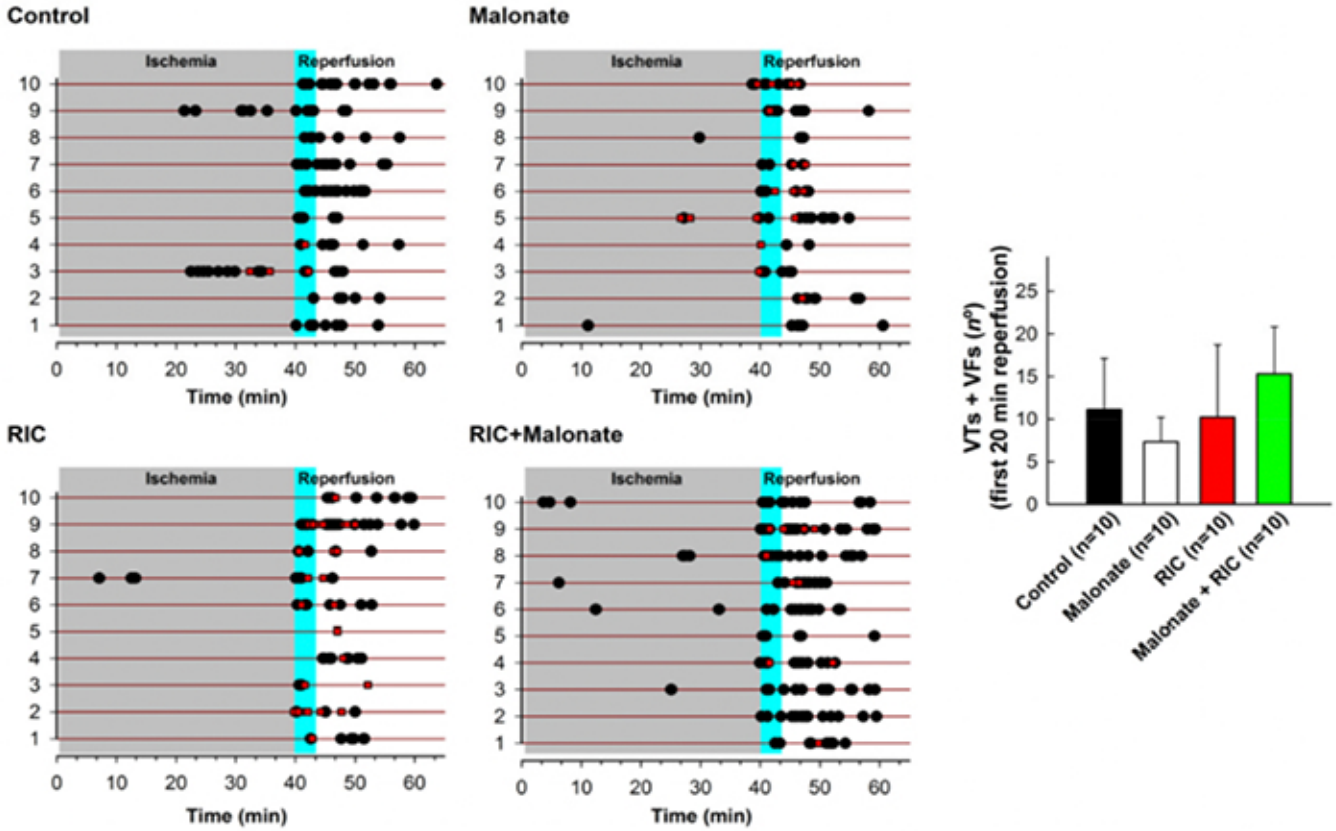

Figure 4. Incidence of ventricular tachyarrhythmias (ventricular tachycardias (VTs, black dots) and ventricular fibrillations (VFs, red squares) during ischemia and the first 20 min of reperfusion in control *pigs* submitted to 40 min LAD coronary occlusion followed by reperfusion, and in animals treated with intracoronary malonate, given at the onset of reperfusion, remote ischemic conditioning (RIC), or combined treatment. Right figure indicates the total number of ventricular tachyarrhythmias.

2.2. *Targeted LC-MS/MS Analysis of Citric Acid Cycle Metabolites in Porcine Plasma Samples*

Analysis of peripheral blood samples obtained from control *pigs* submitted to transient coronary occlusion did not show any significant change in plasma concentrations for succinate, fumarate, malate, or lactate during the first 10 min of reperfusion (Figure 5A–C,E, blank dots), whereas a slight and continuous increase in citrate was observed in these samples following ischemia (Figure 5D, blank dots). Only modest enhancements in fumarate (from 0.80 ± 0.50 µmol/L at baseline to 1.97 ± 1.93 at the end of the experiment, Student's *t* test, $p = 0.039$) and malate (from 2.45 ± 0.75 µmol/L to 4.89 ± 3.49, Student's *t* test, $p = 0.031$) were noticeable 2 h after reperfusion. In contrast, plasma samples obtained from the great cardiac vein depicted, in this group of animals, a marked increase in all analyzed metabolites, peaking, in most cases, at 5 min of reperfusion (Figure 5A–E, black dots). Differences in baseline values between peripheral and great cardiac vein samples were apparent for succinate, fumarate, and especially, lactate. Malonate was not detected in these animals at any time.

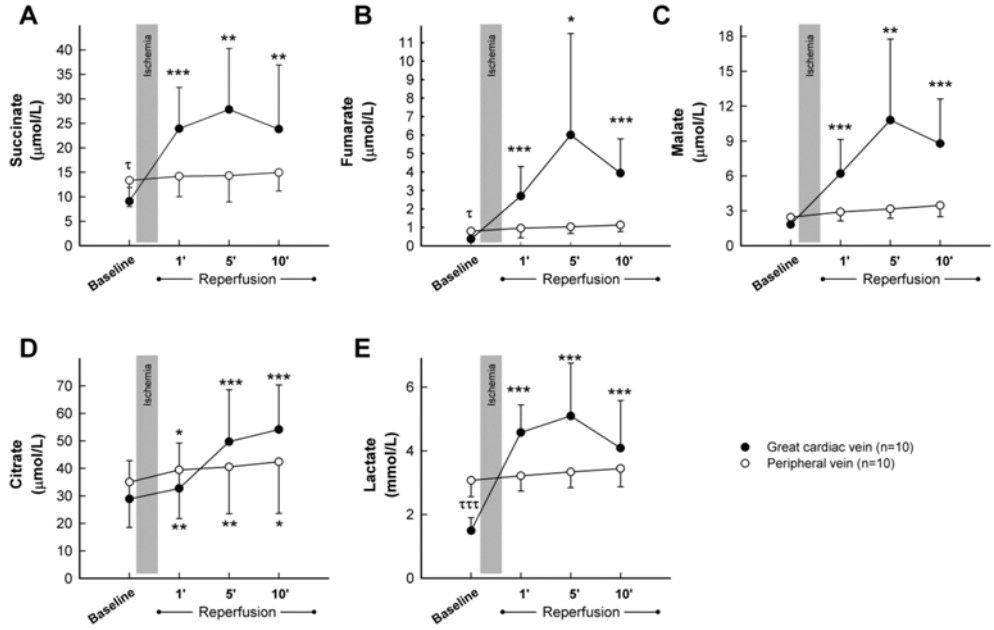

Figure 5. Concentrations of the citric acid cycle metabolites succinate (**A**), fumarate (**B**), malate (**C**), and citrate (**D**), together with lactate (**E**), assessed by LC-MS/MS, in plasma samples obtained from the great cardiac and femoral veins in control *pigs* submitted to 40 min of LAD coronary artery occlusion followed by 2 h of reperfusion. * ($p < 0.05$), ** ($p < 0.01$) and *** ($p < 0.001$) indicate significant differences vs. the corresponding baseline value (repeated measures ANOVA and Tukey tests). τ ($p < 0.05$) and ττ τ ($p < 0.001$) indicate significant differences between both baseline values (Student's *t* test).

As these results demonstrate that citric acid cycle metabolites are only enhanced in plasma samples obtained from the great cardiac vein, we decided to assess the influence of malonate, RIC, or combined treatment only in blood from this source. Accordingly, repeated measures ANOVA analysis demonstrated significantly enhanced levels of succinate during reperfusion in all experimental groups, with no differences between treatments (Figure 6A). In contrast, the increase in fumarate and malate detected during initial reperfusion was significantly attenuated by cardioprotective maneuvers. Indeed, repeated measures ANOVA demonstrated a significant effect of group allocation for both fumarate and malate, together with positive interactions between group allocation and the time course of concentration changes (Figure 6B,C). In addition, the enhancement in citrate levels observed in control animals was also attenuated in all treated groups (Figure 6D), whereas a marginally significant effect of group allocation was detected for lactate (Figure 6E). Measurement of malonate, used as a positive control, demonstrated an increase in its plasma concentration only in animals treated with this reversible SDH inhibitor (Figure 6F).

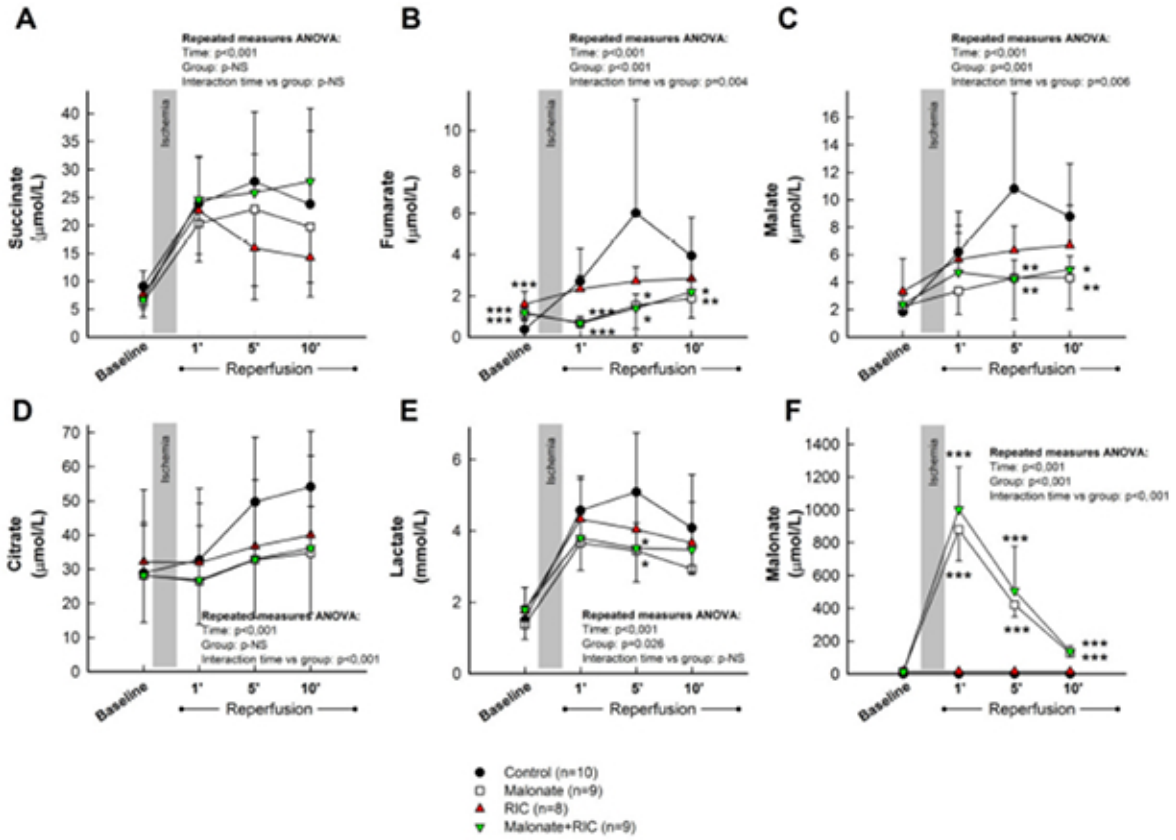

Figure 6. Concentrations of the citric acid cycle metabolites succinate (**A**), fumarate (**B**), malate (**C**) and citrate (**D**), together with lactate (**E**) and malonate (**F**), assessed by LC-MS/MS, in plasma samples obtained from the great cardiac vein in control *pigs*, submitted to 40 min of LAD coronary artery occlusion followed by 2 h of reperfusion, and in animals treated with intracoronary malonate, given at the onset of reperfusion, remote ischemic conditioning (RIC), or malonate + RIC. * ($p < 0.05$), ** ($p < 0.01$) and *** ($p < 0.001$) indicate significant differences vs. the corresponding value in the control group (ANOVA and Tukey tests).

When analyzed independently of the control group, pooled samples from the two groups receiving malonate showed a trend of having higher succinate concentrations than those receiving RIC alone (repeated measures ANOVA, $p = 0.051$ for interaction), and significantly reduced levels of fumarate (repeated measures ANOVA, $p = 0.014$ for interaction and $p < 0.001$ for group allocation) and malate (repeated measures ANOVA, $p = 0.019$ for group allocation).

Interestingly, concentrations of succinate, fumarate, malate, and lactate, obtained 5 min after reperfusion from the great cardiac vein, significantly correlated with infarct size, expressed as percentage of ventricular weight, with good correlation coefficients, particularly for succinate levels (Figure 7A–D). Similar data were obtained when infarct size was expressed in grams (not shown). In contrast, only succinate and lactate concentrations correlated with the size of the area at risk, although in these cases correlation coefficients were slightly lower (Figure 7E,F). No group differences were observed in these correlationships.

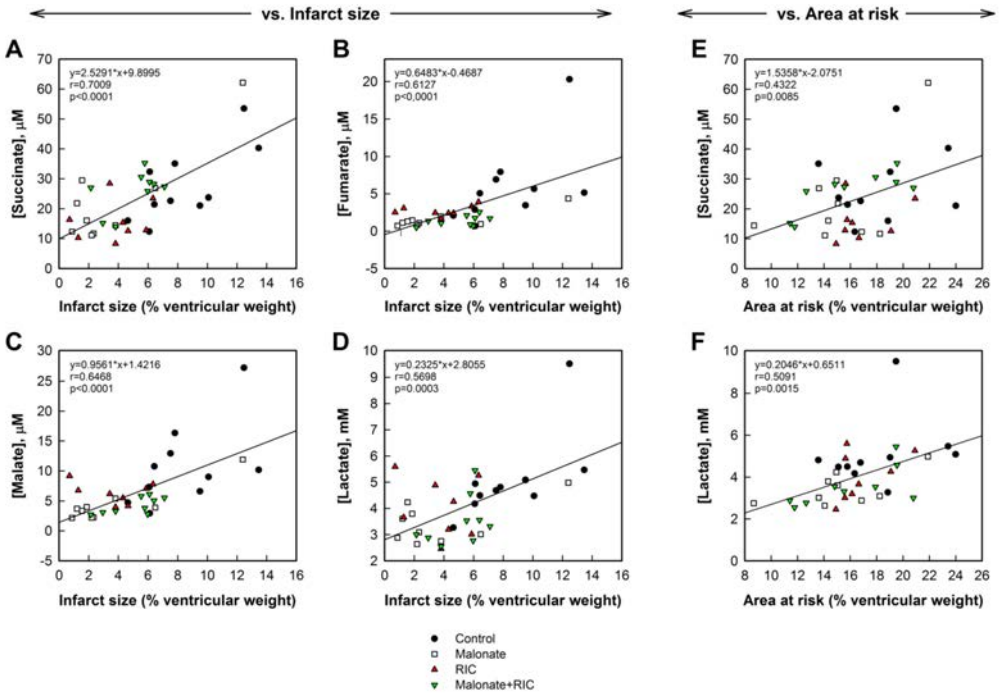

Figure 7. Correlations between infarct size, expressed as percentage of total cardiac weight, and succinate (**A**), fumarate (**B**), malate (**C**), and lactate (**D**) concentrations measured 5 min after reperfusion in plasma obtained from the great cardiac vein in *pigs* from the four experimental groups. Right panels show correlations between area at risk (in percentage of ventricular weight) and succinate (**E**) and lactate (**F**) concentrations in the same plasma samples.

3. Discussion

This study demonstrates that the combination of SDH inhibition during initial reperfusion with intracoronary malonate and RIC exerts non-additive cardioprotective effects in *pigs* submitted to transient coronary occlusion. Moreover, our results show that the enhanced release of citric acid cycle intermediates to the bloodstream, detected in plasma samples from the great cardiac vein during initial reperfusion, is attenuated by cardioprotective maneuvers, and that succinate, fumarate, and malate concentrations significantly correlate with infarct size. These results open up the possibility to use citric acid cycle metabolite concentrations obtained in blood samples from the coronary sinus as new prognosis biomarkers in STEMI patients.

3.1. Cardioprotection by SDH Inhibition and RIC

Prevention of succinate accumulation during ischemia by pretreatment with the reversible SDH inhibitor malonate was demonstrated to reduce myocardial infarct size in several animal models [7,26,27]. Although the mechanisms of succinate accumulation in ischemic tissues are not entirely understood [7,24,28], it was demonstrated that accumulated succinate is rapidly oxidized during reperfusion by forward SDH activity, which, in turn, induces a massive reactive oxygen species (ROS) production by reverse electron transfer from mitochondrial complex II to complex I [7,8]. This oxidative stress is associated with mitochondrial permeability transition pore (MPTP) opening and cell death [7,8]. Furthermore, it has been demonstrated that administration of the SDH inhibitor malonate at the onset of reperfusion reduces myocardial infarct size in several independent experimental models, including Langendorff-perfused isolated mice heart [8], in situ coronary occlusion in mice [26], and in *pigs* submitted to transient coronary occlusion [12]. In all of these mod-

els, the protective effect of malonate was associated with reduced oxidation of succinate during the first minutes of reperfusion, less ROS production, preserved mitochondrial function, and increased calcein retention in isolated mitochondria, suggestive of reduced MPTP opening [8]. Our present results thus support the cardioprotective effects of SDH inhibition when applied at the onset of reperfusion.

RIC activates a variety of endogenous mechanisms of cardioprotection [16–18] and has been shown to exert protective effects in both experimental models [14,19,20], and in proof-of-concept clinical trials in STEMI patients [21,22]. Experimental studies have demonstrated that the cardioprotective signal is transferred from the remote conditioned organ or tissue to the heart, either through the release of humoral factors or through activation of neuronal pathways [16]. In the heart, RIC causes activation of intracellular transduction cascades similar to those of classic, local, ischemic pre- or postconditioning, including the RISK and SAFE pathways [16,17,29], being the mitochondria the end-effectors [16,17,30]. Our present results confirm previous data obtained by our group in the same animal model [14,15], and support the cardioprotective effect of RIC against myocardial infarction. Unfortunately, however, two recently published randomized clinical trials have not been able to find any effect of RIC on clinical outcomes or on infarct size evaluated by cardiac biomarkers or NMR in STEMI patients [31,32]. Different reasons have been proposed to explain the failure of translation of cardioprotective strategies, including presence of comorbidites, such as aging, diabetes, or hypertension, which may alter the efficacy of cardioprotective maneuvers [33], the routine use of different comedications, such as P2Y12 antagonists, which may have protective effects [34], or the lack of uniformity in the method used to quantify infarct size [32]. Optimization of conditioning protocols in the clinical setting may help to improve efficacy of RIC in STEMI patients [32].

Under this situation, emerging evidence suggests that a multitargeted approach using two or more therapies, directed against different signaling pathways or cell targets involved in ischemia-reperfusion injury, would be advantageous in STEMI patients in order to reduce final infarct size [13]. Additive protection may be reached when the mechanisms of action of the combined interventions are different and would be especially interesting when the efficacy of the individual treatments is expected to be reduced by comorbidities or comedications. To date, some of the combined strategies that have demonstrated additive protection are addressed to different cell targets, such as coronary circulation or microvascular obstruction vs. cardiomyocytes [35]. This is the case of the combination of the antiplatelet cangrelor (a $P2Y_{12}$ receptor antagonist) and cariporide (a Na^+/H^+ exchanger inhibitor) or hypothermia, the last two acting mostly on cardiomyocytes, which has been shown to exert additive protection in open-chest rats submitted to transient coronary occlusion [36]. Other strategies have used treatment combinations acting on different signaling pathways within cardiomyocytes, including those targeting ischemic and reperfusion injury separately. In this regard, additive protection was found between RIC and local ischemic postconditioning in an in vivo rat model of ischemia-reperfusion [37], a finding that was later extended to STEMI patients [38]. Similarly, we have previously demonstrated additive effects between treatments modulating myocardial energy metabolism (glucose-insulin-potassium (GIK) or exenatide, a mimetic of the incretin glucagon-like peptide-1 (GLP-1)) and RIC [14,15]. Furthermore, synergistic effects between inhibition of succinate accumulation, oxidation, and hypothermia have been also described in rabbits [39]. However, not all treatment combinations are equally effective. Thus, protection by long-term nitroglycerine and RIC was shown to be abrogated when both individual treatments were combined in rats [40]. Similarly, no additive effects were found between aminooxyacetate, a malate-aspartate shuttle inhibitor, and local ischemic preconditioning in isolated rat hearts [41]. Unfortunately, our present results demonstrate that the addition of the SDH inhibitor malonate to RIC does not exert additive cardioprotective effects in *pigs* submitted to transient coronary occlusion.

As conduction arrhythmias may severely affect cardiac performance during reperfusion, we assessed whether our two individual treatments and the combination of both was

able to modify the incidence of ventricular tachyarrhythmias during initial reperfusion. Accordingly, we observed that none of the three treatments were able to modify the total number of ventricular tachyarrhythmias following ischemia. However, the incidence of VF during initial reperfusion was significantly higher in animals treated with malonate and RIC as compared with controls, although this enhancement was, in part, compensated with a trend towards a lower number of VTs in these two groups. In contrast to these findings, we have previously demonstrated that neither malonate [12], nor RIC [15], were able to modify the incidence of VFs in the same animal model. Reasons for these discrepancies are unknown. It is plausible that smaller, patchier, infactions in malonate and RIC-treated animals in the present study would create the ideal substrate for VF to evolve, at the expense of a lower number of VTs. Nevertheless, the higher incidence of VFs in these two groups in the present study would not modify our main conclusion, as defibrillation has been associated with higher infarctions in the *pig* model [42]. Thus, even smaller infactions would be expected in these two groups in the absence of VF, thus magnifying its protective action. On the contrary, the incidence of VF in *pigs* receiving the treatment combination was not modified, thus supporting the fact that both treatments have no additive effect on infarct size.

3.2. Targeted Analysis of Citric Acid Cycle Metabolites by LC-MS/MS

Part of the succinate that accumulated during myocardial ischemia is released into the bloodstream after flow restoration [23–25]. In fact, conditions during early reperfusion might not be so favorable for reverse electron transfer, and the rapid decay in succinate occurring during reperfusion [7,8] has been suggested to be due, at least in part, to efflux rather than oxidation [43]. Indeed, it has been quantified that about two-thirds of accumulated succinate is washed into the perfusate within the first 5 min of reperfusion, while approximately one-third is metabolized [24]. Supporting the existence of this efflux, succinate, together with other citric acid cycle metabolites, including fumarate, malate and citrate, have been found to accumulate in the interstitial space during ischemia and initial reperfusion in isolated rat hearts [41]. Similar findings were obtained in the right ventricular interstitial space of newborn *pigs* submitted to 10 cycles of 3 min ischemia followed by 3 min of reperfusion, as determined using microdialysis catheters [44]. However, analysis of interstitial metabolite concentrations in newborn animals in the last study might not be directly translated to changes occurring in adult hearts, as a gradual switch in cardiac energy generation from glycolysis to fatty acid oxidation occurs over the first postnatal weeks [44]. Furthermore, short bouts of ischemia in that study [44] may not completely reflect changes occurring after myocardial infarction. Importantly, Prag and coworkers have recently suggested that succinate release upon reperfusion of the ischemic heart is mediated by the monocarboxylate transporter 1 (MCT1), in a process that is facilitated by ischemic acidification of the myocardium [25].

Several studies have characterized the plasma metabolome in patients with STEMI. Using a non-targeted LC-MS approach in 27 STEMI patients who underwent primary percutaneous coronary intervention (pPCI), it was demonstrated that the largest cohort of molecules undergoing significant changes, 2 to 48 after pPCI, were lipid metabolites, although citric acid metabolites, and especially succinate were also increased [45]. In contrast, others found a decrease in succinate, fumarate, and citrate in serum obtained 1 h after symptom onset in 20 STEMI patients [46]. Significantly, peripheral blood might not be appropriate to analyze these changes, which could explain these discrepancies. Indeed, it was demonstrated in STEMI patients, and in a porcine model of transient coronary occlusion, that the greatest increase in succinate concentrations occurred when blood was taken, immediately after reperfusion, from the coronary sinus [23,25]. However, whether release of succinate and other citric acid cycle metabolites to the bloodstream during reperfusion is modified by protective maneuvers was until now unknown. In this sense, our present results demonstrate that the enhanced levels of fumarate, malate, and citrate, detected in the plasma from the great cardiac vein in control animals during

initial reperfusion, are reduced by both individual treatments and by a combination of RIC with malonate. In addition, it was unknown whether citric acid cycle metabolite concentrations might have a prognostic value during myocardial ischemia-reperfusion. In the study by Kohlhauer et al. including STEMI and non-STEMI patients, a modest correlation between coronary sinus succinate concentrations and edema volume, but not irreversible myocardial injury (i.e., final myocardial infarct size at 6 months, as measured by cardiac magnetic resonance, or troponins, determined during the first 48 h), was found [23]. Edema volume was quantified, in the aforementioned study, by T2-weighted nuclear magnetic resonance imaging performed 2 days after pPCI, a supposed surrogate of area at risk and acute injury [23]. However, it has been suggested that T2-weighted edema might not constitute an accurate surrogate for the area at risk [47], especially when it is not determined in a time window ranging between 4 and 7 days post myocardial infarction [48] and when cardioprotective therapies are applied [49]. Our present results using a targeted LC-MS/MS approach demonstrate that not only succinate, but also fumarate and malate, are significantly enhanced during initial reperfusion in blood from the great cardiac vein, confirm a moderate correlation between succinate (and lactate) concentrations measured 5 min after reperfusion with the size of the area at risk, and suggest positive correlations between succinate, fumarate, and malate and myocardial infarct size. These data are suggestive that citric acid metabolite concentrations obtained in blood samples from the coronary sinus might constitute a new prognosis tool to predict final infarct size in STEMI patients.

The increase in citric acid cycle intermediates seen after reperfusion can be due to two different mechanisms that may work simultaneously. Membrane rupture would cause a massive release of intracellular metabolites, and in this sense, our present results may merely reflect differences in the amount of cell death. However, it may also reflect differences in the metabolic profile of cardiac cells and active release of metabolites. Accordingly, our present data demonstrate that groups receiving malonate had higher succinate plasma concentrations as compared with those receiving RIC alone. As these groups of animals have similar infarctions, these differences can only be ascribed to the effect of malonate on SDH activity [7,8]. Furthermore, these differences seem to extend to fumarate and malate.

4. Materials and Methods

This study complies with Directive 2010/63/EU of the European Parliament on the protection of animals used for scientific purposes and the NIH Guide for the Care and Use of Laboratory Animals (NIH publications N°. 85-23, revised 1996, updated in 2011). The study was approved by the Ethics Committee of our institution (reference number: CEEA 33/17).

4.1. Animals and Instrumentation

Forty hybrid farm *pigs* (25–30 kg, 12 h fasting) were premedicated with tiletamine-zolazepam (4–6 mg/kg, IM) and anesthetized with sodium thiopental (25 mg/kg, IV, plus continuous infusion at 6–14 mg/kg/h) and fentanyl (5 µg/kg, IV, plus continuous infusion at 3–6 µg/kg/h). Following ventilation, the thorax was opened, and the left anterior descending (LAD) coronary artery was dissected free below the first diagonal branch [12,14]. Electrocardiogram, left ventricular (LV) pressure, LV dP/dt and coronary blow flow were recorded in a computer as previously described [12,14]. At the end of the experiments, animals were sacrificed by a pentobarbital overdose (100 mg/kg, IV).

4.2. Regional Myocardial Function

Two pairs of hemispherical polystyrene crystals were inserted into the remote LV myocardium and in the area at risk to monitor regional myocardial function, as previously described [12,14,50]. Systolic segment shortening ratio (SS) was calculated as SS = (EDL − ESL)/EDL, where EDL is end-diastolic length and ESL corresponds to end-systolic length [12,14,50].

4.3. Study Protocols

All animals were intravenously administered with sodium heparin (100 UI/kg). Immediately, a Judkins 8F guiding catheter was inserted into a carotid artery, and a 2.8/2.5F intracoronary infusion catheter (TRANSIT, Cordis Neurovascular Inc., Miami, FL, USA) was advanced through it into the LAD, until crossing the dissection site selected for coronary occlusion [12]. To assess the effects of treatments on ischemia-reperfusion injury, *pigs* were then submitted to 40 min of LAD coronary artery occlusion, followed by 2 h of reperfusion. This time of ischemia (40 min) was selected based on previous publications from our group that demonstrated that this duration induced an infarct size of about 50% of the area at risk [12,14]. Myocardial ischemia was performed by occluding the LAD coronary artery around the infusion catheter using an elastic snare. Animals were randomly assigned to four different experimental groups (n = 10/group). Control *pigs* received intracoronary saline for 6 min, beginning at 39 min of ischemia and lasting for the first 5 min of reperfusion, at a flow rate of 15 mL/min (37 °C). Malonate-treated animals received intracoronary saline containing disodium malonate at a concentration of 10 mmol/L. Conditioned animals (RIC) were submitted, in addition to intracoronary saline infusion, to four cycles of 5 min of right lower limb ischemia followed by 5 min of reperfusion, starting simultaneously with LAD ligature, using an elastic snare placed around the right femoral artery. Finally, a fourth treatment group consisted in the combination of both treatments.

Blood samples were obtained in all cases at baseline and 1, 5, and 10 min after the onset of reperfusion, both from the great cardiac vein (or anterior interventricular vein), running parallel to the LAD coronary artery, and from the left femoral vein. An additional peripheral blood sample was obtained at the end of reperfusion (2 h). Blood was collected in heparinized tubes, centrifuged at 1500 g for 10 min (4 °C) to obtain plasma, and stored at −80 °C until analysis.

4.4. Area at Risk and Infarct Size

Two hours after reperfusion, the LAD was reoccluded and the size of the area at risk and of infarction were determined by 10% fluorescein and 1% 2,3,5-triphenyltetrazolium chloride (TTC) staining, respectively, as previously described [51]. Area at risk was expressed as percentage of total ventricular weight and infarct size as percentage of area at risk.

4.5. Reperfusion Arrhythmias

Recordings were analyzed for the incidence of ventricular tachycardia (VT) and ventricular fibrillation (VF) during ischemia and the first 20 min of reperfusion. VT was defined as three or more consecutive premature beats of ventricular origin at a heart rate faster than 120 beats/min, and wide QRS durations (>120 ms) [15].

4.6. Targeted LC-MS/MS Analysis of Citric Acid Cycle Metabolites in Porcine Plasma Samples

Separation and detection of the citric acid cycle metabolites succinate, fumarate, malate, and citrate, together with lactate and malonate, was performed on a Waters Acquity Ultra Performance Liquid Chromatographic coupled with a Waters Xevo TQ MS triple quadrupole mass spectrometer (Waters Corporation, Milford, MA, USA).

Standard calibration curves for each analyte were freshly prepared by adding 5 µL of 7 different concentrations of the distinct metabolites to 200 µL of plasma. An additional blank sample lacking analytes was also prepared. Linearity for the standard calibration curves was obtained between 3.125 and 500 µmol/L for succinate, 0.1 and 20 µmol/L for fumarate, 0.5 and 40 µmol/L for malate, 7.8125 and 125 µmol/L for citrate, 0.005 and 2500 µmol/L for malonate, and 500 and 8000 µmol/L for lactate. Metabolites were then extracted by adding 200 µL or 400 µL of methanol, containing 0.05 mmol/L succinic acid-2,2,3,3-d_4 (#293075, Merck KGaA, Darmstadt, Germany) as an internal standard, to 100 µL of each sample or 200 µL of each calibration standard, respectively. Samples were vortexed, cooled at −20 °C for 20 min, and centrifuged at 11,000 rpm for 30 min, at 4 °C. Supernatants

containing metabolites were transferred to new 1.5 mL propylene tubes, lyophilized, and stored at −20 °C until analysis. Before injection to LC-MS/MS, the purified residues were reconstituted with 100 µL (for samples) or 200 µL (for calibration standards) of a mobile phase solution consisting of mobile phase A (0.2% formic acid in acetonitrile) and mobile phase B (0.2% formic acid in water) at 10:90 *v*/*v*. Samples and calibration standards were vortexed for 5 min and centrifuged again at 11,000 rpm for 5 min, at 4 °C.

Separation was achieved following injection of 4 µL of each sample on an Acquity UPLC HSS C18 column (2.1 × 100 mm, 1.8 µm particle size, Waters Corporation, Milford, MA, USA). A gradient elution program was conducted for chromatographic separation with mobile phase A and mobile phase B as follows: 0–1.5 min hold for 10% eluent A, 1.5–5 min from 95% to 60% eluent A, 5–7 min hold for 60% eluent A, 7–7.5 min from 60% to 10% eluent A and 7.5–9 min hold for 10% eluent A to reequilibrate column before next injection. Pump was operated at a flow rate of 0.3 mL/min with an overall run time of 9 min. The autosampler was held at 6 °C and column oven was set up at 30 °C. The mass spectrometer was operated in multiple reaction monitoring (MRM) using an electrospray (ESI) source in negative mode for all compounds, with a capillary voltage of 2.02 kV. Argon was used as collision gas and flow was 0.17 mL/min. Desolvation temperature was 450 °C with a gas flow of 1100 L/h. Ion transitions and optimal cone voltage and collision energy use for fragments detection are summarized in Table 2. System control and data analysis were carried out using the MassLynx software (Version 4.1, Waters Corporation, Milford, MA, USA) and processed using TargetLynxTM program (Waters Corporation, Milford, MA, USA). For each calibration standard, the ratio between the intermediate peak and the internal standard containing succinic acid-2,2,3,3-d_4 was determined. Linear regressions describing the calibration curves were then calculated using a weighting factor of $1/x^2$, where x was concentration.

Table 2. Ion transitions and optimal cone voltage and collision energy used for fragments detection in LC-MS/MS analysis of citric acid cycle metabolites in porcine plasma samples. IS indicates internal standard.

Compound	Precursor Ion m/z	Product Ion	Cone Voltage	Collision Energy
Succinate	117.10	73.00	16	11
Succinic acid-2,2,3,3-d_4 (IS)	121.10	76.50	15	9
Fumarate	115.09	71.01	13	6
Malate	133.04	115.02	20	10
Citrate	191.13	111.00	18	10
Malonate	103.09	59.00	12	8
Lactate	89.11	43.00	18	10

4.7. Statistical Analysis

All measurements were carried out by a researcher blinded to group allocation. Normal distribution was assessed by Kolmogorov–Smirnov test. Data are expressed as mean±SD. ANOVA and Tukey post-hoc test were used to assess differences in infarct size and area at risk. Changes in the time course of hemodynamic and contractility variables and in metabolomic studies were assessed by repeated measures ANOVA and Tukey post-hoc tests. Student's t test was used to compare metabolite concentrations at a baseline between peripheral and great cardiac vein plasma samples. Non-parametric Kruskal–Wallis test was used to assess differences in the number of ventricular tachyarrhythmias. Incidence of VF was analyzed by the Pearson Chi-square test. Differences were considered significant when $p < 0.05$.

5. Conclusions

Our present results demonstrate that, despite the combination of SDH inhibition during reperfusion and RIC did not result in additive protection, plasma concentrations of

selected citric acid cycle metabolites are attenuated by protective maneuvers and correlate with irreversible injury. Analysis of these metabolites may, therefore, have a prognostic value in STEMI patients.

Author Contributions: Conceptualization, A.R.-S. and I.F.-G.; methodology, A.R.-S.; software, A.R.-S.; validation, M.C., I.B., N.N., B.B., M.R.-M., J.I. and A.R.-S.; formal analysis, M.C., N.N. and I.B.; investigation, A.R.-S., I.F.-G., B.B., M.R.-M. and J.I.; resources, A.R.-S., I.F.-G., B.B., M.R.-M. and J.I.; data curation, M.C. and N.N.; writing—original draft preparation, A.R.-S., M.C. and N.N.; writing—review and editing, M.C., N.N., I.B., B.B., M.R.-M., J.I., I.F.-G. and A.R.-S.; visualization, A.R.-S.; supervision, A.R.-S.; project administration, A.R.-S.; funding acquisition, A.R.-S. and I.F.-G. All authors have read and agreed to the published version of the manuscript.

Funding: This research was funded by the Spanish Ministry of Economy and Competitiveness, Instituto de Salud Carlos III (grants PI17/01397 and CIBERCV) and the Spanish Society of Cardiology (Proyectos de la FEC para Investigación Básica en Cardiología 2018, Sociedad Española de Cardiología), and was cofinanced by the European Regional Development Fund (ERDF-FEDER, a way to build Europe). Antonio Rodríguez-Sinovas has a consolidated Miguel Servet contract.

Institutional Review Board Statement: This study complies with Directive 2010/63/EU of the European Parliament on the protection of animals used for scientific purposes and the NIH Guide for the Care and Use of Laboratory Animals (NIH publications Nº. 85-23, revised 1996, updated in 2011). The study was approved by the Ethics Committee of Vall d'Hebron Institut de Recerca (reference number: CEEA 33/17).

Informed Consent Statement: Not applicable.

Data Availability Statement: The data presented in this study are available on request from the corresponding author.

Conflicts of Interest: The authors declare no conflict of interest.

References

1. Virani, S.S.; Alonso, A.; Benjamin, E.J.; Bittencourt, M.S.; Callaway, C.W.; Carson, A.P.; Chamberlain, A.M.; Chang, A.R.; Cheng, S.; Delling, F.N.; et al. Heart Disease and Stroke Statistics—2020 Update: A Report from the American Heart Association. *Circulation* **2020**, *141*, e139–e596. [CrossRef] [PubMed]
2. Jernberg, T.; Hasvold, P.; Henriksson, M.; Hjelm, H.; Thuresson, M.; Janzon, M. Cardiovascular risk in post-myocardial infarction patients: Nationwide real world data demonstrate the importance of a long-term perspective. *Eur. Heart J.* **2015**, *36*, 1163–1170. [CrossRef]
3. Garcia-Dorado, D.; Ruiz-Meana, M.; Piper, H.M. Lethal reperfusion injury in acute myocardial infarction: Facts and unresolved issues. *Cardiovasc. Res.* **2009**, *83*, 165–168. [CrossRef] [PubMed]
4. Hausenloy, D.J.; Yellon, D.M. Myocardial ischemia-reperfusion injury: A neglected therapeutic target. *J. Clin. Investig.* **2013**, *123*, 92–100. [CrossRef] [PubMed]
5. Dirksen, M.T.; Simoons, M.L.; Duncker, D.J.; Laarman, G.J. Reperfusion injury in humans: A review of clinical trials on reperfusion injury inhibitory strategies. *Cardiovasc. Res.* **2007**, *74*, 343–355. [CrossRef] [PubMed]
6. Ferdinandy, P.; Hausenloy, D.J.; Heusch, G.; Baxter, G.F.; Schulz, R. Interaction of Risk Factors, Comorbidities, and Comedications with Ischemia/Reperfusion Injury and Cardioprotection by Preconditioning, Postconditioning, and Remote Conditioning. *Pharmacol. Rev.* **2014**, *66*, 1142–1174. [CrossRef] [PubMed]
7. Chouchani, E.T.; Pell, V.R.; Gaude, E.; Aksentijević, D.; Sundier, S.Y.; Robb, E.L.; Logan, A.; Nadtochiy, S.M.; Ord, E.N.; Smith, A.C.; et al. Ischaemic accumulation of succinate controls reperfusion injury through mitochondrial ROS. *Nature* **2014**, *515*, 431–435. [CrossRef] [PubMed]
8. Valls-Lacalle, L.; Barba, I.; Miró-Casas, E.; Alburquerque-Béjar, J.J.; Ruiz-Meana, M.; Fuertes-Agudo, M.; Rodríguez-Sinovas, A.; García-Dorado, D. Succinate dehydrogenase inhibition with malonate during reperfusion reduces infarct size by preventing mitochondrial permeability transition. *Cardiovasc. Res.* **2015**, *109*, 374–384. [CrossRef]
9. Pell, V.R.; Chouchani, E.T.; Frezza, C.; Murphy, M.P.; Krieg, T. Succinate metabolism: A new therapeutic target for myocardial reperfusion injury. *Cardiovasc. Res.* **2016**, *111*, 134–141. [CrossRef]
10. Quinlan, C.L.; Orr, A.L.; Perevoshchikova, I.V.; Treberg, J.R.; Ackrell, B.A.; Brand, M.D. Mitochondrial Complex II Can Generate Reactive Oxygen Species at High Rates in Both the Forward and Reverse Reactions. *J. Biol. Chem.* **2012**, *287*, 27255–27264. [CrossRef]
11. Robb, E.L.; Hall, A.R.; Prime, T.A.; Eaton, S.; Szibor, M.; Viscomi, C.; James, A.M.; Murphy, M.P. Control of mitochondrial superoxide production by reverse electron transport at complex I. *J. Biol. Chem.* **2018**, *293*, 9869–9879. [CrossRef]

12. Valls-Lacalle, L.; Barba, I.; Miró-Casas, E.; Ruiz-Meana, M.; Rodríguez-Sinovas, A.; Garcia-Dorado, D. Selective Inhibition of Succinate Dehydrogenase in Reperfused Myocardium with Intracoronary Malonate Reduces Infarct Size. *Sci. Rep.* **2018**, *8*, 2442. [CrossRef]
13. Davidson, S.M.; Ferdinandy, P.; Andreadou, I.; Bøtker, H.E.; Heusch, G.; Ibáñez, B.; Ovize, M.; Schulz, R.; Yellon, D.M.; Hausenloy, D.J.; et al. Multitarget Strategies to Reduce Myocardial Ischemia/Reperfusion Injury. *J. Am. Coll. Cardiol.* **2019**, *73*, 89–99. [CrossRef]
14. Alburquerque-Béjar, J.J.; Barba, I.; Inserte, J.; Miró-Casas, E.; Ruiz-Meana, M.; Poncelas, M.; Vilardosa, Ú.; Valls-Lacalle, L.; Rodríguez-Sinovas, A.; Garcia-Dorado, D. Combination therapy with remote ischaemic conditioning and insulin or exenatide enhances infarct size limitation in *pigs*. *Cardiovasc. Res.* **2015**, *107*, 246–254. [CrossRef]
15. Alburquerque-Béjar, J.J.; Barba, I.; Ruiz-Meana, M.; Valls-Lacalle, L.; Rodríguez-Sinovas, A.; García-Dorado, D. Additive Effects of Exenatide, Glucose-insulin-potassium, and Remote Ischemic Conditioning Against Reperfusion Ventricular Arrhythmias in *Pigs*. *Rev. Esp. Cardiol.* **2016**, *69*, 620–622. [CrossRef]
16. Hausenloy, D.J.; Yellon, D.M. Ischaemic conditioning and reperfusion injury. *Nat. Rev. Cardiol.* **2016**, *13*, 193–209. [CrossRef]
17. Schmidt, M.R.; Redington, A.; Bøtker, H.E. Remote conditioning the heart overview: Translatability and mechanism. *Br. J. Pharmacol.* **2015**, *172*, 1947–1960. [CrossRef]
18. Heusch, G.; Bøtker, H.E.; Przyklenk, K.; Redington, A.; Yellon, D. Remote Ischemic Conditioning. *J. Am. Coll. Cardiol.* **2015**, *65*, 177–195. [CrossRef] [PubMed]
19. Przyklenk, K.; Bauer, B.; Ovize, M.; Kloner, R.A.; Whittaker, P. Regional ischemic 'preconditioning' protects remote virgin myocardium from subsequent sustained coronary occlusion. *Circulation* **1993**, *87*, 893–899. [CrossRef]
20. Schmidt, M.R.; Smerup, M.; Konstantinov, I.E.; Shimizu, M.; Li, J.; Cheung, M.; White, P.A.; Kristiansen, S.B.; Sorensen, K.; Dzavik, V.; et al. Intermittent peripheral tissue ischemia during coronary ischemia reduces myocardial infarction through a KATP-dependent mechanism: First demonstration of remote ischemic perconditioning. *Am. J. Physiol. Circ. Physiol.* **2007**, *292*, H1883–H1890. [CrossRef]
21. Bøtker, H.E.; Kharbanda, R.; Schmidt, M.R.; Bøttcher, M.; Kaltoft, A.K.; Terkelsen, C.J.; Munk, K.; Andersen, N.H.; Hansen, T.M.; Trautner, S.; et al. Remote ischaemic conditioning before hospital admission, as a complement to angioplasty, and effect on myocardial salvage in patients with acute myocardial infarction: A randomised trial. *Lancet* **2010**, *375*, 727–734. [CrossRef]
22. Crimi, G.; Pica, S.; Raineri, C.; Bramucci, E.; De Ferrari, G.M.; Klersy, C.; Ferlini, M.; Marinoni, B.; Repetto, A.; Romeo, M.; et al. Remote Ischemic Post-Conditioning of the Lower Limb During Primary Percutaneous Coronary Intervention Safely Reduces Enzymatic Infarct Size in Anterior Myocardial Infarction. *JACC Cardiovasc. Interv.* **2013**, *6*, 1055–1063. [CrossRef] [PubMed]
23. Kohlhauer, M.; Dawkins, S.; Costa, A.S.H.; Lee, R.; Young, T.; Pell, V.R.; Choudhury, R.P.; Banning, A.P.; Kharbanda, R.K.; Saeb-Parsy, K.; et al. Metabolomic Profiling in Acute ST-Segment–Elevation Myocardial Infarction Identifies Succinate as an Early Marker of Human Ischemia–Reperfusion Injury. *J. Am. Heart Assoc.* **2018**, *7*. [CrossRef] [PubMed]
24. Zhang, J.; Wang, Y.T.; Miller, J.H.; Day, M.M.; Munger, J.C.; Brookes, P.S. Accumulation of Succinate in Cardiac Ischemia Primarily Occurs via Canonical Krebs Cycle Activity. *Cell Rep.* **2018**, *23*, 2617–2628. [CrossRef]
25. Prag, H.A.; Gruszczyk, A.V.; Huang, M.M.; Beach, T.E.; Young, T.; Tronci, L.; Nikitopoulou, E.; Mulvey, J.F.; Ascione, R.; Hadjihambi, A.; et al. Mechanism of succinate efflux upon reperfusion of the ischaemic heart. *Cardiovasc. Res.* **2021**, *117*, 1188–1201. [CrossRef]
26. Prag, H.A.; Pala, L.; Kula-Alwar, D.; Mulvey, J.F.; Luping, D.; Beach, T.E.; Booty, L.M.; Hall, A.R.; Logan, A.; Sauchanka, V.; et al. Ester Prodrugs of Malonate with Enhanced Intracellular Delivery Protect Against Cardiac Ischemia-Reperfusion Injury In Vivo. *Cardiovasc. Drugs Ther.* **2020**, 1–13. [CrossRef]
27. Jespersen, N.R.; Hjortbak, M.V.; Lassen, T.R.; Støttrup, N.B.; Johnsen, J.; Tonnesen, P.T.; Larsen, S.; Kimose, H.-H.; Bøtker, H.E. Cardioprotective effect of succinate dehydrogenase inhibition in *rat* hearts and human myocardium with and without diabetes mellitus. *Sci. Rep.* **2020**, *10*, 10344. [CrossRef]
28. Chinopoulos, C. Succinate in ischemia: Where does it come from? *Int. J. Biochem. Cell Biol.* **2019**, *115*, 105580. [CrossRef]
29. Breivik, L.; Helgeland, E.; Aarnes, E.K.; Mrdalj, J.; Jonassen, A.K. Remote postconditioning by humoral factors in effluent from ischemic preconditioned *rat* hearts is mediated via PI3K/Akt-dependent cell-survival signaling at reperfusion. *Basic Res. Cardiol.* **2010**, *106*, 135–145. [CrossRef]
30. Turrell, H.E.; Thaitirarot, C.; Crumbie, H.; Rodrigo, G. Remote ischemic preconditioning of cardiomyocytes inhibits the mitochondrial permeability transition pore independently of reduced calcium-loading or sarcKATP channel activation. *Physiol. Rep.* **2014**, *2*. [CrossRef]
31. Hausenloy, D.J.; Kharbanda, R.K.; Møller, U.K.; Ramlall, M.; Aarøe, J.; Butler, R.; Bulluck, H.; Clayton, T.; Dana, A.; Dodd, M.; et al. Effect of remote ischaemic conditioning on clinical outcomes in patients with acute myocardial infarction (CONDI-2/ERIC-PPCI): A single-blind randomised controlled trial. *Lancet* **2019**, *394*, 1415–1424. [CrossRef]
32. Del Blanco, B.G.; Otaegui, I.; Rodríguez-Palomares, J.F.; Bayés-Genis, A.; Fernández-Nofrerías, E.; del Olmo, V.V.; Carrillo, X.; Ibáñez, B.; Worner, F.; Casanova, J.; et al. Effect of COMBinAtion therapy with remote ischemic conditioning and exenatide on the Myocardial Infarct size: A two-by-two factorial randomized trial (COMBAT-MI). *Basic Res. Cardiol.* **2021**, *116*, 1–12. [CrossRef]
33. Kleinbongard, P.; Bøtker, H.E.; Ovize, M.; Hausenloy, D.J.; Heusch, G. Co-morbidities and co-medications as confounders of cardioprotection—Does it matter in the clinical setting? *Br. J. Pharmacol.* **2020**, *177*, 5252–5269. [CrossRef]

34. Yang, X.M.; Liu, Y.; Cui, L.; Yang, X.; Liu, Y.; Tandon, N.; Kambayashi, J.; Downey, J.M.; Cohen, M.V. Platelet P2Y(1)(2) blockers confer direct postconditioning-like protection in reperfused rabbit hearts. *J. Cardiovasc. Pharmacol. Ther.* **2013**, *18*, 251–262. [CrossRef]
35. Hausenloy, D.J.; Chilian, W.; Crea, F.; Davidson, S.M.; Ferdinandy, P.; Garcia-Dorado, D.; Van Royen, N.; Schulz, R.; Heusch, G. The coronary circulation in acute myocardial ischaemia/reperfusion injury: A target for cardioprotection. *Cardiovasc. Res.* **2019**, *115*, 1143–1155. [CrossRef]
36. Yang, X.-M.; Cui, L.; Alhammouri, A.; Downey, J.M.; Cohen, M.V. Triple therapy greatly increases myocardial salvage during ischemia/reperfusion in the in situ *rat* heart. *Cardiovasc. Drugs Ther.* **2013**, *27*, 403–412. [CrossRef]
37. Xin, P.; Zhu, W.; Li, J.; Ma, S.; Wang, L.; Liu, M.; Li, J.; Wei, M.; Redington, A.N. Combined local ischemic postconditioning and remote perconditioning recapitulate cardioprotective effects of local ischemic preconditioning. *Am. J. Physiol. Circ. Physiol.* **2010**, *298*, H1819–H1831. [CrossRef]
38. Eitel, I.; Stiermaier, T.; Rommel, K.P.; Fuernau, G.; Sandri, M.; Mangner, N.; Linke, A.; Erbs, S.; Lurz, P.; Boudriot, E.; et al. Cardioprotection by combined intrahospital remote ischaemic perconditioning and postconditioning in ST-elevation myocardial infarction: The randomized LIPSIA CONDITIONING trial. *Eur. Heart J.* **2015**, *36*, 3049–3057. [CrossRef]
39. Kohlhauer, M.; Pell, V.R.; Burger, N.; Spiroski, A.-M.; Gruszczyk, A.; Mulvey, J.F.; Mottahedin, A.; Costa, A.S.H.; Frezza, C.; Ghaleb, B.; et al. Protection against cardiac ischemia-reperfusion injury by hypothermia and by inhibition of succinate accumulation and oxidation is additive. *Basic Res. Cardiol.* **2019**, *114*, 1–9. [CrossRef]
40. Hauerslev, M.; Mørk, S.R.; Pryds, K.; Contractor, H.; Hansen, J.; Jespersen, N.R.; Johnsen, J.; Heusch, G.; Kleinbongard, P.; Kharbanda, R.; et al. Influence of long-term treatment with glyceryl trinitrate on remote ischemic conditioning. *Am. J. Physiol. Circ. Physiol.* **2018**, *315*, H150–H158. [CrossRef]
41. Støttrup, N.B.; Løfgren, B.; Birkler, R.D.; Nielsen, J.M.; Wang, L.; Caldarone, C.A.; Kristiansen, S.B.; Contractor, H.; Johannsen, M.; Bøtker, H.E.; et al. Inhibition of the malate–aspartate shuttle by pre-ischaemic aminooxyacetate loading of the heart induces cardioprotection. *Cardiovasc. Res.* **2010**, *88*, 257–266. [CrossRef]
42. Skyschally, A.; Amanakis, G.; Neuhäuser, M.; Kleinbongard, P.; Heusch, G. Impact of electrical defibrillation on infarct size and no-reflow in *pigs* subjected to myocardial ischemia-reperfusion without and with ischemic conditioning. *Am. J. Physiol. Circ. Physiol.* **2017**, *313*, H871–H878. [CrossRef]
43. Andrienko, T.N.; Pasdois, P.; Pereira, G.C.; Ovens, M.J.; Halestrap, A.P. The role of succinate and ROS in reperfusion injury—A critical appraisal. *J. Mol. Cell. Cardiol.* **2017**, *110*, 1–14. [CrossRef]
44. Hyldebrandt, J.A.; Støttrup, N.B.; Frederiksen, C.A.; Heiberg, J.; Birkler, R.I.D.; Johannsen, M.; Schmidt, M.R.; Ravn, H.B. Citric Acid Cycle Metabolites Predict the Severity of Myocardial Stunning and Mortality in Newborn *Pigs*. *Pediatr. Crit. Care Med.* **2016**, *17*, e567–e574. [CrossRef]
45. Surendran, A.; Aliani, M.; Ravandi, A. Metabolomic characterization of myocardial ischemia-reperfusion injury in ST-segment elevation myocardial infarction patients undergoing percutaneous coronary intervention. *Sci. Rep.* **2019**, *9*, 1–13. [CrossRef]
46. Gundogdu, G.; Senol, O.; Miloglu, F.D.; Koza, Y.; Gundogdu, F.; Hacımüftüoğlu, A.; El-Aty, A.A. Serum metabolite profiling of ST-segment elevation myocardial infarction using liquid chromatography quadrupole time-of-flight mass spectrometry. *Biomed. Chromatogr.* **2019**, *34*, e4738. [CrossRef]
47. Croisille, P.; Kim, H.W.; Kim, R.J. Controversies in Cardiovascular MR Imaging: T2-weighted Imaging Should Not Be Used to Delineate the Area at Risk in Ischemic Myocardial Injury. *Radiology* **2012**, *265*, 12–22. [CrossRef] [PubMed]
48. Fernández-Jiménez, R.; Barreiro-Pérez, M.; Martin-García, A.; Sánchez-González, J.; Agüero, J.; Galán-Arriola, C.; García-Prieto, J.; Díaz-Pelaez, E.; Vara, P.; Martinez, I.; et al. Dynamic Edematous Response of the Human Heart to Myocardial Infarction. *Circulation* **2017**, *136*, 1288–1300. [CrossRef] [PubMed]
49. Fernández-Jiménez, R.; Galán-Arriola, C.; Sánchez-González, J.; Agüero, J.; López-Martín, G.J.; Gomez-Talavera, S.; Garcia-Prieto, J.; Benn, A.; Molina-Iracheta, A.; Barreiro-Pérez, M.; et al. Effect of Ischemia Duration and Protective Interventions on the Temporal Dynamics of Tissue Composition After Myocardial Infarction. *Circ. Res.* **2017**, *121*, 439–450. [CrossRef] [PubMed]
50. Garcia-Dorado, D.; Théroux, P.; Duran, J.M.; Solares, J.; Alonso, J.; Sanz, E.; Munoz, R.; Elizaga, J.; Botas, J.; Fernandez-Avilés, F. Selective inhibition of the contractile apparatus. A new approach to modification of infarct size, infarct composition, and infarct geometry during coronary artery occlusion and reperfusion. *Circulation* **1992**, *85*, 1160–1174. [CrossRef] [PubMed]
51. Garcia-Dorado, D.; Inserte, J.; Ruiz-Meana, M.; González, M.A.; Solares, J.; Juliá, M.; Barrabés, J.A.; Soler-Soler, J. Gap Junction Uncoupler Heptanol Prevents Cell-to-Cell Progression of Hypercontracture and Limits Necrosis During Myocardial Reperfusion. *Circulation* **1997**, *96*, 3579–3586. [CrossRef]

10.2 PUBLICATION 2

Spontaneous reperfusion enhances succinate concentration in peripheral blood from stemi patients but its levels does not correlate with myocardial infarct size or area at risk.

Consegal M, Barba I, García Del Blanco B, Otaegui I, Rodríguez-Palomares JF, Martí G, Serra B, Bellera N, Ojeda-Ramos M, Valente F, Carmona MÁ, Miró-Casas E, Sambola A, Lidón RM, Bañeras J, Barrabés JA, Rodríguez C, Benito B, Ruiz-Meana M, Inserte J, Ferreira-González I, Rodríguez-Sinovas A..

Sci Rep. 2023 Apr 27;13(1):6907. doi: 10.1038/s41598-023-34196-7. PMID: 37106099; PMCID: PMC10140265.

Impact factor (2023): 4.6

scientific reports

Check for updates

OPEN

Spontaneous reperfusion enhances succinate concentration in peripheral blood from stemi patients but its levels does not correlate with myocardial infarct size or area at risk

Marta Consegal[1,2,3], Ignasi Barba[1,2,3,4], Bruno García del Blanco[1,3], Imanol Otaegui[1,3], José F. Rodríguez-Palomares[1,3], Gerard Martí[1,3], Bernat Serra[1,3], Neus Bellera[1,3], Manuel Ojeda-Ramos[1,3], Filipa Valente[1,3], Maria Ángeles Carmona[1,3], Elisabet Miró-Casas[1,3], Antonia Sambola[1,3], Rosa María Lidón[1,3], Jordi Bañeras[1,3], José Antonio Barrabés[1,3], Cristina Rodríguez[3,5], Begoña Benito[1,2,3], Marisol Ruiz-Meana[1,2,3], Javier Inserte[1,2,3], Ignacio Ferreira-González[1,2,6]✉ & Antonio Rodríguez-Sinovas[1,2,3]✉

Succinate is enhanced during initial reperfusion in blood from the coronary sinus in ST-segment elevation myocardial infarction (STEMI) patients and in pigs submitted to transient coronary occlusion. Succinate levels might have a prognostic value, as they may correlate with edema volume or myocardial infarct size. However, blood from the coronary sinus is not routinely obtained in the CathLab. As succinate might be also increased in peripheral blood, we aimed to investigate whether peripheral plasma concentrations of succinate and other metabolites obtained during coronary revascularization correlate with edema volume or infarct size in STEMI patients. Plasma samples were obtained from peripheral blood within the first 10 min of revascularization in 102 STEMI patients included in the COMBAT-MI trial (initial TIMI 1) and from 9 additional patients with restituted coronary blood flow (TIMI 2). Metabolite concentrations were analyzed by ^{1}H-NMR. Succinate concentration averaged 0.069 ± 0.0073 mmol/L in patients with TIMI flow ≤ 1 and was significantly increased in those with TIMI 2 at admission (0.141 ± 0.058 mmol/L, $p < 0.05$). However, regression analysis did not detect any significant correlation between most metabolite concentrations and infarct size, extent of edema or other cardiac magnetic resonance (CMR) variables. In conclusion, spontaneous reperfusion in TIMI 2 patients associates with enhanced succinate levels in peripheral blood, suggesting that succinate release increases overtime following reperfusion. However, early plasma levels of succinate and other metabolites obtained from peripheral blood does not correlate with the degree of irreversible injury or area at risk in STEMI patients, and cannot be considered as predictors of CMR variables.

Trial registration: Registered at www.clinicaltrials.gov (NCT02404376) on 31/03/2015. EudraCT number: 2015-001000-58.

[1]Cardiovascular Diseases Research Group, Department of Cardiology, Vall d'Hebron Institut de Recerca (VHIR), Vall d'Hebron Hospital Universitari, Vall d'Hebron Barcelona Hospital Campus, Passeig Vall d'Hebron 119-129, 08035 Barcelona, Spain. [2]Departament de Medicina, Universitat Autònoma de Barcelona, 08193 Bellaterra, Spain. [3]Centro de Investigación Biomédica en Red (CIBER) de Enfermedades Cardiovasculares (CIBERCV), Instituto de Salud Carlos III, Madrid, Spain. [4]Faculty of Medicine, University of Vic - Central University of Catalonia (UVicUCC), Can Baumann. Ctra. de Roda, 70, 08500 Vic, Spain. [5]Institut de Recerca Hospital de la Santa Creu i Sant Pau (IRHSCSP), Barcelona, Spain. [6]Centro de Investigación Biomédica en Red (CIBER) de Epidemiología y Salud Pública, CIBERESP, Instituto de Salud Carlos III, Madrid, Spain. ✉email: iferregon@gmail.com; antonio.rodriguez.sinovas@vhir.org

Abbreviations

BMI	Body mass index
BSA	Body surface area
CMR	Cardiac magnetic resonance
LCX	Left circumflex coronary artery
LDA	Left descending coronary artery
LV	Left ventricular
LVEF	Left ventricular ejection fraction
MCT1	Monocarboxylate transporter 1
MVO	Relative microvascular obstruction
OAD	Oral antidiabetic drugs
PPCI	Primary percutaneous coronary intervention
RCA	Right coronary artery
STEMI	ST-segment elevation myocardial infarction

Previous studies demonstrated that succinate, the endogenous substrate used by the mitochondrial enzyme succinate dehydrogenase (or mitochondrial complex II), accumulates in ischemic tissues, including the myocardium[1–4], and is massively released into the bloodstream after flow restoration[5–8]. Moreover, it was shown that succinate can be detected in plasma from STEMI patients immediately after stent implantation, both in blood obtained from a peripheral vein or from the coronary sinus, and that its plasma concentrations at the coronary sinus correlate with edema volume[5]. Interestingly, we have recently demonstrated that plasma levels of succinate and other citric acid intermediates are enhanced in the blood obtained from the great cardiac vein 5 min after reperfusion in a pig model of transient coronary occlusion, and that their concentration is reduced by protective maneuvers and correlates with final infarct size[8].

However, obtaining blood from the coronary sinus is not included in the routine practice, is not always feasible and is not without risk. As most STEMI patients have a peripheral via, and as succinate concentration is also enhanced in blood from this origin[5], we aimed to assess whether the concentration of succinate and other metabolites in peripheral plasma, obtained during the coronary procedure, correlates with myocardial edema or infarct size, as determined by CMR, in patients undergoing emergency primary percutaneous coronary intervention (PPCI) in our center (Vall d'Hebron Hospital Universitari, Barcelona, Spain) and included in the randomized COMBAT-MI clinical trial[9].

Methods

The present sub-study analyzes the plasma concentration of succinate and other metabolites in a subgroup of STEMI patients submitted to PPCI (n = 111) and included in the COMBAT-MI clinical trial (registered at www.clinicaltrials.gov (NCT02404376) on 31/03/2015; EudraCT number 2015-001000-58)[9]. The COMBAT-MI trial was a prospective, randomized, multicentric, double blinded, clinical trial comparing the effects of sham procedure, intravenous exenatide, remote ischemic conditioning (RIC), and their combination on infarct size measured by late gadolinium enhancement in CMR in patients with STEMI undergoing PPCI (allocation ratio 1:1:1:1 via a web-based clinical support system accessible 24 h a day (W3NEXUS, Barcelona, Spain); further details in[9]), and main results were published in[9]. The study was conducted in accordance with the Declaration of Helsinki and the European Guidelines for Good Clinical Practice, and was approved by the Agencia Española de Medicamentos y Productos Sanitarios (AEMPS) and the Ethics Committee of participant institutions.

Patients with diagnosis of STEMI, older than 18 years, presenting within 6 h of symptom onset were included in the original study[9]. STEMI was characterized by ischemic symptoms, including chest pain, and ≥ 1 mm ST elevation in 2 leads in the same territory or ≥ 2 mm ST elevation in ≥ 2 V1 through V4 leads or left bundle branch block with ≥ 1 mm concordant ST elevation. Exclusion criteria included TIMI flow grade at admission equal to 2 or 3. Additional exclusion criteria can be found in[9]. Patients eligible were recruited in our center between March 2016 and June 2019 and enrolled in the emergency room or upon entering the catheterization laboratory. Primary and secondary study endpoints can be found in[9].

Although in the original study only patients with TIMI flow ≤ 1 were included, plasma samples were available for 102 patients who met the inclusion criteria and for 9 with TIMI flow equal to 2. PPCI followed guideline recommendations and was performed by experienced operators without any delay. Blood samples were obtained at the time of PPCI from the 111 STEMI patients randomized in our center (in 102 within the first 10 min after revascularization and in 9 with initial TIMI flow ≥ 2 during coronariography) and placed in EDTA tubes. Plasma was obtained after centrifugation at 1500 g for 10 min. The supernatant was then centrifuged again at 2500 g (15 min) and maintained at − 80 °C until use. CMR data were obtained 3–7 days after PPCI[9].

Analysis of plasma samples by nuclear magnetic resonance spectroscopy. Plasma metabolites were extracted using the methanol method and ^{1}H-NMR spectra were acquired on a vertical bore 9.4 T magnet interfaced to a Bruker Avance 400 spectrometer, as previously described[10].

Statistics. Sample size calculation in the original COMBAT-MI clinical trial can be found in[9]. Data in this substudy are expressed as mean ± SEM. Differences in baseline characteristics and outcomes between patients with initial TIMI flow ≤ 1 and those with TIMI flow 2 were analyzed by Student's t test. Linear regression analysis was used to assess the existence of correlations between metabolite concentrations and CMR variables. Predictors for myocardial infarct size, myocardial salvage index, transmurality index, left ventricular ejection fraction

and microvascular obstruction volume, measured by CMR imaging, were determined by stepwise regression analysis. Differences were considered significant when $p < 0.05$.

Ethics approval and consent to particate. The study was conducted in accordance with the Declaration of Helsinki and the European Guidelines for Good Clinical Practice, and was approved by the Agencia Española de Medicamentos y Productos Sanitarios (AEMPS) and the Ethics Committee of participant institutions. All patients provided written informed consent before randomization.

Results

The numbers of participants who were randomly assigned, received intended treatment, and were analyzed for the primary outcome, together with losses and exclusions after randomization, can be found in[9]. Exploratory clinical adverse events during hospitalization can also be found in[9].

For the present substudy, baseline clinical and procedural characteristics and CMR outcomes of the 102 patients originally included in the COMBAT-MI clinical trial (TIMI flow ≤ 1) were similar to those of patients with TIMI flow ≥ 2 (Table 1). The mean age of the pooled population was 61.41 ± 1.07 years, and 96 (85.5%) of the patients were male.

Metabolomic profile of plasma samples from STEMI patients by nuclear magnetic resonance spectroscopy. ^{1}H-NMR spectra of plasma extracts allowed identification of succinate and other metabolites including lactate, 3-hydroxybutirate, acetate, glucose, alanine, creatine, creatinine, threonine, and tyrosine. Succinate concentration averaged 0.069 ± 0.0073 mmol/L in patients with TIMI flow ≤ 1 (Fig. 1), in the range of previous studies[11], and was significantly enhanced in the 9 additional patients with TIMI flow ≥ 2 (0.141 ± 0.058 mmol/L, $p < 0.05$, Fig. 1, Table 2). Similar trends were observed for other metabolites, especially creatine (Fig. 1).

Correlations between metabolite concentrations in peripheral plasma and CMR variables. Regression analysis did not show any significant correlation between the concentrations of the different metabolites analyzed, including succinate, and infarct size (determined as percentage of left ventricular mass or as absolute weight), myocardial salvage index, transmurality index, extent of edema, left ventricular ejection fraction (LVEF) or microvascular obstruction volume. Furthermore, with the exception of creatine for myocardial salvage index ($p = 0.008$) and transmurality index ($p = 0.039$), stepwise regression analysis did not identify any metabolite as predictor of any of the analyzed variables.

Discussion

This study shows that the presence of restituted blood flow at the culprit vessel before PPCI in STEMI patients, most likely due to spontaneous reperfusion, resulted in enhanced levels of succinate in peripheral blood as compared with patients with TIMI flow ≤ 1. These data suggests that the concentration of this metabolite achieved in the peripheral blood of STEMI patients undergoing successful reperfusion increases over time, and that a delay before blood sampling might be needed to attain higher levels of this metabolite. Unfortunately, however, plasma concentrations of succinate and other metabolites obtained early after PPCI from peripheral blood does not correlate with the degree of irreversible injury (i.e., infarct size) or the size of the area at risk in these patients, and cannot be considered a predictor of CMR variables.

Previous studies have shown that succinate accumulates in ischemic tissues, including the myocardium[1–4]. At the onset of reperfusion succinate is rapidly oxidized to fumarate by forward succinate dehydrogenase activity. Succinate oxidation, in turn, induces a massive reverse electron transfer from mitochondrial complex II to complex I, leading to ROS production, mitochondrial permeability transition pore opening and cell death[1,2]. In fact, prevention of succinate accumulation during ischemia or of its oxidation during reperfusion has been demonstrated to reduce myocardial infarct size in several animal models, including isolated mice hearts and in pigs submitted to transient coronary occlusion[1,2,12–14].

Importantly, part of the succinate that accumulated during myocardial ischemia is released into the bloodstream following reperfusion[5–8], in a process that is dependent on monocarboxylate transporter 1 (MCT1) activity[7]. Indeed, it has been quantified that more than half of total succinate accumulated in the ischemic myocardium is released into the circulation during initial reperfusion, while about one-third is oxidized[6]. In agreement with this, succinate and other citric acid cycle metabolites can be detected in the interstitium during initial reperfusion in isolated rat hearts[15], and in the blood of pigs subjected to transient coronary occlusion[8]. Furthermore, several citric acid cycle intermediates, including succinate, were shown to be increased in plasma from 27 STEMI patients, 2 to 48 h after PPCI[16]. In this regard, our present study, using ^{1}H-NMR spectroscopy analysis, shows that STEMI patients with TIMI flow ≥ 2 at the time of PPCI (and therefore having experienced spontaneous reperfusion), had increased levels of succinate as compared with patients with TIMI ≤ 1, which may indicate that peripheral succinate concentration increases over time after reperfusion. These data suggests that some delay after reperfusion, before blood sampling, might be required to attain higher plasma metabolite concentrations in peripheral blood. However, the potential correlation between succinate concentration in peripheral plasma at longer time intervals after PPCI and the size of myocardial infarction or area at risk deserves further investigation. On the other hand, and in contrast with previous studies, other authors found a decrease in succinate and other citric acid cycle intermediates 1 h after symptom onset in the same type of patients[17]. Reasons for these discrepancies are unclear.

Kohlhauer and coworkers found increased concentration of succinate in the blood of STEMI patients obtained from a peripheral vein or the coronary sinus immediately after stent implantation[5]. A similar increase in succinate

		TIMI ≤ 1 (n = 102)	TIMI = 2 (n = 9)	*p* value
Male, n° (%)		87 (85.29%)	9 (100%)	NS
Age (years)		61.80 ± 1.15	56.89 ± 2.09	NS
Body weight (kg)		78.81 ± 1.22	83.89 ± 4.08	NS
Height (cm)		168.98 ± 0.78	174.33 ± 2.62	NS
BMI (kg/m^2)		27.54 ± 0.35	27.77 ± 1.71	NS
Body surface area (BSA) (m^2)		1.92 ± 0.02	2.01 ± 0.05	NS
Comorbidities:				
Smoking, n° (%)	Active	44 (43.14)	6 (66.67)	NS
	Ex-smoker	34 (33.33)	1 (11.11)	
Hypertension, n° (%)		44 (43.14)	5 (55.55)	NS
Dyslipidemia, n° (%)		59 (55.84)	6 (66.67)	NS
Diabetes, n° (%)	With diet	5 (4.90)	0 (0.00)	NS
	Insulin	4 (3.92)	0 (0.00)	
	OAD	17 (16.67)	2 (22.22)	
	Insulin + OAD	1 (0.98)	0 (0.00)	
Killip class	1	83 (81.37)	8 (88.89)	NS
	2	11 (10.78)	1 (11.10)	
	3	1 (9.80)	0 (0.00)	
	4	4 (3.92)	0 (0.00)	
Procedural details				
Infarct-related artery	RCA	48 (47.06)	4 (44.44)	NS
	LDA	44 (43.14)	4 (44.44)	
	LCX	10 (9.80)	1 (11.11)	
Symptom-to-door (min)		151.29 ± 7.09	134.44 ± 13.92	NS
Symptom-to-ballon (min)		168.25 ± 7.01	153.33 ± 14.29	NS
Sum of ST-seg. elevation		3.93 ± 0.33	4.71 ± 0.92	NS
Systolic pres. (mmHg)		131.91 ± 2.58	136.22 ± 5.09	NS
Diastolic pres. (mmHg)		78.28 ± 1.60	89.00 ± 4.92	NS
Heart rate (beats/min)		72.13 ± 1.53	83.67 ± 4.21	NS
TIMI flow (post-proced.)	TIMI = 1, n°(%)	1 (0.98)	0 (0.00)	NS
	TIMI = 3, n°(%)	7 (6.86)	2 (22.22)	
	TIMI = 4, n°(%)	93 (91.18)	7 (77.78)	
CMR outcomes				
Infarct size (% of LV mass)		23.60 ± 1.14	22.99 ± 3.48	NS
Infarct size (g)		29.88 ± 1.62	30.09 ± 4.95	NS
Myocardial salvage index (%)		9.09 ± .073	7.46 ± 1.46	NS
Transmurality index		47.70 ± 1.21	44.93 ± 3.47	NS
Heart rate (beats/min)		65.83 ± 1.17	72.11 ± 7.49	NS
LVEF (%)		45.00 ± 0.99	42.89 ± 3.90	NS
Extent of edema (g)		38.56 ± 1.85	37.56 ± 4.86	NS
MVO (%)		0.82 ± 0.16	0.81 ± 0.60	NS
Cardiac mass (g)		124.79 ± 2.79	129.48 ± 6.11	NS
Cardiac mass/BSA		64.59 ± 1.28	64.56 ± 2.93	NS

Table 1. Baseline clinical and procedural characteristics, comorbidities and CMR outcomes of patients with initial TIMI flow ≤ 1 versus those with TIMI flow at admission equal to 2. BMI, body mass index; BSA, body surface area; LCX, left circumflex coronary artery; LDA, left descending coronary artery; LV, left ventricular; LVEF, left ventricular ejection fraction; MVO, relative microvascular obstruction; OAD, oral antidiabetic drugs; pres., pressure; post-proced., post-procedure; RCA, right coronary artery; seg., segment.

levels during initial reperfusion was described by our group in the blood of the great cardiac vein in a pig model of transient coronary occlusion[8]. However, whereas in the first study succinate plasma concentration at the coronary sinus correlated with edema volume, a surrogate of acute ischemic injury, but not with irreversible myocardial injury (i.e., myocardial infarct size at 6 months measured by CMR or troponins quantified during the first 48 h)[5], in our previous study succinate concentration at the great cardiac vein correlated with infarct size and was reduced by protective maneuvers[8]. In contrast with these previous observations, our present analysis shows that succinate concentration in peripheral blood, obtained early after PPCI, does not correlate with the

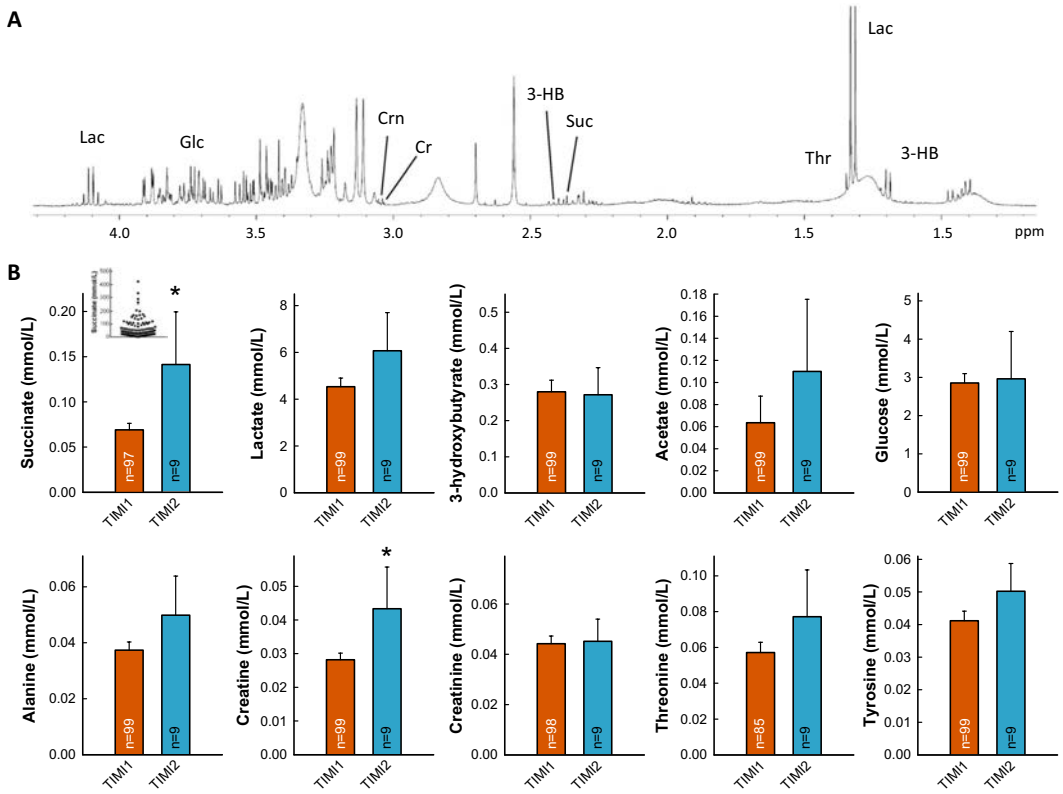

Figure 1. (**A**) Representative ^{1}H-NMR spectra obtained from plasma extracts in a STEMI patient included in the COMBAT-MI clinical trial. Abbreviations: 3-HB: 3-hydroxybutyrate; Cr: Creatine; Crn: Creatinine; Glc: Glucose; Lac: Lactate; Suc: Succinate; Thr: Threonine. (**B**) Concentrations of selected metabolites (mmol/L) analyzed by ^{1}H NMR spectroscopy in plasma extracts obtained from peripheral blood samples in STEMI patients with initial TIMI flow 1 as compared with data from those with initial TIMI flow 2. * ($p < 0.05$) indicates significant differences vs. TIMI 1 group. Inset shows variability in succinate concentrations in control TIMI 1 patients (data in µmol/L).

	TIMI 1	TIMI 2
Succinate	0.069 ± 0.007	0.141 ± 0.058 *
Lactate	4.537 ± 0.369	6.071 ± 1.631
3-hydroxybutyrate	0.280 ± 0.032	0.272 ± 0.075
Acetate	0.064 ± 0.024	0.110 ± 0.065
Glucose	2.855 ± 0.242	2.962 ± 1.240
Alanine	0.037 ± 0.003	0.050 ± 0.014
Creatine	0.028 ± 0.002	0.043 ± 0.012 *
Creatinine	0.044 ± 0.003	0.045 ± 0.089
Threonine	0.057 ± 0.006	0.077 ± 0.026
Tyrosine	0.041 ± 0.003	0.050 ± 0.009

Table 2. Concentrations of selected metabolites (mmol/L) analyzed by ^{1}H NMR spectroscopy in plasma extracts obtained from peripheral blood samples in STEMI patients with initial TIMI flow 1 as compared with data from those with initial TIMI flow 2. * ($p < 0.05$) indicates significant differences versus TIMI 1 group.

degree of irreversible injury (i.e., infarct size) or the size of the area at risk in STEMI patients undergoing PPCI, limiting the applicability of this metabolite as a prognostic biomarker in STEMI patients.

A possible explanation for the lack of correlation in our present study is that we measured metabolite concentrations in blood from a peripheral origin, as we tried to mimic the clinical situation in which a peripheral via is available in most, if not all, STEMI patients. In contrast, previous studies measured succinate concentrations at the coronary sinus[5,8], where they may represent a better picture of what is happening into the area at risk. Indeed, succinate was found to be the only metabolite significantly increased in coronary sinus blood compared with peripheral venous blood in STEMI patients[5]. Whether its concentration at this location correlates with the area at risk (acute ischemic injury)[5] or final infarct size[8] deserves further investigation.

Lack of correlations in our present study might be also explained by methodological differences, as compared with previous ones. Whereas here CMR data were obtained 3–7 days after PPCI[9], in the study by Kohlhauer and coworkers edema volume was quantified by T2-weighted CMR 2 days after PPCI[5]. However, T2-weighted edema may not constitute an accurate surrogate for the area at risk[18], particularly when it is determined outside a time window ranging between 4 and 7 days post myocardial infarction[19]. Similarly, in our previous study in pigs, infarct size was measured by triphenyltetrazolium staining soon after coronary occlusion[8], an experimental methodology very different to that used in the clinical context.

Succinate concentrations in plasma seem to have a great variability between studies. In the work by Sadagopan, serum succinate concentrations, as measured by liquid chromatography tandem mass spectroscopy (HPLC) in samples from hypertensive or diabetic patients, ranged between 1 and 8 µmol/L[20], values similar to those found by Kohlhauer in patients with angina or acute myocardial infarction[5]. However, others have found, using the same technique, values around 1–3 mmol/L in patients with acute myocardial infarction or coronary artery disease, and undetectable levels in healthy controls[21]. No clear explanation is currently available for these discrepancies, apart from methodological errors. But even within the same work, huge variations have been described. D'Alessandro et al., also using HPLC, found mean values or 10.1 ± 22.7 µmol/L in a control population with traumatic injuries that was increased to 96.1 ± 144.2 µmol/L in deceased patients, but values ranged from below 5 to more than 200 µmol/L (40x)[22]. Similarly, patients with aortic diseases had a median of 35.15 µmol/L, significantly higher than healthy controls (15.30 µmol/L), but again values ranged from about 10 to near 200 µmol/L (20x)[23], whereas Osuna-Prieto and coworkers showed that succinate plasma levels ranged from 11 to 130 µmol/L in young adults (11x)[11]. In our study we measured succinate concentrations by ^{1}H-NMR spectroscopy in plasma, and our values were in the range of some of those previous studies (about 69 ± 7 µmol/L in TIMI 1 and 141 ± 58 in TIMI 2 patients), and near to those we found in plasma from a pig model of transient coronary occlusion (from 9.1 ± 0.9 to 27.8 ± 3.9 µmol/L) in blood from the great cardiac vein[8], but also shows a high variability (from 40 to 423 µmol/L, 10x). Reasons for this high variability are unknown but may be due, in part, to the different conditions within each individual patient, to the analytical technique (NMR vs. HPLC), to the extraction method, or to the use of plasma vs. serum.

Conclusions

In conclusion, the present data suggest that spontaneous reperfusion enhances succinate levels in peripheral blood from STEMI patients, but do not support the utility of succinate and other citric acid intermediates assessed early during PPCI in plasma from that origin as prognostic biomarkers in these patients.

Data availability

The datasets used and/or analysed during the current study are available from the corresponding authors on reasonable request.

Received: 5 August 2022; Accepted: 25 April 2023
Published online: 27 April 2023

References

1. Valls-Lacalle, L. *et al.* Succinate dehydrogenase inhibition with malonate during reperfusion reduces infarct size by preventing mitochondrial permeability transition. *Cardiovasc. Res.* **109**(3), 374–384 (2016).
2. Chouchani, E. T. *et al.* Ischaemic accumulation of succinate controls reperfusion injury through mitochondrial ROS. *Nature* **515**(7527), 431–435 (2014).
3. Goldberg, N. D., Passonneau, J. V. & Lowry, O. H. Effects of changes in brain metabolism on the levels of citric acid cycle intermediates. *J. Biol. Chem.* **241**(17), 3997–4003 (1966).
4. Krebs, H. A. Rate control of the tricarboxylic acid cycle. *Adv. Enzyme Regul.* **8**, 335–353 (1970).
5. Kohlhauer, M. *et al.* Metabolomic profiling in acute ST-segment–elevation myocardial infarction identifies succinate as an early marker of human ischemia–reperfusion injury. *J. Am. Heart Assoc.* https://doi.org/10.1161/JAHA.117.007546 (2018).
6. Zhang, J. *et al.* Accumulation of succinate in cardiac ischemia primarily occurs via canonical krebs cycle activity. *Cell Rep.* **23**(9), 2617–2628 (2018).
7. Prag, H. A. *et al.* Mechanism of succinate efflux upon reperfusion of the ischaemic heart. *Cardiovasc. Res.* **117**(4), 1188–1201. https://doi.org/10.1093/cvr/cvaa148 (2020).
8. Consegal, M. *et al.* Citric acid cycle metabolites predict infarct size in pigs submitted to transient coronary artery occlusion and treated with succinate dehydrogenase inhibitors or remote ischemic perconditioning. *Int. J. Mol. Sci.* **22**(8), 4151 (2021).
9. García del Blanco, B. *et al.* Effect of COMBinAtion therapy with remote ischemic conditioning and exenatide on the Myocardial Infarct size: a two-by-two factorial randomized trial (COMBAT-MI). *Basic Res. Cardiol.* **116**(1), 4 (2021).
10. Lema, C. *et al.* ^{1}H NMR serum metabolomic profiling of patients at risk of cardiovascular diseases performing stress test. *Sci. Rep.* **10**(1), 17838 (2020).
11. Osuna-Prieto, F. J. *et al.* Elevated plasma succinate levels are linked to higher cardiovascular disease risk factors in young adults. *Cardiovasc. Diabetol.* **20**(1), 151 (2021).

12. Valls-Lacalle, L. *et al.* Selective inhibition of succinate dehydrogenase in reperfused myocardium with intracoronary malonate reduces infarct size. *Sci. Rep.* **8**(1), 2442 (2018).
13. Prag, H. A. *et al.* Ester prodrugs of malonate with enhanced intracellular delivery protect against cardiac ischemia-reperfusion injury in vivo. *Cardiovasc. Drugs Ther.* **36**, 1–13. https://doi.org/10.1007/s10557-020-07033-6 (2020).
14. Jespersen, N. R. *et al.* Cardioprotective effect of succinate dehydrogenase inhibition in rat hearts and human myocardium with and without diabetes mellitus. *Sci. Rep.* **10**(1), 10344 (2020).
15. Stottrup, N. B. *et al.* Inhibition of the malate-aspartate shuttle by pre-ischaemic aminooxyacetate loading of the heart induces cardioprotection. *Cardiovasc. Res.* **88**(2), 257–266 (2010).
16. Surendran, A., Aliani, M. & Ravandi, A. Metabolomic characterization of myocardial ischemia-reperfusion injury in ST-segment elevation myocardial infarction patients undergoing percutaneous coronary intervention. *Sci. Rep.* **9**(1), 11742 (2019).
17. Gundogdu, G. *et al.* Serum metabolite profiling of ST-segment elevation myocardial infarction using liquid chromatography quadrupole time-of-flight mass spectrometry. *Biomed. Chromatogr.* **34**(2), e4738 (2020).
18. Croisille, P., Kim, H. W. & Kim, R. J. Controversies in cardiovascular MR imaging: T2-weighted imaging should not be used to delineate the area at risk in ischemic myocardial injury. *Radiology* **265**(1), 12–22 (2012).
19. Fernandez-Jimenez, R. *et al.* Dynamic edematous response of the human heart to myocardial infarction: Implications for assessing myocardial area at risk and salvage. *Circulation* **136**(14), 1288–1300 (2017).
20. Sadagopan, N. *et al.* Circulating succinate is elevated in rodent models of hypertension and metabolic disease. *Am. J. Hypertens.* **20**(11), 1209–1215 (2007).
21. Aguiar, C. J. *et al.* Succinate causes pathological cardiomyocyte hypertrophy through GPR91 activation. *Cell Commun. Signal.* **12**, 78 (2014).
22. D'Alessandro, A. *et al.* Plasma succinate is a predictor of mortality in critically injured patients. *J. Trauma Acute Care Surg.* **83**(3), 491–495 (2017).
23. Cui, H. *et al.* Untargeted metabolomics identifies succinate as a biomarker and therapeutic target in aortic aneurysm and dissection. *Eur. Heart J.* **42**(42), 4373–4385 (2021).

Acknowledgements

Plasma samples were provided by the Vall d'Hebron University Hospital Biobank (PT20/00107), integrated in the Spanish National Biobanks Network, and they were processed following standard operating procedures with the appropriate approval of the Ethical and Scientific Committees.

Author contributions

A.R.S. and I.F.G. conceived the study. M.C., I.B., E.M.C., M.A.C., M.R.M., C.R. and J.I. obtained 1H-NMR spectra from plasma samples and analyzed the data. B.G.d.B., I.O., G.M., B.S., N.B. and M.O.R. performed the PPCI and obtained blood samples. J.F.R.P. and F.V. obtained CMR data. R.M.L., J.B., A.S. and B.B. obtained clinical data. A.R.S. and I.F.G. wrote the initial draft of the manuscript and all authors contributed to its final version. All authors have read and approved the final manuscript. No identifable individual data is provided in the article.

Funding

This work was supported by the Spanish Ministry of Economy and Competitiveness, Instituto de Salud Carlos III (Grants PI17/01397 and CIBERCV) and the Spanish Society of Cardiology (Proyectos de la FEC para Investigación Básica en Cardiología 2018, Sociedad Española de Cardiología), and was cofinanced by the European Regional Development Fund (ERDF-FEDER, a way to build Europe). Antonio Rodríguez-Sinovas has a consolidated Miguel Servet contract.

Competing interests

The authors declare no competing interests.

Additional information

Correspondence and requests for materials should be addressed to I.F.-G. or A.R.-S.